VOLTAMMETRIC SENSORS FOR HIGHLY SENSITIVE DETERMINATION OF BIOMOLECULES AND DRUGS

Ph.D. THESIS

by

NEERAJ KUMAR

**DEPARTMENT OF CHEMISTRY
INDIAN INSTITUTE OF TECHNOLOGY ROORKEE
ROORKEE-247667 (INDIA)
APRIL, 2019**

VOLTAMMETRIC SENSORS FOR HIGHLY SENSITIVE DETERMINATION OF BIOMOLECULES AND DRUGS

A THESIS

Submitted in partial fulfilment of the requirements for the award of the degree

of

DOCTOR OF PHILOSOPHY

in

CHEMISTRY

by

NEERAJ KUMAR

DEPARTMENT OF CHEMISTRY
INDIAN INSTITUTE OF TECHNOLOGY ROORKEE
ROORKEE–247667 (INDIA)
APRIL, 2019

INDIAN INSTITUTE OF TECHNOLOGY ROORKEE
ROORKEE

CANDIDATE'S DECLARATION

I hereby certify that the work which is being presented in the thesis entitled **"VOLTAMMETRIC SENSORS FOR HIGHLY SENSITIVE DETERMINATION OF BIOMOLECULES AND DRUGS"** in partial fulfilment of the requirements for the award of the Degree of Doctor of Philosophy and submitted in the Department of Chemistry of the Indian Institute of Technology Roorkee, Roorkee is an authentic record of my own work carried out during the period from December, 2014 to April, 2019 under the supervision of Dr. R.N. Goyal, Emeritus Professor and Dr. M.R. Maurya, Professor, Department of Chemistry, Indian Institute of Technology Roorkee, Roorkee.

The matter presented in this thesis has not been submitted by me for the award of any other degree of this or any other Institute.

(NEERAJ KUMAR)

This is to certify that the above statement made by the candidate is correct to the best of my knowledge.

(M.R. Maurya)
Supervisor

(R.N. Goyal)
Supervisor

Date:

ABSTRACT

The analysis of biomolecules and drugs has great importance in medical science and in the pharmaceutical industries. In both the cases accuracy is the main factor, which can affect the health of living mankind. From the previous literature, it has been concluded that small concentration of biomolecules and drugs is responsible to regulate the various biological activities. Any imbalance in their concentration can disturb the human physiological system, which leads to various serious diseases. Therefore, rapid, sensitive and highly selective methods are needed for the selective determination of biomolecules and drugs in clinical diagnosis and quantification of drugs in pharmaceutical analysis. Voltammetric sensors have many advantages in term of excellent sensitivity and selectivity for the determination of electro-active biomolecules, drugs, organic compounds and inorganic compounds. As a result of this, several unmodified and modified voltammetric sensors have been developed for the analysis of the trace amount of biologically significant biomolecules and drugs.

In the present thesis, various voltammetric sensors have been fabricated, characterized and used for the determination of biomolecules and drugs. The fabrication, characterization, behavior, results and applications of these sensors are summarized into five chapters.

The **first chapter** of the thesis is "General Introduction". It describes important aspects of electrochemical, voltammetric techniques, conventional electrodes, types of surface modifiers and analytes of interest. This chapter also presents the methodology applied in the present studies.

The **second chapter** describes the fabrication of unmodified and nanopalladium grained polymer nanocomposite based sensors for the sensitive determination of a biomolecule, Melatonin (MEL) in human biological samples and pharmaceutical samples. This chapter has been divided into two sections. In the **first section**, the unmodified glassy carbon sensor is employed for the determination of MEL using cyclic voltammetry (CV) and square wave voltammetry (SWV). Irreversible oxidation of MEL was found to proceed through an adsorption controlled pathway at the surface of glassy carbon. The quantitative estimation of MEL was performed using SWV in a linear concentration range of 5–200 µM with a sensitivity of 0.0491 µM/µA and a limit of detection of 0.3432 µM was observed. The proposed protocol was also applied for determining MEL content in pharmaceutical samples and recovery studies in human urine samples were also

performed. The observed results demonstrated a good agreement with the stated values. In the **second section,** the electrocatalytic properties of the palladium nanoparticles based polymer nanocomposite towards sensing of MEL are presented. The modification protocol involved a single step fabrication and was achieved using CV. The sensing surface was characterized using voltammetry, Field Emission Scanning Electron Microscopy (FE-SEM), Energy dispersive X-ray analysis (EDX) and Electron Impedance Spectroscopy (EIS). Quantitative estimation of MEL has also been carried out using SWV in the linear concentration range of 5–100 μM and sensitivity and limit of detection of 0.1235 μA/μM and 0.09 μM respectively have been achieved. The surface modified sensor exhibited almost 3 fold improvement in the sensing properties in comparison to the unmodified surface. The proposed method was also successfully extended for the determination of MEL in commercially available pharmaceutical formulations and human urine samples.

The **third chapter** of the thesis presents the development of melamine based molecularly imprinted, palladium nanoparticles decorated multi-walled carbon nanotubes and silver nanoparticles decorated graphene nanorribon modified sensor for the determination of biomolecules. For the sake of clarity, this chapter has been divided into three sections. The **first section,** describes a sensitive and facile molecularly imprinted sensor for the determination of 8-hydroxydeoxyguanosine (8-OHdG), an important oxidative DNA damage product. The molecularly imprinted polymer film was fabricated by electropolymerization of melamine in the presence of 8-OHdG, on glutaraldehyde/poly-1,5-diaminonaphthalene modified edge plane pyrolytic graphite (EPPG) surface. The imprinted sensor surface was characterized by using FE-SEM, EIS, CV, SWV and UV-visible spectroscopy. The calibration response was linear over a concentration range of 0.020–3 μM for 8-OHdG with sensitivity and limit of detection (3σ/b) as 10.59 μM/μA and 3 nM respectively. The common metabolites in urine, like uric acid, ascorbic acid, xanthine and hypoxanthine did not interfere up to 100-fold concentration. The imprinted sensor is also successfully employed for the determination of 8-OHdG in human urine sample of a renal failure patient. The **second section**, deals with the nano palladium decorated multi walled carbon nanotubes (PdNP:MWCNT) modified sensor for the determination of 5-hydroxytryptophan, an important serotonin (5-HT) precursor. PdNP:MWCNT was synthesized in a simple single step, followed by the characterization using FE-SEM, EDX, Film-X-ray diffraction (XRD), EIS and voltammetry. The PdNP:MWCNT was then used for the surface modification of

glassy carbon electrode (GCE) and applied for the electrochemical analysis of 5-hydroxytryptophan (5-HTP), a serotonin precursor. A significant increment in the peak current response was observed and peak potential also shifted towards less positive potentials indicating the facilitated oxidation process at PdNP:MWCNT/GCE. The quantitative determination of 5-HTP was carried out by using SWV and the anodic peak current was found to increase with increasing 5-HTP concentration in the linear range of 2–400 µM with a sensitivity and limit of detection of 0.2122 µA/µM and 77 nM respectively. The fabricated sensor further displayed excellent selectivity for 5-HTP in the presence of major interfering biomolecules in the urine with excellent recovery. The **third section,** of this chapter demonstrates the simple, rapid and sensitive voltammetric sensor for the determination of histamine (HTM); a neurotransmitter. The graphene nanoribbons were prepared by chemical method and silver nanoparticles (AgNPs) were prepared by the reduction of silver nitrate. The composite of graphene nanoribbons (GNRs) and AgNPs was drop casted on the surface of EPPG and the GNRs-AgNP exhibited superior catalytic activity towards the oxidation of HTM. To characterize the modified surface film-XRD, EDX, Raman Spectroscopy, Transmission Electron Microscopy (TEM), High Resolution Transmission Electron Microscopy (HRTEM), FE-SEM, EIS and CV have been used. The SWV has been used for the quantitative analysis of HTM and the GNRs-AgNP modified sensor demonstrated a linear calibration plot in the concentration range of 1–500 µM with sensitivity 0.158 µA/µM and the limit of the detection was found to be 0.049 µM. The GNRs-AgNPs sensor was highly selective in the presence of common interfering compounds present in biological fluids. The good recoveries (> 99%) were found in blood plasma samples. The determination of HTM was carried out in red wine by using standard addition method and the results were validated by using HPLC. The proposed sensor can be effectively applied for the determination of HTM in real samples.

The **fourth chapter** deals with the fabrication of a gold-palladium nanoparticles decorated electrochemically reduced graphene oxide (AuNP-PdNP-ErGO) modified glassy carbon sensor for the individual and simultaneous determination of lomefloxacin (LMF) and amoxicillin (AMX). A new sensing platform exploiting the beneficial interaction of gold, palladium and ErGO has been prepared involving a one-step electrochemical process, and is characterized using FE-SEM, Elemental Mapping, TEM, Raman Spectroscopy, film-XRD and EIS. The calibration curves for LMF and AMX have been constructed using square wave voltammetry and exhibited a linear response in the concentration range of 4–500 µM and 30–350 µM respectively. The sensitivity and

limit of detection were 0.0773 µA/µM and 81 nM; 0.0376 µA/µM and 9 µM for LMF and AMX respectively. The proposed protocol was successfully applied for detecting the presence of LMF and AMX in the complex matrix like urine and in the solutions containing excess of potentially interfering substances like ascorbic acid, uric acid, hypoxanthine etc.

The **fifth chapter** is divided into two sections, **first section** describes a simple, facile and sensitive method for the fabrication of molecularly imprinted sensor for the determination of hydrochlorothiazide (HCTZ). The sensor is fabricated by the deposition of iron oxide nanoparticles followed by the electropolymerization of melamine monomer in the presence of HCTZ at the surface of EPPG. The surface of the imprinted sensor was characterized by using FE-SEM, EDX, EIS, film-XRD, CV and SWV. The oxidation of HCTZ occurred in a single, well-defined peak and the peak current was dependent on the concentration of HCTZ in the range 0.025–10 µM. The sensitivity and limit of detection ($3\sigma/b$) were found to be 2.342 µM/µA and 4 nM respectively. The proposed method was applied for the determination of HCTZ in the presence of common metabolites present in the human system. The obtained results indicated that uric acid, ascorbic acid, hypoxanthine and xanthine did not interfere up to 100 fold concentration. The imprinted sensor was successfully applied for the determination of HCTZ in real samples. The **second section** of this chapter deals with a simple, facile, selective and cost effective electrochemical method for the determination of telmisartan (TMS); a drug used for the treatment of hypertension. A sodium dodecyl sulfate (SDS) modified EPPG is prepared by the simple immersion of EPPG in SDS solution at concentration greater than critical micelle concentration (CMC). The modified sensor exhibited superior sensing properties towards the oxidation of TMS. The modified surface was characterized by using the EDX, FE-SEM, EIS and CV. The quantitative investigations of the TMS were performed by applying the SWV. The micelles of SDS form a pseudo complex with cation radical of TMS and catalyse the oxidation. The proposed sensor showed the linear calibration plot in the concentration range of 5–100 µM with sensitivity 0.2983 µA/µM and limit of the detection 0.082 µM. The specificity of the developed sensor was also evaluated in the presence of commonly present interfering substances in biological samples. The amount of TMS excreted in urine of the patients undergoing treatment has also been determined. The proposed method can be effectively applied for the investigation of TMS in pharmaceutical formulations and biological samples.

****

ACKNOWLEDGEMENTS

My friends have constantly been a pool of support and happiness. I owe my thanks to the friends from the other laboratories of the department, Ramesh Chandra, Sundeep Kumar, Raj Kumar, Ankur Maji, Gaurav, Ankur Malik, Jatin, Rahul, Ankit, Amit, Waheed and Nitish.

I would like to bestow acknowledgement to my late grandmother Smt. **Murthi Devi**, for her support, prayers and blessings.

I would like to sincerely thank the most important people in my life, my parents and my family. My vocabulary is less to express my gratitude towards Maa and Papa, who have always supportive to me in every step of life. Their patience and diligent nature is pillar of my strength and inspiration, which promote my own potential and give me a positive attitude. With the core of my heart, I would like to give a special thanks to my family members; father Shri **Devendra Kumar**, mother Smt. **Rekha Devi**, sisters **Pooja, Rajni and Kajal**, and younger brother **Tarun** whose support, belief and patience in me enable this thesis to be completed. The thesis is dedicated to my family.

Date: **(NEERAJ KUMAR)**

****

LIST OF PUBLICATIONS

[1] **Neeraj Kumar**, Rosy and Rajendra N. Goyal, "Electrochemical behavior of melatonin and its sensing in pharmaceutical formulations and in human urine", **Current Pharmaceutical Analysis,** 13(1) (2017) 85-90.

[2] **Neeraj Kumar**, Rosy, Rajendra N. Goyal, "Nanopalladium grained polymer nanocomposite based sensor for the sensitive determination of Melatonin", **Electrochimica Acta** 211 (2016) 18–26.

[3] **Neeraj Kumar**, Rosy, Rajendra N. Goyal, "A melamine based molecularly imprinted sensor for the determination of 8- hydroxydeoxyguanosine in human urine", **Talanta** 166 (2017) 215–222.

[4] **Neeraj Kumar**, Rosy, Rajendra N. Goyal, "Palladium nano particles decorated multi-walled carbon nanotubes modified sensor for the determination of 5-hydroxytryptophan in biological fluids", **Sensors and Actuators B** 239 (2017) 1060–1068.

[5] **Neeraj Kumar**, Rajendra N. Goyal, "Silver nanoparticles decorated graphene nanoribbon modified pyrolytic graphite sensor for determination of histamine", **Sensors and Actuators B** 268 (2018) 383–391.

[6] **Neeraj Kumar**, Rosy, Rajendra N. Goyal, "Gold-palladium nanoparticles aided electrochemically reduced graphene oxide sensor for the simultaneous estimation of lomefloxacin and amoxicillin", **Sensors and Actuators B** 243 (2017) 658–668.

[7] **Neeraj Kumar**, Rajendra N. Goyal, "Melamine/Fe_3O_4 nanoparticles based molecular imprinted highly sensitive sensor for determination of hydrochlorothiazide: An Antihypertensive drug", **Journal of the Electrochemical Society**, 164 (6) B240–B246 (2017).

[8] **Neeraj Kumar**, Rajendra N. Goyal, "A simple and highly selective determination of telmisartan at sodium dodecyl sulfate modified pyrolytic graphite surface", **Electroanalysis,** 30 (2018) 1–10.

****

LIST OF CONFERENCES/SEMINARS ATTENDED

[1] An oral presentation on the topic "Determination of Histamine by using graphene nano-ribbon based nanocomposite modified pyrolytic graphite sensor" in the International conference on CEAMCR 2018 organized by the Indian Society for ElectroAnalytical Chemistry (ISEAC) during, February 15-17, 2018 at DAE Convention centre, Anushaktinagar, BARC, Mumbai 400094.

[2] A poster presentation on "Silver nanoparticles decorated graphene nano-ribbon modified sensor for determination of histamine" in the National Seminar on "Recent Trends in Nanobiosensors" (NBS 2018) University of Madras, 22nd and 23rd Feb 2018.

[3] An oral presentation on "A sodium dodecyl sulfate modified pyrolytic graphite sensor for determination of Telmisartan; an anti-hypertensive drug" in International Conference on Nanotechnology: Ideas, Innovations and Initiatives (ICN:3I-2017), December 06-08, 2017 at IIT Roorkee, Uttarakhand, India.

[4] A poster presentation on "Determination of 5-hydroxytryptophan, a serotonin precursor, by using nano palladium decorated glassy carbon electrode" in the 12th ISEAC Discussion Meet in Electrochemistry (12th ISEAC-DM-2016) organized by Indian Society for ElectroAnalytical Chemistry (ISEAC) at The Acres Club, Chembur, Mumbai, India, December 7-8, 2016.

****

LIST OF ABBREVIATIONS

CV	Cyclic Voltammetry
FE-SEM	Field Emission Scanning Electron Microscopy
SWV	Square Wave Voltammetry
EIS	Electrochemical Impedance Spectroscopy
TEM	Transmission Electron Microscopy
HRTEM	High Resolution Transmission Electron Microscopy
HPLC	High Performance Liquid Chromatography
XRD	X-ray powder diffraction
CNTs	Carbon Nanotubes
MWNTs	Multi Walled Carbon Nanotubes
SWNTs	Single Walled Carbon Nanotubes
p-AHNSA	Poly(4-amino-3-hydroxy-1-naphthalenesulfonic acid)
p-DAN	Poly-1,5-diaminonapthalene
MIPs	Molecularly Imprinted Polymers
NIPs	Non Imprinted polymers
Ag/AgCl	Silver-Silver Chloride Electrode
GCE	Glassy Carbon Electrode
EPPGE	Edge Plane Pyrolytic Graphite Electrode
HOPGE	Highly Oriented Pyrolytic Graphite Electrode
BPPGE	Basal Plane Pyrolytic Graphite Electrode
PdNPs	Palladium Nanoparticles
AuNPs	Gold Nanoparticles
AgNPs	Silver nanoparticles
XT	Xanthine
UA	Uric Acid
AA	Ascorbic Acid
HX	Hypoxanthine
LMF	Lomefloxacin
5-HT	Serotonin
AMX	Amoxicillin
HTM	Histamine

8-OHdG	8-Hydroxydeoxyguanosine
GA	Glutaraldehyde
MM	Melamine
CMC	Critical micelle concentration
SDS	Sodium dodecyl sulfate
TMS	Telmisartan
MEL	Melatonin
5-HTP	5-Hydroxytryptophan
HCTZ	Hydrochlorothiazide
E_p	Peak Potential
i_p	Peak Current
f	Square Wave Frequency
ν	Scan Rate
RSD	Relative Standard Deviation

****

CONTENTS

CHAPTER 4

Au-PdNPs-rGO MODIFIED SENSOR FOR SIMULTANEOUS DETERMINATION OF LOMEFLOXACIN AND AMOXICILLIN

Chapter 1

General Introduction

1.1 ELECTROCHEMISTRY: AN OVERVIEW

The branch of science that employed with the relationship between electricity to chemical changes and with the interconversion of chemical and electrical energy or vice versa is known as electrochemistry. In other words, the science of the electrochemistry involves the study of the inter-relationship between chemical and electrical energy at the solution/electrode interface. Electrochemical reactions are chemical reactions in which electrons are transferred in between electrode and electro-active species (ionic conductor, such as electrolyte). Oxidation-reduction refers to electrochemical processes; occur via transfer of electrons in the substrate (molecules, atoms or ions) and causes change in oxidation state. Redox processes are involved in all living organisms for conversion of energy and substrate metabolism. In plants, solar energy (solar radiation) is converted into chemical energy and in human system metabolism of several natural substances (neurotransmitter, drugs and xenobiotic etc.) occurs by oxidation- reduction processes. The redox nature suggests that electrochemical methods can be effective tools to elucidate the kinetics, thermodynamics and mechanistic processes of biological redox reactions. Thus, electrochemical investigations provide the information about oxidation and reduction potential, pathway of reaction, reaction intermediate and mechanism of a reaction. Electrochemistry is playing an important role in a broad range of research and analytical areas including the dynamic applications in the field of organic and inorganic compounds, biological and biochemical research, energy conversion and storage, corrosion, pollution control, nano scale investigation, fuel cells and solar cells etc. Several electrochemical methods have been applied to investigate the oxidation or reduction of biologically significant compounds.

The credit of first electrochemistry experiment goes to Luigi Galvani (1791) and stabilizes a bridge between chemical reaction and produced electricity by placing the metal pieces into frog's legs in his experiment. In the year 1800, Alessandro Volta invented the first battery, described as 'Voltaic Pile' and two new fields of study opened; they were chemical production of electricity and the effect of electricity on chemicals due to continous production of current in this experiment. Hydrogen and oxygen were successfully separated in water electrolysis by Johann Wilhelm Ritter and William Nicholson. Many more experiments and theories have been described by the scientists in this period, such as electroplating, thermo-electricity etc. to develop the electrochemistry. In 1832, Michael Faraday describesd the two important fundamental laws of electrolysis, which were named as Faraday's law in electrochemistry and also defined some terms, frequently used in the electrochemistry, like anion, cation, anode, cathode, electrode and electrolyte. In the year 1888,

Nernst proposed the electromotive force theory of the voltaic cell and developed the method for the determination of dielectric constants. Nernst also constructed an equation, which was related to the voltage of the cells to its properties and is known as "Nernst equation". In 1922, Czech chemist Jaroslav Heyrovsky performed his famous experiment on polarography and received the Nobel Prize in chemistry in 1959, for his excellent work and development of polarographic technique. The branch of the electrochemistry now known as voltammetry was developed from polarography. The advent of operational amplifiers in 1960's led to various improvements in all the fileds of instrument, methodology and theory of voltammetry. Electroanalytical techniques have ability to detect the extremely short-lived, reactive intermediate species formed during the electrode reactions [1-8].

In recent years electrochemical sensors have been developed to very high level, which improved the sensitivity and expended the field of sensors for routine analysis of drugs, biomolecules and clinically relevant substances. Electrochemical sensors are based on the determination of electrical signal produced by electro-active species. The modern electrochemical strategies have better subtle platform for detection of redox reactions of biomolecules at an electrode. The biomolecules, like neurotransmitters, proteins, small molecules, genetic materials, amino acids, etc. are having prospective clinical importance [9]. Biomolecules have crucial importance for living beings to regulate the numerous biological activities in the human body. The analysis of these biomolecules is very important due to the increasing pathological imbalance in natural metabolites. Irregularities in biological functions and alteration in biomolecules concentration lead to several kinds of cancerous, metabolic and genetic diseases, which require a stable, accurate and highly sensitivity equipment for quick and specific detection [10]. The clinical diagnosis in laboratories is a time consuming process and expensive too. Hence, there is an increasing demand of simple, rapid and inexpensive techniques for the diagnosis of biological and clinically significant substances. Electrochemical sensors/biosensors are serving as an alternative tool for solving this problem due to their high sensitivity, selectivity, low-cost and rapid response time. Thus, the analytical techniques can be considered an important option for clinical and pharmaceutical analysis due to inexpensive analytical device, less complicated procedure and simplicity of operation [11-15]. The developed methods must be able to determine various compounds in the real samples with high sensitivity and accuracy. Electrochemical sensors are ideally suitable for the determination of trace amount of clinical and biological compounds [9-15].

The major efforts during the present studies have been made to develop highly sensitive voltammetric sensors for the determination of biomolecules and drugs in biological fluids.

1.2 ELECTROCHEMICAL TECHNIQUES

Electroanalysis has applications in environmental, metal industry, and pharmaceutical industry. It has various advantages, including high sensitivity, low operating cost, ease of operation and high-speed analysis. The pulse techniques are widely used for the drug analysis and biological sample analysis these days.

Voltammetry basically deals with the analysis and interpretation of current-voltage curves. In voltammetry, voltage-current-time relationship is recorded in an electrochemical cell, having three electrodes: reference electrode, working electrode and counter or auxiliary electrode (**Fig.1.1**). The transfer of electrons to substrate or vice-versa occurs at the working electrode. In practice, there is practically no flow of current through the reference electrode, which possesses a constant potential over the process, and calomel electrode and silver/silver chloride electrode are most frequently used in aqueous solution as reference electrodes. Third electrode, an auxiliary (counter) electrode made of an inert metal or carbon (graphite) is used to make a connection with electrolyte and almost 99% current flows between the working and auxiliary electrodes. A supporting electrolyte is used to ensure the conductivity of the medium or solution. The mass transport of the substrate to the working electrode surface and generation of current leads to the oxidation or reduction of an electroactive substance at a suitable applied potential at the working electrode [4,7, 16-18].
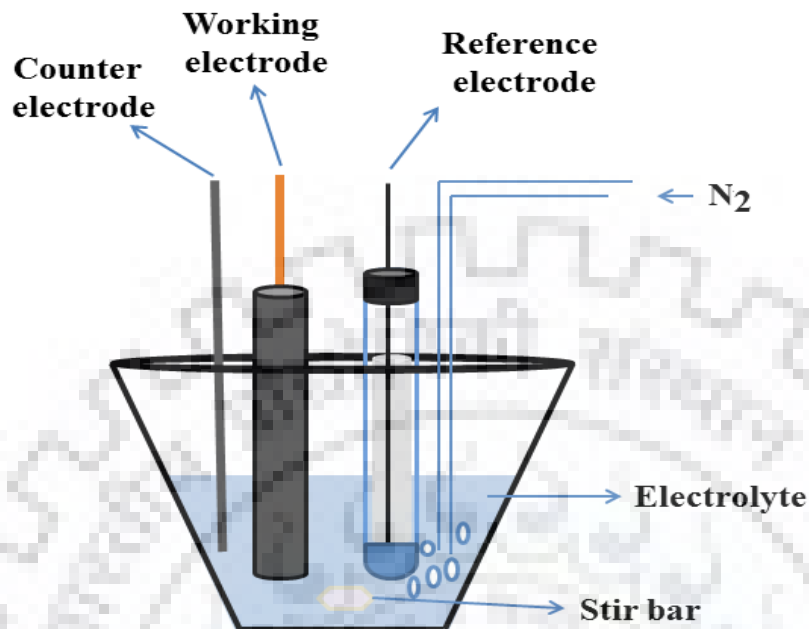
Fig. 1.1: Electrochemical cell setup commonly used in electroanalysis.

1.2.1 Cyclic voltammetry

Cyclic voltammetry (CV) is an electroanalytical technique, which is widely used in many areas of chemistry. This technique is rarely applied for quantitative determination, but commonly used for examination of redox processes, electron transfer kinetics, stability of reaction products, reversibility of the reaction, investigation of reaction products and understand the reaction intermediates. In CV, applied potential is varied in forward and reverse directions and resulting current is monitored at certain scan rate. The initial scan can be in the negative or positive direction and reaching at switching potential, the direction of the scan would be reversed. In CV experiment, the potential waveform is applied at the working electrode, excitation signal is a linear potential scan swept between two values of electrode potential, from an initial potential value (E_i) to a final potential value (E_f) in one direction and then reversed back to the initial potential. The potential at which the direction is reversed is known as switching potential **(Fig.1.2A)**. The current response vs. potential plot is referred as the cyclic voltammogram **(Fig.1.2B)**, from which important information regarding cathodic and anodic peak potentials (E_{pa}, E_{pc}) and peak current (i_{pa}, i_{pc}) respectively, can be acquired. Based on the requirement of analysis, a partial cycle, a full single cycle or a series of cycles can be executed [3-4,7, 16-20].
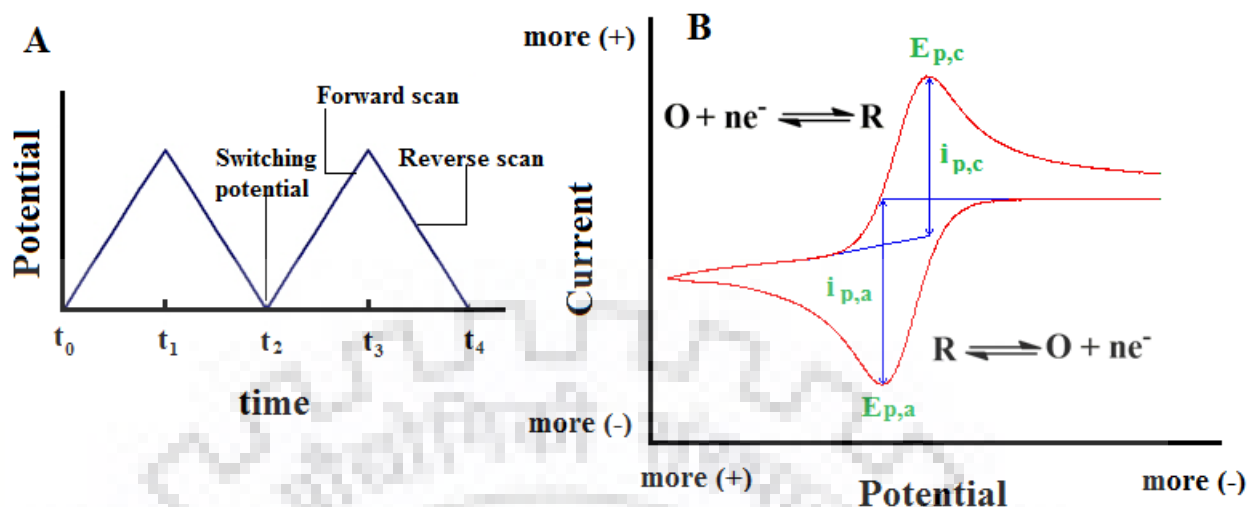
Fig. 1.2: (A) Typical triangular potential-excitation signal in cyclic voltammetry (B) A typical cyclic voltammogram for reversible redox process.

In a reversible process, the number of electrons in the electrochemical reaction can be evaluated by using the difference in anodic potential 'E_{pa}' and cathodic potential 'E_{pc}'

$$\Delta Ep = [E_{pa} - E_{pc}] = 2.303RT/nF = 0.059/n$$

where, n is the number of electrons, F is Faraday constant (96485 C), T is the absolute temperature (298 K) and R is the universal gas constant (8.314 J mol^{-1} K^{-1}). Thus, for an electrochemically reversible one electron event the difference between the two peak potentials is about 59 mV at 25 ^{o}C. The peak to peak separation for a two-electron transfer will be 29.5 mV instead of 59 mV and the process is reversible. A process is named as electrochemically irreversible, when the electron transfer process at electrode surface is slower than mass transport [21].

In voltammetry, for an electrochemical reversible process the quantitative information can be described by the Randles-Sevcik equation (at 25°C):

$$i_p = (268600) \, n^{3/2} \, A \, C \, D^{1/2} \, v^{1/2}$$

where, i_p is the peak current in ampere, A is the electrode surface area (cm^2), n is the number of electrons transferred in redox event, D is the diffusion coefficients of analyte (cm^2/s), C is the concentration of analyte (mol/L) and *v* is the scan rate (V/s). According to this relation, i_p is proportional to the square root of scan rate ($v^{1/2}$) and concentration. This technique enables to study the reducible or oxidizable species in the wide potential window even at a high scan rate. However, for quantitative analysis more sensitive pulse techniques (square wave voltammetry, differential

pulse voltammetry etc.) are used, which enhance the sensitivity by minimizing charging current [21-23].

1.2.2 Square wave voltammetry

In 1957, square wave polarography and its applications are reported by C.G. Barker. Later a staircase waveform was combined with a square wave and the technique was named as square wave voltammetry (SWV). Modern, SWV is developed from the Barker square wave polarography [24-28]. SWV technique is much faster than the normal and differential pulse technique and can use up to 1 V/s or higher, permitting much faster analysis [29]. The improvements in analog and digital electronics have made it possible to complete the experiment in few seconds using SWV. This technique contains a symmetrical square wave pulse of constant amplitude, which is superimposed on a base staircase waveform. The current is sampled twice for each cycle, first at the end of the first pulse, known as forward current (i_f) in the direction of staircase scan and second at the end of the second pulse, known as reverse current (i_r) as shown in **Fig.1.3**.
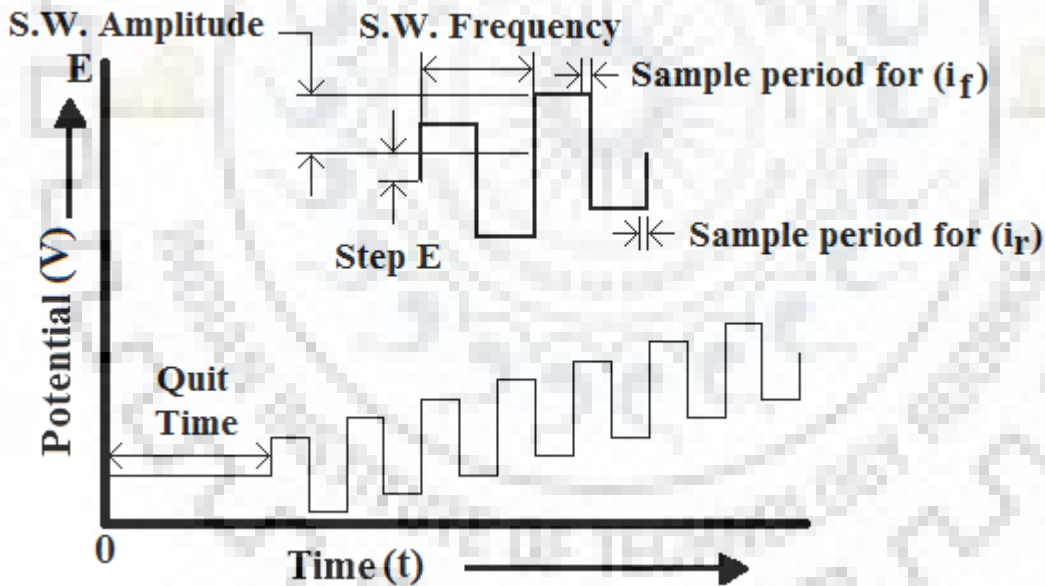
Fig. 1.3 Potential wave form commonly used for square-wave voltammetry

Fig. 1.4: Epsilon EC-USB system used for electrochemical studies

The resulting current, difference of forward and reverse current ($i_f - i_r$) is plotted against the staircase potential. The peak height or current is directly related to the concentration of analytes (electroactive substance). SWV is one of the superior electroanalytical techniques of the family of pulse techniques in term of excellent sensitivity. Thus, it is commonly used for the quantification of various compounds, such as biomolecules, antioxidants, environmental pollutants and medications, etc. The advantages of SWV are its speed to perform the experiments and low background currents. In recent years, the application of SWV has increased drastically due to its feasibility and has replaced highly expensive, sophisticated, lengthy and time consuming chromatographic and spectroscopic techniques in various studies. Thus, SWV has found various applications in different fields, including detection of substances at trace level, study of the electrode kinetics with regard to preceding, following, or catalytic homogeneous chemical reactions [2,7, 30-32]. SWV has been used for the quantification of vitamins, proteins, phenols, pesticides, fungicides and herbicides, terpenoids, alkaloids, metal traces and drugs [30-32]. In the present studies, the electrochemical studies of several biomolecules and drugs have been carried out using SWV.

1.3 WORKING ELECTRODS

The first electrochemical sensor invented by Max Cremer in 1906, was named as glass electrode [8, 15]. The modern concept of electrochemistry for the determination of biologically important molecules using sensors has attracted attention after the invention of the very first glucose electrochemical biosensor by Clark and Lyons in 1962, based on enzyme glucose oxidase [8, 11]. Electrochemical sensors have high performance, low cost, simple to operate and portable in comparison to conventional analytical techniques. Electrochemical sensors are widely used these days as they possess high sensitivity, precision and accuracy, larger linear dynamic range and comparatively low-cost instrumentation.

Working electrode is defined as a platform at which reaction of interest is carried out, and response and change in signal are investigated. Different electrode materials behave differently with electro-active compounds. Hence, the study of the material is very important to know the surface morphology and chemistry of materials. The material of electrode is responsible for the redox reaction to occur or not at an electrode interface. Electrochemical reactions proceed through the exchange of electrons at the electrode-electrolyte interface. Thus, the chemical, physical and electronic properties of the electrode material are of prime importance. The effectiveness of the electrode towards the redox system also depends upon the material of electrode. Therefore, the choice of the working electrode material plays a crucial role to enhance the reproducibility and sensitivity of the electrode. The ideal working electrode should possess properties, such as fast rate of electron transfer, reproducible and low background for the entire potential range for the target analyte.

Some important feature of an ideal electrode are :

- ➢ Easy availability and cost effectiveness
- ➢ Renewable and reproducible surface
- ➢ Wide potential window and low residual current
- ➢ Resistance to chemical attack
- ➢ Fast electron transfer rate
- ➢ Long term stability and easy to handle
- ➢ Easy to fabricate

If a working electrode is having low charge carrier mobility (i.e. weak electronic properties), the flow of the current response will be limited. Generally the working electrodes are made up of carbon based materials, but some other materials also have been considered for the construction of the electrode. Typical electrode materials are the carbon based electrodes (glassy carbon, diamond film, carbon paste, pyrolytic graphite, carbon fibers, nanotubes etc.), semiconductor electrode (ITO; Indium tin oxide, Si), metal electrodes (Au, Pt, Ag, Cu, Ni etc.) and liquid electrodes (Hg, amalgam etc.). A variety of mercury based electrodes, such as hanging mercury drop electrode (HMDE), mercury film electrode and dropping mercury electrode (DME) have also been used. HMDE and DME have been extensively applied for the investigation of inorganic and organic electro-active substances due to reliability, simplicity and easily renewable surface. However, due to serious problems associated with the use of mercury, such as contamination, risk of potent poisoning and disposal of the used mercury, it has been completely banned/restricted in many developed and developing countries [3-4, 33-38]. Carbon based electrodes are widespread in electroanalysis because of their low cost, low background current, broad potential window, rich surface chemistry, chemical inertness and suitability for countless detection and sensing applications [3]. In the present studies, pyrolytic graphite and glassy carbon sensors have been used for the analysis of analytes.

1.3.1 Pyrolytic graphite electrode

Pyrolytic graphite is an ultra-pure form of graphite and is manufactured by decomposition of a hydrocarbon gas at very high temperature (more than ~2500 ^{o}K) in a vacuum furnace. Highly oriented pyrolytic graphite (HOPG) is the result of annealing of pyrolytic graphite under compressive stress at ~3300 ^{o}K and it is highly pure form of pyrolytic graphite. The pyrolytic graphite is extremely anisotropic in nature and a polycrystalline form of graphite. The material is characterized by anisotropic of thermal, mechanical and electrical properties and based on these properties two types of pyrolytic graphite surfaces are formed. One is basal plane pyrolytic graphite and other is edge plane pyrolytic graphite. The basal plane pyrolytic graphite contains layers of graphite that lie parallel to the surface and with ~3.35 Å inter-layer spacing. The other is edge plane pyrolytic graphite, which consists of perpendicular graphite layers to the surface of the disc and the defect occurs due to these steps **(Fig. 1.5)**. The high electrochemical activity of the edge plane is assigned to the step edges.
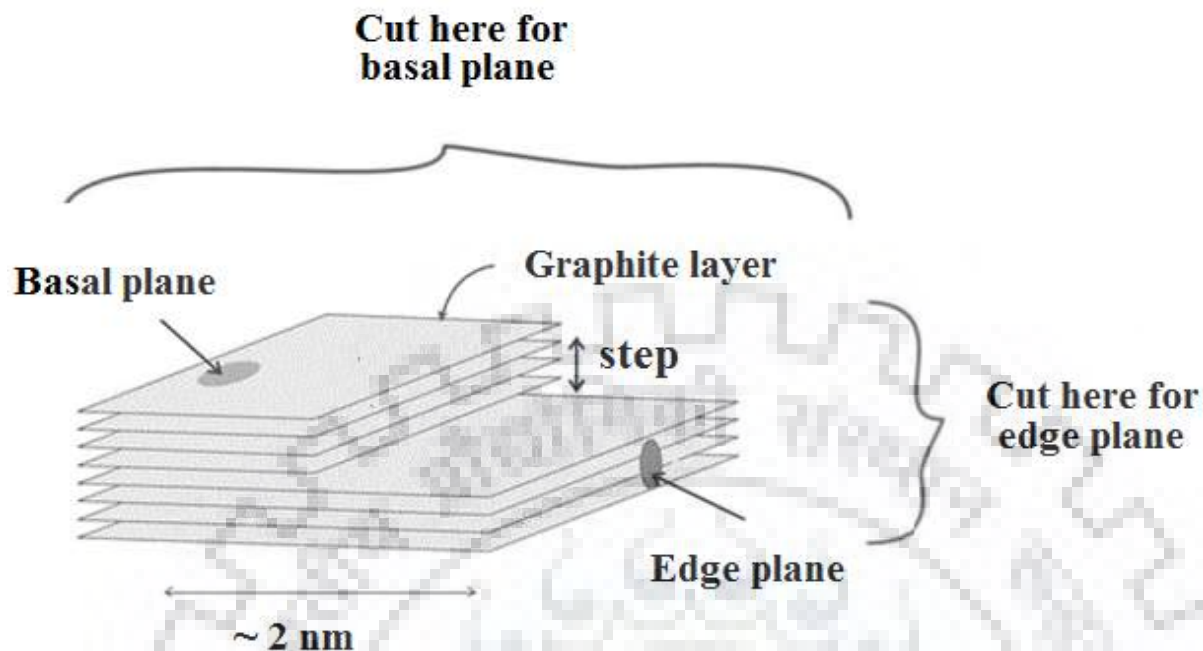
Fig.1.5 Schematic representation of pyrolytic graphite electrode
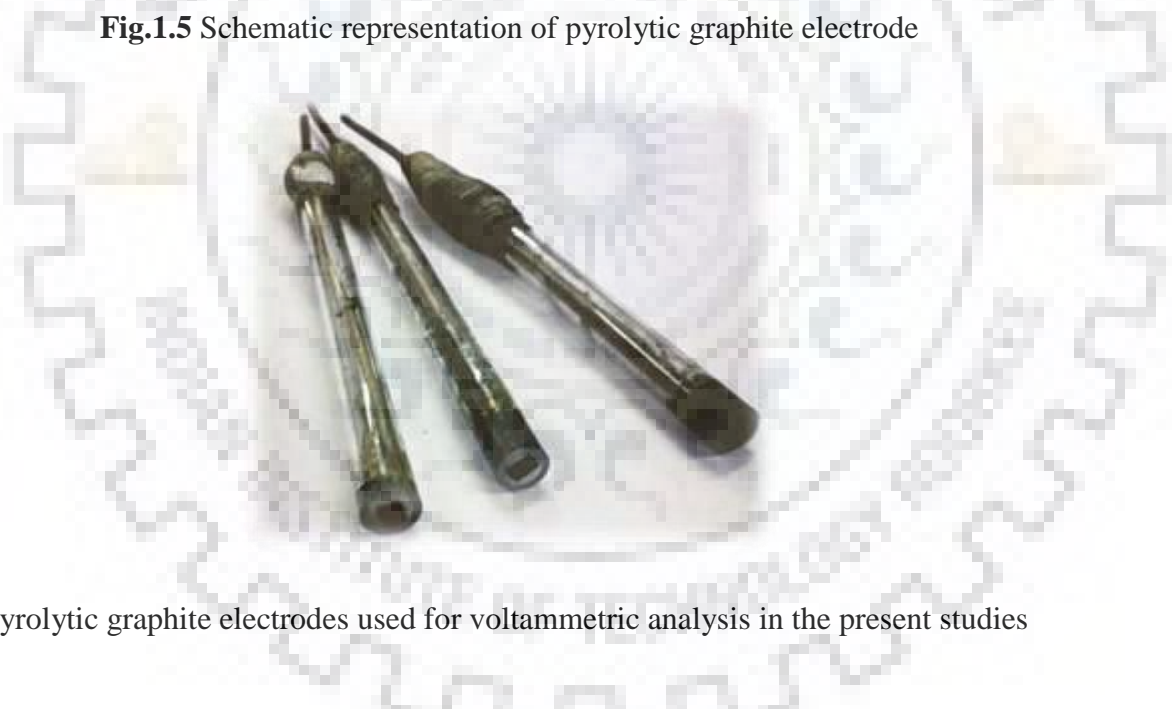
Fig. 1.6 Pyrolytic graphite electrodes used for voltammetric analysis in the present studies

The edge plane and basal plane pyrolytic graphite demonstrate different electrochemical properties and different electron transfer kinetics due to the nature of the chemical binding in graphite. For electrochemistry, edge plane pyrolytic graphite (EPPG) in general exhibits more reactivity in comparison to the basal plane pyrolytic graphite (BPPG) towards the electro-catalytic activity, adsorption and electron transfer reactions. The reactivity of EPPG is assigned to the larger surface area, high capacitance, high electronic density, surface roughness, high adsorption sites and larger

functional groups. Moreover, EPPG also exhibits low background currents and wide potential window. The EPPG has been used for the electrochemical investigations of various electro-active compounds, such as neurotransmitters, steroids, nucleic acid, DNA damage, NADH oxidation, glucose, myoglobin, hemoglobin etc., that demonstrate the low background currents and wide potential window [4, 39-51]. In the present investigation, basal plane and edge plane electrodes were prepared in the laboratory and are depicted in **Fig. 1.6**.

1.3.2 Glassy carbon electrode

The credit of preparing glassy carbon goes to Yamada and Sato [52], by using phenolic resin as the starting material. Glassy carbon was prepared under controlled heating of polymeric (phenol-formaldehyde) resin in an inert atmosphere. The carbonization process starts at 300 $^{\circ}$C to 1200 $^{\circ}$C to ensure the elimination of non-carbon atoms like nitrogen and oxygen (300–500 $^{\circ}$C) and hydrogen (500–1200 $^{\circ}$C) and the process gives a product known as glassy carbon. The resultant product has high resistance to chemical attack (alkali and strong acid) and holds isotropic properties and possess thin, interwoven ribbons like structure **(Fig.1.7)**.
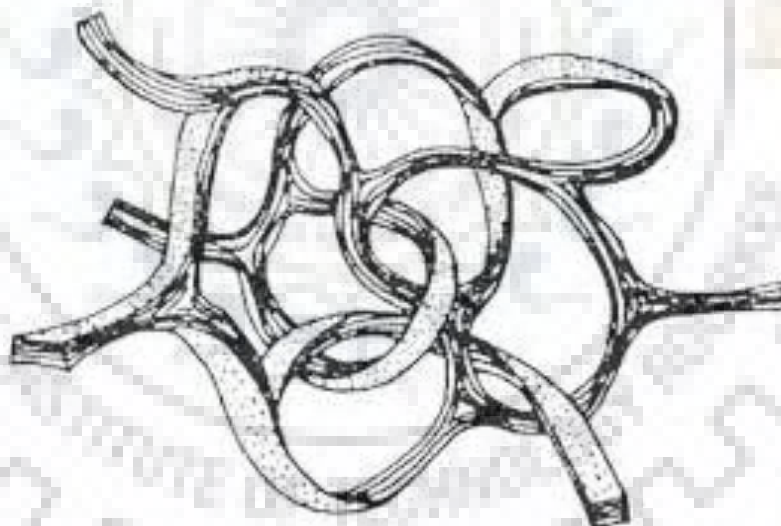
Fig.1.7 Schematic structural representation of glassy carbon interwoven ribbon stacks

Glassy carbon is very hard as compared to graphite and also has extremely low permeability to liquids or gases. It is obtained in various forms, like rods, disk and plates. The glassy carbon electrode (GCE) has been extensively used in the voltammetric sensing **(Fig.1.8)** due to its low residual current in aqueous medium and aqueous-micellar medium in the potential range - 1V to + 1V. Some important factors, which can affect the electron-transfer kinetics at the electrode

11

interface are microstructure, surface roughness, and cleanliness and surface functional groups. GCE has characteristic properties, such as good electrical conductivity, excellent mechanical properties, extremely low porosity, wide potential window and reproducibility. It is widely used for the determination of various drugs and biologically important compounds, such as uric acid, glucose, ascorbic acid, neurotransmitters, steroids, nucleosides, biogenic amines, NADH oxidation, etc. [52-65].

Fig.1.8 Commercially available glassy carbon electrodes

1.4 SURFACE MODIFICATION

The turn of the last decade has seen an extraordinary growth in the area of nanotechnology. Various potential applications of nano materials in the area of electrochemistry have also been reported. The realm of nanotechnology is referred as analysis, manufacturing, use in nano devices and nano-structures. These new materials and devices lead to various technological and commercial applications, in medicine, bioencapsulation, drug delivery, biomaterials energy production, analytical chemistry, mechanical, optical and electronic devices etc. Nanotechnology is involved to accelerate and excite the field of activity, used for creation and manipulation of materials with structural properties on atom, bulk material and molecular scale. Normally, nano-materials are having a size in between 1–100 nm scale and in chemistry these are related to micelles, polymer molecules, colloids, phase-separated regions in block copolymers and polymer nano-composite [66-70]. The main advantages of the nanomaterials are that they help to attain the larger surface to volume ratio, shape, physicochemical properties of compositions and binding characteristics. The shapes, sizes, dimension, porosity and surface area of nanomaterials makes

them highly interesting material and suitable for catalysis, energy storage and conversion, gas storage and chemical and biosensing and related applications [71-72]. Applications of nanomaterials in electrochemical sensing allow many new signal transducers methodologies in their fabrications. The use of nanomaterials in electroanalysis has revolutionized the fields of biological and chemical sensing due to their unique size, shape and compositions. The nanomaterials have been classified as nanotubes, nanowires, nanoparticles, graphene, quantum dots, graphene nanoribbons, nano-silica, magnetic nanoparticles, conjugated polymer nanocomposite, and nanostructured and nano-channels surfaces [73-76].

Surface modification is used to improve the surface properties of electrode, such as electrical, mechanical and physical properties and also to facilitate the electrochemical reaction at the electrode interface. In order to achieve the highly sensitive and selective working surface, chemical modification is carried out by using various methods. The main aim of the surface modification is to develop the specific properties, which are not naturally found in substrates and thus desired functional groups are incorporated to the working surface by using surface modifiers, like conducting polymers, enzymes, nanomaterials, chemical substance, biological recognition elements etc. The modified film on the working surface can be prepared by using several methods, such as adsorption, spin coating, electrochemical deposition, covalent attachment, entrapment (gel or paste or polymer), microencapsulations, cross-linking etc. [78-82]. Adsorption method is the simplest method to modify the surface by simple dorp casting. The use of surface modified sensors has been found extremely sensitive and selective for the analysis of electro-active compounds.

1.4.1 Graphene

Graphene is an important allotrope of carbon, and was discovered by A.K. Geim and K.S. Novoselov in the year 2004, and is considered an excellent electronic material. Graphene is a monoatomic two dimensional (2D) graphite sheet of sp^2-bonded carbon atoms with a honeycomb like network as shown in **Fig. 1.9**. It is involved to form the other carbon allotropes by modification of their structure, conformation, like rolled to form one dimensional (1D) nanotubes, stacked sheet to form three dimensional (3D) graphite and wrapped to form zero dimensional (0D) fullerenes. Graphene is having extraordinary thermal, electronic and mechanical properties due to long-term π-conjugation. Graphene has many advantages, such as high carrier mobility, high surface area, 2D morphology, excellent thermal conductivity, electrical conductivity, potential biocompatibility and extraordinary behavior towards the metals, π-conjugated system and with

other materials. These properties of graphene generated titanic growth in the possible implementation of graphene in electronic devices, gas sensors, super capacitors, batteries, fuel cell, electrochemical sensors and biosensors, energy storage, drug delivery, photonic devices and numerous biomedical applications. Several methods have been implemented to prepare the graphene including, reduction of graphene oxide, mechanical exfoliation, chemical vapor deposition, thermal decomposition of graphite oxide, chemical exfoliation and cleavage, epitaxial growth, thermal decomposition of SiC and unzipping of carbon nanotubes [83-85]. Graphene oxide is an oxidized form of graphene and highly oxygen functional groups present in it makes it easier and compatible with various nanoparticles, polymers and solvent. The biocompatibility of graphene permitted the immobilization of enzyme, proteins, DNA and other biological recognition elements. It is reported that by using the graphene and graphene related materials with metal nanoparticles and polymers leads to specific and sensitive determination of drugs and biomolecules using electrochemical sensors [66, 86-89].
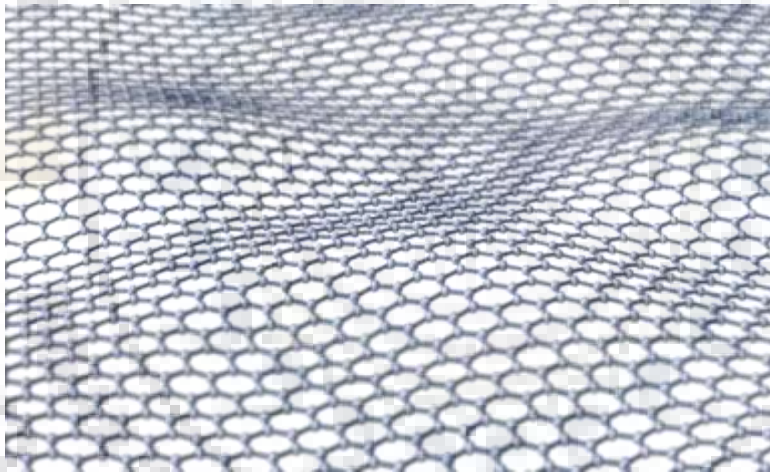
Fig.1.9: Structure representation of graphene sheet

1.4.2 Carbon nanotubes

Carbon nanotubes (CNTs) can be classified into two groups as single-walled carbon nanotubes and multi-walled carbon nanotubes based on their specific structural features and properties **(Fig. 1.10)**. In 1991, Sumio Iijima synthesized multi-walled carbon nanotubes (MWCNT) with inner diameter ~4 nm. Later in 1993, D.S. Bethune of IBM and Sumio Iijima of NEC, Corporation independently synthesized the single walled carbon nanotubes (SWCNTs). The individual SWCNTs tubes contain a very small diameter of around 1 nm. SWCNTs have only one rolled graphene sheet with diameters range 0.4–4 nm. These are hollow cylindrical molecules

formed with carbon atoms with unique 1D structure. CNTs contain length in nano, micro, or even millimeter-scale and diameters in nanometer-scale. The basic building block of carbon nanotubes is long-term cylindrical and monoatomic thick wall nanostructure of the carbon and rolled form of graphene sheets. To synthesize the CNTs, various methods have been utilized, but most common methods are chemical vapor deposition (CVD), arc discharge, flame synthesis and laser ablation. In the last two decades carbon nanotubes have attracted a lot of attention of chemists, physicists, electronic device engineers and material scientists because of their exceptional properties. These cylindrical nanostructure molecules have exceptional electronic, chemical, optical, and mechanical properties. Characteristic of carbon nanotubes (CNTs) including electrical, chemical, physical and high thermal properties makes them suitable for potential applications, such as electrochemical sensing, fuel cells, atomic force microscopy probes, drug carriers, microelectrodes, electronics (semiconductor material) and adsorbents for removal of pollutant from waste water.
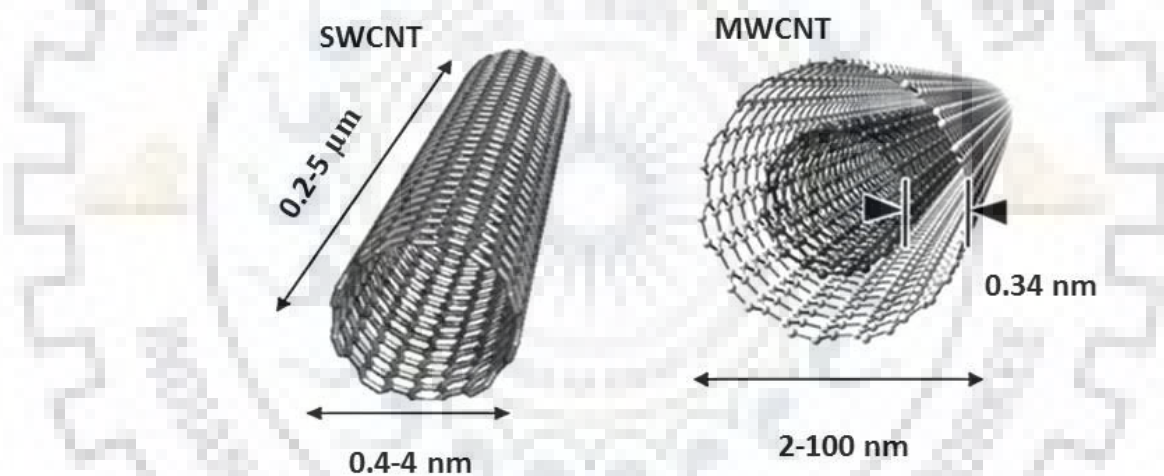
Fig. 1.10: A typical representation of single and multi-walled carbon nanotubes

Pristine CNTs are hydrophobic in nature and can be modified by using surfactants to disperse the nanotubes. In order to introduce more dispersible properties in the nanotubes functionalization is required. The various organic moieties or functional groups can be easily added to the sidewalls of CNTs for their specific applications [90-97].

1.4.3 Metal nanoparticles

Metal particles at nano-scale are especially interesting due to the simplicity with which they can be synthesized chemically. Various approaches have been suggested to synthesize the

nanoparticles over the last few decades. In many methods, the main objective of nanoparticle synthesis was to control the particle morphology; to control and minimize the particle size; to hold in the crystallinity and to preserve the narrow size distribution [98-100]. The variation in size, shape and crystal structure of particles leads to different chemical and physical properties to metal nanoparticles. Metal nanoparticles are having dynamic medical, biomedical and pharmaceutical applications in the fields of gene delivery, drug delivery, biomarker mapping, targeted cancer remedy and molecular imaging. Since the initial development of nanotechnology, the main challenge is to develop the simple, high yield and low cost methods for the synthesis of nanoparticles. Different bottom-up and top-down methods have been proposed for the preparation of metal nanoparticles, such as sol-gel process, sonochemical methods, nanosphere lithography, mechanical milling, photochemical, chemical, electrochemical, templating, photolithography, thermal reduction, biogenic synthesis, laser ablation and lithography strategies. Several metallic and semiconductor nanoparticles, such as palladium, silver, cobalt, gold, copper, platinum, iron, zinc, cadmium and some of their metal oxides have been prepared [101-104]. The metallic nanoparticles have been used to develop sensors, biosensors, gas sensors, and electrochemical sensors for sensing of organic and inorganic compounds with high sensitivity (**Fig. 1.11**). Due to their chemical stability, high conductivity and excellent catalytically activity nanoparticles have found applications in medical science, molecular diagnostics, medical imaging, probing of DNA structure, gene and drug delivery, treatment of cancer etc. Some other important applications of nanoparticles are in the cancer diagnostics (metal nanoparticles, magnetics nanoparticles), antibacterial creams (Ag), biolabeling and detection (Ag, Au quantum dots) and MRI contrast agents (Fe_3O_4, Fe_2O_3) [105-116]. In the present studies palladium, gold, silver and iron oxide nanoparticles have been prepared and used for the fabrication of sensors for the sensitive and selective analysis of biomolecules and drugs.
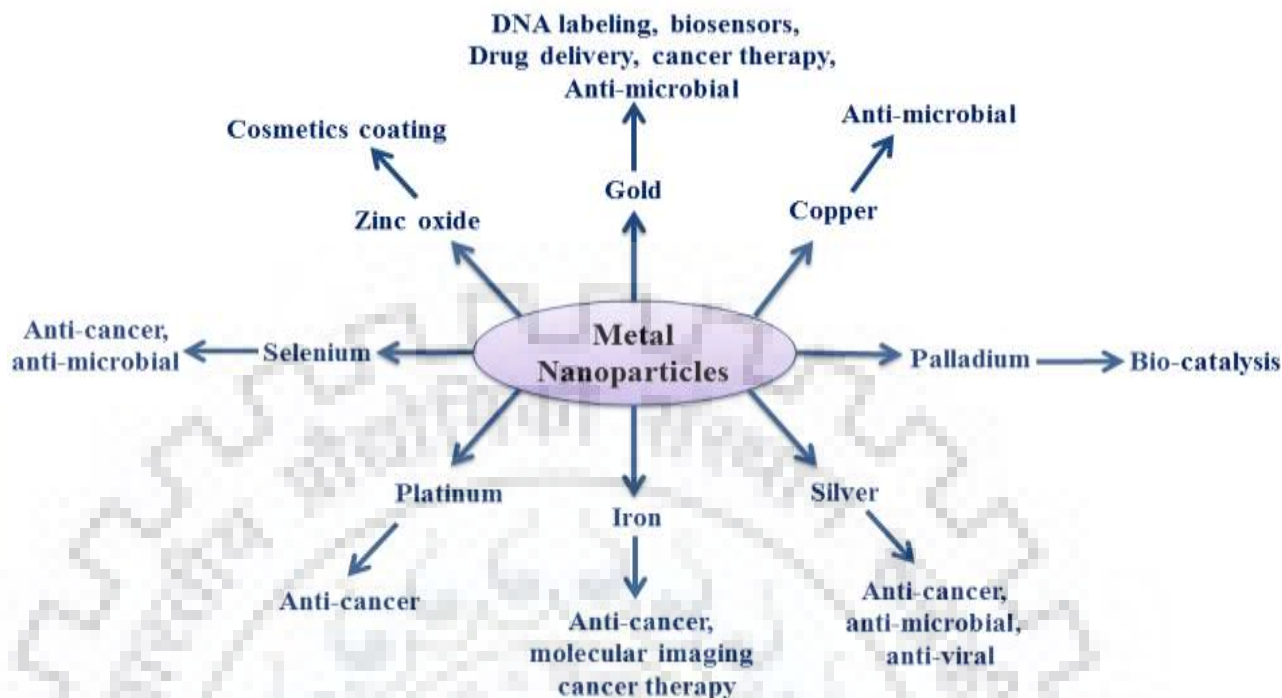
Fig. 1.11 Types of metal nanoparticles and their applications in biotechnology

1.4.4 Conducting polymers

Conducting polymers are a special class of organic polymers, which conduct electricity and conceived as "synthetic metals" by various researchers. In 1997, the first conducting polymer is introduced by H. Shirakawa, A.J.M. Diarmid and A.J. Heeger, who were awarded the noble prize in the year 2000 for their development and discovery of conducting polyacetylene. Conducting polymers are also known as promising materials due to the presence of excellent electronics, optical and magnetic properties, like semiconductors and metals. The unusual electronic properties of conducting polymers, such as high electron affinity, electrical conductivity, biocompatible nature, low ionization potential, and low energy optical transitions are attributed to the π-electron backbone. The conducting polymers have π-conjugation system in the polymer chain (i.e. alternative single and double bonds) and their conductivity is due to the delocalization of π-electron system over the polymeric backbone. The inter-chain and intra-chain interaction, conjugated length, and degree of crystallinity most effectively influence their physical properties. Conducting polymers have various advantages, including low density, chemical diversity, flexibility, corrosion resistance, tunable conductivity, controllable morphology and shape. However, these properties are not completely compatible with semiconductors and metals.

Therefore, properties of conducting polymers have also been enhanced by mixing them with other materials, to overcome their inherent boundaries in terms of conductivity, stability, and solubility. The excellent properties of conducting polymer nanocomposites led to important applications in chemical sensors, bio-sensors, energy storage devices, nanoelectronics devices, catalysis or electro-catalysis, microwave absorption, ER fluid, EMI shielding, and biomedical research (**Fig.1.12**).
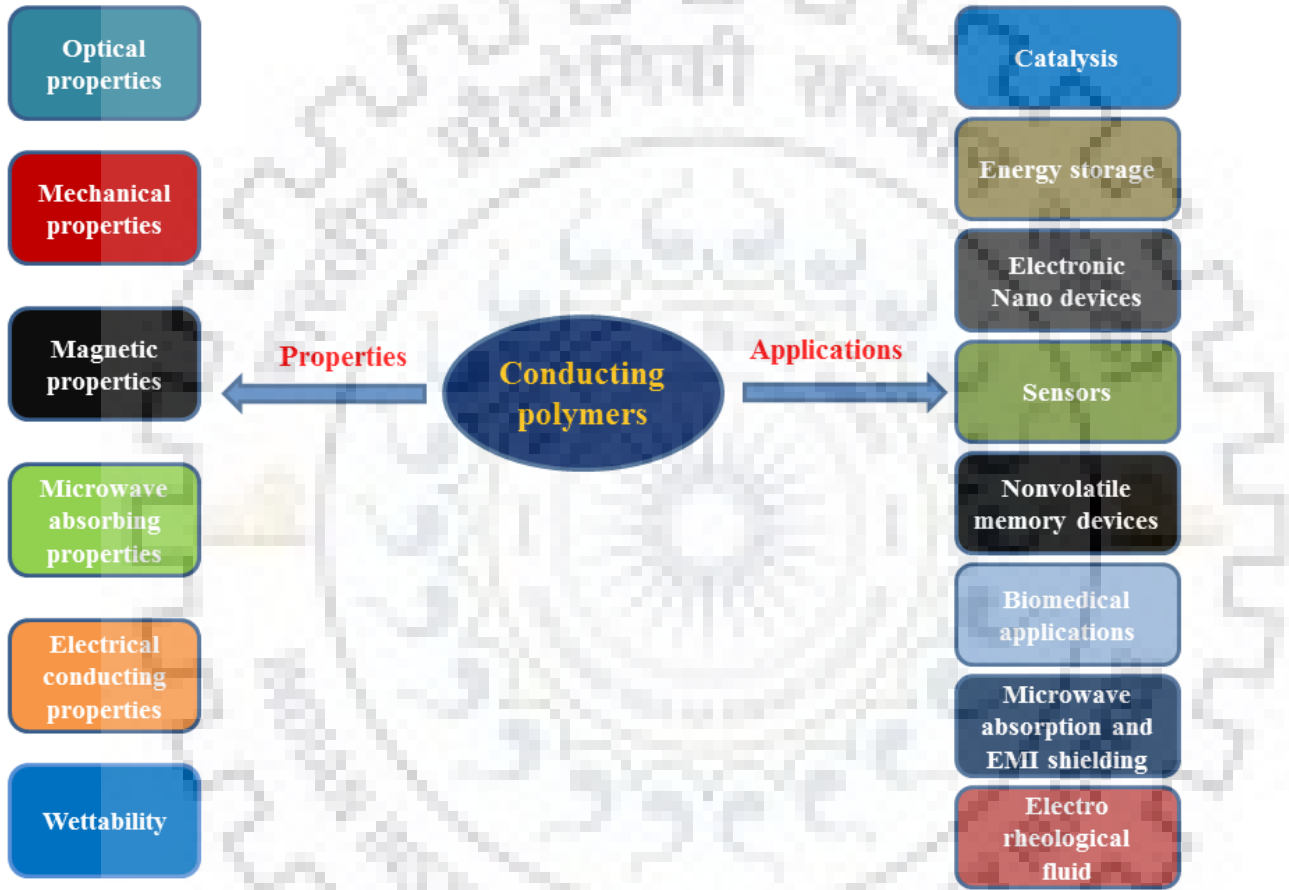
Fig. 1.12 Properties and applications of conducting polymers

In the last few decades, thousands of articles related to conducting polymers including polydiaminonapthalene, polypyrrole, polymelamine, polyindole, polythiophene, poly(4-amino-3-hydroxy-1-naphthalenesulfonic acid, polyfluorine, poly(3,4-ethylenedioxythiophene), polycarbazole and their composites with nanomaterials have appeared and voltammetric sensors based on them have been developed. The structure of some common conducting polymers is presented in **Fig.1.13**. The conducting polymers are generally synthesized by the electrochemical or chemical polymerization method. Chemical polymerization provides different routes to prepare

the polymers, such as condensation or addition polymerization. The electropolymerization and some physical methods, like mechanical stretching and electro-spinning can be applied to synthesize the polymer nanofibers. The electropolymerization is a simple and a single step method for the synthesis of the thin film of conducting polymer on the sensor surface. The electropolymerization of polymer on the surface of sensors is not only simple but can also be used to control the morphology and thickness of the film. Thus, electropolymerization method is generally applied for the fabrication of conducting polymer and polymer nanocomposite based sensors/biosensors [117-125]. In the present dissertation, conducting polymer nanocomposites have been used for the modification of surface of the sensors for the sensitive determination of drugs and biomolecules.
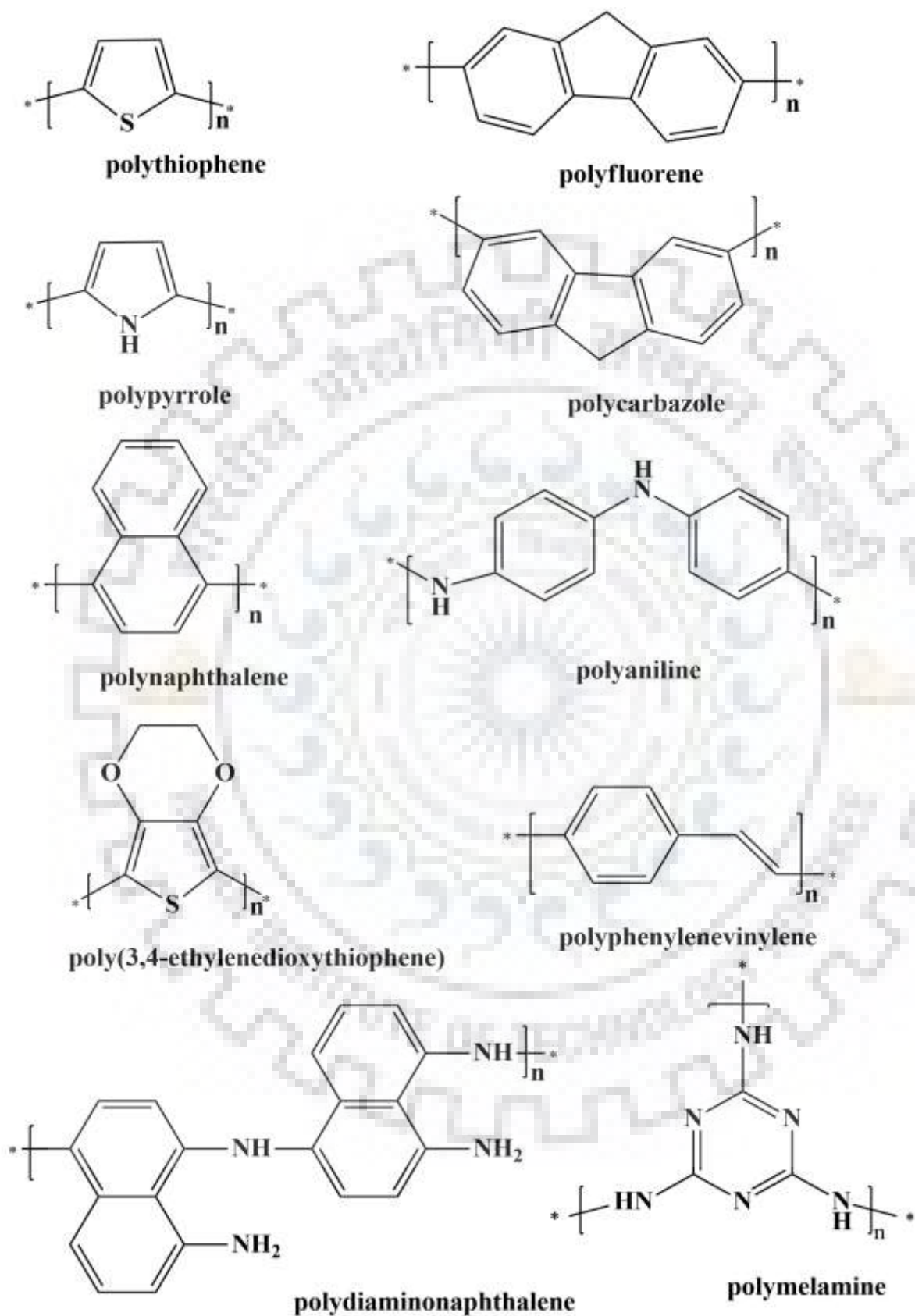
Fig. 1.13: Structure of some commonly used conducting polymers

20

1.4.5 Molecularly imprinted polymer

Molecularly imprinting technique is an approach to generate the artificial recognizing binding sites on a polymer having specific affinity for a substrate. Molecularly imprinted polymer is prepared by polymerizing the suitable monomer with template molecules. The recognized sites are specific and selective for the target analytes. The covalent or non-covalent bonds are formed in between functional groups of polymers and template molecules. Generally, two steps are involved in the synthesis of the molecularly imprinted sensor. In the first step, the formation of complex or polymerization with monomer and template molecules takes place, and in the second step the removal of template molecules, which leave behind the recognized sites of the template molecule in polymer matrix **(Fig.1.14)**. The developed recognized/binding sites are highly selective for the target analytes. The molecularly imprinted polymers are currently gaining high attention, in organic synthesis due to their easy accessibility, stability, high specificity, and low cost.
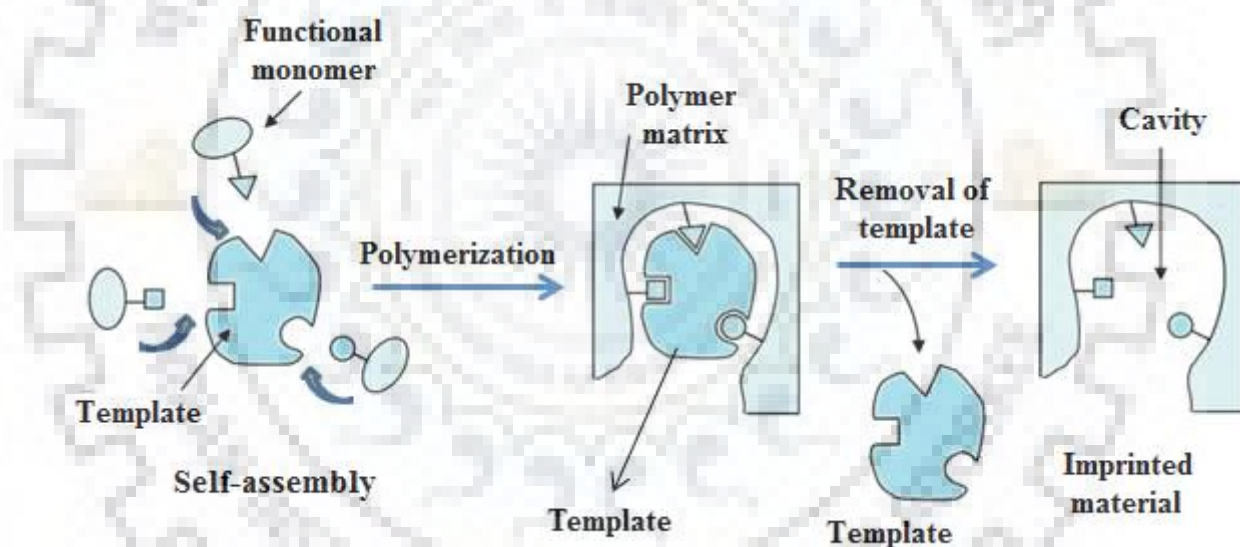
Fig. 1.14: Representation of synthesis of molecularly imprinted polymer

In comparison to natural receptor, molecularly imprinting method has various significant features, like robustness, low cost, long term stability and high binding sites. Recently, the nanocomposite hybrid and core-shell nanoparticles conducting polymers based molecularly imprinted sensors have been developed. The molecularly imprinting technique is promising and versatile and may be used to distinguish both chemical and biological molecules, such as nucleotide derivatives, drugs, amino acids and proteins, food and pollutants [126-129]. The molecularly imprinted methods have also been applied in drug delivery, separation sciences and purification, catalysis, sensor technology,

nanotechnology, biological antibodies and biological receptors etc. The molecularly imprinted electrochemical sensor has several advantages, such as high sensitivity, low detection limit, high selectivity, highly reproducible, ease to renewal and lower cost [130-135]. In recent years, molecularly imprinting technique has also gained interest in the industries. An attempt has been made to prepare molecularly imprinted sensor in the present dissertation for the determination of biomolecules and drugs.

1.5 ANALYTES OF INTEREST

In the present studies, two groups of analytes are selected for the determination. First is the biomolecules and second is drugs. Biomolecules are the fundamental substance of the all living beings and are essential to regulate the biological processes. The small concentration of the biomolecules plays a crucial role in maintaining various biological activities in the human system. The imbalance of their concentration level leads to numerous pathological disorders, physical and mental illness, and degenerative diseases. Thus, the investigation of concentration of biomolecules is highly desirable for clinical and biological applications. The pharmaceutical drugs are prescribed to cure or to prevent the symptoms of disease or medical condition in a controlled way. The overdose of the drugs causes various abnormalities and unwanted side effects in the human body. Thus, selective and highly sensitive methods are required for the detection of biomolecules and drugs in biological fluids and pharmaceutical formulations.

1.5.1 Biomolecules

Neurotransmitters are endogenous brain chemicals, which allow the signal from one neuron to the next neuron through chemical synapses. **Melatonin** is a neurohormone, well known for regulating the sleep-wake cycles (circadian rhythm) and produced by the pineal gland. In physiological conditions, the concentration of melatonin in plasma is low at light and becomes high at dark. The disruption due to the regular exposure of light in the night, the internal body clock restricts the secretion of melatonin in body and causes several sleep-wake related disorders. Melatonin plays an important role in the regulation of mood, immunologic functions, dreaming, sexual maturation and reproduction etc. It also has potent antioxidant effect, immunomodulation effect in cancer therapy and act as an anti-inflammatory agent [136-139]. Thus, melatonin has significant effect in clinical and biological diagnosis and is a subject of an intensive research. Hence, an electrochemical method is applied for the sensitive and selective determination of

melatonin in biological fluids and pharmaceutical formulations by using the polymer nanocomposite modified and unmodified glassy carbon electrodes. It is believed that the results will provide a new platform for biomedical research and quality control of pharmaceutical formulations having melatonin.

Melatonin
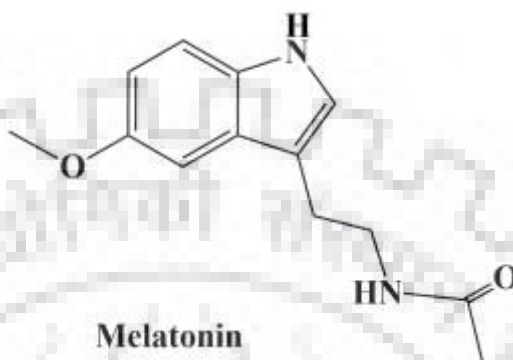
8-Hydroxydeoxyguanosine (8-OHdG) is a product of deoxyguanosine in DNA under the oxidative conditions. 8-OHdG in peripheral blood leukocytes is related to cancer and mutation risk and its level in urine is associated with total DNA damage due to the long term oxidative stress. 8-OHdG has been considered as biomarker for gastric cancer, malignant teratoma, brain tumor, breast cancer, pancreatic cancer, colorectal cancer and lung cancer [140-141]. The quantification and identification of 8-OHdG with accuracy is very important to understand its repair, mechanism of formation and biological significance. Therefor, determination of 8-OHdG contributes to the fast, simple, sensitive and selective method to analyze its concentration in biological samples, like plasma and urine samples. Thus, a polymer nano-composite based molecularly imprinted sensor has been fabricated on pyrolytic graphite surface for the selective and sensitive detection of 8-OHdG. It is believed that the developed sensor will be helpful for the analysis of 8-OHdG in real samples with accuracy.

5-Hydroxy-L-tryptophan is a naturally occurring amino acid and a chemical precursor in the biosynthesis of neurotransmitter, serotonin. 5-Hydroxy-L-tryptophan has been considered as a dietary supplement in various developed countries and used as an appetite suppressant, antidepressant and for the treatment of insomnia [142]. It is reported that on administration of 5-hydroxy-L-tryptophan, the concentration of serotonin increases, which is responsible for protecting the immune system and support health during the first week of the life of a new born baby [143]. It also plays an important role in regulating the physiological processes in the central nervous system. Therefore, voltammetric sensor has been developed for the sensitive determination of 5-

hydroxy-L-tryptophan in biological fluids. The voltammetric sensor was prepared by using palladium nano particles decorated multi-walled carbon nanotubes modified glassy carbon surface for the effective analysis of this analyte. It is believed that the developed method will be helpful in determining 5-hydroxy-L-tryptophan in biological fluids.

Histamine is a neurotransmitter for brain, uterus and spinal cord and is also involved in regulating the physiological functions in the gut. It is involved as a mediator of itching and inflammatory response. Fermented foods and protein rich foods contain high concentration of histamine, like wine, beer, processed meat, cheese and fish. Low concentration of histamine in foodstuffs is not considered a serious health risk, but high level in histamine-rich foods or drugs or alcohol may cause serious allergy-like reactions, headache, urticaria, diarrhea, hypertension and other effects due to the intolerance of histamine. In human body, it acts as an important mediator to regulate the various pathological and physiological processes, such as neurotransmission and several brain functions, to regulate the gastrointestinal and circulatory functions [144-146]. Therefore, a silver nano-particle decorated graphene nano ribbon based sensor is developed for the determination of histamine in red wine and plasma samples.

8-Hydroxydeoxyguanosine

5-Hydroxytryptophan

Histamine
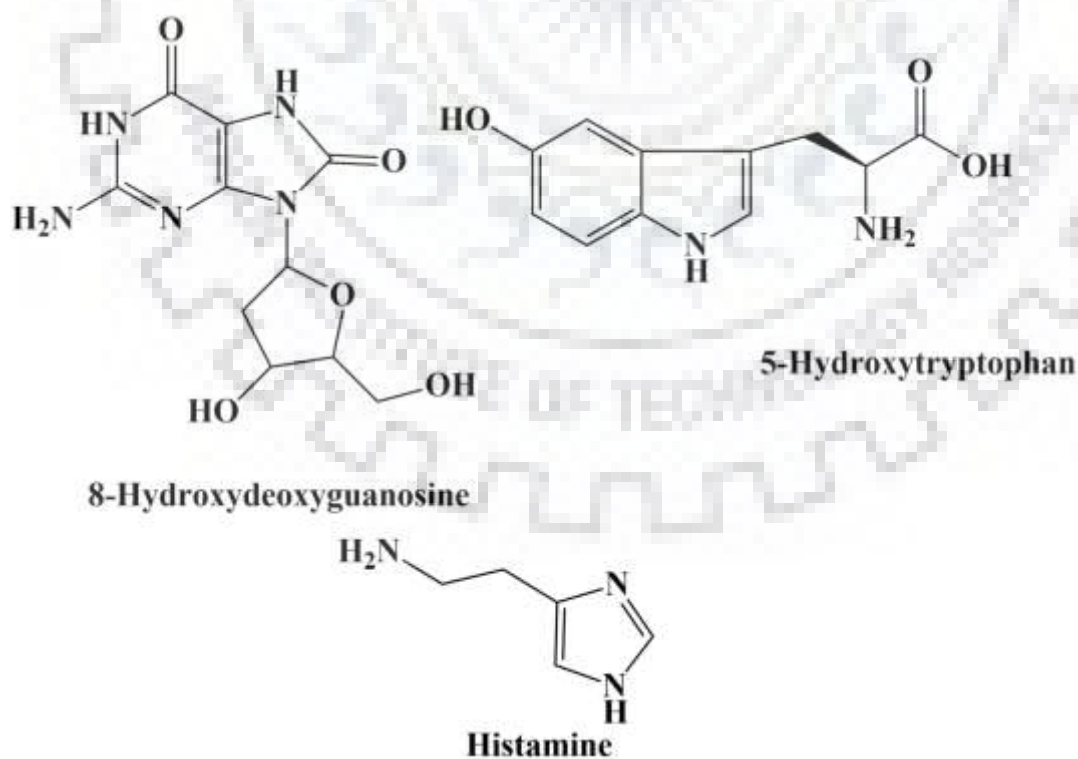
1.5.2 Drugs

Antibiotics are a class of drugs, which revolutionized the medical science in the 20th century. These are most frequently suggested to prevent or treatment of bacterial infections. These drugs may either kill or prevent the growth of bacteria. **Lomefloxacin** (LMF) is a second generation fluoroquinolone antibiotic, used for the treatment of several bacterial infections, including urinary tract infections, bronchitis, sexually transmitted diseases, skin infections and prostatitis. It is also used topically in ear and eye drops to inhibit the bacterial conjunctivitis and treatment of otitis media and externa [147-148]. LMF has broad range antibacterial activity against a larger range of gram positive and gram negative bacteria. Moreover, it is likewise associated with some serious side effects due to overdoses, such as phototoxicity, headache, diarrhea, insomnia and vomiting. Therefore, its various biological effects attracted great attention in developing a method for the determination of LMF in pharmaceutical formulation and biological samples. **Amoxicillin** (AMX) is a third generation aminopencillin family antibiotics and is used for treatment of numerous bacterial infections, such as bronchitis, gonorrhea, pneumonia, nose, ears, throat, skin and urinary tract infections [149-150].

Lomefloxacin

Amoxicillin
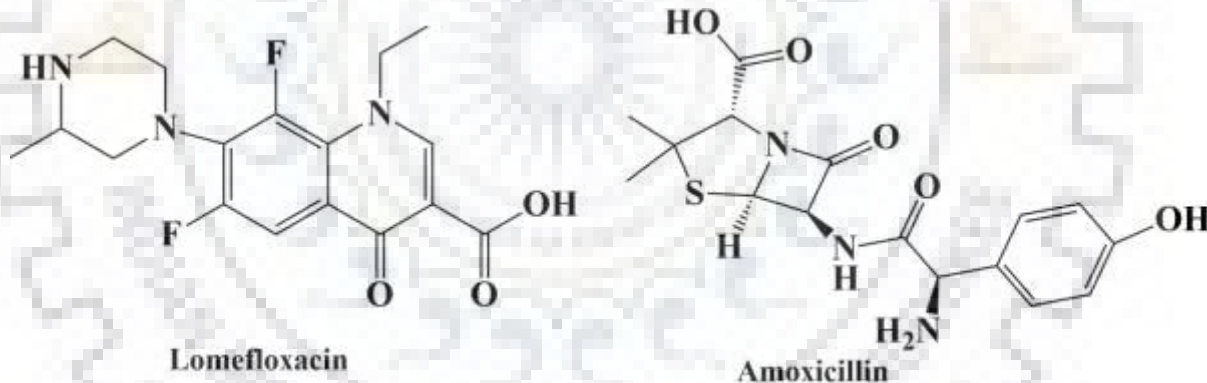
These antibiotics can cause severe allergic reactions including swelling of mouth, face, lips and numbness in the feet or hand etc. The combination of LMF and AMX has been used in many diseases and found effective in patients with chlamydia trachomatis infections. As drug-drug interaction has been found harmful in elderly patients an attempt has been made for the simultaneous determination of LMF and AMX in pharmaceutical formulations and biological samples.

Antihypertensive drugs belong to a class of drugs, which are useful for the treatment of high blood pressure (hypertension). Antihypertensive therapy is used to reduce the complications

of hypertension, like myocardial infarction and stroke [151]. Several drugs are used for the treatment of hypertension and different antihypertensive drugs behave differently to lower the blood pressure. Among most significant antihypertensive drugs are, thiazide diuretics, beta blockers, and calcium channel and angiotensin II receptor antagonists. **Hydrochlorothiazide and Telmisartan** both are antihypertensive drugs and used for treatment of hypertension and to regulate the blood pressure [152]. The main aim of the treatment is to prevent the endpoints of hypertension, like stroke, heart failure and heart attack. Hydrochlorothiazide drug is a diuretic medication and works by causing to make more urine. It decreases extra body fluid in the body, which is caused by the diseases of heart, kidney or liver. It is used alone or in the combination with other medicines to effectively treat the hypertension. The polymer nanocomposite based molecularly imprinted sensor was fabricated for the determination of hydrochlorothiazide in the urine samples and pharmaceutical formulations in the present studies. Telmisartan is an angiotensin II receptor antagonist also widely prescribed to prevent the hypertension. A dose of 20 to 160 mg telmisartan has been found to decrease the systolic and diastolic blood pressure by 10 to 15 mm Hg respectively [151-157].

Telmisartan   Hydrochlorothiazide
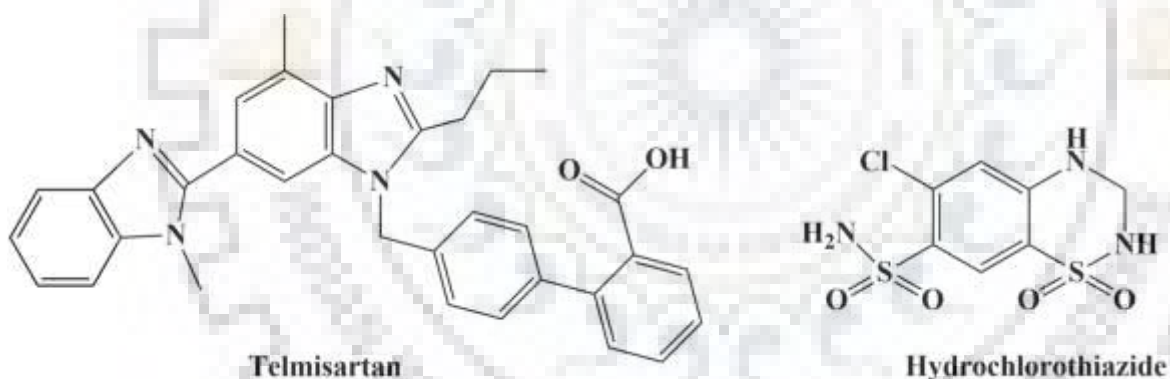
In many cases a combination of telmisartan with hydrochlorothiazide is prescribed (40 mg telmisartan and 12.5 mg hydrochlorothiazide) to control the blood pressure. In the view of the importance of these medicines, a sodium dodecyl sulfate modified pyrolytic graphite sensor has been suggested in the present studies for sensitive and exact determination of telmisartan in real samples, like pharmaceutical formulations and urine samples. The approach to determine the hydrochlorothiazide and telmisartan will be useful in the quality control in the pharmaceutical industries and will also be helpful in their analysis in biological samples.

1.6 THESIS LAYOUT

For clear understanding of the results of present studies the thesis has been divided into five chapters and they are systematically arranged in the dissertation as follows:

Chapter 1: General Introduction.

Chapter 2: Voltammetric sensors for the determination of melatonin.

Chapter 3: Highly sensitive sensors for the determination of biomolecules.
Chapter 4: Au-PdNPs-rGO modified sensor for simultaneous determination of Lomefloxacin and Amoxicillin.

Chapter 5: Sensors for the determination of antihypertensive drugs.

1.7 REFERENCES

[1]   L. Hart, "Electrochemistry and electrochemical engineering", Larsen and Keller Education, Library press, USA (2018).

[2]   A.J. Bard, L.R. Faulkner, "Electrochemical methods fundamentals and applications", 2nd edition, John Wiley & Sons, Inc. (2001).

[3]   J. Wang, "Analytical electrochemistry", 3rd edition, John Wiley & Sons, Inc. (2000).

[4]   C.G. Zoski, "Handbook of electrochemistry", 1st edition, Elsevier (2007).

[5]   G. Dryhurst, "Applications of electrochemistry in studies of the oxidation chemistry of central nervous system indoles", Chem. Rev. 90 (1990) 795–811.

[6]   A.K. Shukla, T.P. Kumar, "Pillars of modern electrochemistry: A brief history", Central Electrochemical Research Institute, Karaikudi, India, (2008), http://knowledge.electrochem. org/encycl/art-p05-pillars-of-ec.htm

[7]   F.A. Settle, "Handbook of instrumental techniques for analytical chemistry", Prentice Hall PTR, Upper Saddle River, NJ (1997).

[8]   K.H. Lubert, K. Kalcher, "History of electroanalytical methods", Electroanalysis 22 (2010) 1937–1946.

[9]   M. Labib, E.H. Sargent, S.O. Kelley, "Electrochemical methods for the analysis of clinically relevant biomolecules", Chem. Rev. 116 (2016) 9001−9090.

[10]   Dhanjai, A. Sinha, X. Lu, L. Wu, D. Tan, Y. Li, J. Chen, R. Jain, "Voltammetric sensing of biomolecules at carbon based electrode interfaces: A review", Trends Anal. Chem. 98 (2018) 174–189.

[11]   Y. Wang, H. Xu, J. Zhang, G. Li, "Electrochemical sensors for clinical analysis", Sensors 8 (2008) 2043–2081.

[12]   R. Monosil, M. Stred'ansky, E. Sturdik, "Application of electrochemical biosensors in clinical diagnosis", J. Clin. Lab. Anal. 26 (2012) 22−34.

[13]   D.W. Kimmel, G. LeBlanc, M.E. Meschievitz, D.E. Cliffel, "Electrochemical sensors and biosensors", Anal Chem. 84(2) (2012) 685–707.

[14]   M.L.Y. Sin, K.E. Mach, P.K. Wong, J.C. Liao, "Advances and challenges in biosensor-based diagnosis of infectious diseases", Expert Rev Mol Diagn. 14(2) (2014) 225–244.

[15]   N. Bhalla, P. Jolly, N. Formisano, P. Estrela, "Introduction to biosensors", Essays Biochem. 60 (2016) 1–8.

[16] O.A. Farghaly, R.S.A. Hameed, A.A.H. Abu-Nawwas, "Analytical application using modern electrochemical techniques, Int. J. Electrochem. Sci. 9 (2014) 3287–3318.

[17] H.A. Laitinen, I.M. Kolthoff, "Voltammetry with stationary microelectrodes of platinum wire", J. Phys. Chem. 45(7) (1941) 1061–1079.

[18] F. Rouessac, A. Rouessac, "Chemical analysis modern instrumentation methods and techniques", 2nd edition, John Wiley & Sons Inc. (1994).

[19] A.M. Bond, "Analysis of simulated reversible cyclic voltammetric responses for a charged redox species in the absence of added electrolyte", J. Phys. Chem. B 102 (1998) 9966–9974.

[20] R.S. Nicholson, "Theory and application of cyclic voltammetry for measurement of electrode reaction kinetics", Anal. Chem. 37(11) (1965) 1351–1355.

[21] N. Elgrishi, K.J. Rountree, B.D. McCarthy, E.S. Rountree, T.T. Eisenhart, J.L. Dempsey, "A practical beginner's guide to cyclic voltammetry", J. Chem. Educ. 95 (2018) 197–206.

[22] P.T. Kissinger, "Cyclic voltammetry", J. Chem. Educ. 60 (1983) 702–706.

[23] A.H. Suroviec, "Introduction to electrochemistry", J. Lab. Chem. Educ. 1(3) (2013) 45–48.

[24] J.A. Turner, J.H. Christie, M. Vukovic, R.A. Osteryoung, "Square wave voltammetry at the dropping mercury electrode: Experimental", Anal. Chem. 49(13) (1997) 1904–1908.

[25] Square wave voltammetry, Anal. Chem. 52(2) (1980) 229–230. (DOI: 10.1021/ac50052a801)

[26] L. Ramaley, M.S. Krause, "Theory of square wave voltammetry", Anal. Chem. 41(11) (1969) 1362–1365.

[27] J.H. Christie, J.A. Turner, R.A. Osteryoung, "Square wave voltammetry at the dropping mercury electrode: Theory", Anal. Chem. 49(13) (1977) 1899–1903.

[28] R.A. Osteryoung, "Square wave voltammetry" Anal. Chem. 57(1) (1985) 101A–110A.

[29] Application Note S-7, Square wave voltammetry, Princeton Applied Research, 801 S. Illinois Avenue, Oak Ridge, TN 37830.

[30] V. Mirceski, R. Gulaboski, "Recent achievements in square-wave voltammetry a review", Maced. J. Chem. Chem. Eng. 33(1) (2014) 1–12.

[31] V. Mirceski, R. Gulaboski, M. Lovric, I. Bogeski, R. Kappl, M. Hoth, "Square-wave voltammetry: A review on the recent progress", Electroanalysis 25(11) (2013) 2411–2422.

[32] J.J. O'Dea, J. Osteryoung, R.A. Osteryoung, "Theory of square wave voltammetry for kinetic systems", Anal. Chem. 53(4) (1981) 895–701.

[33]   F. Scholz, "Electroanalytical Methods", 2nd edition, Verlag Berlin Heidelberg (2010).

[34]   D.A. Skoog, D.M. West, F.J. Holler, S.R. Crouch, "Fundamental of analytical chemistry", 9th edition, Mary Finch, USA (2014).

[35]   R.L. McCreery, "Carbon electrode surface chemistry: Optimization of bioanalytical performance", in: "Voltammetric methods in brain systems", A.A. Boulton, G.B. Baker, R.N. Adams (Eds.,), Humana Press Inc, New Jersey, 27 (1995) 1–26.

[36]   M.C. Granger, M. Witek, J. Xu, J. Wang, M. Hupert, A. Hanks, M.D. Koppang, J.E. Butler, G. Lucazeau, M. Mermoux, J.W. Strojek, G.M. Swain, "Standard electrochemical behavior of high-quality, boron-doped polycrystalline diamond thin-film electrodes", Anal. Chem. 72 (2000) 3793–3804.

[37]   A.E. Fischer, Y. Show, G.M. Swain, "Electrochemical performance of diamond thin-film electrodes from different commercial sources", Anal. Chem. 76 (2004) 2553–2560.

[38]   V. Vyskocil, J. Barek, "Mercury electrodes–possibilities and limitations in environmental electroanalysis", Crit. Rev. Anal. Chem. 39(3) 173–188.

[39]   J. Pappis, S.L. Blum, "Properties of pyrolytic graphite", J. Am. Ceram. Soc. 44(12) (1961) 592–597.

[40]   C.E. Banks, R.G. Compton, "New electrodes for old: from carbon nanotubes to edge plane pyrolytic graphite", Analyst 131 (2006) 15–21.

[41]   C.E. Banks, R.G. Compton, "Edge plane pyrolytic graphite electrodes in electroanalysis: An overview", Anal. Sci. 21 (2005) 1263–1268.

[42]   L.F. Coffin, "Structure-property relations for pyrolytic graphite", J. Am. Ceram. Soc. 47(10) (1964) 473–478.

[43]   R. Bowling, R.T. Packard, R.L. McCreery, "Mechanism of electrochemical activation of carbon electrodes: Role of graphite lattice defectst", Langmuir 5(1989) 683–688.

[44]   G. Zhang, A.S. Cuharuc, A.G. Guell, P.R. Unwin, "Electrochemistry at highly oriented pyrolytic graphite (HOPG): Lower limit for the kinetics of outer-sphere redox processes and general implications for electron transfer models", Phys. Chem. Chem. Phys. 17 (2015) 11827–11838.

[45]   J.P. Randin, E. Yeager, "Differential capacitance study on the edge orientation of pyrolytic graphite and glassy carbon electrodes", J. Electroanal. Chem. Interf. Electrochem. 58 (1975) 313–322.

[46]   P. Gupta, R.N. Goyal, "Polymelamine modified edge plane pyrolytic graphite sensor for the electrochemical assay of serotonin", Talanta 120 (2014) 17–22.

[47]   R.N. Goyal, V.K. Gupta, S. Chatterjee, "Electrochemical investigations of corticosteroid isomers-testosterone and epitestosterone and their simultaneous determination in human urine", Anal. Chim. Acta 657 (2010) 147–153.

[48]   P. Gupta, M. Oyama, R.N. Goyal, "Electrochemical investigations of 8-hydroxydeoxyguanosine and its determination at an edge plane pyrolytic graphite electrode", RSC Adv. 6 (2016) 1722–1728.

[49]   A. Salimi, R.G. Compton, R. Hallaj, "Glucose biosensor prepared by glucose oxidase encapsulated sol-gel and carbon-nanotube-modified basal plane pyrolytic graphite electrode", Anal. Biochem. 333 (2004) 49–56.

[50]   E.V. Ivanova, E. Magner, "Direct electron transfer of haemoglobin and myoglobin in methanol and ethanol at didodecyldimethylammonium bromide modified pyrolytic graphite electrodes", Electrochem. Commun. 7 (2005) 323–327.

[51]   C.E. Banks, R.G. Compton, "Exploring the electrocatalytic sites of carbon nanotubes for NADH detection: an edge plane pyrolytic graphite electrode study", Analyst 130 (2005) 1232–1239.

[52]   S. Yamada, H. Sato, "Some physical properties of glassy carbon", Nature 193 (1962) 261–262.

[53]   W.E. Van der Linden, J.W. Dieker, "Glassy carbon as electrode material in electroanalytical chemistry", Anal. Chim. Acta 119 (1980) 1–24.

[54]   G.N. Kamau, "Surface preparation of glassy carbon electrodes", Anal. Chim. Acta 207 (1988) 1–16.

[55]   F.C. Cowlard, J.C. Lewis, "Vitreous carbon - a new form of carbon", J. Mater. Sci. 2 (1967) 507–512.

[56]   J.C. Bokros, "Carbon biomedical devices", Carbon 15 (1977) 355–371.

[57]   R.J. Rice, N.M. Pontikos, R.L. McCreery, "Quantitative correlations of heterogeneous electron-transfer kinetics with surface properties of glassy carbon electrodes", J. Am. Chem. Soc. 112(12) (1990) 4618–4622.

[58]   R.N. Goyal, V.K. Gupta, A. Sangal, N. Bachheti, "Voltammetric determination of uric acid at a fullerene-C60- modified glassy carbon electrode", Electroanalysis 17(24) (2005) 2217 – 2223.

[59]   A.A. Ensafi, M. Taei, T. Khayamian, A. Arabzadeh, "Highly selective determination of ascorbic acid, dopamine, and uric acid by differential pulse voltammetry using poly(sulfonazo III) modified glassy carbon electrode", Sens. Actuators B-Chem. 147 (2010) 213–221.

[60]   X. Kang, Z. Mai, X. Zou, P. Cai, J. Mo, "A novel glucose biosensor based on immobilization of glucose oxidase in chitosan on a glassy carbon electrode modified with gold–platinum alloy nanoparticles/multiwall carbon nanotubes", Anal. Biochem. 369 (2007) 71–79.

[61]   Rosy, R.N. Goyal, "Determination of 8-Hydroxydeoxyguanosine: A potential biomarker of oxidative stress, using carbon-allotropic nanomaterials modified glassy carbon sensor", Talanta 161 (2016) 735–742.

[62]   R.N. Goyal, V.K. Gupta, M. Oyama, N. Bachheti, "Voltammetric determination of adenosine and guanosine using fullerene-C60-modified glassy carbon electrode", Talanta 71 (2007) 1110–1117.

[63]   L. Saghatforoush, M. Hasanzadeh, N. Shadjou, "Polystyrene–graphene oxide modified glassy carbon electrode as a new class of polymeric nanosensors for electrochemical determinationof histamine", Chin. Chem. Lett. 25 (2014) 655–658.

[64]   R.F. Lane, A.T. Hubbard, "Differential double pulse voltammetry at chemically modified platinum electrodes for in vivo determination of catecholamines", Anal. Chem. 48(9) (1976) 1287–1293.

[65]   F. Pariente, F. Tobalina, G. Moreno, L. Hernandez, E. Lorenzo, H.D. Abruna, "Mechanistic studies of the electrocatalytic oxidation of NADH and ascorbate at glassy carbon electrodes modified with electrodeposited films derived from 3,4-dihydroxybenzaldehyde", Anal. Chem. 69 (1997) 4065–4075.

[66]   W. Ahmed, "Nanomaterials and nanotechnology", One Central Press Ltd, UK (2016).

[67]   C.R. Martin, D.T. Mitchell "Template-synthesized nanomaterials in electrochemistry", in: "Electroanalytical Chemistry: A series of advances", A.J. Brad, I. Rubinstein (Eds.,), Marcel Dekker, Inc., New York, Basel 21 (1998).

[68]   G.M. Whitesides, "Nanoscience, nanotechnology, and chemistry", Small 1(2) (2005) 172–179.

[69]   S. Viswanathan, J. Radecki, "Nanomaterials in electrochemical biosensors for food analysis– A Review", Pol. J. Food Nutr. Sci. 58(2) (2008) 157–164.

[70]   J. Wang, "Nanomaterial-based electrochemical biosensors", Analyst 130 (2005) 421–426.

[71]   G. Aragay, F. Pino, A. Merkoci, "Nanomaterials for sensing and destroying pesticides", Chem. Rev. 112 (2012) 5317–5338.

[72]   F.P. Zamborini, L. Bao, R. Dasari, "Nanoparticles in measurement science", Anal. Chem. 84 (2012) 541−576.

[73]   S. Pandit, D. Dasgupta, N. Dewan, P. Ahmed, "Nanotechnology based biosensors and its application", Pharma Innov. 5(6) (2016) 18–25.

[74]   K.K. Yadav, J.K. Singh, N. Gupta, V. Kumar, "A review of nanobioremediation technologies for environmental cleanup: A novel biological approach", J. Mater. Environ. Sci. 8(2) (2017) 740–757.

[75]   J.E. Pearson, A. Gill, P. Vadgama, "Analytical aspects of biosensors", Ann. Clin. Biochem. 37 (2000) 119–145.

[76]   R.C. Alkire, D.M. Kolb, J. Lipkowski, P.N. Ross, "Chemically modified electrodes", in: advances in electrochemical science and engineering", Wiley-VCH Verlag GmbH & Co. KGaA, 11 (2009).

[77]   P. Malik, V. Katyal, V. Malik, A. Asatkar, G. Inwati, T.K. Mukherjee, "Nanobiosensors: concepts and variations", ISRN Nanomaterials 2013 (2013) 1–9. (http://dx.doi.org/10.1155/2013/327435).

[78]   A.J. Bard, "Chemical modification of electrodes", J. Chem. Educ. 64(4) (1984) 302–304.

[79]   R.W. Murray, "Chemically modified electrodes", Acc. Chem. Res. 13 (1980) 135–141.

[80]   A. Gentile, F. Ruffino, M.G. Grimaldi, "Complex-morphology metal-based nanostructures: Fabrication, characterization, and applications", Nanomaterials 6 (2016) 1–33.

[81]   B.S. Murty, P. Shankar, B. Raj, B B Rath, J. Murday, "Chapter 4 - Applications of Nanomaterials" in: "Textbook of Nanoscience and Nanotechnology", Universities Press, India (2013).

[82]   B.R. Eggins, "Chemical sensors and biosensors", John Wiley & Sons Ltd, UK (2002).

[83]   J.R. Gong, "Graphene-synthesis, characterization, properties and applications", InTech, Croatia (2011).

[84]   M.J. Allen, V.C. Tung, R.B. Kaner, "Honeycomb carbon: A review of graphene", Chem. Rev. 110 (2010) 132–145.

[85]   Y. Zhu, S. Murali, W. Cai, X. Li, J.W. Suk, J.R. Potts, R.S. Ruoff, "Graphene and graphene oxide: Synthesis, properties, and applications", Adv. Mater. 22 (2010) 3906–3924.

[86] W. Choi, I. Lahiri, R. Seelaboyina, Y.S. Kang, "Synthesis of graphene and its applications: A review", Crit. Rev. Solid State Mater. Sci. 35 (2010) 52–71.

[87] C. Riedl, C. Coletti, U. Starke, "Structural and electronic properties of epitaxial graphene on SiC(0 0 0 1): A review of growth, characterization, transfer doping and hydrogen intercalation", J. Phys. D: Appl. Phys. 43 (2010) 1–17.

[88] K.S. Novoselov, A.K. Geim, S.V. Morozov, D. Jiang, Y. Zhang, S.V. Dubonos, I.V. Grigorieva, A.A. Firsov, "Electric field effect in atomically thin carbon films", Science 306 (2004) 666–669.

[89] T. Kuilla, S. Bhadrab, D. Yao, N.H. Kim, S. Bosed, J.H. Lee, "Recent advances in graphene based polymer composites", Prog. Poly. Sci. 35 (2010) 1350–1375.

[90] S. Iijima, T. Ichihashi, "Single-shell carbon nanotubes of 1-nm diameter", Nature 363 (1993) 603–605.

[91] P.J.F. Harris, "Carbon nanotube science synthesis, properties and applications", Cambridge University Press, New York (2009).

[92] S. Suzuki, "Physical and chemical properties of carbon nanotubes", InTech, Croatia (2013).

[93] A. Jorio, G. Dresselhaus, M.S. Dresselhaus, "Carbon nanotubes advanced topics in the synthesis, structure, properties and applications", Springer-Verlag, Berlin Heidelberg, (2008).

[94] R.H. Baughman, A.A. Zakhidov, W.A. de Heer, "Carbon nanotubes the route toward applications", Science 297 (5582) 787–792.

[95] J. Prasek, J. Drbohlavova, J. Chomoucka, J. Hubalek, O. Jasek, V. Adam, R. Kizek, "Methods for carbon nanotubes synthesis review", J. Mater. Chem. 21 (2011) 15872–15884.

[96] M.S. Dresselhaus, G. Dresselhaus, P. Avouris, "Carbon nanotubes synthesis, structure, properties, and applications", Springer-Verlag, Berlin Heidelberg (2001).

[97] S.B. Dutt, M.L. Minus, R. Jain, D. Nepal, S. Kumar, "Chemistry of carbon nanotubes for everyone", J. Chem. Educ. 89 (2012) 221–229.

[98] V.M. Arole1, S.V.Munde, "Fabrication of nanomaterials by top-down and bottom-up approaches-An overview", JAAST:Material Science (Special Issue) 1(1) (2014) 89–93.

[99] T.P. Yadav, R.M. Yadav, D.P. Singh, "Mechanical milling: A top down approach for the synthesis of nanomaterials and nanocomposites", Nanosci. Nanotechnol. 2(3) (2012) 22–48.

[100] Y. Tak, K. Yong, "Controlled growth of well-aligned ZnO nanorod array using a novel solution method", J. Phys. Chem. B 109 (2005) 19263–19269.

[101] M.M. Oliveira, D. Ugarte, D. Zanchet, A.J.G. Zarbin, "Influence of synthetic parameters on the size, structure, and stability of dodecanethiol-stabilized silver nanoparticles", J. Colloid Interface Sci. 292 (2005) 429–435.

[102] L.H. Madkour, "Biogenic–biosynthesis metallic nanoparticles (MNPs) for pharmacological, biomedical and environmental nanobiotechnological applications", Chron. Pharm. Sci. 2(1) (2018) 384–444.

[103] A.G. Skirtach, C. Dejugnat, D. Braun, A.S. Susha, A.L. Rogach, W.J. Parak, H. Mohwald, G.B. Sukhorukov, "The role of metal nanoparticles in remote release of encapsulated materials", Nano Lett. 5(7) (2005) 1371–1377.

[104] R. Tan, D. Wu, S. Xu, Y. Zhu, D. Xiong, L. Wang, P. Yang, P.K. Chu, "Electrocatalytic hydrogen evolution of palladium nanoparticles electrodeposited on nanographene coated macroporous electrically conductive network", Int. J. Hydrog. Energy 43(2018) 2171–2183.

[105] G. Doria, J. Conde, B. Veigas, L. Giestas, C. Almeida, M. Assuncao, J. Rosa, P.V. Baptista, "Noble metal nanoparticles for biosensing applications", Sensors 12(2012) 1657–1687.

[106] V. Leso, I. Iavicoli, "Palladium nanoparticles: Toxicological effects and potential implications for occupational risk assessment", Int. J. Mol. Sci. 19 (2018) 1–19.

[107] S. Thota, D.C. Crans, "Metal nanoparticles: Synthesis and applications in pharmaceutical sciences", Wiley-VCH Verlag GmbH, Germany (2018).

[108] F.P. Zamborini, S.M. Gross, R.W. Murray, "Synthesis, characterization, reactivity, and electrochemistry of palladium monolayer protected clusters", Langmuir 17 (2001) 481–488.

[109] I. Turel, "Special issue: Practical applications of metal complexes", Molecules 20 (2015) 7951–7956.

[110] M. Hazarika, D. Borah, P. Bora, A.R. Silva, P. Das, "Biogenic synthesis of palladium nanoparticles and their applications as catalyst and antimicrobial agent", PLOS ONE 12(9) (2017) e0184936. (https://doi.org/10.1371/journal.pone.0184936).

[111] R.A. Sperling, P.R. Gil, F. Zhang, M. Zanella, W.J. Parak, "Biological applications of gold nanoparticles", Chem. Soc. Rev. 37 (2008) 1896–1908.

[112] J.S. Gullon, A. Rodes, V. Montiel, A. Aldaz, J. Clavilier, "Electrochemical characterisation of platinum-palladium nanoparticles prepared in a water-in-oil microemulsion", J. Electroanal. Chem. 554-555 (2003) 273–284.

[113] S. Tymen, A.C. Scheinost, M.J.L. Rodriguez, C. Friebe, U.S. Schubert, "From cubic palladium to concave core-shell platinum palladium nanoparticles: evolution of the structure and their electrochemical properties", J. Electrochem. Soc. 165(3) (2018) H67–H77.

[114] B. Wiley, Y. Sun, B. Mayers, Y. Xia, "Shape-controlled synthesis of metal nanostructures: The case of silver", Chem. Eur. J. 11 (2005) 454– 463.

[115] T. Teranishi, M. Miyake, "Size control of palladium nanoparticles and their crystal structures", Chem. Mater. 10 (1998) 594–600.

[116] M.R. Ghazanfari, M. Kashefi, S.F. Shams, M.R. Jaafari, "Perspective of Fe_3O_4 nanoparticles role in biomedical applications", Biochem. Res. Int. 2016 (2016) 1–32. (http://dx.doi.org/10.1155/2016/7840161).

[117] T.H. Le, Y. Kim, H. Yoon, "Electrical and electrochemical properties of conducting polymers", Polymers 9 (2017) 1–32.

[118] G. Kaur, R. Adhikari, P. Cass, M. Bown, P. Gunatillake, "Electrically conductive polymers and composites for biomedical applications", RSC Adv. 5 (2015) 37553–37567.

[119] M.M. Barsan, M.E. Ghica, C.M.A. Brett, "Electrochemical sensors and biosensors based on redox polymer/carbon nanotube modified electrodes: A review", Anal. Chim. Acta 881 (2015) 1–23.

[120] T.K. Das, S. Prusty, "Review on conducting polymers and their applications", Polym. Plast. Technol. Eng. 51 (2012) 1487–1500.

[121] M. Gerard, A. Chaubey, B.D. Malhotra, "Application of conducting polymers to biosensors", Biosens. Bioelectron. 17 (2002) 345–359.

[122] Rajesh, T. Ahuja, D. Kumar, "Recent progress in the development of nano-structured conducting polymers/nanocomposites for sensor applications", Sens. Actuators B-Chem. 136 (2009) 275–286.

[123] J.M. Moon, N. Thapliyal, K.K. Hussain, R.N. Goyal, Y.B. Shim, "Conducting polymer-based electrochemical biosensors for neurotransmitters: A review", Biosens. Bioelectron. 102 (2018) 540–552.

[124] M. Naseri, L. Fotouhi, A. Ehsani, "Recent progress in the development of conducting polymer-based nanocomposites for electrochemical biosensors applications: A mini-review", Chem. Rec. 18 (2018) 599–618.

[125] S. Baskar, C.W. Liao, J.L. Chang, J.M. Zen, "Electrochemical synthesis of electroactive poly(melamine) with mechanistic explanation and its applicability to functionalize carbon surface to prepare nanotube–nanoparticles hybrid", Electrochim. Acta 88 (2013) 1–5.

[126] B. Sellergren, C.J. Allender, "Molecularly imprinted polymers: A bridge to advanced drug delivery", Adv. Drug Deliv. Rev. 57 (2005) 1733–1741.

[127] J. Liu, T. Qian, M. Wang, X. Liu, N. Xu, Y. You, C. Yan, "Molecularly imprinted polymer enables high-efficiency recognition and trapping lithium polysulfides for stable lithium sulfur battery", Nano Lett. 17 (2017) 5064–5070.

[128] K. Haupt, K. Mosbach, "Molecularly imprinted polymers and their use in biomimetic sensors", Chem. Rev. 100 (2000) 2495–2504.

[129] M.J. Whitcombe, N. Kirsch, I.A. Nicholls, "Molecular imprinting science and technology: a survey of the literature for the years 2004–2011", J. Mol. Recognit. 27 (2014) 297–401.

[130] G. Vasapollo, R.D. Sole, L. Mergola, M.R. Lazzoi, A. Scardino, S. Scorrano, G. Mele, "Molecularly imprinted polymers: Present and future prospective", Int. J. Mol. Sci. 12 (2011) 5908–5945.

[131] Y. Saylan, F. Yilmaz, E. Ozgur, A. Derazshamshir, H. Yavuz, A. Denizli, "Molecular imprinting of macromolecules for sensor applications", Sensors 17 (2017) 2–30.

[132] A. Verma, G.M. Murray, "A path to soluble molecularly imprinted polymers", J. Funct. Biomater. 3 (2012) 1–22.

[133] H. Liu, T. Ni, L. Mu, D. Zhang, J. Wang, S. Wang, B. Sun, "Sensitive detection of pyrraline with a molecularly imprinted sensor based on metal-organic frameworks and quantum dots", Sens. Actuators B-Chem. 256 (2018) 1038–1044.

[134] A.Z. Galvez, C.C.M. Matinez, C. Parolo, J. Pons, A. Merkoci, "Magnetic nanoparticle-molecular imprinted polymer: A new impedimetric sensor for tributyltin detection", Electrochem. Commun. 82 (2017) 6–11.

[135] J. Pan, W. Chen, Y. Ma, G. Pan, "Molecularly imprinted polymers as receptor mimics for selective cell recognition", Chem. Soc. Rev. 47 (2018) 5574–5587.
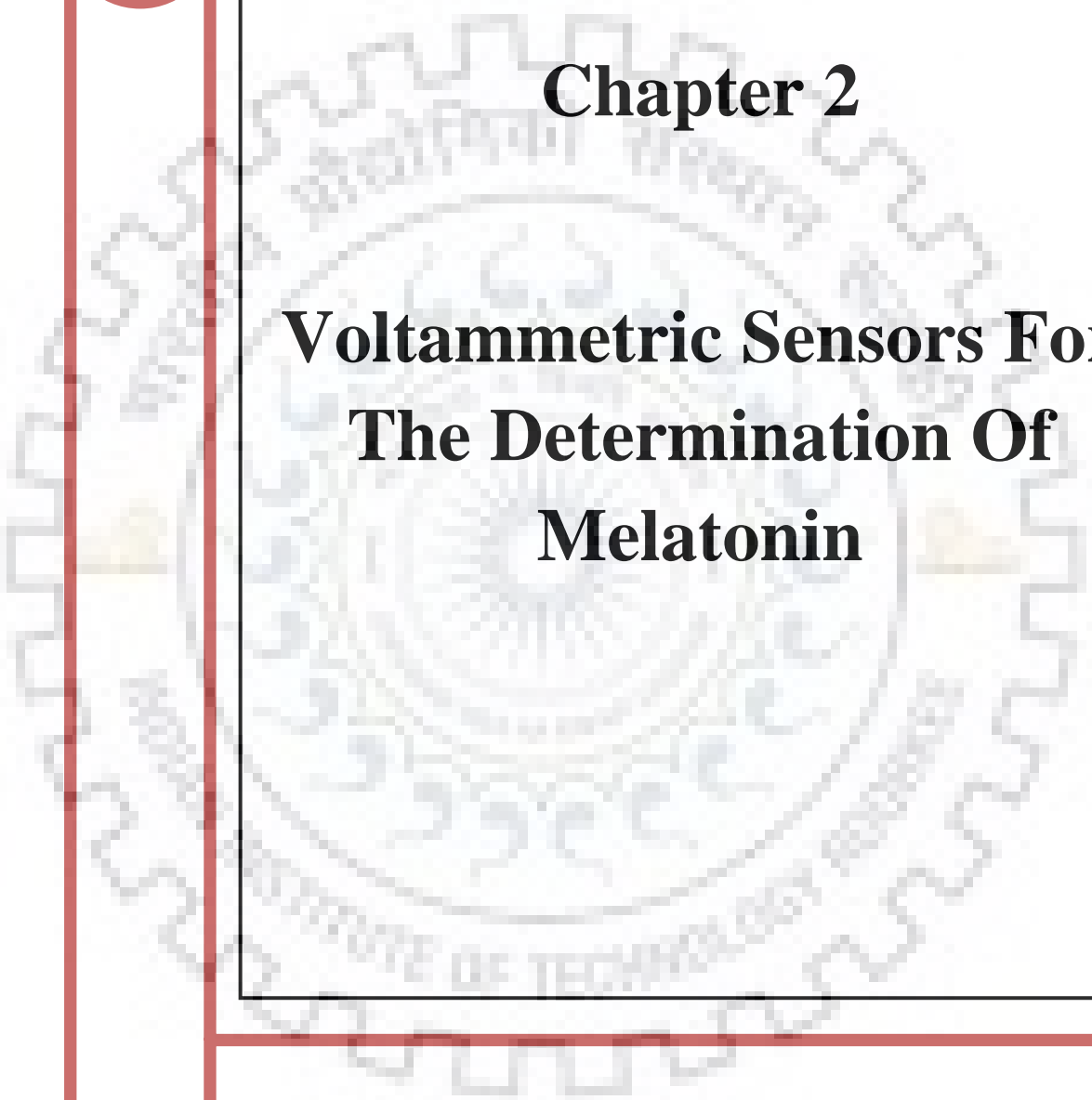
[136] P.P. Posadzki, R. Bajpai, B.M. Kyaw, N.J. Roberts, A. Brzezinski, G.I. Christopoulos, U. Divakar, S. Bajpai, M. Soljak, G. Dunleavy, K. Jarbrink, E.E.K. Nang, C.K. Soh, J. Car, "Melatonin and health: An umbrella review of health outcomes and biological mechanisms of action", BMC Med. 16 (2018) 2–18.

[137] I.S. Abdelgadir, M.A. Gordon, A.K. Akobeng, "Melatonin for the management of sleep problems in children with neurodevelopmental disorders: A systematic review and meta-analysis", Arch Dis Child 103(12) (2018) 1–8. (http://dx.doi.org/10.1136/archdischild-2017-314181)

[138] S.M. Nabavi, S.F. Nabavi, A. Sureda, J. Xiao, A.R. Dehpour, S. Shirooie, A.S. Silva, A. Baldi, H. Khan, M. Daglia, "Anti-inflammatory effects of Melatonin: A mechanistic review", Crit. Rev. Food Sci. Nutr. (2018). (https://doi.org/10.1080/10408398.2018.1487927)

[139] Z. Xin, S. Jiang, P. Jiang, X. Yan, C. Fan, S. Di, G. Wu, Y. Yang, R.J. Reiter, G. Ji, "Melatonin as a treatment for gastrointestinal cancer: A review", J. Pineal Res. 58 (2015) 375–387.

[140] D.J. Weiss, C.E. Lunte, "Detection of a urinary biomaker for oxidative DNA damage 8-hydroxydeoxyguanosine by capillary electrophoresis with electrochemical detection", Electrophoresis 21(10) (2000) 2080–2085.

[141] D. Wu, B. Liu, J. Yin, T. Xu, S. Zhao, Q. Xu, X. Chen, H. Wang, "Detection of 8-hydroxydeoxyguanosine (8-OHdG) as a biomarker of oxidative damage in peripheral leukocyte DNA by UHPLC–MS/MS", J. Chromatogr. B 1064 (2017) 1–6.

[142] L.E.H. Castellano, R. Ozcelik, L.L. Hernandez, R.M. Bruckmaier, "Short communication: Supplementation of colostrum and milk with 5-hydroxy-L-tryptophan affects immune factors but not growth performance in newborn calves", J. Dairy Sci. 101 (2018) 794–800.

[143] X. Wang, B. Yang, A. Zhang, H. Sun, "Chapter 20 - Metabolic profiling and biomarkers analysis of insomnia, and the intervention effects of suanzaoren decoction, and its related active ingredients", in: "Chinmedomics: The integration of serum pharmacochemistry and metabolomics to elucidate the scientific value of traditional chinese medicine", X. Wang, A. Zhang, H. Sun (Eds.), Chinmedomics, Academic Press, (2015) 305–325.

[144] Z.S. Stojanovic, E. Mehmeti, K. Kalcher, V. Guzsvany, D.M. Stankovic, "SWCNT-modified carbon paste electrode as an electrochemical sensor for histamine determination in alcoholic beverages", Food Anal. Method 9 (2016) 2701–2710.

[145] L. Maintz, N. Novak, "Histamine and histamine intolerance", Am. J. Clin. Nutr. 85 (2007) 1185–1196.

[146] H.C. Chen, Y.R. Huang, H.H. Hsu, C.S. Lin, W.C. Chen, C.M. Lin, Y.H. Tsai, "Determination of histamine and biogenic amines in fish cubes (Tetrapturus angustirostris) implicated in a food-borne poisoning", Food Control 21 (2010) 13–18.

[147] R.I. Al-Wabli, "Lomefloxacin", in: "Profiles of drug substances, excipients, and related methodology", H.G. Brittain (Ed.), Elsevier 42 (2017) 193–240.

[148] M. Gao, L. Li, S. Lu, Q. Liu, H. He, "Silver nanoparticles for the visual detection of lomefloxacin in the presence of cysteine", Spectrochim. Acta A Mol. Biomol. Spectrosc. 205 (2018) 72–78.

[149] M.M.A. Galeil, H.S. El-Desoky, E.M. Ghoneim, A. Matsuda, "Application of montmorillonite clay and mesoporous carbon as modifiers to carbon paste electrode for determination of amoxicillin drug", J. Electrochem. Soc. 164 (14) (2017) H1003–H1012.

[150] P.B. Deroco, R.C.R. Filho, O.F. Filho, "A new and simple method for the simultaneous determination of amoxicillin and nimesulide using carbon black within a dihexadecylphosphate film as electrochemical sensor", Talanta 179 (2018) 115–123.

[151] S. Laurent, "Antihypertensive drugs", Pharmacol. Res. 124 (2017) 116–125.

[152] M.P Maillard, M. Burnier, "Is the fixed-dose combination of telmisartan and hydrochlorothiazide a good approach to treat hypertension?", Vasc. Health Risk Manag. 3(3) (2007) 265–278.

[153] P. Gosse, "A review of telmisartan in the treatment of hypertension: blood pressure control in the early morning hours", Vasc. Health Risk Manag. 2(3) (2006) 195–201.

[154] Y. Lacourciere, "A New Fixed-dose Combination for Added Blood Pressure Control: Telmisartan plus Hydrochlorothiazide", J. Int. Med. Res. 30 (2002) 366–379.

[155] M. Law, N. Wald, J. Morris, "Lowering blood pressure to prevent myocardial infarction and stroke: A new preventive strategy", Health Technol Assess 7(31) (2003) 1–94.

[156] O.V. Ivanova, O.A. Fomicheva, L.M. Sergakova, N.A. Chernova, A.N. Rogoza, Y.A. Karpov, "Angiotensin II receptor blocker telmisartan: Effect on blood pressure profile and left ventricular hypertrophy in patients with arterial hypertension", J. Int. Med. Res. 33 (Suppl 1) (2005) 21A–29A.

[157] M. Sharpe, B. Jarvis, K.L. Goa, "Telmisartan: a review of its use in hypertension", Drugs 61 (2001) 1501–1529.

Chapter 2

Voltammetric Sensors For The Determination Of Melatonin

2.1 INTRODUCTION

Melatonin (MEL) is a methoxyindole hormone secreted by the mammalian pineal gland present in the brain [1], which plays a crucial role in regulating the sleep-wake cycle and biological circadian rhythm [2]. In biological systems, it is synthesized by tryptophan via serotonin following a pathway catalyzed by two enzymes named arylalkylamine N-acetyltransferase and acetylserotonin-O-methyltransferase [3-5]. Besides regulating the biological clock, MEL also acts as a potent antioxidant and anti-inflammatory agent due to its propensity to scavenge free radicals, specifically radical oxygen and nitrogen species [1,6-9]. The pineal hormone, MEL, is associated with mood regulation, sleep efficiency, dreaming, immunologic functions, retinal physiology, seasonal affective disorder, sexual maturation, reproduction [6,10-11] and is an effective antioxidant and anti-inflammatory agent. MEL is known to be a very effective free radical scavenger, which has the ability to protect tissues from the reactive oxygen and nitrogen species [12-13]. In medical sciences, MEL has been used as immunomodulater in cancer therapy, septic shock, Ebola viral infection and tumor growth inhibition. [14-16]. Large number of studies in the field of medical sciences have addressed the direct relation of MEL concentration with many physiological disorders, like metabolic diseases, mental illness, insomnia, stress related disorders, and neuroprotective action of MEL in some cases of neurodegenerative diseases like Alzheimer and Parkinson's disease has also been observed [9, 17-19]. Thus, its quantification in human fluids and tissues calls for an intensive research, which can lead to early diagnosis of many physiological and behavioural problems. In view of such an importance of MEL, it was considered desirable to prepare sensitive sensors for its determination. Two approaches have been used in the present investigation for the determination of MEL, the first was unmodified glassy carbon surface and second was glassy carbon surface modified with polymer nanocomposite.

Last few years have seen use of palladium nanoparticle (PdNPs) for enhancing electrochemical reactions as they have effective catalytic activity and unique mechanical and electrical properties [20-21]. Moreover, palladium can interact and bind strongly to graphene due to more interaction state and transmission channels developed between them [21-22]. Thus, it is thought that the PdNPs can readily grow on the surface of graphene due to the presence of oxygenated functional group on its surface and can enhance the catalytic activity of the reduced graphene oxide based polymer nanocomposite. Hence, the electrodeposition of PdNPs on the surface of glassy carbon electrode (GCE) has been attempted.

Graphene is a two dimensional sp^2-hybrid carbon material with a honeycomb lattice like structure [23-24]. It has some outstanding properties, like high intrinsic mobility [25-26], tunable band gap [27], high electrical conductivity and good biocompatibility [28], which renders it a potential to attract the interest of scientists working in the various fields of applications including energy storage and supercapacitor [29], sensor and biosensor [30], nanocomposite [31], electrical and optical devices [32], single molecule gas detection [33] and so on. At present, several methods have been developed to prepare graphene, such as chemical vapor deposition [34], epitaxial growth [35], chemical reduction of graphene oxide and mechanical exfoliation [20, 36]. Among these methods, chemical reduction method is the most frequently used method for the reduction of GO to prepare reduced graphene oxide (rGO). But since, the chemical reduction of GO to rGO requires a number of highly toxic chemicals, like hydrazine or hydroquinone this method has to be replaced by some other simple method of equal productivity [36]. Thus, an alternative, environmental friendly and green method has been used now a days for the synthesis of reduced graphene oxide (rGO) by carrying out the electrochemical reduction of graphene oxide (GO). This method provides a fast, clean and inexpensive tool to carry out the reduction of GO [21] without involving any extra hazardous chemicals. But, electrochemically reduced graphene oxide (ErGO) has the tendency to aggregate or reconvert into the graphite, thus, to avoid the agglomeration of ErGO, conducting polymer 4-amino-3-hydroxy-1-naphthalenesulfonic acid (AHNSA) has been used to prevent the aggregation and to stabilize the graphene like film. The covalent binding of polymer to graphene and the concept of synergy further provides the reason to develop a polymer nanocomposite by combining these materials [37].

The screening of the literature revealed that for the determination of MEL, various analytical methods have been developed, such as gas chromatography- mass spectroscopy (GC-MS) [38], HPLC (high pressure liquid chromatography) [39-41], liquid chromatography-mass spectrometry (LC-MS) [42-44], mass spectrometry (MS) [45], colorimetry [46-47], radioimmunoassay (RIA) [48-51], chemiluminescence [52] etc. However, most of these reported techniques are expensive sophisticated processes and usually require time consuming sample processing prior to the analysis. While, on the other hand electrochemical and voltammetric methods are suitable and less expensive than conventional analytical methods. Voltammetric technique has high sensitivity, selectivity and reproducibility with fast response and low cost [53] and thus proved to be an emerging choice for the scientists working in the analytical field. Various types of electrodes with different types of surface modifications have been used as a working

electrode in the electrochemical analysis of MEL including boron-doped diamond (BDD) electrode [54], carbon paste electrodes [55], carbon disc electrode [56], manganese hexacyanoferrate (MnHCF) mixed-valent poly(3,4-Ethylenedioxythiophene) (PEDOT) hybrid film modified glassy carbon electrode [57], BT-drug membrane sensors [58], glassy carbon electrode [59], RGO/RuO$_2$/GCE [60] etc. However, the previously reported sensors have a limitation of small linear concentration range, higher limits of detection, complex modifications and in some cases high cost like BDD electrode. Moreover metabolites like ascorbic acid and uric acid, which are usually present in high concentration in biological fluids, interfere in the selective determination of MEL. Previously, our research group has also fabticated a molecular imprinted sensor for assaying MEL [61], but the low stability, complex multistep modification, and time consuming incubation process involved in the sensing inspired us to develop a more practical sensor by overcoming the drawbacks of molecular imprinted sensor. Thus, the purpose of the present research is to fabricate and characterize a sensor to carry out a selective and sensitive determination of MEL in biological and pharmaceutical samples. A single step approach for the fabrication of PdNPs, ErGO and AHNSA polymer nanocomposite modified GCE has been presented in this chapter and the application of the surface modified sensor has been tested in the quantification of MEL in complex matrix, like human urine as well as in the commercially available pharmaceutical formulations.

2.2 EXPERIMENTAL

2.2.1 Reagents and materials

Melatonin (MEL), 4-amino-3-hydroxy-1-naphthalenesulfonic acid (AHNSA), graphene oxide, hypoxanthine (HX), uric acid (UA), ascorbic acid (AA), palladium chloride anhydrous (PdCl$_2$), hydrochloric acid, and nitric acid were purchased from Sigma-Aldrich Chemical Co (USA). Phosphate buffers (μ = 1.0 M) in the pH range of 2.4–10.0 were prepared by using analytical grade Na$_2$HPO$_4$, NaH$_2$PO$_4$ and NaOH, according to the method described by Christian and Purdy [62]. All the stock solutions used throughout the experiment were prepared using double distilled water.

2.2.2 Instrumentation

Electrochemical deposition and other qualitative and quantitative studies were carried out using a Bio-analytical system (BAS, West Lafayette, USA) CV-50 voltammetric analyzer. The experiment was performed by using a three electrode system in a glass cell consisting of Ag/AgCl

(3M NaCl) as reference, platinum wire as the auxiliary and glassy carbon electrode (GCE) as the working electrode. Phosphate buffer has been used as the supporting electrolyte and the pH of the solutions was measured by using a digital pH meter (Eutech, model pH 700). The surface morphology and the composition of the fabricated sensor were investigated using Field Emission Scanning Electron Microscopy (FE-SEM; Zeiss ultra plus 55) and Electron Energy Dispersive X-ray spectroscopy (EDX). The Electrochemical Impedance Spectroscopy (EIS) was performed to calculate the charge transfer resistance by using galvanostat VERSA STAT 3 (PAR, USA).

2.2.3 Voltammetric procedure and sample preparation

The electrochemical study of MEL oxidation was carried out using cyclic and square wave voltammetry. The stock solution was prepared by dissolving required amount of MEL in double distilled water. The required stock solution was added in a glass cell already containing 2 mL of phosphate buffer (pH 7.2) as supporting electrolyte, and the total volume was made 4 mL using double distilled water. After each voltammogram, the surface of unmodified GCE was cleaned and regenerated by rubbing it gently over slurry of zinc oxide (ZnO) and alumina on micro cloth pad. The voltammograms were recorded under optimized parameters. The optimized conditions for square wave voltammetric parameters were: initial potential (E_i): 100 mV, final potential (E_f): 1200 mV, potential step: 4 mV, square wave amplitude: 25 mV, square wave frequency (f): 15 Hz and the optimized parameters for cyclic voltammetry were associated as: initial potential (E_i): -400 mV, switching potential (E): 1600 mV, final potential (E_f): -400 mV and scan rate 100 mV/s. The surface of the modified sensor was cleaned each time by applying a potential of -800 mV for 300 sec in the blank solution.

2.2.4 Synthesis of GO

GO was synthesized according to the modified Hummer's method as described earlier [20]. Briefly, GO was synthesized using graphite powder and $KMnO_4$ in the presence of H_3PO_4 and H_2SO_4 (20:180) mixture. The mixture was then heated for 12 h at 50ºC, which finally resulted in a brown colored suspension that becomes yellow on the addition of double distilled water followed by H_2O_2 (30%). The final suspension thus obtained was centrifuged and the sediment was washed several times with water, HCl and ethanol to get GO.

2.2.5 Fabrication of modified sensors

For the modification of the bare glassy carbon electrode (GCE), its surface was firstly polished with the slurry of alumina and ZnO on a micro cloth pad. To carry out the electropolymerization of AHNSA directly on the surface of GCE, 15 cyclic voltammetry scans in 2 mM AHNSA solution (prepared in 0.1M HNO_3) were recorded in the potential window -1000 to 2000 mV. After the completion of 15 scans (optimized), the polymer modified GCE was rinsed with double distilled water and stabilized by recording voltammograms in 0.5 M H_2SO_4 between −1.0 and +1.0 V at 100 mVs^{-1} till the overlapping voltammograms were not obtained [63]. Final sensing surface thus obtained was named as AHNSA/GCE and was characterized using FE-SEM.

To fabricate and electrodeposit the ErGO, AHNSA composite on GCE (ErGO:AHNSA/GCE), 2 mg of GO was first suspended in 4 mL phosphate buffer solution (pH 7.2) and was sonicated for 30 min to ensure uniform dispersion. 2 mL of the above prepared suspension was then taken along with 2 mL of 2 mM AHNSA in an electrochemical glass cell and potential in the range of -1000 to 2000 mV was applied using cyclic voltammetry for 19 continuous runs (optimized). Final sensing surface so obtained was washed with double distilled water, dried and characterized using FE-SEM

To modify the GCE with PdNPs and AHNSA, 1 mM Palladium chloride solution was prepared by dissolving the required quantity of $PdCl_2$ in 10% hydrochloric acid. The electrochemical deposition on the precleaned GCE surface was performed in a 1:1 mixture of the above prepared $PdCl_2$ (1mM) and AHNSA (2mM) solutions, by transversing the potential in the range of -400 to 1600 mV at a sweep rate of 100 mV s^{-1} for 15 cycles (optimized). The resulting surface PdNPs:AHNSA/GCE was characterized using FE-SEM after rinsing with double distilled water.

The single step fabrication of the polymer nanocomposite of PdNPs, AHNSA and GO was also attempted directly on the surface of GCE. For the synthesis of polymer nano composite required amount of $PdCl_2$ (1 mM) was dissolved in 4 mL of GO suspension. The solution so formed was further sonicated for 25 min. The 1:1 mixture of the above prepared $PdCl_2$:GO suspension and 2 mM AHNSA solution was taken in a glass cell in order to carry out the electrochemical reduction of GO, electropolymerization of AHNSA and electrodeposition of the polymer nanocomposite simultaneously in a single step using cyclic voltammetry. The single step fabrication is achieved by applying the potential range -400 to 1600 mV at the sweep rate 100 mV/s for 5–25 scans. The best results were obtained when 19 continuous scans were carried out,

(greater number of scans leaded to the aggregation, whereas less number of scans resulted in less uniform deposition) hence, 19 scans have been used as the modification protocol throughout the experiment. Obtained surface modified sensor was then rinsed with double distilled water and permitted to dry at room temperature. The characterization of the surface was then carried out by using Voltammetry, FE-SEM, EDX and EIS.

2.2.6 Pharmaceutical tablets analysis

To investigate pharmaceutical samples, tablets (3 mg) of MEL were purchased from the local market of Roorkee, India. The tablets were emptied in a clean mortar for powdering and the required amount of powder was weighed and transferred to the 10 ml volumetric flask to prepare 1mM stock solution.

2.2.7 Urine sample analysis

Urine samples from two healthy volunteers (Male, Age 26 and Female, age 23) were collected from the Institute hospital of IIT Roorkee and filtered using whatman 42 filter paper. The filtered solution was then diluted twice with pH 7.2 phosphate buffer and spiked with 1 mM MEL solution. This solution was then treated as stock solution and subsequent dilution was done in order to prepare the required test solutions having concentration ranging between the working range.

The present chapter presents results for the determination of MEL using unmodified and modified surface of glassy carbon. For the sake of clarity, the chapter is divided into two sections:

Section 1: deals with the determination of melatonin; a neurotransmitter, using unmodified glassy carbon electrode;

Section 2: deals with the electrochemical determination of melatonin by using polymer nanocomposite (AHNSA:PdNPs:ErGO) modified glassy carbon sensor.

SECTION 1: DETERMINATION OF MELATONIN USING UNMODIFIED GLASSY CARBON ELECTRODE

2.3. RESULTS AND DISCUSSION

2.3.1 Cyclic Voltammetry

Initial studies for MEL analysis were carried out using cyclic voltammetry as CV has been widely used to investigate the electrochemical behavior of electro-active species, and to study the

kinetics and nature of the electron transfer processes involved in the electrochemical reactions. Cyclic voltammogram of 200 µM MEL solution was recorded at a glassy carbon electrode (GCE) by scanning the potential from 200 to 1400 mV at a sweep rate of 100 mVs^{-1}. **Fig 2.1** demonstrates the cyclic voltammograms in presence and absence of 100 µM MEL. An intense oxidation peak was observed at 770 mV, whereas no reduction peak was observed in the reverse scan indicating the irreversible nature of MEL.
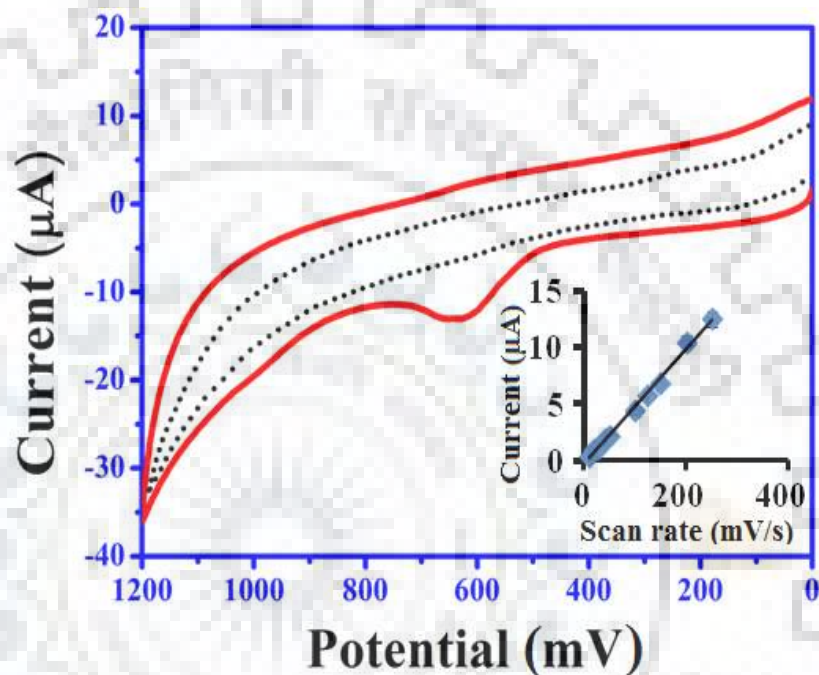
Fig. 2.1: Cyclic voltammograms recorded in the presence and absence of 200 µM MEL using bare GCE. Inset is the plot representing linear variation of 50 µM MEL peak current with scan rate at pH 7.4.

In order to investigate the nature of the electron transfer involved in the oxidation of MEL, scan rate study was carried out. It was found that on increasing the scan rate the oxidation peak current increases and the peak potential shifted towards the more positive potentials. The peak current (i_p) was found to increase with increasing sweep rate and a linear relation between i_p versus v was obtained in the range of 10–250 mV/s for a 50 µM solution of MEL (inset of Fig.1), indicating the adsorption controlled nature of electron transfer process. The variation of peak current with scan rate can be documented by the following regression equations;

$$i_p = 0.051 \ v - 0.2836, \ R^2 = 0.9932$$

$$\log i_p = 1.0448 \log v - 1.4177, \ R^2 = 0.9950$$

46

where, i_p is the peak current, v is the scan rate and R^2 is the correlation coefficient. As the slope of log i_p vs log v was found to be nearly equal to 1, it further indicated that oxidation process of MEL proceeded via adsorption controlled pathway [64].

2.3.2 Square wave voltammetry

The square wave voltammetry (SWV) being a pulse technique is more sensitive and fast in comparison to the conventional cyclic voltammetry. So, further electrochemical studies of MEL were carried out using SWV. A peak at ~625 mV was obtained corresponding to the oxidation of MEL. The peak obtained in the SWV or CV was attributed to the abstraction of 2 electrons and one proton from MEL moiety, thereby resulting into a quinoneimine as shown in **Scheme 2.1** [55].
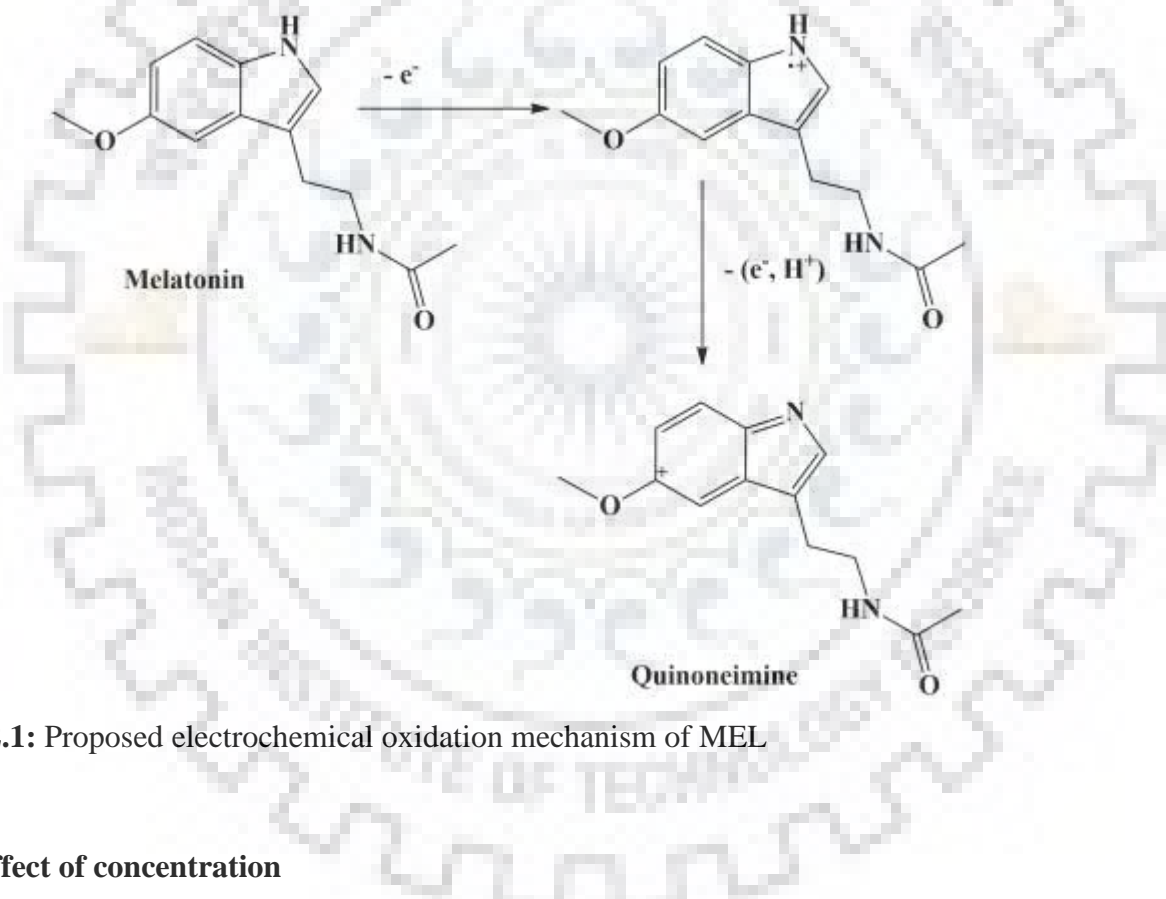
Scheme 2.1: Proposed electrochemical oxidation mechanism of MEL

2.3.2.1 Effect of concentration

To analyze the limit of detection and in order to carry out quantitative analyses of MEL, effect of concentration on MEL peak current was studied. For carrying out concentration study, SW volttamograms were recorded in the potential window of 300 to 1000 mV at different concentration of MEL using bare GCE. It is observed that the anodic peak current (i_p) increases linearly with increasing concentration of MEL in the range of 5 to 200 μM as shown in **Fig. 2.2**. The peak current versus concentration was linear and observed the following linear relation:

$$i_p = 0.0437[C] + 0.5407, R^2 = 0.9909$$

where, C is the concentration of MEL. From the regression equation, the sensitivity of the electrode is found to be 0.0491 µM/ µA.
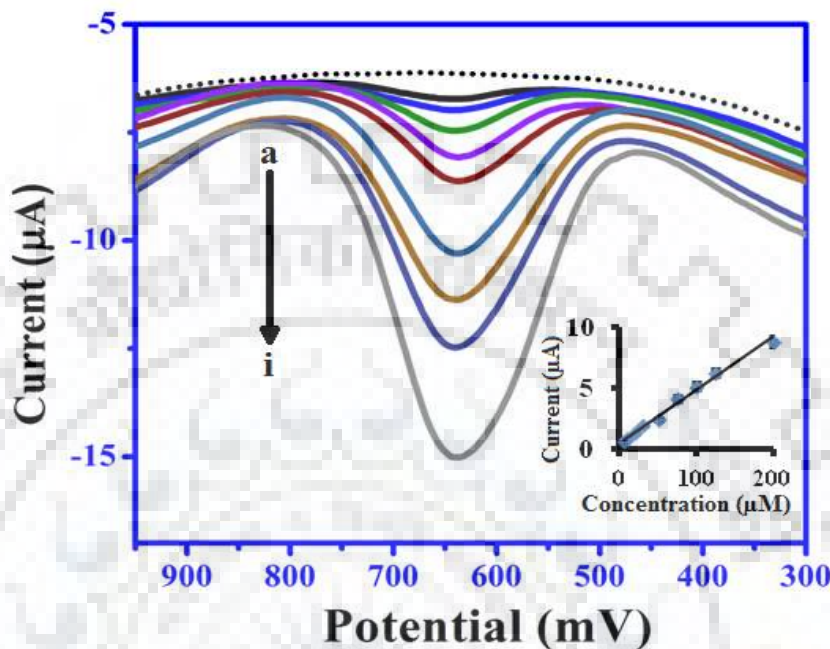
Fig. 2.2: Square wave voltammograms recorded for (a) 5 µM, (b) 10 µM, (c) 20 µM, (d) 30 µM, (e) 50 µM, (f) 75 µM, (g) 100 µM, (h) 125 µM and (i) 200 µM MEL concentrations using bare GCE. Voltammogram corresponding to the background is shown by the dotted line. Inset is the calibration plot in the concentration range 5–200 µM.

The limit of detection (L.O.D.) was also calculated using $3\sigma/b$, where σ is the standard deviation of blank and b is the slope of the calibration plot. Using the above mentioned formula the L.O.D. was found to be 0.3432 µM. The validation parameters of the proposed analytical methodology for the determination of MEL are tabulated in **Table 2.1**.

Table 2.1: Validation parameters for analytical procedure proposed for the determination of MEL.

S.No.	Validation Parameters	Values
1	Concentration range (μM)	5–200
2	Correlation coefficient (R^2)	0.9909
3	Detection limit (μM)	0.3432
4	Limit of quantification (μM)	1.144
5	Sensitivity (μA/μM)	0.0437
6	Standard error of slope (α, 0.025)	±0.0036
7	Standard error of intercept (α, 0.025)	±0.3329

2.3.2.2 Effect of pH

The pH of the supporting electrolyte has a significant effect on the electro-oxidation of MEL. The effect of pH on the oxidation peak potential and peak current of 50 μM MEL were studied in the range of 2.0–10.0 pH. It was found that by increasing the pH of supporting electrolyte the peak potential shifted towards the less positive values **(Fig. 2.3)**. The plot between peak potential and pH was found to be linear and the dependence of E_p on pH can be documented by the relation:

$$E_p \text{ (mV)} = -37.91 \text{ pH} + 912.87, \quad R^2 = 0.9938$$

The slope value 37.91 mV/pH indicates that an unequal number of electron and proton are involved in the oxidation of MEL, which is also in accordance with the mechanism shown in **Scheme 2.1** [55, 61].
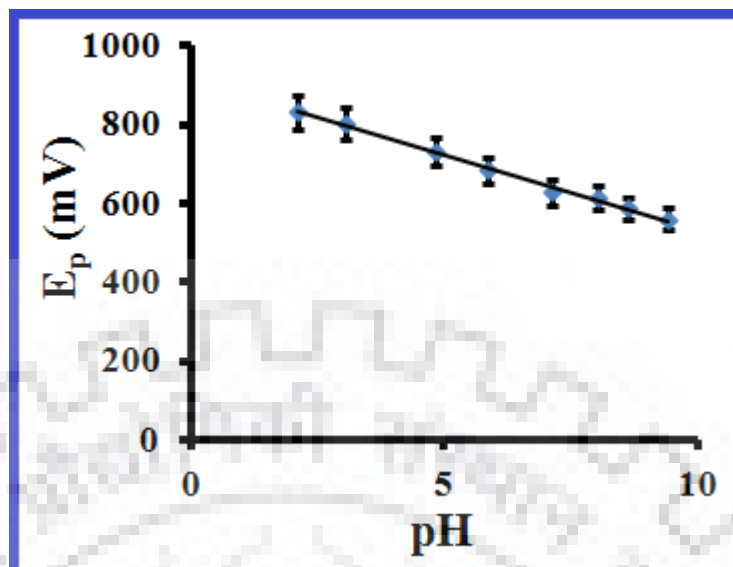
Fig. 2.3: Dependence of 50 μM MEL peak potential observed on the pH of the supporting electrolyte.

2.3.2.3 Effect of frequency

The effect of frequency on the anodic peak current of 50 μM MEL was studied in the range 5 to 50 Hz using GCE. It was found that the peak current increases linearly with the increasing frequency **(Fig. 2.4)** and can be represented by the following linear equation;

$$i_p = 0.2252\,f - 0.5942, R^2 = 0.9930$$

$$\log(i_p) = 1.1319\,\log(f) - 0.8933, R^2 = 0.9977$$

where, f is the frequency, i_p is the peak current and R^2 is the correlation coefficient. The linearity of the i_p versus f plot as well as the slope value (nearly equal to 1) for the log plot demonstrated the involvement of adsorption in the oxidation of MEL, which was also concluded from the scan rate study [64].
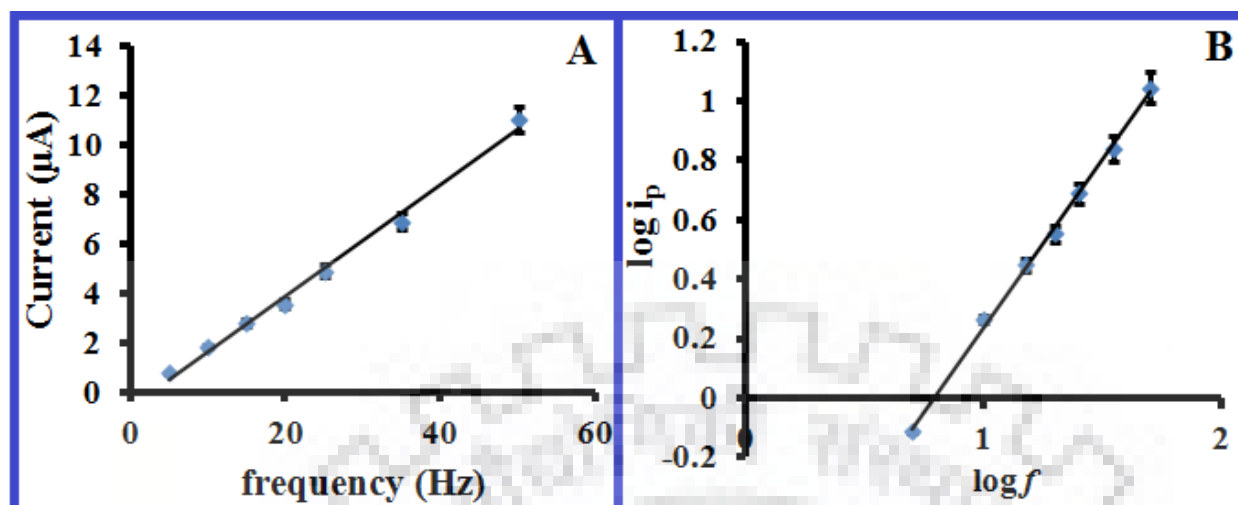
Fig. 2.4: Dependence of (A) peak current (i_p) on increasing frequency and (B) log i_p on log f for 50 µM MEL.

2.3.3 Interference study

Several metabolites present in the blood and urine, have potential to interfere in the determination of the targeted compounds and thus it is very important to check the voltammetric response of desired analyte in the presence of such compounds. As the presence of commonly present biological compounds such as hypoxanthine (HX), ascorbic acid (AA), uric acid (UA) etc. may alter the electrochemical signal of the MEL and can also affect the selectivity of the developed sensor, hence, the voltammetric behavior of MEL in the presence of these compounds has been investigated. The voltammograms were recorded in the presence of 10-fold excess concentration of these interferants at fixed MEL concentration (50 µM). Some typical voltammograms observed are presented in **Fig 2.5**. In all these voltammograms, well separated peaks at -100, 277 and 965 mV corresponding to the oxidation of AA, UA, and HX can be seen in addition to MEL peak at 625 mV. From **Fig 2.5**, it can be seen that no substantial deviation in the peak current or peak potential of the oxidation peak of MEL in the presence of high concentration of potential interfering compounds was observed, which clearly indicated that the sensor can be successfully employed for the determination of MEL.
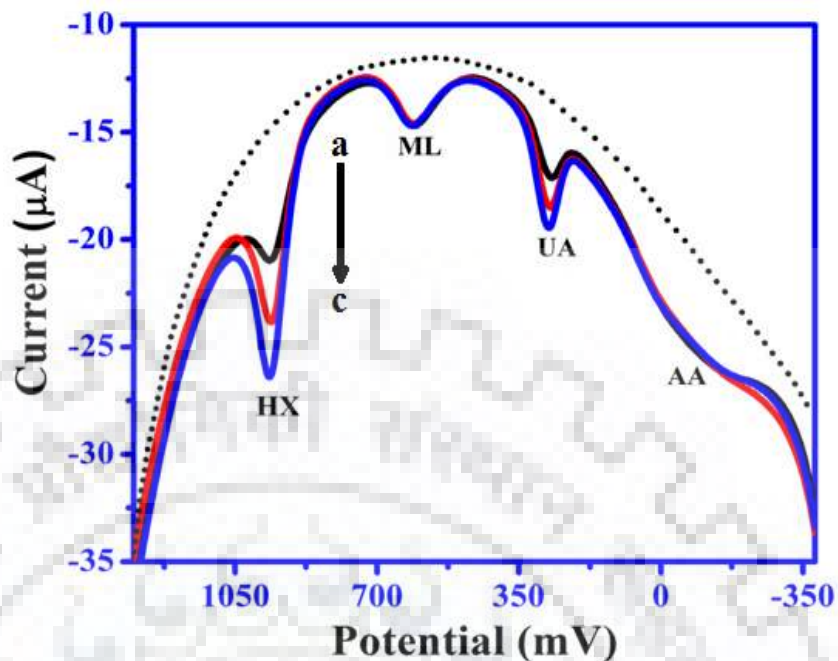
Fig. 2.5: Square wave voltammograms observed for a solution containing (a) 50 µM AA + 10 µM UA + 50 µM MEL + 25 µM HX (b) 50 µM AA + 25 µM UA+ 50 µM MEL + 50 µM HX and (c) 50 µM AA + 50 µM UA+ 50 µM MEL + 75 µM HX. Background is represented by the dotted line.

2.3.4. ANALYTICAL APPLICATION

2.3.4.1 Analysis of Pharmaceutical Formulations

To investigate the analytical applicability of the sensor, two commercially available tablets named Eternex (Dabur Pharmaceuticals Ltd, Baddi, Himachal Pradesh) and Zytonin (Cadila Healthcare Ltd, Ahmedabad, Gujarat) were analyzed. The stock solutions of the tablets were prepared by the dissolution of finally powdered tablets in the double distilled water. The stock solutions were then subsequently diluted to bring the concentration of melatonin in the working range. Square wave voltammograms were then recorded and by keeping dilution factor in mind, the MEL content present in the solution was calculated using peak current. The results thus obtained demonstrate that the observed values are in good agreement with the stated labels of pharmaceutical samples as shown in **Table 2.2**.

Table 2.2: Detemination of MEL content in commercially available pharmaceutical formulations.

Tablet	Stated content (mg)	Observed content (mg)	Error %
Zytonin	3	2.91	3.00
Eternex	3	2.89	3.67

2.3.4.2 Urine sample assay

In order to check the practical application of the proposed method, analysis of MEL in complex matrix like urine has also been investigated. Inspite of our best efforts, urine samples of patients undergoing treatment with MEL could not be obtained and thus standard addition method was performed in the urine samples of healthy volunteers. The collected urine sample was diluted twice with pH 7.2 phosphate buffer and then was spiked with 1mM solution of MEL. The above prepared solution was used as a stock solution, and solutions having concentration in the calibration range were prepared by the subsequent dilutions. Square wave voltammograms were then recorded and an oxidation peak at 625 mV was observed along with an additional peak at 279 mV, which corresponded to the oxidation of UA present in the urine. The concentration of MEL was then back calculated by substituting the peak current values in the calibration equation. The results obtained are summarized in **Table 2.3** and it can be seen that a good recovery > 90% has been observed, thereby indicating the successful application of the proposed method in urine analysis.

Table 2.3: Recovery data of MEL determination in human urine sample

S.No.	Spiked amount (µM)	Detected amount (µM)[*]	Recovery %
Sample 1			
1	100	91.22	91.22
2	150	138.02	92.01
3	200	192.45	96.22
Sample 2			
1	50	46.74	93.48
2	75	67.89	90.52
3	100	93.26	93.26

*RSD for the determination was 0.61% for n=3

2.3.5 STABILITY

An additional advantage of using unmodified GCE is its high stability and reproducibility. As the sensor is utilized without any surface modification, it is extremely stable and can be used for months without suffering from any significant current drop.

2.4. CONCLUSION

In the proposed method, bare GCE has been successfully employed to develop an alternative electrochemical method for the qualitative as well as quantitative analysis of MEL. Literature survey has shown similar sensitivities for MEL determinations at other unmodified electrodes using different voltammetric techniques **(Table 2.4)** in recent years [54-56, 58-59], whereas in this section an extremely simple method with high stability and precision and comparable limits of detection has been suggested. The practical utility of the proposed protocol in MEL analysis in commercially available pharmaceutical formulations and complex matrix like urine has also been checked and demonstrated a good agreement of the obtained values with the stated ones. Thus, the studies confer a feasible, precise and extremely simple methodology for the determination of MEL in both clinical and pharmaceutical investigations.

Table 2.4: Comparison of Limit of Detection (L.O.D) obtained for MEL using the proposed method with the previously reported unmodified sensors

Electrode/Technique	Linear range	L.O.D (µM)	Analysis	Reference
Boron doped diamond electrode (SWV)	0.5–4 mM	11	Urine, Drug	54
Carbon paste electrode (LSV)	3–550 µM	2.3	Capsules	55
Carbon disc electrode (CE-ED)	2.5–100 µM	1.3	Drug	56
Glassy carbon electrode (DPV)	20–80 µM	5.86	Nil	59
BT-drug ion pair PVC (potentiometric sensor)	10–10^4 µM	7	Urine, Drug	58
Glassy Carbon Electrode (SWV)	5–200 µM	0.3432	Urine, Drug	**Present work**

SWV: Square wave voltammetry; LSV: Linear sweep voltammetry; PVC: Poly vinylchloride DPV: Differential pulse voltammetry; CE-ED: Capillary electrophoresis-Electrochemical detection; BT: Bismus tetraiodate; PVC: Poly vinylchloride

SECTION 2: DETERMINATION OF MELATONIN BY USING POLYMER NANOCOMPOSITE MODIFIED GLASSY CARBON SENSOR

2.5 RESULTS AND DISCUSSION

2.5.1 Characterization of PdNPs, p-(AHNSA) film and GO

The successive cyclic voltammograms obtained during the electropolymerization of AHNSA at the surface of GCE are presented in **Fig. 2.6 (A)**. In the first cyclic voltammogram, two anodic peaks a and a' and one cathodic peak b were observed at 66 mV, 397 mV and -71 mV respectively [63]. However, an additional peak c also appeared around ~ 1700 mV in further scans. The current response of peak a, a' and b was found to increase with the increasing number of scans, which indicated the electrochemical deposition of the conducting polymer thin film over the GCE surface. A weak peak a' at 66 mV represent the generation of cationic free radical, which reacts with similar species to form dimer during the polymerization, while the peak a is attributed to the loss of proton from the dimer and the peak b corresponds to the consecutive cathodic reduction of the protons as reported in the literature [65].

Fig. 2.6 (B) indicates the consecutive cyclic voltammogram of PdNPs on GCE surface. Majorly, six peaks I_a, I_b, II, III_a, III_b and IV were observed at -152, 8, 463, 620, 385 and -284 mV respectively. The cathodic wave at -284 mV (peak IV) was thought to be attributed to the reduction of Pd^{2+} to Pd(0) and the peak at 423 mV (Peak II) could be because of stripping of Pd(0) deposited on the surface of GCE [66]. The peak I_a and I_b signifies the reduction of proton adsorbed on the PdNPs surface to hydrogen and demonstrates the nano crystalline behavior of Pd [67-68]. Based on the previous studies the remaining two peaks at 620 and 385 mV can be assigned to the PdO_2 formation and its conversion back to Pd(0) respectively [66-67].

Fig. 2.6 (C) represent the single step electrochemical deposition of the polymer nanocomposite (AHNSA:PdNPs:ErGO) over the surface of GCE. From the voltammograms, it can be seen that the peaks corresponding to the polymerization of AHNSA were masked by the redox peaks observed for electrodeposition of PdNPs. Six peaks named I_a, I_b, II, III_a, III_b and IV were observed at -125, 25, 359, 724, 295, and -278 mV respectively, which are similar to those obtained in the electrodeposition of PdNPs. An additional irreversible peak at 1374 mV was also observed after first few cycles, which can also be seen in voltammograms observed during AHNSA polymerization **(Fig. 2.6(A))**. From **Fig. 2.6(C)**, it can be seen that the peaks which were observed during the electrodeposition of the PdNPs and electropolymerization of AHNSA exhibited a

substantial negative potential shift as well as peak separation, which indicated the successful surface modification and also demonstrated electrocatalytic properties of the fabricated sensor.
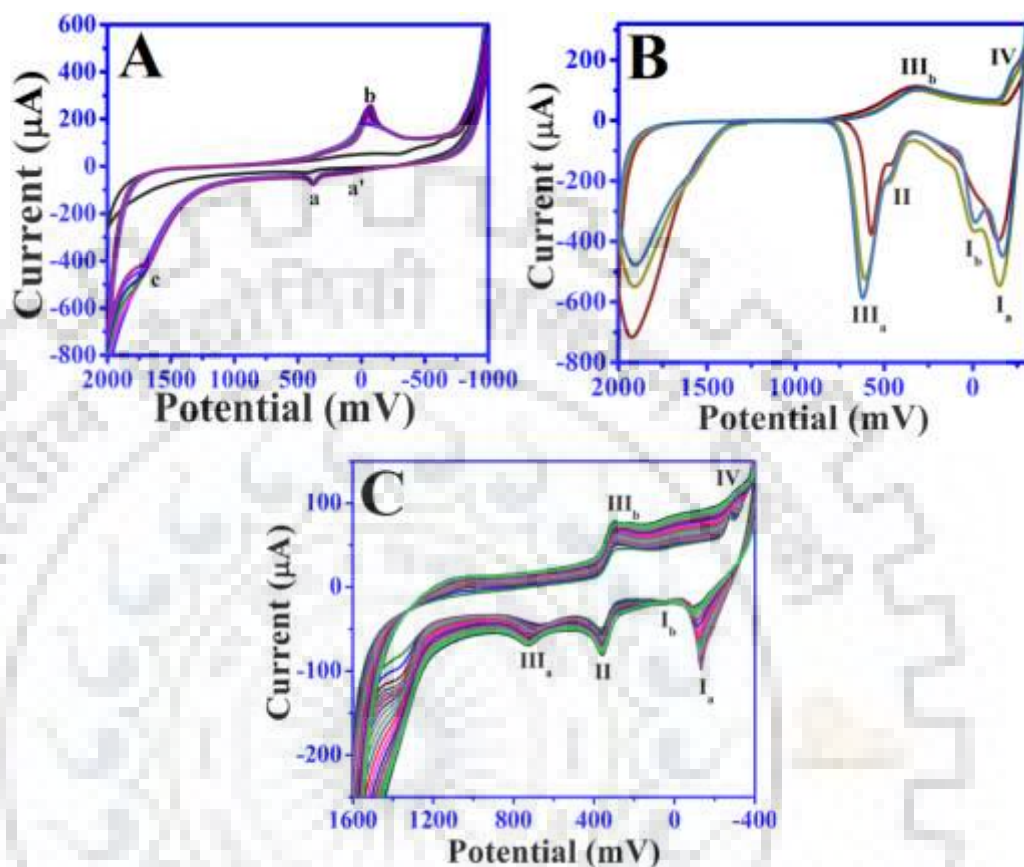
Fig. 2.6: Cyclic voltammograms observed for (A) electropolymerization of 2 mM AHNSA solution (prepared in 0.1 M nitric acid) at a sweep rate of 100 mV s^{-1} (B) electrodeposition of PdNPs and (C) Electrofabrication of palladium based polymer nanocomposite AHNSA:PdNPs:ErGO.

To characterize the changes produced on the sensing surface during the electrochemical deposition of AHNSA:PdNPs:ErGO polymer nanocomposite, FE-SEM images were recorded at different steps of modification. From the FE-SEM images shown in **Fig. 2.7**, it can be clearly seen that surface of the GCE has been successfully modified and showed different topological characteristics in comparison to the unmodified GCE surface **(Fig. 2.7(A))**. From the figure 2.7B, the electrodeposition of PdNP's on the nanotriangles of AHNSA can be clearly evidenced which can also be seen in **Fig. 2.7 (C)** along with the crumbled and folded sheets corresponding to ErGO thereby representing simultaneous presence of PdNP, ErGO and AHNSA in the

AHNSA:PdNPs:ErGO/GCE. The presence of Pd has also been confirmed from the Electron Energy Dispersive X-ray spectroscopy (EDX), which demonstrated the 3.70 atomic % of Pd in the AHNSA:PdNPs:ErGO polymer nanocomposite as presented in **Fig. 2.7 (D)**.
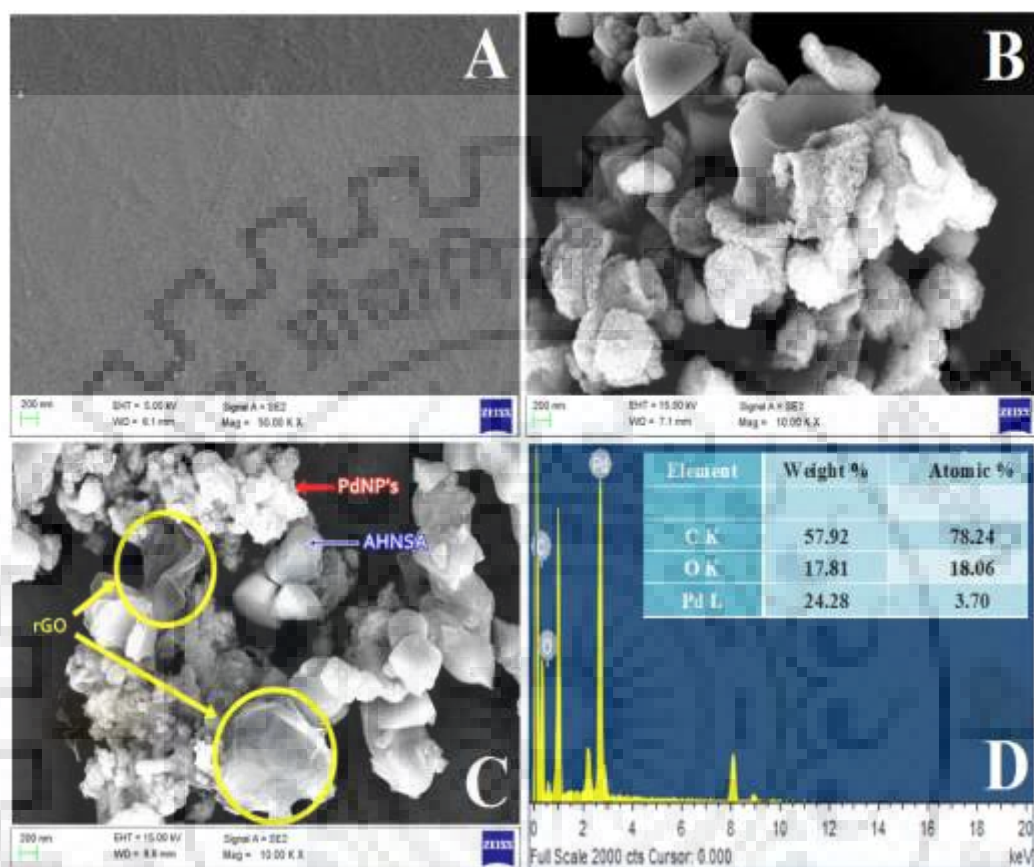
Fig. 2.7: FE-SEM images demonstrating surface morphology of (A) unmodified GCE, (B) AHNSA:PdNPs/GCE, (C) AHNSA:PdNPs:ErGO/GCE and (D) EDX data demonstrating presence of Pd in AHNSA:PdNPs:ErGO/GCE.

EIS measurement was used to further investigate the changes produced on the surface of glassy carbon after the electrochemical deposition of AHNSA:PdNPs:ErGO at GCE surface. The experiment was carried out in 1:1 mixture of 5 mM $K_3Fe(CN)_6$ and 0.1 M KCl solution over the frequency range 1000 kHz to 1 mHz. A typical Nyquist plot observed consisted of two portions, one was the semi-circular and another was the linear portion. The diameter of the semicircle represents the charge transfer resistance (R_{CT}) at a higher frequency and the linear portion response at lower frequency is an indicator of the mass transfer effects [20]. The Nyquist plots corresponding to modified and unmodified GCE have been presented in **Fig. 2.8,** from which a semicircle with a smaller diameter in comparison to the one obtained for the unmodified GCE

demonstrates the faster electron transfer process at AHNSA:PdNPs:ErGO/GCE. The value of R_{CT} for the redox process was calculated by fitting the Randle's circuit **(inset of Fig. 2.8)** and was found to be 547 Ω and 976 Ω for the polymer nanocomposite modified and unmodified sensor respectively. The lower value of the R_{CT} indicates that the electron transfer reaction at the surface of the modified GCE is facilitated by the AHNSA:PdNPs:ErGO polymer nanocomposite.
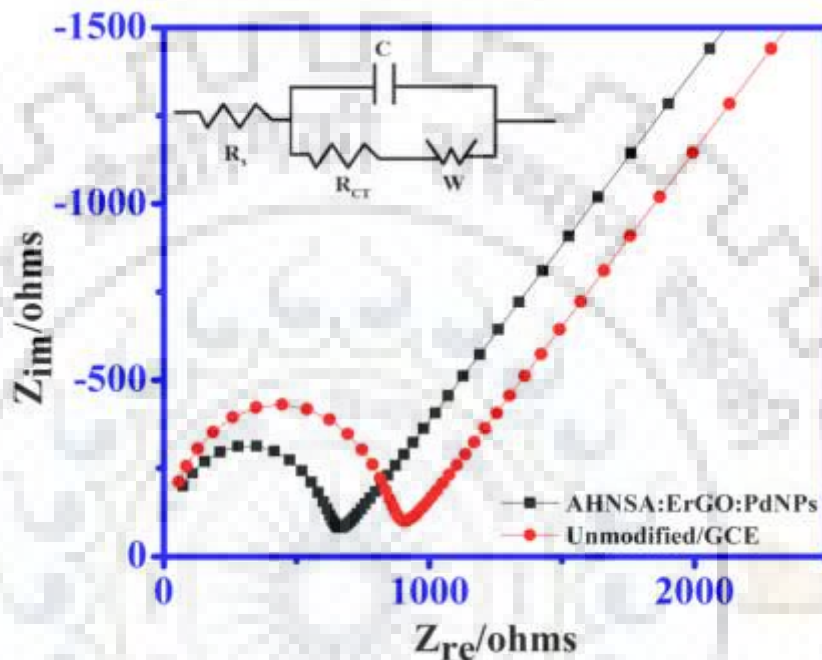
Fig. 2.8: Typical Nyquist plot obtained for AHNSA:PdNPs:ErGO/GCE and unmodified GCE during electrochemical impedance spectroscopy in 1:1 mixture of 5 mM $K_3Fe(CN)_6$ and 0.1 M KCl solution over the frequency range 1000 kHz to 1 mHz.

2.5.2 Cyclic Voltammetry

Cyclic voltammetry has been widely used in order to investigate the redox behavior of electro-active analyte, and to study the nature of the electrochemical reaction involved. Hence, the initial study of MEL was carried out using cyclic voltammetry (CV) technique. Cyclic voltammograms of 100 µM MEL were recorded in phosphate buffer solution (pH 7.2) at 100 mV/s sweep rate using bare and modified glassy carbon electrode (GCE). A broad oxidation peak was observed at 686 mV at bare GCE, whereas a sharp peak at reduced peak potential (~656 mV) with much enhanced peak current has been observed at AHNSA:PdNPs:ErGO/GCE as shown in **Fig. 2.9**. In the reverse scan no reduction peak was observed, which indicated the irreversible oxidation process of MEL. The reduced peak potential and significant enhancement in the peak current of

MEL demonstrates the electrocatalytic activity of the polymer nano composite, which has facilitated the electron transfer and thus developed our interest to carry out further MEL investigations using AHNSA:PdNPs:ErGO/GCE.
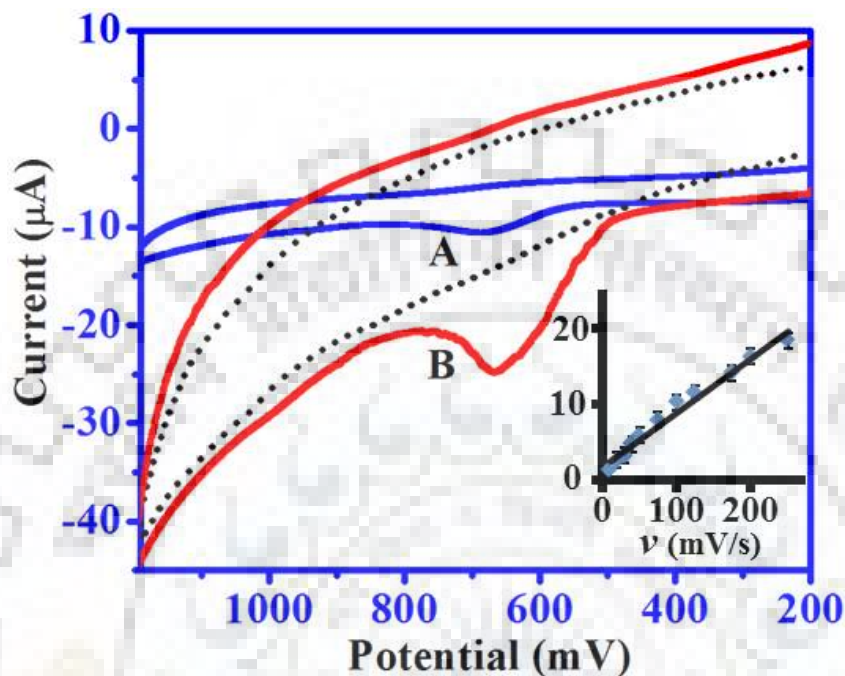
Fig. 2.9: Comparative cyclic voltammograms corresponding to 100 µM MEL in pH 7.2 phosphate buffer at 100 mV/s scan rate using (A) unmodified GCE and (B) AHNSA:PdNPs:ErGO/GCE.

In order to comprehend the nature of the electron transfer reaction involved in the oxidation of MEL, scan rate study was performed. During the scan rate study, anodic peak current of MEL was found to increase with the increasing scan rate. A linear relation was found between peak current (i_p) and scan rate (v) in the range of 5–250 mVs^{-1} for 100 µM MEL solution (inset of Fig. 2.9) and the dependence of i_p on v can be represented by the following regression equation:

$$i_p \ (\mu A) = 0.0707 \ v \ (mVs^{-1}) + 1.8756, \ R^2 = 0.990$$

$$\log i_p = 0.7703 \log v - 0.5833, \ R^2 = 0.993$$

where, R^2 is regression coefficient. From the linearity of i_p versus v and the slope value of $\log i_p$ versus $\log v$ (> 0.5) the involvement of adsorption controlled electron transfer reaction in the oxidation of MEL has been concluded [68].

2.5.3 Square wave voltammetry

The square wave voltammetric technique (SWV) has also been used for the analysis of MEL due to its high sensitivity and better peak resolution in comparison to the conventional cyclic voltammetry technique. Square wave voltammograms were recorded for 20 µM MEL in phosphate buffer (pH 7.2) using unmodified GCE, AHNSA/GCE, PdNPs:AHNSA/GCE, GO:AHNSA/GCE and AHNSA:PdNPs:ErGO/GCE. A comparative voltammograms have been demonstrated in **Fig. 2.10**, which clearly indicates the superior response of AHNSA:PdNPs:ErGO/GCE in comparison to all other modifications as much enhanced peak current (4.26 µA) can be witnessed along with a shift of 37 mV in peak potential in comparison to the unmodified GCE. Hence, all the studies were carried out using AHNSA:PdNPs:ErGO/GCE.
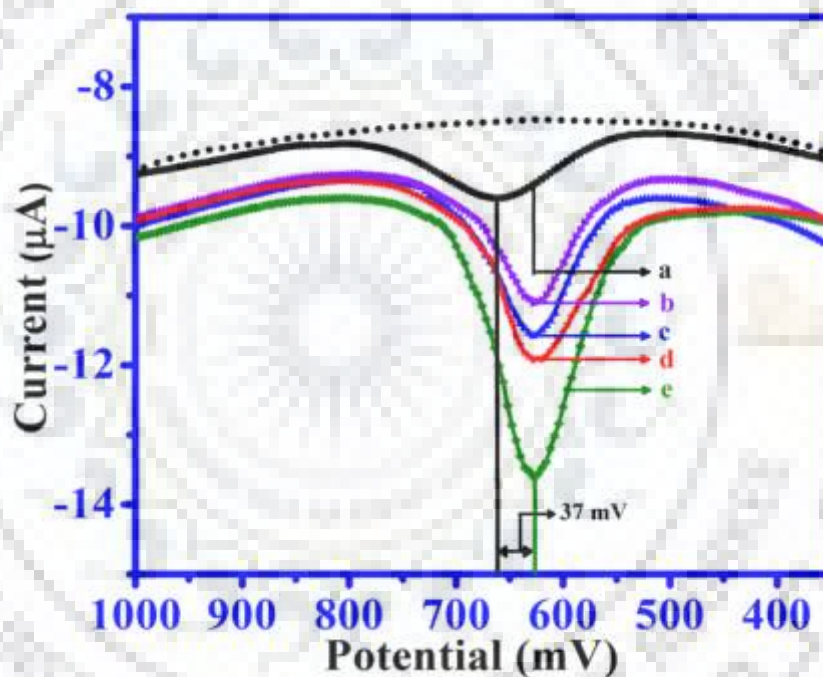
Fig. 2.10: Comparative square wave voltammograms recorded for 20 µM MEL in pH 7.2 phosphate buffer at modified (a) unmodified GCE, (b) AHNSA/GCE, (c) AHNSA:PdNPs/GCE, (d) AHNSA:GO/GCE and (e) AHNSA:PdNPs:ErGO/GCE.

2.5.3.1 Effect of concentration

The concentration study has been carried out to determine the limit of detection and sensitivity of the modified sensor. For the concentration study, the square wave voltammograms for the different concentration of MEL were recorded using the AHNSA:PdNPs:ErGO/GCE in pH 7.2 phosphate buffer solution at the optimal SWV parameter **(Fig. 2.11)**. The quantitative

evaluation of MEL has been done by measuring its oxidation peak current using SWV technique. A linear relation between the peak current (i_p) and the increasing concentration of MEL for the modified as well as unmodified GCE has been established and are given by the following regression equations:

$$i_p = 0.0437 \text{ [C 5-200 μM]} + 0.5407, R^2 = 0.9909 : \textbf{unmodified GCE}$$

$$i_p = 0.1235 \text{ [C 5-100 μM]} + 1.6863, R^2 = 0.9745: \textbf{AHNSA:PdNPs:ErGO/GCE}$$

where, C is the concentration of MEL. From the regression equation, it can be concluded that modification with polymer nano composite resulted in ~ 3 fold increase in the sensitivity of the sensor towards MEL.
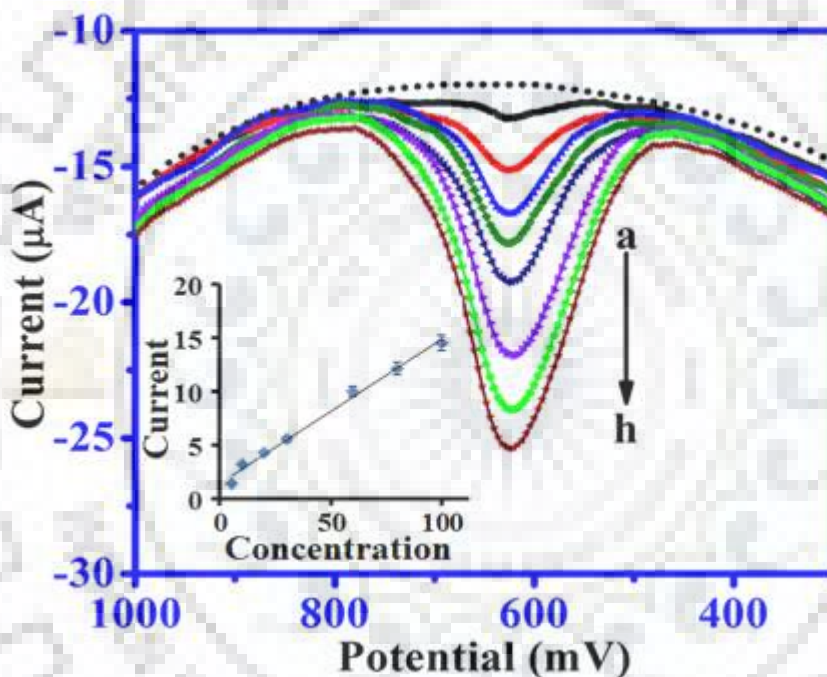
Fig. 2.11: Square wave voltammograms recorded for (a) 5 μM, (b) 10 μM, (c) 20 μM, (d) 30 μM, (e) 50 μM, (f) 60 μM, (g) 80 μM and (h) 100 μM MEL concentrations using AHNSA:PdNPs:ErGO/GCE. The dotted line demonstrates the background current. Inset is the calibration plot in the MEL concentration range of 5–100 μM.

The limit of detection (L.O.D.) has also been calculated by using formula 3σ/b, where b is the sensitivity obtained from the calibration plot and σ is the standard deviation of 'n' blank voltammograms. The limit of detection for MEL using AHNSA:PdNPs:ErGO/GCE was found to be 0.09 μM which is much lower in comparison to the recently reported analytical techniques as showcased in **Table 2.5**.

Table 2.5: Comparison of Limit of Detection (LOD) obtained for MEL using the proposed method with the previously reported sensors.

S.No	Modification/electrode	LOD(μM)	Concentration range	Reference
1	Carbon paste electrode (LSV)	2.3	3–550 μM	**[55]**
2	Carbon disc electrode (CE-ED)	1.3	2.5–1000 μM	**[56]**
3	BDD electrode (SWV)	0.11	0.5–4.0 μM	**[54]**
4	MnHCF_PEDOT /GCE	100	100–4600 μM	**[57]**
5	BT-drug ion pair PVC (potentiometry)	7	1–10000 μM	**[58]**
6	Glassy Carbon Electrode (SWV)	5.86	20–80 μM	**[59]**
7	RGO/RuO$_2$/GCE	0.18	2–20 μM	**[60]**
8	AHNSA:PdNPs:ErGO/GCE	0.09	5–100 μM	**Present work**

LSV: Linear sweep voltammetry, CE-ED: Capillary electrophoresis with electrochemical detection, SWV: square wave voltammetry, DPV: Differential pulse voltammetry, BT: Bismus tetraiodate; PVC: Poly vinyl chloride, MnHCF: maganese hexacyanoferrate, PEDOT: poly(3,4-Ethylenedioxythiophene, BDD : Boron Doped Diamond

2.5.3.2 Effect of pH

The pH of the supporting electrolyte plays a significant role in the oxidation of MEL. The effect of pH on the electro-oxidation of MEL was investigated by using SWV, and the experiment was performed using 50 μM MEL in the pH range 2.4 to 10.0. It was found that the pH of the supporting electrolyte affects the oxidation peak potential and peak current of MEL. On increasing the pH the anodic peak potential shifted towards less positive potentials and a linear relation was observed between anodic peak potential (E_p) and pH, which can be expressed by the following equation:

$$E_p \, (mV) = -37.828 \, pH + 910.2, \quad R^2 = 0.9816$$

where, R^2 is the correlation coefficient.The slope (dE_P/dpH) has a value of 37.828 mV/pH which clearly demonstrated the involvement of an unequal number of electrons and protons in the oxidation of MEL [61]. The 2e, 1H$^+$ oxidation of melatonin in aqueous and non-aqueous media has been represented in the literature [55].

2.5.3.3 Effect of frequency

The effect of frequency on the oxidation of MEL was studied at AHNSA:PdNPs:ErGO/GCE by recording the SWV response for 20 μM MEL in pH 7.2 phosphate buffer by varying the frequency in the range of 5 to 50 Hz. The peak current has been found to increase with the increasing frequency and a linear plot between $\log i_p$ and $\log f$ can be represented by the following linear equation;

$$\log i_p = 0.855 \log f - 0.4051, R^2 = 0.9772$$

Where, i_p is the peak current, f is frequency and R^2 is the correlation coefficient. The slope value >0.5 indicated that the oxidation of MEL process was adsorption controlled and thus further supported the results observed in the scan rate study [68].

2.5.4 Interference study

High concentration of several metabolites like ascorbic acid (AA), hypoxanthine (HX), uric acid (UA) etc. are present in the human blood and urine, which can alter the voltammetric response of the developed sensor and can also affect its selectivity. Thus to investigate the effect of these metabolites on the peak potential and the peak current of MEL, interference study has been carried out using the developed sensor. The voltammograms were recorded at a fixed concentration (30 μM) of MEL in the presence of excess of interferants as represented in **Fig. 2.12**. The well defined oxidation peak was observed at -100 mV, 309 mV, 988 mV for AA, UA, and HX respectively, in addition to the peak of MEL at 623 mV. A peak of AA has not been shown due to no significant importance, as the peak potential lies far away from the working range. The voltammograms thus obtained clearly indicated that the oxidation peak potential and the peak current response of MEL suffer from no significant change in the presence of potentially interfering substances. Hence, modified sensor can be successfully used for the investigation of MEL in blood and urine samples.
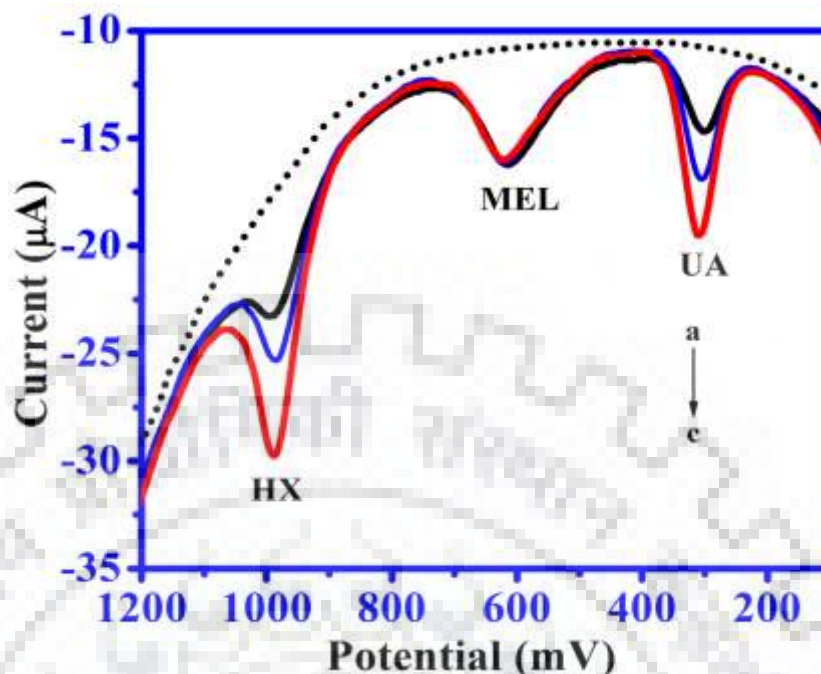
Fig. 2.12: Square wave voltammograms observed for a solution containing (a) 25 μM AA + 10 μM UA + 30 μM MEL + 10 μM HX, (b) 50 μM AA + 25 μM UA+ 30 μM MEL + 25 μM HX and (c) 100 μM AA + 50 μM UA+ 30 μM MEL + 50 μM HX. Background is represented by the dotted line.

2.5.5 ANALYTICAL APPLICATION

2.5.5.1 Analysis of Pharmaceutical Formulations

To determine the pharmaceutical application of the developed sensor, MEL containing two tablets named Eternex (Dabur Pharmaceuticals Ltd, Baddi, Himachal Pradesh) and Zytonin (Cadila Healthcare Ltd, Ahmedabad, Gujarat) were purchased from the local market of Roorkee, India. The stock solution for pharmaceutical analysis was prepared by dissolving the required amount of the powdered tablets in double distilled water and then the stock solution so obtained was further diluted to bring the concentration in the working range. Square wave voltammograms were then recorded at the optimal parameter and under the identical conditions that were employed at the time of the calibration plot. The obtained results are summarized in **Table 2.6** and show that the observed results are in good agreement with the stated values. Thus, the developed sensor can be extended to ensure the apt amount of MEL content in the tablets and can prove to be of significant importance to the pharma industry.

Table 2.6: Detemination of MEL content in pharmaceutical drug formulations using a modified sensor.

Tablet	Stated content (mg)	Observed content (mg)	Error %
Zytonin	3	2.96	1.33
Eternex	3	2.94	2.00

2.5.5.2 Urine sample assay

In order to investigate the practical application of the proposed sensor, the PdNPs:AHNSA:GO/GCE was used to measure the MEL content in the complex matrix like human urine or plasma samples. Inspite of our best efforts samples of the patients on any form of MEL treatment could not be obtained and thus recovery studies in the urine sample of two healthy volunteers were carried out. For the recovery studies, collected urine samples were diluted twice by using pH 7.2 phosphate buffer solutions in order to reduce the matrix complexity. The diluted urine sample was spiked with the known concentration of MEL and the square wave voltammograms were recorded. The oxidation peak of MEL was observed at 622 mV with an additional oxidation peak at 304 mV corresponding to the oxidation of UA in the urine samples. The concentration of MEL in the urine sample is then back calculated by putting the peak current value in the regression equation and the results obtained are listed in **Table 2.7**. The good recovery with low RSD value demonstrates the accuracy and reproducibility of the proposed method.

Table 2.7: Recovery data of MEL determination in human urine sample.

S.No.	Spiked amount (µM)	Detected amount (µM)[*]	Recovery %
Sample 1			
1	20	19.92	99.60
2	30	29.85	99.50
3	100	99.65	99.65
Sample 2			
1	10	9.87	98.70
2	25	24.89	99.56
3	50	49.81	99.62

*RSD for the dtermination was 1.03% for n=3

2.5.6 STABILITY

For monitoring the stability of the AHNSA:PdNPs:ErGO/GCE sensor the anodic peak current of MEL at a fixed concentration was examined in phosphate buffer of pH 7.2. The voltammograms were recorded every day for 30 days and the current response so obtained indicated a fluctuation of 6.0% in the first 20 days, however, after 20 days, current response decreased by up to 8.57%. Thus, obtained results suggested that the developed sensor possesses excellent stability.

To examine the intraday reproducibility of the AHNSA:PdNPs:ErGO/GCE, five voltammograms were scanned consequently for 100 μM MEL and the calculated R.S.D value was found to be 2.73% for n=3. The low R.S.D. value indicated the accuracy and reproducibility of the proposed method.

The sensor to sensor variation has also been evaluated by modifying three different GCE (having similar backgrounds) following the same modification protocol. Using each of the modified GCE, voltammograms were recorded in 30 μM MEL solution and deviation in the current response of the three sensors with each other were calculated. It was observed that the peak current of the three modified sensors varies only by a R.S.D of 3.29%. Thus, it was concluded that the fabricated sensor bears appreciable stability and reproducibility.

2.6 CONCLUSION

A facile, single step method for the surface modification of GCE with polymer nanocomposite (AHNSA:PdNPs:ErGO) has been demonstrated which includes the simultaneous electrochemical reduction of GO to ErGO, electropolymerization of AHNSA and electrodeposition of PdNPs on the surface of GCE. Surface modified voltammetric sensor thus obtained has been characterized using CV, FE-SEM, EDX and EIS. The developed sensor has been extended for the qualitative as well as quantitative analysis of MEL in the range 5 to 100 μM and can also be utilized successfully for the analysis of MEL in pharmaceutical and human biological samples. The presented protocol for the surface modification not only provides higher surface area but also facilitated the oxidation process of MEL, which resulted in much enhanced peak current as well as reduced peak potential for the oxidation of MEL. Thus the modification resulted in a sensitive determination of MEL in comparison to other recently reported methods in the literature. The developed sensor offers a long term stability and appreciable reproducibility therefore, holds a potential to commence research in the field of polymer nanocomposites as surface modifiers. A

comparison of L.O.D. of unmodified and modified sensors clearly indicated that modification of the surface caused a decrease from 0.343 to 0.090 μM.

2.7 REFERENCES

[1]   F.A.M. Al-Omary, "Melatonin: comprehensive profile", in: "Profiles of drug substances, excipients and related methodology", H.G. Brittain (Ed.), 1st edition, Elsevier, 38 (2013) 159–226.

[2]   T.B. Grivas, O.D. Savvidou, "Melatonin the "light of night" in human biology and adolescent idiopathic scoliosis", Scoliosis (2007) 2:6 (doi:10.1186/1748-7161-2-6).

[3]   D.P. Cardinali, V. Srinivasan, A. Brzezinski, G.M. Brown, "Melatonin and its analogs in insomnia and depression", J. Pineal Res. 52 (2012) 365–375.

[4]   A.B. Hickman, D.C. Klein, F. Dyda, "Melatonin biosynthesis: The structure of serotonin N-acetyltransferase at 2.5 Å resolution suggests a catalytic mechanism", Molecular Cell 3 (1999) 23–32.

[5]   D.X. Tan, L.C. Manchester, M.P. Terron, L.J. Flores, R.J. Reiter, "One molecule, many derivatives: A never ending interaction of melatonin with reactive oxygen and nitrogen species?", J. Pineal Res. 42 (2007) 28–42.

[6]   A. Brzezinski, "Melatonin in humans", N. Engl. J. Med. 336 (1997) 186–195 (DOI: 10.1056/NEJM199701163360306)

[7]   F. Waldhauser, M. Dietzel, "Daily and annual rhythms in human melatonin secretion: role in puberty control", Ann. N. Y. Acad. Sci. 453 (1985) 205–214. (doi: 10.1111/j.1749-6632.1985.tb11811.x)

[8]   G. M. Brown, D.P. Cardinali, S.R. Pandi-Perumal, "Melatonin and mental illness" S.R. Pandi-Perumal, M. Krame (Eds.), In: "Sleep and Mental Illness" Cambridge University Press (2010) pp 119–129.

[9]   J.R. Johns, J.A. Platts, "Theoretical insight into the antioxidant properties of melatonin and derivatives", Org. Biomol. Chem. 12 (2014) 7820–7827.

[10]   M.M. Macchi, J.N. Bruce, "Human pineal physiology and functional signification of melatonin", Front Neuroendocrinol. 25 (2004) 177–195.

[11]   V. Srinivasan, G.J.M. Maestroni, D.P. Cardinali, A.I. Esquifino, S.R.P. Perumal, S.C. Miller, "Melatonin, immune function and aging", Immun. Ageing (2005) 2:17 (doi:10.1186/1742-4933-2-17).

[12]   R.J. Reiter, D.X Tan, C. Osuna, E. Gitto, "Actions of melatonin in the reduction of oxidative stress", J. Biomed. Sci. 7 (2000) 444–458.

[13]   R.J. Reiter, D.X. Tan, L.C. Manchester, W. Qi, "Biochemical reactivity of melatonin with reactive oxygen and nitrogen species", Cell Biochem. Biophys. 34 (2001) 237–256.

[14]   D.X. Tan, A. Korkmaz, R.J. Reiter, L.C. Manchester, "Ebola virus disease: Potential use of melatonin as a treatment", J. Pineal Res. 57 (2014) 381–384.

[15]   E. Gitto, M. Karbownik, R.J. Reiter, D.X. Tan, S. Cuzzocrea, P. Chiurazzi, S. Cordaro, G. Corona, G. Trimarchi, I. Barberi, "Effects of melatonin treatment in septic newborns", Pedi. Resear. 50 (2001) 756–760.

[16]   V. Srinivasan, S.R.P. Perumal, D.P. Cardinali, B. Poeggeler, R. Hardeland, "Melatonin in Alzheimer's disease and other neurodegenerative disorders", Behav. Brain Funct. 2 (2006) 15.

[17]   J.C. Mayo, R.M. Sainz, D.X. Tang, I. Antolin, C. Rodriguez, R.J. Reiter, "Melatonin and parkinson's disease", Endocrine 27 (2005) 169–178.

[18]   J. Wang, Z. Wang, "Role of melatonin in Alzheimer-like neurodegeneration", Acta Pharm. Sinic. 27(2006) 41–49.

[19]   V. Srinivasan, G. Gobbi, S.D. Shillcutt, S. Suzen, "Melatonin: Therapeutic value and neuroprotection", CRC Press, Taylor and Francis group (2015).

[20]   Rosy, S.K. Yadav, B. Agrawal, M. Oyama, R.N. Goyal, "Graphene modified palladium sensor for electrochemical analysis of norepinephrine in pharmaceuticals and biological fluids", Electrochim. Acta 125 (2014) 622–629.

[21]   X.M. Chen, Z.X. Cai, Z.Y. Huang, M. Oyama, Y.Q. Jiang, X. Chen, "Ultrafine palladium nanoparticles grown on graphene nanosheets for enhanced electrochemical sensing of hydrogen peroxide", Electrochim. Acta 97 (2013) 398–403.

[22]   P.A. Khomyakov, G. Giovannetti, P.C. Rusu, G. Brocks, J. van den Brink, P.J. Kelly, "First-principles study of the interaction and charge transfer between graphene and metals", Phys. Rev. B 79 (2009) 19–15.

[23]   L. Liao, H. Peng, Z. Liu, "Chemistry makes graphene beyond graphene", J. Am. Chem. Soc. 136 (2014) 12194–12200.

[24]   S.D. Sarma, S. Adam, E.H. Hwang, E. Rossi, "Electronic transport in two-dimensional graphene", Rev. Mod. Phys. 83 (2011) 407–412.

[25]   R.S. Shishir, D.K. Ferry, "Intrinsic mobility in graphene", J. Phys. Condens. Matter 21 (2009) 232204.

[26]   S.V. Morozov, K.S. Novoselov, M.I. Katsnelson, F. Schedin, D.C. Elias, J.A. Jaszczak, and A.K. Geim, "Giant intrinsic carrier mobilities in graphene and its bilayer", Phys. Rev. Lett. 100 (2008) 016602.

[27]   Y. Zhang, T.T. Tang, C. Girit, Z. Hao, M.C. Martin, A. Zettl, M.F. Crommie, Y.R. Shen, F. Wang, "Direct observation of a widely tunable bandgap in bilayer graphene", Nature 459 (2009) 820–823.

[28]   H. Chen, M.B. Muller, K.J. Gilmore, G.G. Wallace, D. Li, "Mechanically strong, electrically conductive, and biocompatible graphene paper", Adv. Mater. 20 (2008) 3557–3561.

[29]   Y. Wang, Z. Shi, Y. Huang, Y. Ma, C. Wang, M. Chen, Y. Chen, "Supercapacitor devices based on graphene materials", J. Phys. Chem. C 113 (2009) 13103–13107.

[30]   Y. Shao, J. Wang, H. Wu, J. Liu, I.A. Aksay, Y. Lin, "Graphene based electrochemical sensors and biosensors", Electroanalysis 22 (2010) 1027–1036.

[31]   J.L. Vickery, A.J. Patil, S. Mann, "Fabrication of graphene–polymer nanocomposites with higher-order three-dimensional architectures", Adv. Mater. 21 (2009) 2180–2184.

[32]   G. Jo, M. Choe, S. Lee, W. Park, Y. ho Kahng, T. Lee, "The application of graphene as electrodes in electrical and optical devices", Nanotechnology 23 (2012) 112001.

[33]   V. Dua, S.P. Surwade, S. Ammu, S.R. Agnihotra, S. Jain, K.E. Roberts, S. Park, R.S. Ruoff, S.K. Manohar, "All-organic vapor sensor using inkjet-printed reduced graphene oxide", Angew. Chem. Int. Ed. 49 (2010) 2154–2157.

[34]   S. Bae, H. Kim, Y. Lee, X. Xu, J.S. Park, Y. Zheng, J. Balakrishnan, T. Lei, H. ri Kim, Y. II Song, Y.J. Kim, K.S. Kim, B. Ozyilmaz, J.H. Ahn, B. hee Hong, S. Iijima, "Roll-to-roll production of 30-inch graphene films for transparent electrodes", Nat. Nanotechnol. 5 (2010) 574–578.

[35]   C. Berger, Z. Song, X. Li, X. Wu, N. Brown, C. Naud, D. Mayou, T. Li, J. Hass, A.N. Marchenkov, E.H. Conrad, P.N. First, W.A. de Hee, "Electronic confinement and coherence in patterned epitaxial graphene", Science 312 (2006) 1191–1195.

[36]   Z. Wang, X. Zhou, J. Zhang, F. Boey, H. Zhang, "Direct electrochemical reduction of single-layer graphene oxide and subsequent functionalization with glucose oxidase", J. Phys. Chem. C 113 (2009) 14071–14075.

[37]   H.J. Salavagione, G. Martinez, G. Ellis, "Recent advances in the covalent modification of graphene with polymers", Macromol. Rapid Commun. 32 (2011) 1771–1789.

[38]   L.J.N. Vergara, J.A. Squella, J.C. Sturm, H. Baez, C. Camargo, "Simultaneous determination of melatonin and pyridoxine in tablets by gas chromatography-mass spectrometry", J. Pharm. Biomed. Anal. 26 (2001) 929–938.

[39]   E. Chanut, J.N. Legros, C.V. Botteri, J.H. Trouvin , J.M. Launay, "Determination of melatonin in rat pineal, plasma and retina by high-performance liquid chromatography with electrochemical detection", J. Chromatogr. B 709 (1998) 11–18.

[40]   J. Lin, C. Zhang, Y. Gao, X. Zhao, X. Li, "A Validated HPLC method for determining melatonin in capsule dosage form", Spatula DD 2(3) (2012) 147–151.

[41]   R.M. Chau, B.A. Patel, "Determination of serotonin, melatonin and metabolites in gastrointestinal tissue using high-performance liquid chromatography with electrochemical detection", Biomed Chromatogr. 23(2) (2009) 175–181.

[42]   J. Cao, S.J. Murcha, O'Briena Robert, P.K. Saxena, "Rapid method for accurate analysis of melatonin, serotonin and auxin in plant samples using liquid chromatography–tandem mass spectrometry", J. Chromatogr. A 1134 (2006) 333–337.

[43]   X. Huang, G. Mazza, "Simultaneous analysis of serotonin, melatonin, piceid and resveratrol in fruits using liquid chromatography tandem mass spectrometry", J. Chromatogr. A 1218 (2011) 3890–3899.

[44]   K. Eriksson, A. Ostin, J.O. Lev, "Quantification of melatonin in human saliva by liquid chromatography–tandem mass spectrometry using stable isotope dilution", J. Chromtogr. B 794 (2003) 115–123.

[45]   I.M. Young, R.M. Leone, R.E. Silman, "The mass spectrometric analysis of the urinary metabolites of melatonin and its deuterated analogues, confirming their identity as N-acetylserotonin and 6-hydroxymelatonin", Biol. Mass Spectrom. 12 (1985) 319–337.

[46]   A.A. Gazy, H.H. Abdine, M.H. Abdel-Hay, "Colorimetric and spectrofluorimetric methods for the determination of melatonin in tablets and serum", Spectrosc. Lett. 31(1) (1998) 177–197.

[47]   A.S. Amin, M. Zaky, A.M. El-Beshbeshy, "Colorimetric estimation of melatonin in pharmaceutical formulations", Mikrochim. Acta 35 (2000) 81–85.

[48]   E.A.de Almeida, P. di Mascio, T. Harumi, D.W. Spence, A. Moscovitch, R. Hardeland, D.P. Cardinali, G. M. Brown, S. R. Pandi-Perumal, "Measurement of melatonin in body fluids: Standards, protocols and procedures", Childs Nerv. Syst. 27 (2011) 879–891.
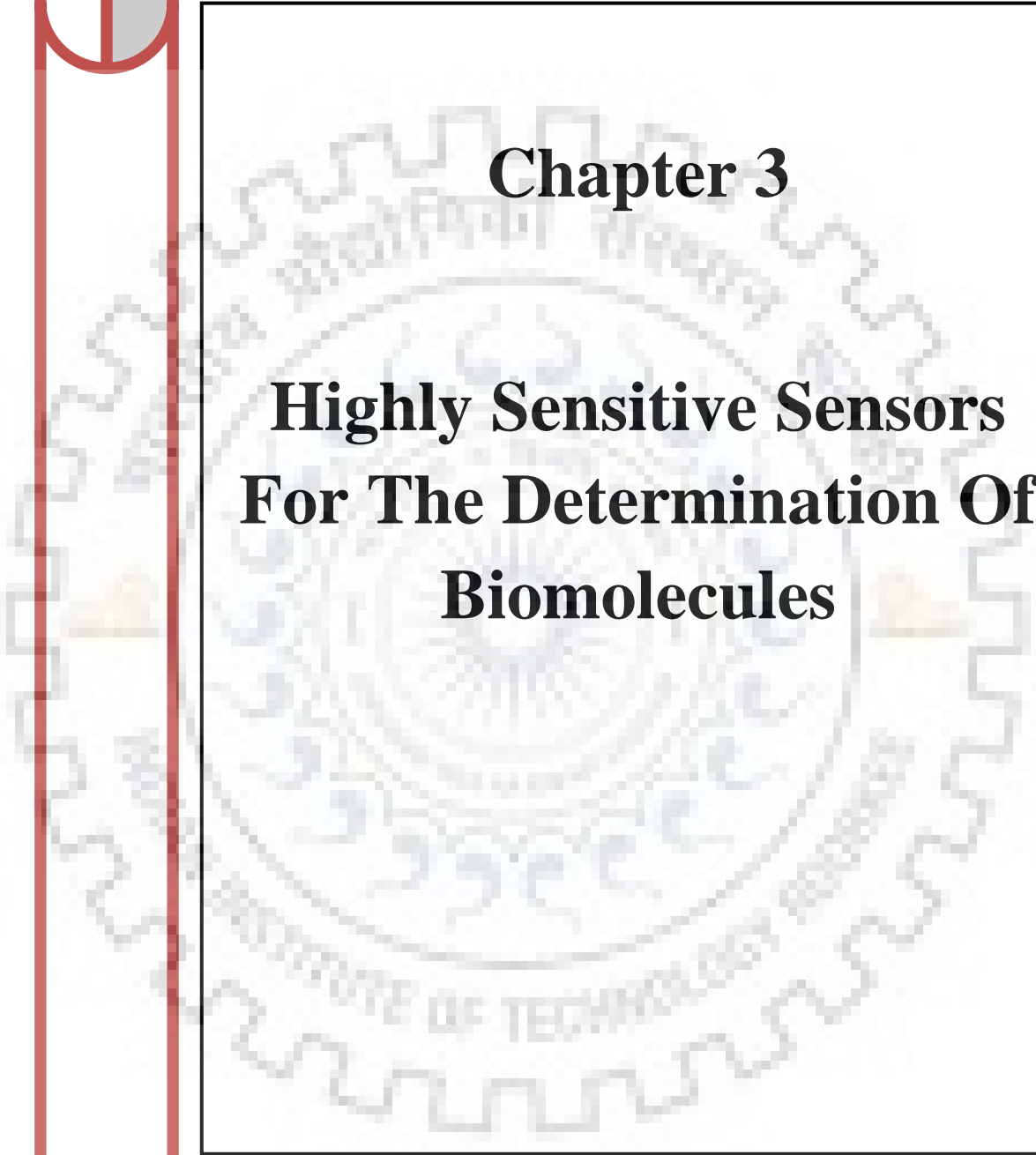
[49]   O. Vakkuri, J. Leppaluoto, O. Vuolteenaho, "Development and validation of a melatonin radioimmunoassay using radioiodinated melatonin as tracer", Acta Endocrinol. 106 (1984) 152–157.

[50]   S. Chegini, B.E. Hofmann, A. Kaider, F. Waldhauser, "Direct enzyme-linked immunosorbent assay and a radioimmunoassay for melatonin compared", Am. Assoc. Clin. Chem. 41 (1995) 381–386.

[51]   S.M. Yie, E. Johansson, G.M. Brown, "Competitive solid-phase enzyme immunoassay for melatonin in human and rat serum and rat pineal gland", Am. Assoc. Clin. Chem. 39 (1993) 2322–2325.

[52]   J. Lu, C. Lau, M.K. Lee, M. Kai, "Simple and convenient chemiluminescence method for the determination of melatonin", Anal. Chim. Acta 455 (2002) 193–198.

[53]   B. Agrawal, P. Chandra, R.N. Goyal, Y.B. Shim, "Detection of norfloxacin and monitoring its effect on caffeine catabolism in urine samples", Biosens. Bioelectron. 47 (2013) 307–312.

[54]   A. Levent, "Electrochemical determination of melatonin hormone using a boron-doped diamond electrode", Diamond Relat. Mater. 21 (2012) 114–119.

[55]   A. Radi, G.E. Bekhiet, "Voltammetry of melatonin at carbon electrodes and determination in capsules", Bioelectrochem. Bioenerg. 45 (1998) 275–279.

[56]   G. Chen, X. Ding, Z. Cao, J. Ye, "Determination of melatonin and pyridoxine in pharmaceutical preparations for health-caring purposes by capillary electrophoresis with electrochemical detection", Anal. Chim. Acta 408 (2000) 249–256.

[57]   T.H. Tsai, Y.C. Huang, S.M. Chen, "Manganese hexacyanoferrate with poly(3,4-ethylenedioxythiophene) hybrid film modified electrode for the determination of catechin and melatonin", Int. J. Electrochem. Sci. 6 (2011) 3238–3253.

[58]   Amr L. Saber, "Novel potentiometric sensors for determination of melatonin and oxomemazine in biological samples and in pharmaceutical formulations", Electroanalysis 22 (2010) 2997–3002.

[59]   B. Uslu, B.T. Demircigil, S.A. Ozkan, Z. Sentürk, H.Y. Aboul-Enein, "Simultaneous determination of melatonin and pyridoxine in tablet formulations by differential pulse voltammetry", Die Pharmazie 56(12) (2001) 938–942.

[60]   B. Devadas, R. Madhu, S.M. Chen, V. Veeramani, M. Rajkuma, "Electrochemical preparation of a reduced graphene oxide/ruthenium oxide modified electrode and its

application to the simultaneous determination of serotonin and melatonin", Sci. Adv. Mate. 6 (2014) 1–9.

[61] P. Gupta, R.N. Goyal, "Graphene and co-polymer composite based molecularly imprinted sensor for ultratrace determination of melatonin in human biological fluids", RSC Adv. 5 (2015) 40444–40454.

[62] G.D. Christian, W.C. Purdy, "The residual current in orthophosphate medium", J. Electroanal. Chem. 3 (1962) 363–367.

[63] P. Gupta, R.N. Goyal, "Sensitive determination of domperidone in biological fluids using a conductive polymer modified glassy carbon electrode", Electrochim. Acta 151 (2015) 1–7.

[64] Rosy, R.N. Goyal, "Estimation of amoxicillin in presence of high concentration of uric acid and other urinary metabolites using an unmodified pyrolytic graphite sensor", J. Electrochem. Soc. 162(1) (2015) G8–G13.

[65] G.C. Marjanovic, M. Trchova, P. Matejka, P. Holler, B. Marjanovic, I. Juranic, "Electrochemical oxidative polymerization of sodium 4-amino-3-hydroxynaphthalene-1 sulfonate and structural characterization of polymeric products", React. Funct. Polym. 66 (2006) 1670–1683.

[66] P. Santhosh, K.M. Manesh, S. Uthayakumar, S. Komathi, A.I. Gopalan, K.P. Lee, "Fabrication of enzymatic glucose biosensor based on palladium nanoparticles dispersed onto poly(3,4-ethylenedioxythiophene) nanofibers", Bioelectrochem. 75 (2009) 61–66.

[67] S. Thiagarajan, R.F. Yang, S.M. Chen, "Palladium nanoparticles modified electrode for the selective detection of catecholamine neurotransmitters in presence of ascorbic acid", Bioelectrochem. 75 (2009) 163–169.

[68] N.F. Atta, M.F. El-Kady, A. Galal, "Simultaneous determination of catecholamines, uric acid and ascorbic acid at physiological levels using poly(N-methylpyrrole)/Pd-nanoclusters sensor", Anal. Biochem. 400 (2010) 78–88.

Chapter 3

Highly Sensitive Sensors For The Determination Of Biomolecules

3.1 INTRODUCTION

Biomolecules are organic molecules which naturally occur in the living organism and are necessary for the existence of all known forms of life. There are various types of biomolecules, such as genetic materials (molecules involved heredity), lipids (energy providing molecules and building blocks of biological membranes), hormones (regulate the metabolic process and several other roles in organism), neurotransmitters (sent over synapses between neurons), carbohydrates (provision of energy and storage of energy), etc. Amino acids and proteins also play an important role in the living organisms, and contribute in the synthesis of proteins, in the genetic code and as biomolecules that involve in other processes, like transport of lipids. Neurotransmitters and hormones are different chemical messengers however, some molecules act as hormone as well as neurotransmitter, viz., norepinephrine. Neurotransmitters are involved in various biological activities and facilitate the nerve impulse transmission. Also, these biomolecules can be used as biomarkers for the diagnosis of various diseases [1-4]. The analysis of biomolecules is important in the fields, like clinical diagnostics, environmental monitoring, food safety analysis and pharmaceutical industries [1].

Purines and their derivatives are involved in nucleic acids and are excreted by the human system through biological fluids such as blood urine. Purine nucleosides are well-known for their metabolic and biological effects in human system. Their determination has attracted considerable attention in the field of biomedical research owing to their importance in normal cellular functions. The importance of such determinations is due to the fact that even small changes in their concentration leads to various diseases [5]. 8-Hydroxydeoxyguanosine (8-OHdG) is an oxidized product of deoxyguanosine residues in DNA, produced by the attack of reactive oxygen at C-8 position of guanine.

Indoles are aromatic heterocyclic compounds in which a benzene ring is fused with pyrrole unit. They have been found in natural environment and can also be produced by bacteria. Substituted indoles have the capability of binding with high affinity to multiple receptors.
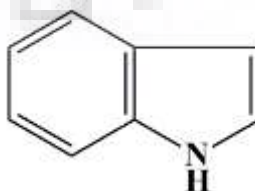
Indole

Hence, many of the indole derivatives act neurotransmitters. The presence of amino acid in indoles makes it an important molecule as neurotransmitter, hormone, indole alkaloid etc. 5-Hyroxytryptophan is a substituted derivative of indole. It is a naturally occurring amino acid and an important intermediate for the biosynthesis of an important neurotransmitter, Serotonin. Serotonin or 5-hydroxytryptamine is a monoamine neurotransmitter, widely distributed in the brain and plays a significant role in various pharmacological, physical and biological processes. 5-Hyroxytryptophan excretes primarily through urine. It's quantification is important during alcohol intoxication, when metabolism of serotonin shifts from 5-hydroxyindole-3-acetic acid to 5-hydroxytryptophan due to inhibition of aldehyde dehydrogenase.
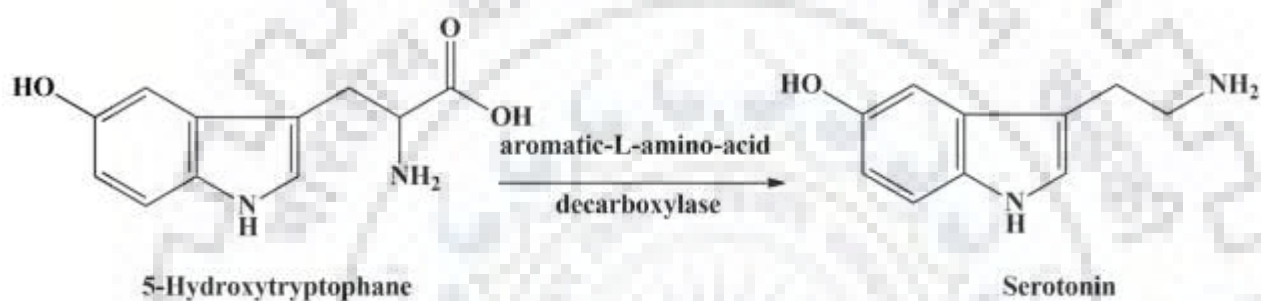
Histamine is a biogenic amine present in various food products and also regulate the physiological functions in the gut and acts as a neurotransmitter for brain, uterus and spinal cord. It is derived by the decarboxylation of histidine by the enzyme L-histidine decarboxylase.

This chapter deals with fabrications, characterization and use of three different kinds of modified sensors. For a clear presentation, the chapter has been divided into three sections: the first section of this chapter deals with the conducting polymer based Molecularly Imprinted sensor for the determination of 8-OHdG. The second section of this chapter is dedicated to the estimation of 5-Hydroxytryptophan in biological fluids. In this section, the composite effect of nano palladium and multi walled carbon nanotubes (PdNP:MWCNT) has been used to fabricate the sensor, while, the third section of this chapter has been devoted to the graphene nanoribbons and silver nanoparticles composite (GNRs-AgNPs) based sensor for estimating histamine; a neurotransmitter.

Section A: A Molecularly Imprinted sensor for determination of 8-Hydroxydeoxyguanosine.

Section B: Nano palladium decorated carbon nanotube modified sensor for the sensitive determination of 5-Hydroxytryptophan.

Section C: Graphene nanoribbons–silver nanoparticles (GNRs-AgNPs) composite modified sensor for estimation of Histamine; an important biogenic amine.

SECTION A: A MOLECULARLY IMPRINTED SENSOR FOR DETERMINATION OF 8-HYDROXYDEOXYGUANOSINE

In recent years, the molecular imprinted polymers (MIPs) have acquired the interest of the scientific community in the sensor development because of their extraordinary sensitivity and long-term stability. In the place of biological receptors, such as antibody–antigen and enzymes, MIPs bear various potential advantages like superior stability, durability, affordability and easy preparation [6-7]. These properties attribute them an efficient and attractive creature in the shape of artificial and robust recognition materials. MIPs are considered as an efficient access to develop specific cavities in the polymer matrix, introduced by polymerization of monomer in the presence of template molecules. Later on, the removal of the template molecules from the polymer matrix, leaves the permanent 'memory' of the template. The template molecules can easily reach to the imprinting site in rebinding step [8]. Several methods have been developed for the preparation of MIP films such as drop coating method [9], electropolymerization [10] and composite membrane techniques [11]. Among these methods electropolymerization has more advantages over others in the generation of rigid, uniform, compact and stable MIP film with good adherence onto sensor surface of different configuration and size. Also, the thickness of the MIP film and morphology can also be controlled by using electropolymerization methods [12-13]. Hence, electropolymerization technique has been widely used for constructing the MIP sensor.

Conducting polymers have received extensive interest due to their unique application in the field of chemical and biological sensors. The electro-oxidative polymerization of 1,5-diaminonaphthalene (1,5-DAN) has received much attention because of its chelating and reduction properties as the polymer chain contains electron donating amino groups [14-15]. Glutaraldehyde (GA) is a bi-functional cross-linking agent, most effectively used to immobilize the proteins and amino functional groups containing polymers. GA reacts rapidly with amine functional groups at around neutral medium and most frequently used in the protein immobilization. It is also a thermally and chemically stable crosslinking reagent [16-17]. The amino functional groups of 1,5-DAN can bind with –CHO groups of GA. The template molecules were polymerized with melamine (MM) on the GA/1,5-DAN modified edge plane pyrolytic graphite (EPPG) surface because melamine and template molecules contain amino functional groups, which can establish the covalent and hydrogen bond with the surface molecules, and template molecules are locked between the sensing surface of the electrode and MM films.

8-Hydroxydeoxyguanosine (*8-OHdG* or *8-oxo-7,8-dihydro-2'-deoxyguanosine*) is an oxidized product of the deoxyguanosine residues in DNA, which is produced by the attack of reactive oxygen species (like hydroxyl radical) at the C-8 position of guanine [18-19]. The level of the 8-OHdG in the urine is directly associated with the total DNA damage in the body and its level in the target tissues are also correlated with various cancers in animal models [18, 20-23]. The urinary 8-OHdG is known as a potential contributor for risk assessment in certain disorders related to carcinogenesis, degenerative diseases, aging, cardiovascular disease, malignant tumors and environmental health [24-25]. The increase in 8-OHdG in serum has been found to increase in the patients with advanced chronic kidney diseases [26]. Hence, it has an impact on analytical science to develop a sensitive, fast, reproducible and selective method for the determination of 8-OHdG. Various analytical methods such as HPLC with electrochemical detection (HPLC-ED) [21], capillary electrophoresis electrochemical detection (CE-ED) [20], Gas Chromatography-Mass Spectrometry (GC-MS) [27], etc. have been used for the determination of 8-OHdG in urine samples. However, most of these techniques suffer from the basic limitation like expensive instrumentation with sophisticated process, large solvent requirement, and complicated sample pre-treatment. While the electrochemical and voltammetric techniques attract attention due to the simple, cost effective, reproducible, rapid and sensitive analysis of biomolecules, drug and electro-active compounds in comparison to the conventional analytical methods. Many surface modified or unmodified electrodes have been used for the analysis of 8-OHdG [28-35]. Several of these electrodes were not explored in biological fluids and demonstrated the low sensitivity and low selectivity. The electrochemical determination of 8-OHdG using composite of graphene oxide and single walled carbon nanotube modified glassy carbon electrode has also been reported by our laboratory [35]. However, only recovery after spinking was reported for the determination of 8-OHdG in human urine samples. Thus, still a more sensitive method is required for determination of trace amount of 8-OHdG in complex matrix like urine of the patients of different diseases. Hence, a molecular imprinted sensor has been developed in the present studies for the determination of 8-OHdG and the applicability of the method is demonstrated by determining 8-OHdG in the urine sample of a renal failure patient, undergoing dialysis once in a week.

In this section, we report a cost effective, sensitive and selective approach based on MIP for the determination of 8-OHdG. The 1,5-DAN and GA used as supporting materials, while melamine monomer has been used for constructing the MIP film on the GA/1,5-DAN modified sensor

surface. The recognition properties of the MIP sensor (EPPG/1,5-DAN/GA/MIP) are highly attractive for the 8-OHdG.

3.2. EXPERIMENTAL

3.2.1 Materials and instrumentation

8-OHdG, uric acid (UA), ascorbic acid (AA), hypoxanthine (HX), xanthine (X), glutaraldehyde (GA), 1,5-diaminonaphthalene (1,5-DAN) and melamine (MM) were purchased from Sigma Aldrich (USA). Potassium ferricyanide ($K_3[Fe(CN)_6]$) and Potassium chloride (KCl) were purchased from E. Merck (India). The pieces of edge plane pyrolytic graphite electrode (EPPG) were obtained from Pfizer, USA as a gift. The phosphate buffer solution of pH 7.2 was prepared using the method of Christian and Purdy [36].

Voltammetric studies were performed by using an Epsilon EC-USB voltammetric analyzer (BAS, West Lafayette, USA). The voltammetric and electrochemical impedance studies were carried out by using the three electrode system in a single glass cell equipped with Ag/AgCl as reference electrode, imprinted sensor as working electrode and platinum wire as auxiliary electrode. Field Emission Scanning Electron Microscopy (FE-SEM) has been used to investigate the changes of the surface morphology of the modified and unmodified sensor by using Ziess ultra plus 55 instrument. Using a Shimadzu spectrophotometer (model UV-2450) UV-vis studies were performed in order to investigate the removal of the template molecule (8-OHdG) from the surface of the MIP sensor. To examine the impact of the modification on the charge transfer resistance, Electrochemical Impedance Spectroscopy (EIS) studies were performed at different stages of modification using Versastat 3 galvanostat (Princeton Applied Research, USA).

3.2.2 Fabrication of modified sensors

Prior to modification, the surface of EPPG was mechanically scratched on the emery paper (P-400) and washed well with double distilled water. Firstly, the electro-polymerization of 1,5-DAN was carried out by transversing the potential range -0.1 to 1.0 V at 100 mV/s sweep rate, in 4 mL of 2 mM 1,5-DAN solution (prepared in 1M $HClO_4$) for 15 optimised cyclic voltammetric scans. The obtained film was rinsed with double distilled water and dried at room temperature. Secondly, 1,5-DAN modified sensor was immersed in the glutaraldehyde solution for 30 min to grow the glutaraldehyde film. After that the sensor was kept at the room temperature for complete drying. Thirdly, the electro-polymerization of melamine with 8-OHdG as template was carried out

on the surface of GA/1,5-DAN modified EPPG. For this purpose, 1:2 mixture of 1 mL of 2 mM solution of melamine (prepared in 0.1 M H_2SO_4) and 2 mL of 8-OHdG was taken in an electrochemical cell and electro-polymerized in the potential range between 0 to 1600 mV at 100 mV/s scan rate for optimized 20 scans [37]. The obtained film was washed with double distilled water so as to remove unreactive monomer from the surface of the sensor. Finally, the modified sensor was cycled in 0.1M H_2SO_4 solution between -1000 to +1000 mV at 100 mV/s scan rate for 25 scans in order to release the template molecules. A non-imprinted polymer (NIP) sensor was also prepared under identical conditions except that the electro-polymerization in the third step was carried out in the absence of the template molecules.

3.2.3 Voltammetric procedures and sample preparation

Voltammetric technique has been used to investigate the electrochemical oxidation of the 8-OHdG. The stock solution of 8-OHdG (1mM) solution was prepared by dissolving the required amount of the 8-OHdG in double distilled water. To prepare the test solution, the required volume of the 8-OHdG stock solution was taken in a glass cell, having 2 mL of phosphate buffer of pH 7.2 and the total volume was made 4 ml using double distilled water.

The optimized operating parameters for square wave voltammetry (SWV) were initial potential (E_i): 100 mV, the final potential (E_f): 1200 mV, square wave amplitude (E_{sw}): 25 mV, square wave frequency (f): 15 Hz, potential step (E): 4 mV. Similarly, the optimum operating condition for cyclic voltammetry (CV) were initial potential (E_i): 0 mV, switching potential (E): 1000 mV, the final potential (E_f): 0 mV and scan rate (v) 100 mV/s. To remove dissolved oxygen from the test solutions, nitrogen gas was purged for 10–12 min before recording each voltammogram. The template molecules were removed from the sensing surface of the imprinted sensor after recording the voltammogram by applying a potential of -400 mV for 150 s in the blank solution.

3.2.4 Biological samples

To examine the 8-OHdG content in the urine sample from a patient suffering from renal failure (Male, age 65, 95 kg), the first urine of the morning was obtained from the Institute hospital of I.I.T. Roorkee after the permission of Ethical Clearance Committee. The patient was undergoing dialysis once in a week. The collected urine sample was diluted four times by using a phosphate

buffer solution of pH 7.2 and the amount of 8-OHdG was determined using standard addition method and a calibration curve was plotted.

For the recovery studies the urine samples of two healthy volunteers (Male, age 26 and Female, age 22) were collected from the Institute hospital of I.I.T. Roorkee (Ethical Committee Permission No. BIOTECH/IHEC/AP/15/1). The obtained urine samples were filtered by using the Whatman 42 filter paper and the filtrate was diluted two times by using a phosphate buffer solution of pH 7.2 in order to remove the complexity of the urine. The test samples for recovery study were prepared by spiking the diluted urine samples with required amount of the 8-OHdG.

3.3 RESULT AND DISCUSSION

3.3.1 Characterization of nano composite

The FE-SEM micrographs were recorded in order to study the changes occurring during the fabrication of imprinted sensing surface. **Fig. 3.1** clearly shows the difference in the morphology of the imprinted sensor in comparison to the NIP/EPPG. **Fig. 3.1(A)** and **3.1 (B)**, shows cubical, crystalline structures for the melamine, which are distributed evenly at the GA/1,5-DAN modified EPPG surface. These nano cubes are expected to provide increased effective surface area and roughness and affect the sensing properties of sensor.
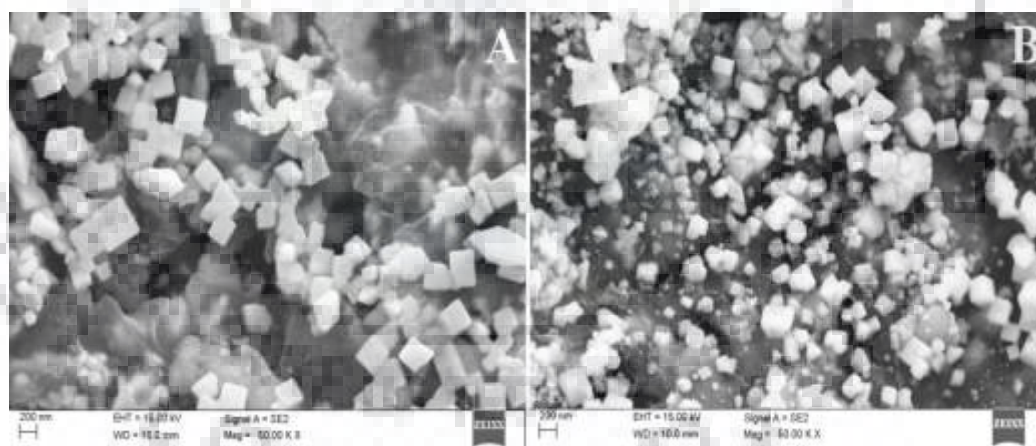
Fig. 3.1: FE-SEM images demonstrating surface morphology of (A) NIP/EPPG, (B) MIP/EPPG.

EIS was employed to examine the changes in the impedance after surface modification and for characterizing the electrochemical performance at different steps of the modification protocol. The experiment was carried out in the 1:1 solution of 5 mM $K_3[Fe(CN)_6]$ and 0.1 M KCl over the frequency range of 1000 kHz to 10 mHz. Randle's equivalent circuit **(inset Fig. 3.2)** was used to

obtain the data of different stages of modification. A Nyquist plot consists two portions, one is semi-circle portion indicating R_{CT} values and other one is a linear portion, which represents the mass transfer effects at lower frequency [38]. **Fig. 3.2** presents the results obtained in the impedance studies corresponding to the unmodified EPPG, molecularly imprinted EPPG, non-imprinted EPPG and MIP in the presence of the template surfaces. The R_{CT} values were calculated by fitting the Randle's circuit and the values observed for the unmodified EPPG, MIP/EPPG without template, NIP/EPPG and MIP bound to template were 1000 Ω, 734 Ω, 576 Ω and 504 Ω respectively. From the figure, it can be seen that the lowest semicircle diameter was observed for MIP in the presence of the template molecules indicating the special affinity of the recognition sites for the template molecules. However, the MIP exhibited higher R_{CT} values in comparison to the NIP, which may be attributed to the absence of cavities in NIP film that resulted in continuous coating of the conducting polymer on the sensor surface whereas, due to the presence of cavities in MIP film, a discontinuous surface of conducting MM film was obtained. This resulted a higher resistance to the charge transfer.
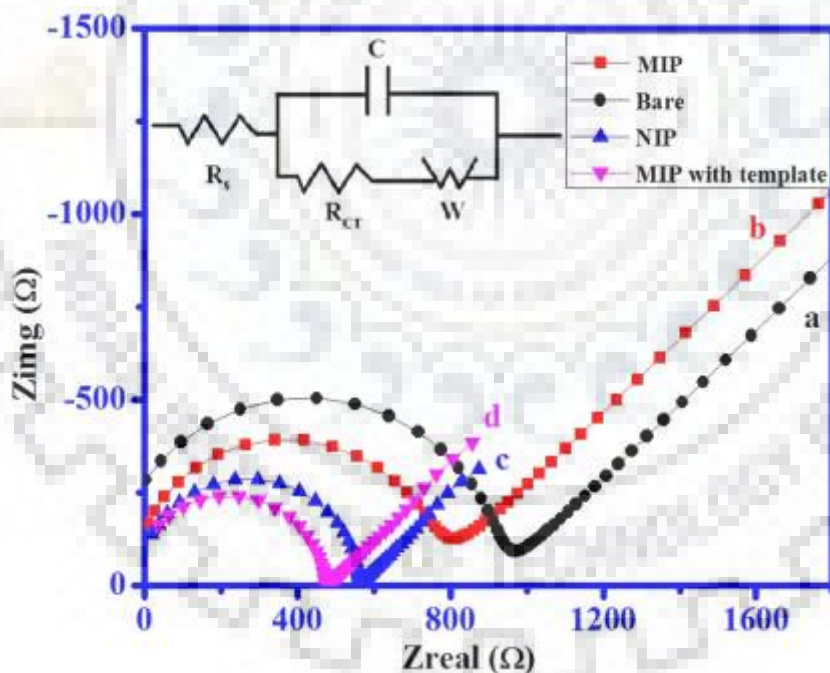
Fig. 3.2: Typical Nyquist plot observed for (a) unmodified/EPPG, (b) MIP/EPPG, (c) NIP/EPPG and (d) MIP with template during the electrochemical impedance spectroscopy in 1:1 mixture of 5 mM $K_3Fe(CN)_6$ and 0.1 M KCl solution over the frequency range 1000 kHz to 1 mHz.

3.3.2 Incubation time and removal of template from the MIP sensor

　　　　Incubation time plays an important role in enhancing the sensitivity of a MIP sensor. The interaction between imprinted film and analyte molecules was evaluated by incubating 1 μM concentration of 8-OHdG in phosphate buffer (pH 7.2) solution for 5 to 35 min. and current response was measured.　It was found that the peak current increased with increasing incubation time till 20 min and then became constant due to the saturation of all the active molecular recognition sites **Fig. 3.3**. Hence, the incubation time was used as 20 min for subsequent studies.
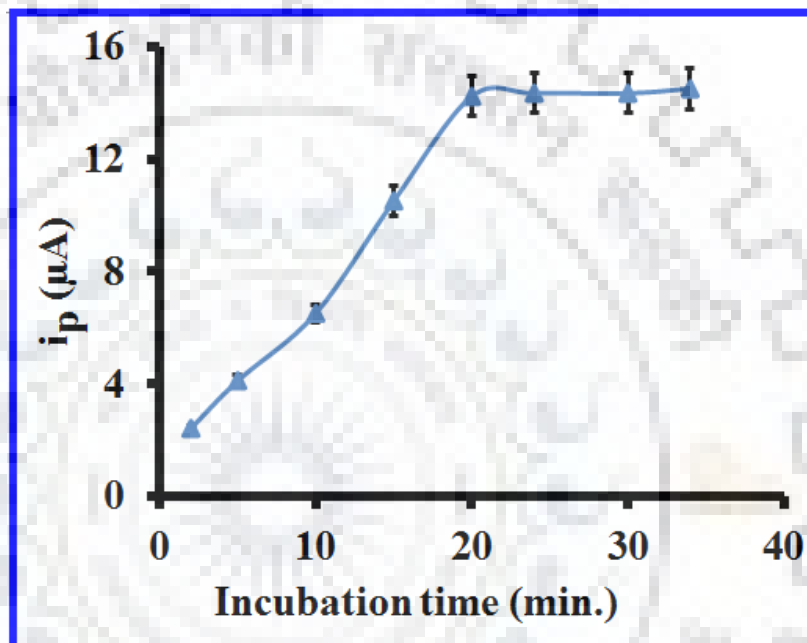
Fig. 3.3: Effect of incubation time on the anodic peak current response of 1μM 8-OHdG observed using the imprinted sensor at pH 7.2.
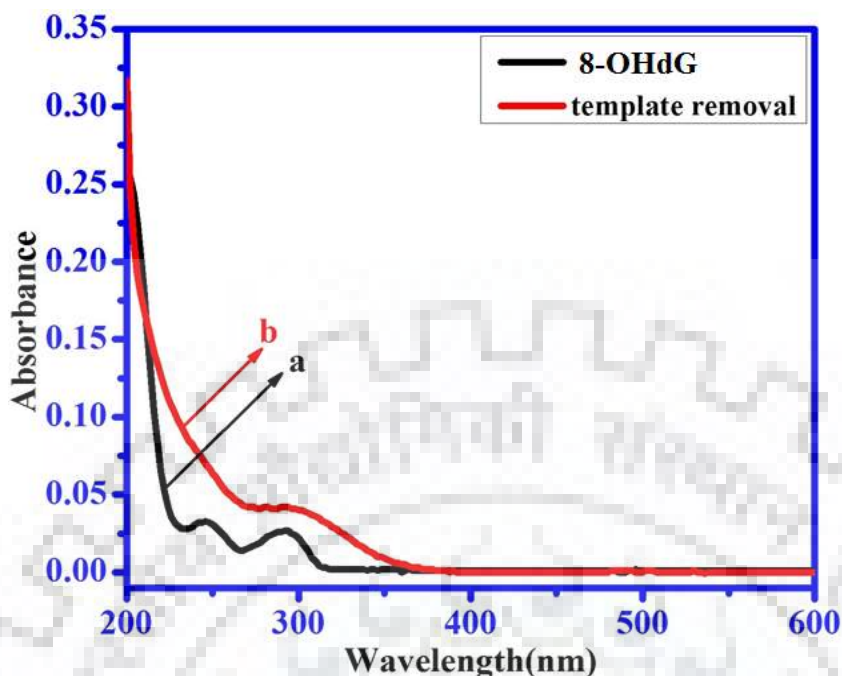
Fig. 3.4: UV-vis absorption spectrum for (a) 4μM 8-OHdG solution and (b) removal of template molecules in the 0.5M H_2SO_4.

Similarly, In order to confirm the removal of template molecules from the sensor surface, UV-visible spectrum was recorded in the H_2SO_4 solution in which template molecules were removed by the afore mentioned procedure. The obtained spectrum is shown in Fig. 3.4 (b), and exhibits two bands at 245 nm and 294 nm. these bands were essentially similar to the bands exhibited by the pure solution of 8-OHdG (Fig. 3.4 (a)) [34]. Thus, the two UV spectra confirmed the successful removal of the template molecules at the imprinted sensor in H_2SO_4 solution in between the desire potential range.

3.3.3 Cyclic Voltammetry

The cyclic voltammetric studies are commonly performed for exploring the redox behavior of the electro-active species and to examine the nature of electrochemical reactions. For exploring the electrochemical characteristics of 8-OHdG, cyclic voltammograms of 1μM 8-OHdG were recorded at MIP/EPPG and NIP/EPPG sensors in the phosphate buffer of pH 7.2 at scan rate of 100 mV/s. A single irreversible oxidation peak was observed for 8-OHdG at both the sensing surfaces. A comparison of voltammograms has been presented in **Fig. 3.5**. A well defined oxidation peak is observed at the imprinted sensor in comparison to the NIP/EPPG sensor at less

positive potentials. The large anodic peak current at imprinted sensor represents the higher sensitivity of the sensing surface towards the oxidation of 8-OHdG.
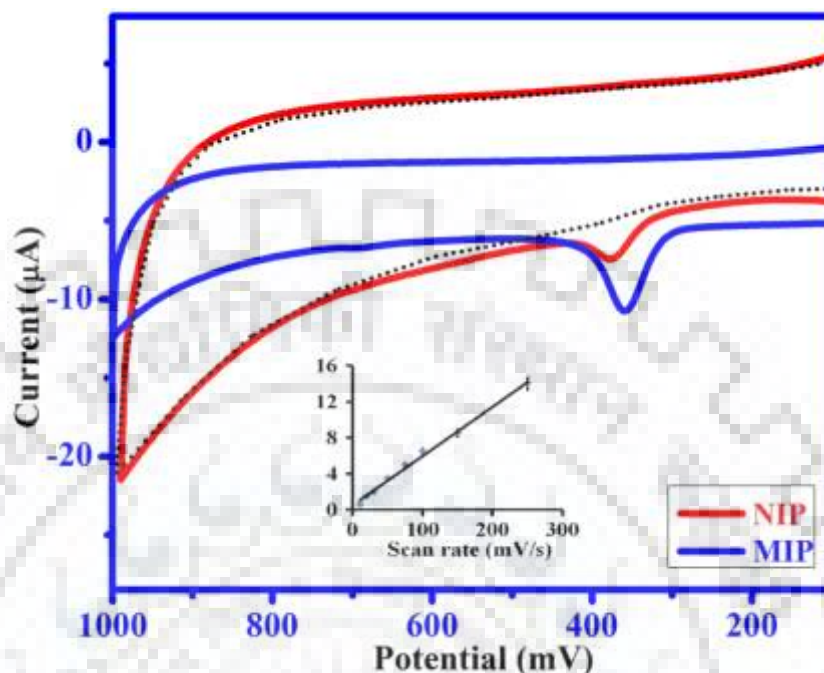
Fig. 3.5: Comparative cyclic voltammograms corresponding to 1 μM 8-OHdG in phosphate buffer of pH 7.2 at 100 mV/s scan rate using (A) NIP/EPPG and (B) MIP/EPPG.

To ascertain the nature of the electron transfer process at the MIP sensor, scan rate study was performed for 1μM 8-OHdG in the range of 10–250 mV/s. It was found that peak current (i_p) of 8-OHdG was increased with increasing the sweep rate (v). The linear relation between i_p and v can be expressed by the relation (**Inset Fig. 3.5**);

$$i_p = 0.0547\ v + 0.5167,\ R^2 = 0.994$$

where, i_p is the oxidation peak current in μA, v is the sweep rate in mV/s and R^2 is correlation coefficient. The linear plot between i_p vs. v, indicates that the oxidation of 8-OHdG at imprinted sensor is adsorption controlled, which is further confirmed by the dependence of log i_p on log v. The plot between log i_p and log v was linear and the dependence can be expressed by the equation;

$$\log i_p = 0.9521 \log v - 1.109,\ R^2 = 0.992$$

The slope value (d log i_p)/ (d log v) near to ~1 for log i_p vs. log v plot further confirmed that the electron transfer process for oxidation of 8-OHdG proceeded by an adsorption controlled pathway [34,39].

3.3.4 Square Wave Voltammetry

The detailed electrochemical study of the 8-OHdG was carried out by using square wave voltammetry (SWV). To analyze the extent of electro-catalytic behavior of imprinted sensor, square wave voltammograms were recorded for 0.5 µM 8-OHdG solutions in pH 7.2 phosphate buffer using unmodified EPPG, 1,5-DAN/EPPG, GA/1,5-DAN/EPPG, NIP/EPPG and MIP/EPPG sensors as shown in **Fig. 3.6 (A)**. A weak anodic peak for the electrochemical oxidation of 8-OHdG was observed at bare EPPG sensor, whereas, at MIP/EPPG a sharp anodic peak at ~339 mV with the highest peak current (i_p) as demonstrated in **Fig. 3.6 (A)** was noticed. In addition, no peak was noticed, if the voltammogram is extended for the reverse direction. Since, the best response for the oxidation of the 8-OHdG was obtained at MIP/EPPG, hence, further studies were performed by using this imprinted sensor. **Fig. 3.6 (B)** demonstrates the oxidation response of 0.5 µM 8-OHdG at imprinted sensor in the first scan and second scan. It can be clearly seen that in the first scan oxidation of 8-OHdG takes place however, in the second scan no oxidation peak of 8-OHdG was observed. This clearly demonstrates that the oxidation of only entrapped 8-OHdG occurs at the MIP/EPPG surface.
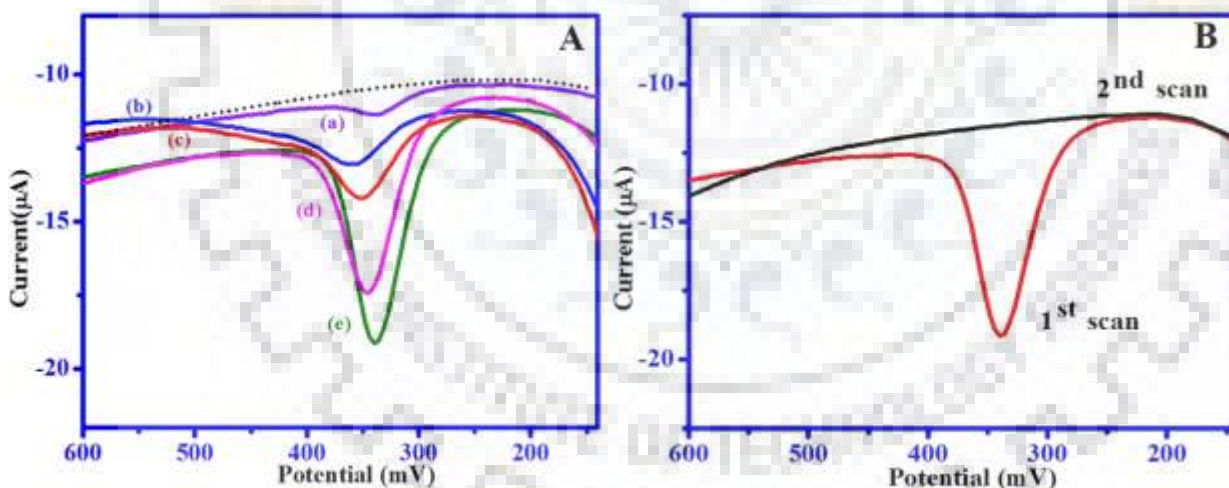
Fig. 3.6: A) Comparative SW voltammograms recorded for 0.5 µM 8-OHdG at pH 7.2 phosphate buffer at (a) unmodified EPPG, (b) 1,5-DAN/EPPG, (c) GA/1,5-DAN/EPPG, (d) NIP/EPPG and (e) MIP/EPPG sensors. The dotted line represents the background current B) Effect of number of scans on the oxidation of 8-OHdG at MIP/EPPG sensor.

3.3.4.1 Effect of pH

The effect of pH on peak potential of 8-OHdG was studied in the pH range 2.4–10.0 by using SWV at MIP sensor. The SW voltammograms were recorded at a fixed concentration of 1 µM 8-OHdG. It was observed that the anodic peak potential (E_p) of 8-OHdG shifted toward the less positive potential with the increasing pH of the supporting electrolyte as demonstrated in **Fig. 3.7**. The linear dependence of anodic peak potential (E_p) on pH can be expressed by the relation:

$$E_p = -58.07 \, (pH, 2.0–10.0) + 768.23, R^2 = 0.994$$

having a correlation coefficient of 0.994. The slope value dE_p/dpH close to 59 (~58 mV/pH) suggests that equal number of electrons and protons are involved in the electro-oxidation of 8-OHdG.
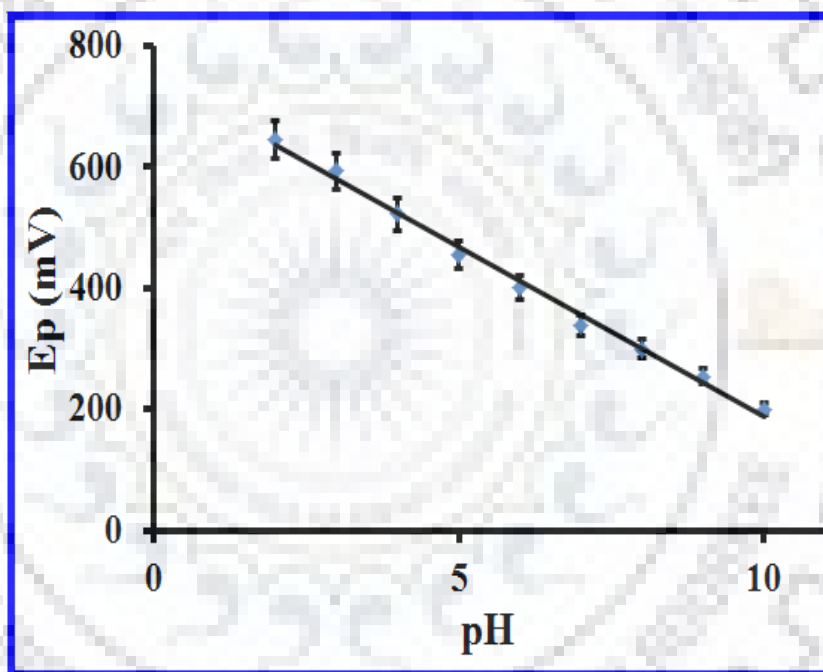
Fig. 3.7: Dependence of peak potential (E_P) on the pH of the supporting electrolyte for 1 µM 8-OHdG.

The Laviron's equation has also been used to further calculate the electron involved in the oxidation of 8-OHdG [40]. For this purpose, the oxidation of 8-OHdG was examined by using cyclic voltammetry. The cyclic voltammograms were recorded for 1 µM 8-OHdG at different scan rates (v) between 10–250 mVs^{-1}. The anodic peak potential (E_p) was found to increase with the increasing scan rate (v) for 8-OHdG and the linear variation can be expressed by the expression:

$$E_p = 52.863 \log v + 257.23, R^2 = 0.991$$

According to the Laviron's equation, the slope ($dE_P/dlog\ v$) of the plot E_p vs. log v gives the value of αn, where α is the electron transfer coefficient. For a totally irreversible electron transfer, the value of α is usually assumed as 0.5 [41]. Using the laviron equation, The number of electrons involved in the oxidation of 8-OHdG was found to be 2.23. The obtained results indicates the participation of 2e⁻, 2H⁺ in the electro-oxidation of 8-OHdG following the mechanism as shown in **Scheme 3.1** [35].
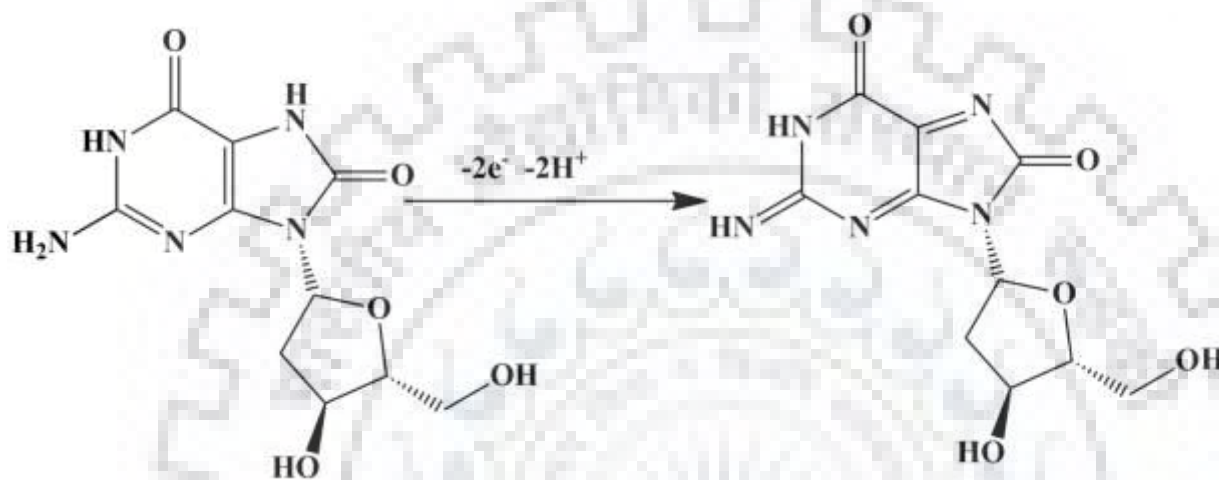
Scheme 3.1: Proposed oxidation mechanism of 8-OHdG.

3.3.4.2 Effect of frequency

The effect of frequency on the oxidation of 1µM 8-OHdG was evaluated in the range 5–75 Hz by using the SWV. It was found that with the increasing square wave frequency, the oxidation peak current of 8-OHdG increased. The linear relation of frequency (f) and peak current (i_p) was witnessed, which indicated the adsorption controlled oxidation of 8-OHdG at the imprinted sensor **(Fig. 3.8)**. The linear relation between i_p vs. f and log i_p vs. log f can be represented by the equations;

$$i_p = 1.003\,f - 3.5503, \ldots\ldots\ldots\ R^2 = 0.992$$
$$\log i_p = 1.2587 \log f - 0.4617, \ldots.. \ R^2 = 0.984$$

where, f is the square wave frequency in Hz and R^2 is correlation coefficient. The log plot having a slope ~ 1 further indicated the adsorption controlled electron transfer process in the oxidation of 8-OHdG at the imprinted sensing surface [34,39].
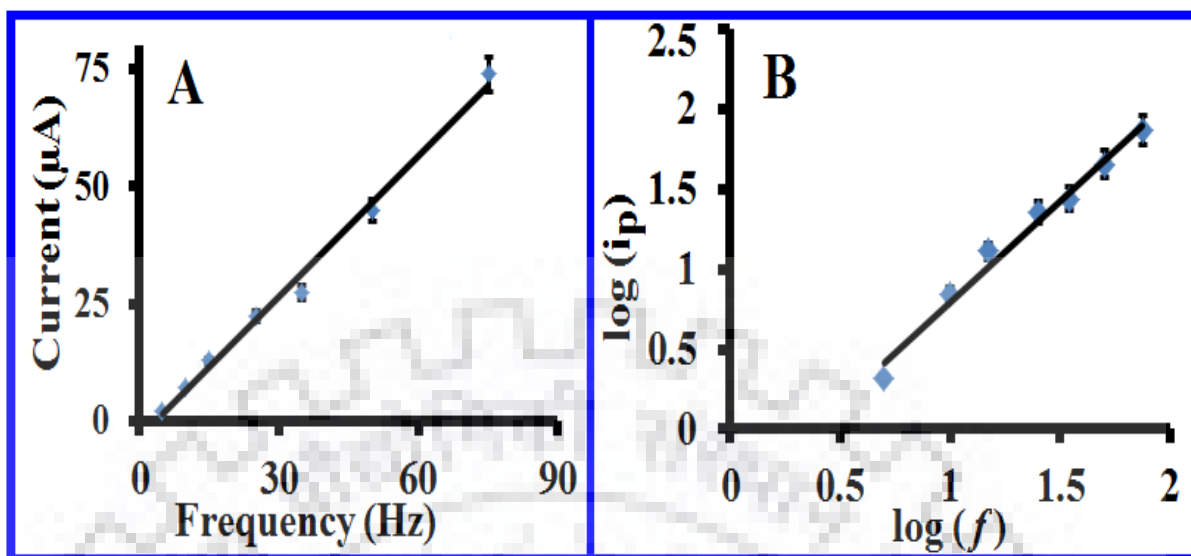
Fig. 3.8: Variation of (A) anodic peak current (i_p) with the square wave frequency (f) and (B) log (i_p) with log (f) for 1 μM 8-OHdG.

3.3.4.3 Effect of concentration

The concentration study was performed to determine the sensitivity and the limit of detection of the developed MIP sensor. The SW voltammograms were recorded for the different concentration of 8-OHdG at the unmodified EPPG and imprinted sensor at pH 7.2 phosphate buffer at the optimal SWV conditions. The optimized incubation time of 20 min was used for the concentration studies. It was found that the peak current increased with increase in concentration of 8-OHdG **(Fig 3.9)**. At unmodified EPPG, no peak was observed at concentration < 0.5 μM. The quantitative determination of 8-OHdG was carried out by measuring the oxidation peak current. A linear relation was found between peak current (i_p) and increasing concentration of the 8-OHdG in the range of 0.020–3 μM at the imprinted sensor as demonstrated in the inset of **Fig. 3.9**. The linear dependence can be expressed by the equations:

$$i_p = 10.59 \ [C, 0.02\text{-}3] + 2.2783, \ R^2 = 0.9934 \ldots\ldots\ldots\ldots\ldots \ \textbf{MIP/EPPG}$$

$$i_p = 1.0183 \ [C, 0.5\text{-}80] + 0.0702, \ R^2 = 0.9969 \ldots\ldots\ldots\ldots \ \textbf{unmodified EPPG}$$

Where, C is the concentration of 8-OHdG in μM. From the regression equations, it is observed that the imprinted sensor has ~ 10 fold higher sensitivity towards the 8-OHdG in comparison to the unmodified sensor. The analytical parameters found for the quantitative analysis of 8-OHdG at MIP/EPPG and bare EPPG sensors have been summarized in **Table 3.1**.
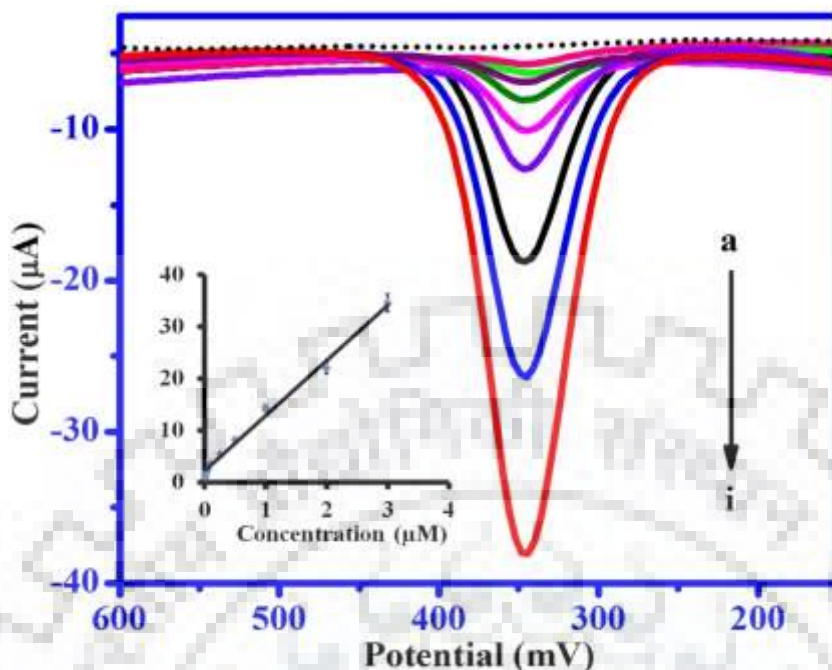
Fig. 3.9: Square wave voltammograms recorded for (a) 0.02 µM, (b) 0.03 µM, (c) 0.05 µM, (d) 0.1 µM, (e) 0.25 µM, (f) 0.5 µM, (g) 1 µM, (h) 2 µM and (i) 3 µM 8-OHdG using MIP sensor. Background current is demonstrated by the dotted line. A calibration plot of 8-OHdG concentration in inset is the range of 0.020–3 µM.

The limit of detection (L.O.D.) for 8-OHdG has been calculated by using formula $3\sigma/b$, where σ is the standard deviation of 'n' (n=3) blank voltammograms and b is the sensitivity observed in the calibration plot. The limit of detection was found to be 3 nM at MIP/EPPG.

Table 3.1: A comparison of analytical parameters obtained for the quantitative analysis of 8-OHdG at MIP/EPPG and bare EPPG.

S.No.	Validation Parameters	MIP	BARE
1	Concentration (µM)	0.020–3	0.5–80
2	Sensitivity (µA/µM)	10.67	1.0205
3	Correlation coefficient (R^2)	0.9923	0.9970
4	Standard error of slope	0.3544	0.0227
5	Standard error of intercept	0.4472	0.8164

A comparison of the L.O.D values reported in recent year for 8-OHdG are presented in **Table 3.2** and it is found that the L.O.D. value is lower than reported earlier.

Table 3.2: A comparison of limit of detection (L.O.D.) observed with the reported for 8-OHdG in recent years.

S.No.	Technique	Linear range	Detection Limit	Real Sample	Reference
1.	CE-ED	10–100 nM	20 nM	Yes	[20]
2.	MWCNT/GCE (CV)	0.08–5 µM	9 nM	No	[28]
3.	CNT-PEI/GCE (DPASV)	0.5–30 µM	100 nM	No	[29]
4.	DNA/P3MT /GCE (CV)	0.28–4.2 µM, 4.2–19.6 µM	56 nM	Yes	[30]
5.	P3MT/GCE (CV)	0.7–35 µM 35–70 µM	100 nM	Yes	[31]
6.	SWCNT-Nafion/GCE (DPV)	0.03–1.25 µM	8 nM	No	[32]
7.	SWCNT-Lysine /GCE (VAS)	0.30–10.0 µM	97 nM	No	[33]
8.	EPPG (SWV)	0.5–100 µM	28 nM	No	[34]
9.	MWCNT/ErGO/GCE (SWV)	3–75 µM	35 nM	No	[35]
10.	MIP Sensor (SWV)	0.020–3 µM	3 nM	Yes	**Present work**

CE-ED: Capillary electrophoresis with electrochemical detection; DPASV: Differential pulse anodic stripping voltammetry; PEI: Polyethylenimine; P3MT: Poly(3-methylthiophene); DVP: Differential pulse voltammetry; VAS: Voltammetric adsorptive stripping

3.3.5 Interference study

To determine the selectivity of the proposed imprinted sensor in the presence of potential interfering substances, which are normally present in the biological fluids such as UA, X, AA and HX are evaluated. For this purpose, the SW voltammetric peak current response of 1 µM 8-OHdG was recorded in the presence of 10–100 fold concentration of interfering substances. The experimental results indicate that no effect of the interfering substances was obtained on the peak current response of 8-OHdG upto 100 fold concentration as depicted in **Fig. 3.10**. These observed results expressed appreciable sensitivity and specificity of the binding cavity of the imprinted sensor towards the 8-OHdG. These results demonstrated that the imprinted sensor can be successfully applied for the quantitative analysis of 8-OHdG in biological fluids.
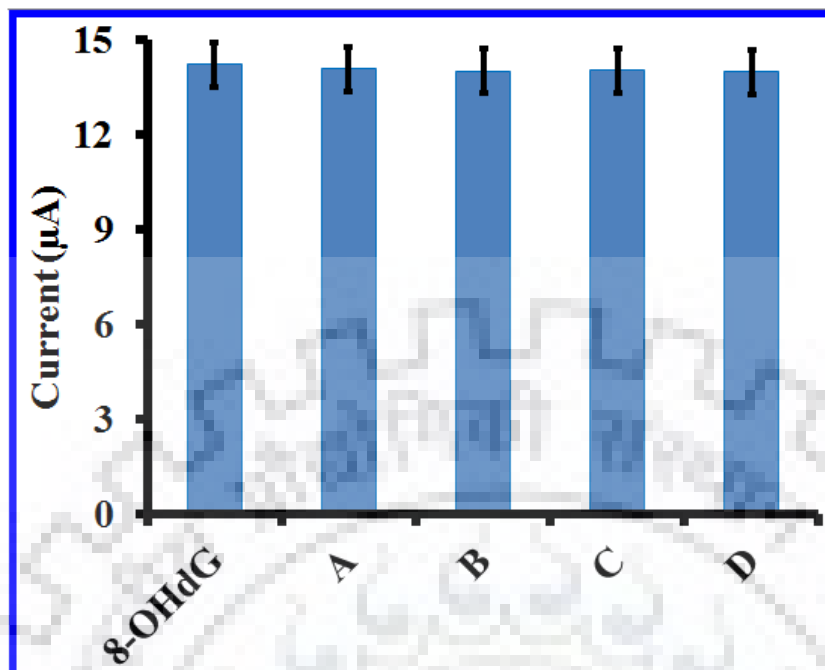
Fig. 3.10: Effect of interfering substances on the peak current of 1 μM 8-OHdG in presence of (A) 400 μM uric acid, (B) 600 μM ascorbic acid, (C) 300 μM hypoxanthine and (D) 400 μM xanthine.

3.3.6 ANALYTICAL APPLICATION

3.3.6.1 Real sample assay

In order to examine the biological applicability of the developed method, imprinted sensor has been used for the analysis of 8-OHdG content in complex matrix such as urine by using the standard addition method. The urine sample of a renal failure patient was collected for performing the biological assay. The collected urine sample was diluted four times by using a phosphate buffer solution of pH 7.2 in order to reduce the matrix complexity. The square wave voltammograms were recorded in the dilute urine sample spiked with the known 8-OHdG concentration. An oxidation peak of 8-OHdG was observed at 339 mV with a small additional peak at 304 mV corresponding to UA in the urine samples. A calibration curve was plotted between the peak current and spiked content of 8-OHdG and on extrapolating the graph the concentration of the 8-OHdG was evaluated as indicated in the **Fig. 3.11**.
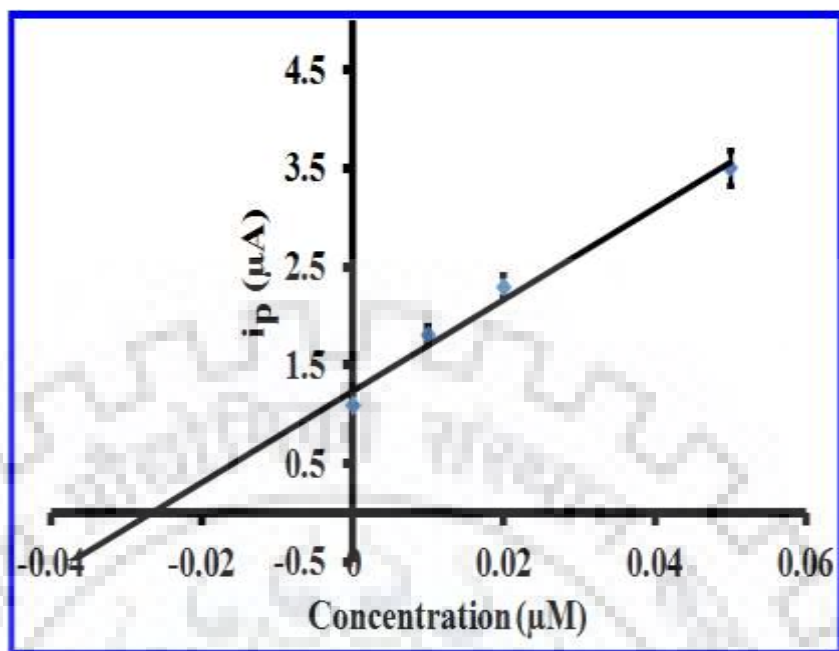
Fig. 3.11: The observed standard addition plot for 8-OHdG in urine sample of renal failure patient.

The observed results are listed in **Table 3.3**. The negative intercept value of x-axis is insignificant. By considering the dilution factor, the detected concentration of 8-OHdG was found to be 26 nM in urine sample. The lower value of RSD ($\pm$1.63%) demonstrates the good accuracy and reliability.

Table 3.3: Biological assay data for determination of 8-OHdG in urine sample of a renal failure patient.

S.No.	Spiked (µM)	Observed (µM)	Actual (µM)	Recovery %	Error%
1	0	0.026	0.026	___	___
2	0.01	0.036	0.026	100.00	0
3	0.02	0.0459	0.0259	99.61	-0.39
4	0.05	0.0761	0.0261	100.03	+0.03

*RSD for the determination was ±1.63 % for n=3
The observed values are sum of 8-OHdG present + spiked amount.
The actual amount is observed - spiked amount.

3.3.6.2 Recovery study

To examine the utility of the imprinted sensor in urine samples, 8-OHdG recovery studies were also carried out in the two healthy human urine samples. The collected urine samples were diluted two times by using pH 7.2 phosphate buffer solutions. SW voltammograms of urine samples were recorded after spiking with different concentrations of the 8-OHdG. The peak of 8-OHdG was noticed at ~*339* mV in addition to the peaks of common metabolites in urine samples. The amount of 8-OHdG was back calculated by using the peak current in the calibration equation and the results observed are presented in **Table 3.4**. The recovery data of spiked 8-OHdG were observed in the range of 98.4–101% **(Table 3.4)**. The robustness test has also been used to investigate the results obtained during recovery studies by examining the effect of pH. From this study, it was found that no significant effect was observed in the results of recovery studies by consciously altering the pH from 7.2 to 5.0.

Table 3.4: Recovery data of 8-OHdG determined in a healthy human urine samples.

S.No.	Spiked amount (µM)	Detected amount (µM)*	Recovery %	Error %
Sample 1				
1	0.05	0.0499	99.80	-0.20
2	0.10	0.101	101.00	+1.00
3	0.25	0.249	99.60	-0.40
Sample 2				
1	0.5	0.497	99.40	-0.60
2	1	1.020	100.20	+0.20
3	2	2.010	100.50	+0.50

*RSD for the determination was 1.56% for n=3

3.3.7 Stability and reproducibility of imprinted sensor

To evaluate the stability of the imprinted sensor, the peak current response at a fixed concentration of 8-OHdG (1µM) was examined in phosphate buffer of pH 7.2 by recording the four consecutive voltammograms per day for 25 days. The experimental results show the minimal variation in anodic peak current response at the imprinted sensor for first 15 days. However, the

current response dropped upto 6.2% for next 10 days, which indicated the excellent stability of the fabricated imprinted sensor.

In order to investigate the intraday reproducibility of the imprinted sensor, five successive voltammograms were recorded for 8-OHdG at an interval of 1 h, and the R.S.D was calculated. From the calculations, R.S.D came out to be 4.53% (n=5), which suggested the excellent reproducibility of the developed imprinted sensor. Hence, it is concluded that the presented imprinted sensor shows appreciable stability and reproducibility. To examine the sensor to sensor variation, five different MIP/EPPG were fabricated independently by following the same modification protocol. By using each of the imprinted sensor, voltammograms were recorded in 1 μM 8-OHdG solution and variation in the peak current response was calculated. It was observed that the current of the five imprinted sensors varied by a RSD 2.43%. Hence, it's concluded that the developed imprinted sensor shows excellent stability and reproducibility.

3.3.8. Ruggedness studies

The ruggedness test was performed to examine the problems in interlaboratory studies of the developed method. For this purpose two electrochemical systems of different laboratories were used by two different analysts. The voltammetric studies were performed at two voltammetric analyzers viz., Epsilon EC-USB and CV-50 (BAS, West Lafayette, USA) to examine the intermediate precision and performance of the MIP sensor. The obtained results of two different instruments were compared and the fluctuation in the electrochemical response at sensor was found to be < 1.6%, indicating the excellent precision of the proposed protocol. There was no significant difference in the observed recovery results from the two instruments as summarized in **Table 3.5**. Hence, MIP sensor was found to be a reliable, rugged and robust tool for the determination of 8-OHdG in the complex matrix.

Table 3.5: The Robustness and ruggedness of the MIP sensor for recovery data of 8-OHdG determination in human urine samples.

Variables	Recovery % ± R.S.D
Robustness at pH=7.2	98.72 ± 1.41
Ruggedness Analyst 1	
Instrument: Epsilon EC-USB	99.18 ± 1.12
Instrument: CV 50W	98.59 ± 1.47
Ruggedness Analyst 2	
Instrument: Epsilon EC-USB	98.26 ± 1.58
Instrument: CV 50W	99.34 ± 1.23

3.4. CONCLUSION

The proposed protocol deals with the fabrication of suitable and extremely selective imprinted sensor for monitoring of 8-OHdG in urine samples. The developed method is based on an imprinted technique in which melamine was electro-polymerized with 8-OHdG at the surface of the GA/1,5-DAN modified EPPG. The surface of the molecular imprinted sensor has been characterized using CV, SWV, FE-SEM and EIS. The proposed sensor can be successfully applied for the quantitative as well qualitative analysis of 8-OHdG. A linear relation was observed between the peak current and 8-OHdG concentration in the range of $20 \times 10^{-9} - 3 \times 10^{-6}$ M with a detection limit of 3×10^{-9} M. Such a low detection limit is sufficient for the determination of excreted 8-OHdG in the urine of patients suffering from various diseases. The fabricated sensor exhibited excellent selectivity, sensitivity, long term stability and reproducibility. Thus, it is concluded that the developed protocol can be successfully employed for the electrochemical measurement of 8-OHdG content in the urine samples and other complex biological fluids.

SECTION B: NANO PALLADIUM DECORATED CARBON NANOTUBE MODIFIED SENSOR FOR SENSITIVE DETERMINATION OF 5-HYDROXYTRYPTOPHAN

5-Hydroxy-L-tryptophan (5-HTP, *2-amino-3-(5-hydroxy-1H-indol-3-yl) propanoic acid, I*) is a naturally occurring aromatic amino acid, produced by one of the essential amino acid L-tryptophan. Its synthesis in the human system is catalyzed by the enzyme, '*tryptophan hydroxylase*', present in the serotonergic neurons. 5-HTP is an intermediate precursor in the biosynthesis of an important neurotransmitter, Serotonin (5-HT) [42-44]. It is also considered as over the counter medicine in several developed countries as a dietary supplement. Past clinical research studies have proved that 5-HTP can easily cross the blood-brain barrier and can bypass the routine rate-limiting step of 5-HT biosynthesis, leading to the abnormally increased serotonin level in the brain and central nervous system (CNS) which is responsible for many disturbed physiological conditions, like insomnia, depression, pain, sexual behavior, anxiety and temperature. [42-43,45-47]. The estimation of 5-HTP is thus directly related to the level of 5-HT and its altered concentration can result in the elevated levels of some clinically important hormones in the living body, such as prolactin and serum corticosterone [45]. It also plays a significant role in the various mental disorders and has also been employed in the effectual treatment of a number of clinical conditions, such as depression, cerebellar ataxia, fibromyalgia, chronic headaches, obesity and insomnia [42, 45-49]. 5-HTP not only maintains the serotonin level but is also used as a dietary supplement in the case of weight loss and body building [46], excessive use of which can result in extreme muscle tenderness (myalgia), blood abnormalities (eosinophilia), sexual problems, heart burns, nausea, vomiting, diarrhea etc. As a result, determination of 5-HTP in biological fluids is of prime importance. For the quantification of 5-HTP, various types of technique have been developed such as liquid chromatography–mass spectrometry (LC–MS) [50], high-performance liquid chromatography [51-52], UV-Spectrophotometry [53], fluorescence spectrometry [54], liquid chromatography–ionspray tandem mass spectrometry (LC–MS) [55], capillary electrophoresis (CE) [56] etc. However, most of these techniques suffer from disadvantages like expensive instrumental setup, sophisticated and time consuming procedure, lengthy processing of samples prior to analysis, large solvent requirement, hectic pre cleaning steps etc. due to which the interest of analytical community is shifting towards finding a more simple, accurate, sensitive and fast technique. Electrochemical methods especially voltammetry has attracted interest in the recent years as it offers a more feasible, cost-effective and selective determination of electro-active analytes [57]. Various types of the surface modified

electrodes such as Indium tin oxide/nanoscale pores sol–gel/cobalt hexacyanoferrate (ITO/npSG/CoHCF) electrode [58], RuOx/GCE [59], carbon disk electrode [60], gold modified pencil graphite electrode [61] etc. have been used to electrochemically determine 5-HTP. However, the previously reported methods have lower sensitivity, higher detection limit, small linear concentration range and complex modification procedure. Thus, fabrication of a simple sensor for assaying the trace amount of 5-HTP in biological samples has been attempted in the present section.

Recently, studies have demonstrated that due to the effective catalytic activity, unique electrical properties and biocompatibility, palladium nanoparticles can be used as modifiers for the electrode surface for the analysis of the drugs and bio-molecules [62-64]. However, the isolated nanoparticles (NPs) are unstable due to their small particle size, as a result of which they undergo agglomeration. In order to avoid the agglomeration of the NPs, a support material for the nucleation and growth can be employed, which can result in a new hybrid nanomaterial [65-66]. Among the support materials, carbon nanotubes (CNTs) are one of the most widely used candidate. The literature has shown that growth of metal nanoparticles on CNTs not only prevents agglomeration but also results in their enhanced catalytic-ability [67]. Last decade has witnessed crucial application of CNTs in the development of sensitive and selective electrochemical sensors. Multi-walled carbon nanotubes (MWCNT), the cylindrical molecules with sp^2 carbon, have been of considerable interest to researchers majorly because of their excellent electrical conductivity, unique physical properties, high surface area and chemical stability [68-69]. MWCNT are also known to improve the electrical properties of the sensing surface as they exhibit electro-catalytic properties and thus results in improved electrochemical response of the analyte [69-70]. Hence, MWCNT has been chosen as the support for the deposition of PdNPs so as to fabricate a nanohybrid material having properties superior then both MWCNT and PdNPs alone.

In the last few years, several methodologies had been opted to achieve the Pd/CNT nanocomposites, such as microemulsion [72], electro-less deposition [73], surfactant self-reduction [74], arc-discharge in solution [75], solid state H_2 reduction [76] and ethylene glycol reduction [77]. However, some of them exhibit sophisticated synthetic procedure or complex equipment to achieve Pd/CNTs nanocomposite. In the present section, a facile, simple and effective chemical method has been used to achieve the Pd decorated MWCNT (PdNP:MWCNT) surface. The fabricated surface has been applied as surface modifier for the fabrication of a sensitive, selective and robust electrochemical sensor for assaying 5-HTP.

3.5 EXPERIMENTAL

3.5.1 Materials and instrumentation

5-Hydroxytryptophan (5-HTP; Code H9772 Sigma), uric acid (UA), ascorbic acid (AA), hypoxanthine (HX), xanthine (X), sodium borohydrate (NaBH$_4$), multi-walled carbon nanotubes (MWCNT; code 773840 Sigma), palladium chloride were purchased from the Sigma Aldrich (USA). The phosphate buffer solutions of different pH in the range 2.4–10.0 were used. All the stock solutions used throughout the experimental procedure were prepared in the double distilled water. The voltammetric studies and characterization techniques used were essentially similar to that reported in the section A of this chapter. X-ray diffraction (XRD) data were obtained by using Bruker D8-advance X-ray powder diffractometer and energy dispersive X-ray analysis (EDX) were carried out using Zeiss ultra plus 55 instrument.

3.5.2 Synthesis of PdNPs- MWCNTs

The aqueous solution of dihydrogen tetrachloropalladate (II) (H$_2$PdCl$_4$, 0.50 M) was prepared by dissolving required palladium chloride in minimum amount of concentrated HCl and double distilled water was then used for making up the solution. The MWCNT suspension was prepared by suspending 0.5 mg MWCNT in 1 mL of ethanol. The suspension so obtained was sonicated for 15 minutes in order to get the maximum dispersion. For synthesizing the palladium nanoparticles modified MWCNT, 20 μL of H$_2$PdCl$_4$ aqueous solution was added to 100 μL of MWCNT suspension and to this, 200 μL of freshly prepared NaBH$_4$ solution (0.5 mg/200 μL in double distilled water) was added. The final mixture was then stirred for 60 s at room temperature. NaBH$_4$ was used to reduce the PdCl$_2$ and MWCNT were used as a supporting material for growing the palladium nanoparticles. After stirring, the solution was centrifuged, washed several times with double distilled water and dissolved in 0.3 mL of water to get a suspension of PdNP modified MWCNT.

3.5.3 Fabrication of modified sensors

The glassy carbon electrode (GCE) surface was firstly polished to a mirror like finish by mechanically rubbing it on a micro cloth pad having slurry of ZnO and alumina. The above prepared PdNP:MWCNT suspension was then dropcasted on pre cleaned GCE surface. The volume of PdNP:MWCNT to be drop casted was optimized in the range of 5–35 μL. The best results were found when 15 μL of suspension was dropcasted onto the GCE surface. Thus, for the

fabrication of PdNP:MWCNT/GCE, 15 µL of PdNP:MWCNT suspension was drop-casted on the pre cleaned GCE surface and dried at room temperature. The final sensing surface was then characterized using voltammetry, FE-SEM, EDX, EIS and XRD.

3.5.4 Voltammetric procedures and sample preparation

Cyclic voltammetry (CV) and square wave voltammetry (SWV) have been applied to investigate the electrochemical oxidation of the 5-HTP. To prepare the stock solution of 5-HTP (1.0 mM), the required amount was dissolved in the double distilled water. For preparing the test solution, the required volume of the 5-HTP stock solution was added to the cell already containing 2 mL of pH 7.2 phosphate buffer and the final volume was made to 4 ml by using double distilled water. The optimized experimental conditions used for the square wave voltammetry (SWV) were: initial potential (E_i): 100 mV, final potential (E_f): 1200 mV, square wave amplitude (E_{sw}): 25 mV, square wave frequency (*f*): 15 Hz, potential step (E) 4 mV and the optimized operating parameters for the cyclic voltammetry were initial potential (E_i): 150 mV, switching potential (E): 800 mV, final potential (E_f): 150 mV and scan rate 100 mV/s. The modified sensor surface was cleaned after every run by applying a potential of -400 mV for 100 s in the blank solution.

3.5.4.1 Urine Sample Preparation:

Urine samples of two healthy volunteers (Male, age 24 and Female, age 29) were collected from the Institute hospital of I.I.T. Roorkee and filtered using the whatman 42 filter paper. The filtrate was then diluted twice by using pH 7.2, phosphate buffer. The test solution for the recovery experiments were prepared by spiking the diluted urine sample with the required volume of 5-HTP stock solution (1mM).

3.6 RESULT AND DISCUSSION

3.6.1 Characterization of composite

The FE-SEM micrographs were recorded in order to investigate the nano scale surface changes occurring at the different stages of modification protocol. **Fig. 3.12** clearly shows the different topology of the modified surface in comparison to the bare electrode. It was found that the bare GCE surface was smooth and flat before the drop cast as shown in **Fig. 3.12(A)**. The tube shape structure in **Fig. 3.12(B)** belongs to the MWCNT casted on the GCE surface. Whereas, the simultaneous presence of both PdNPs (>15 nm) and MWCNT can be seen in **Fig. 1(C)**, which

corresponds to the PdNPs decorated MWCNT. From **Fig. 3.12(C)**, it can be visualized that MWCNT acts as a support for the nucleation and growth of PdNPs. The energy dispersion X-ray spectroscopy (EDX) data further indicated the existence of 35.31 atomic % of Pd in the PdNP:MWCNT as represented in **Fig. 3.12 (D)**.
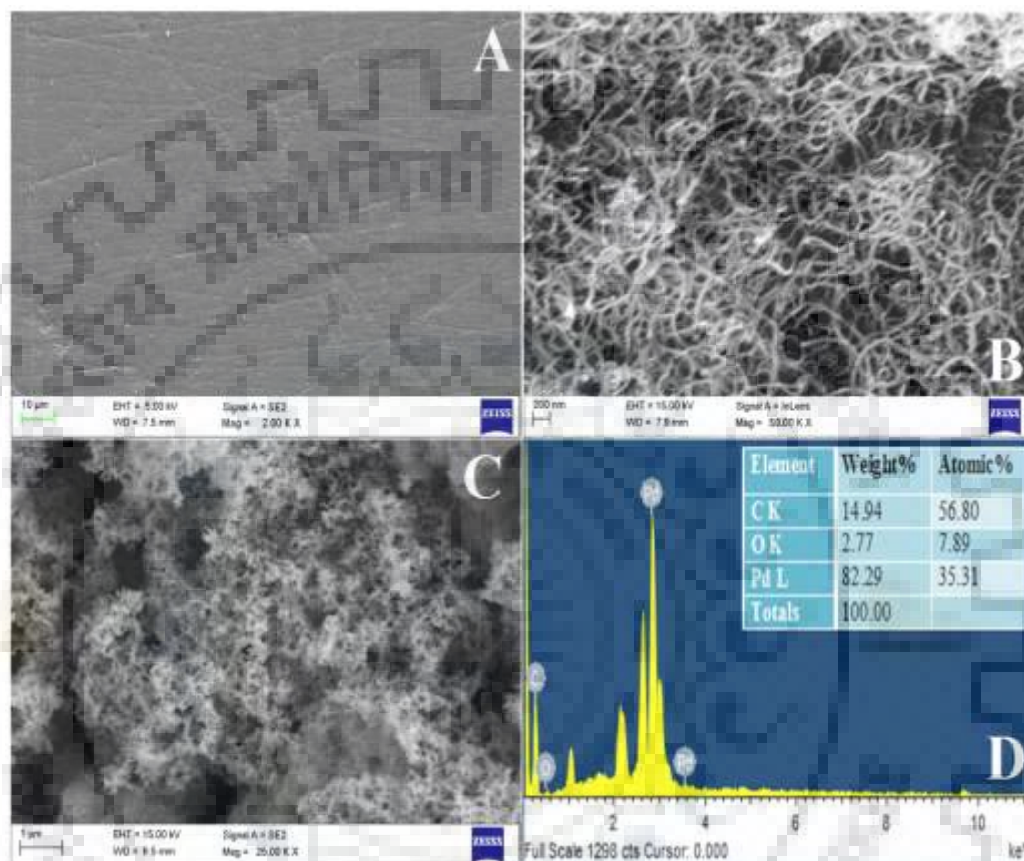
Fig. 3.12: FE-SEM images demonstrating surface morphology of (A) unmodified GCE, (B) MWCNT/GCE, (C) PdNP:MWCNT/GCE and (D) EDX data demonstrating the presence of Pd in PdNP:MWCNT/GCE.

The X-ray diffraction (XRD) spectra of MWCNT, bare Pd and PdNP:MWCNT are presented in **Fig. 3.13**. A broad peak at 2θ = 26° was observed in the MWCNT spectrum which corresponded to the (0 0 2) plane lattice of the MWCNT. Whereas, the diffraction spectrum of PdNP:MWCNT exhibited the major diffraction peaks of Pd at 40.1°, 46.65°, 69°, which corresponds to the (1 1 1), (1 1 0), (1 0 0) planes of crystalline Pd(0) respectively [69, 77], along with a broad peak at 2θ = 26° indicating thereby successful modification of the MWCNT surface with PdNPs and further supports the conclusion made from FE-SEM micrographs.
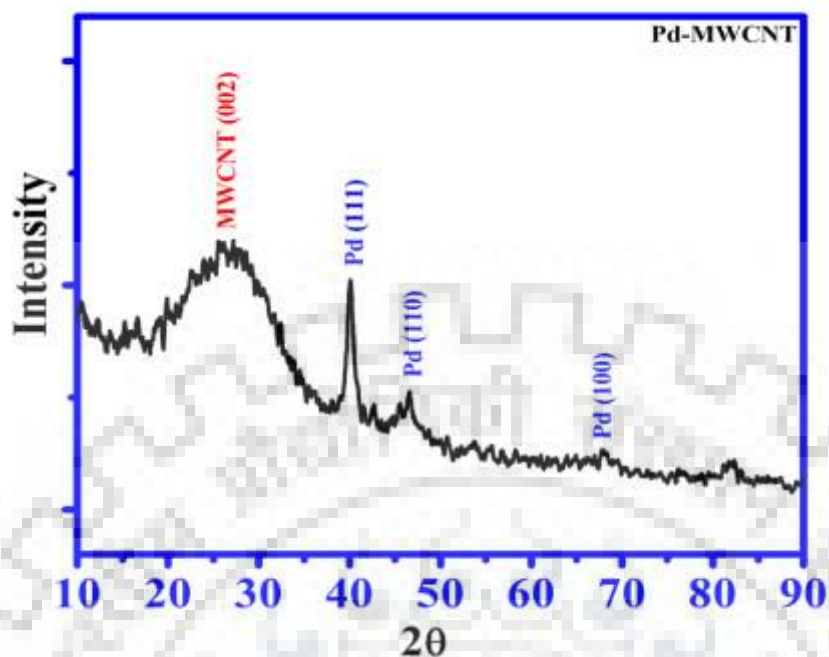
Fig. 3.13: XRD pattern for PdNP:MWCNT.

The EIS experiments have also been carried out for investigating the effect of modification on the electron transport behavior of GCE. The experiment was carried out in the 1:1 mixture of 5 mM $K_3[Fe(CN)_6]$ and 0.1 M KCl solution over 1000 kHz to 0.001 Hz frequency range. A typical Nyquist plot for Randle's circuit consisted of two portions, one is the semi-circular and another is the linear portion. The linear portion represents mass transfer diffusion limited process at lower frequency, while at a high frequency the diameter of the semicircle represents the charge transfer resistance (R_{CT}) [62]. **Fig. 3.14** shows the results of impedance studies carried out using PdNP:MWCNT/GCE, MWCNT/GCE and unmodified GCE. The R_{CT} was calculated by fitting Randle's circuit as shown in the inset of **Fig. 3.14**. The R_{CT} values for PdNP:MWCNT/GCE, MWCNT/GCE and bare GCE were 822 Ω **(curve a)**, 1124 Ω **(curve b)** and 1525 Ω **(curve c)** respectively, which indicates that the rate of electron transfer between the sensor and electrolyte has been promoted by PdNP:MWCNT and thus facilitated the redox processes at the PdNP:MWCNT/GCE.
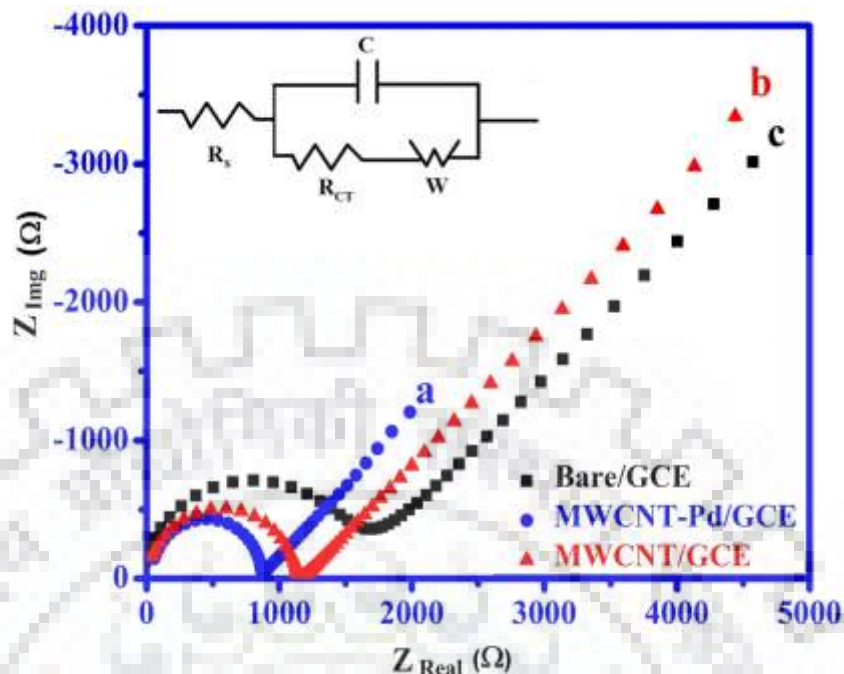
Fig. 3.14: Typical Nyquist plots obtained for (a) PdNP:MWCNT/GCE, (b) MWCNT modified GCE and (c) unmodified GCE in 1:1 mixture of 5 mM $K_3[Fe(CN)_6]$ and 0.1 M KCl solution over the frequency range 1000 kHz to 0.001Hz.

3.6.2 Cyclic Voltammetry

Cyclic voltammetry (CV) is commonly applied to investigate the redox behavior of electro-active species, and for analyzing the nature of the electrochemical reaction involved. Thus, for investigating the electrochemical characteristics of 5-HTP and to study the electro-catalytic ability of PdNP:MWCNT, cyclic voltammograms were recorded for 100 μM 5-HTP in phosphate buffer solution of pH 7.2 using unmodified and PdNP:MWCNT/GCE. As shown in **Fig. 3.15**, a feeble anodic peak at 370 mV was observed at unmodified GCE. On the other hand, a sharp, intense peak at 356 mV with enhanced peak current was observed using PdNP:MWCNT/GCE. As no reduction peak was observed in the reverse scan, it was concluded that 5-HTP oxidation is irreversible in nature. The decrement in the peak potential and significant increment in the peak current of 5-HTP clearly showed the electrocatalytic activity of the nanocomposite, which facilitated the electron transfer reaction and thus created interest to carry out the further investigations of 5-HTP using PdNP:MWCNT/GCE.
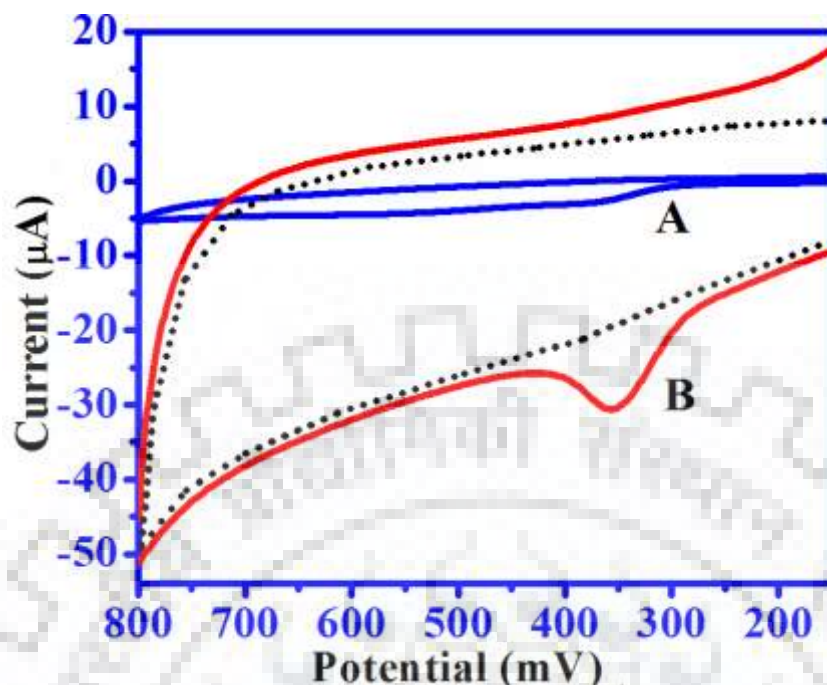
Fig. 3.15: Comparative cyclic voltammograms corresponding to 100 µM 5-HTP in pH 7.2 phosphate buffer at 100 mV/s scan rate using (A) unmodified GCE and (B) PdNP:MWCNT/GCE. Dotted line represents the CV of blank solution at modified sensor.

To examine the nature of the electron transfer process involved in the oxidation of 5-HTP, scan rate study was performed in the range of 5–250 mVs^{-1} and the cyclic voltammograms obtained are shown in **Fig. 3.16**. It is found that on increasing the sweep rate (v), oxidation peak current (i_p) of 5-HTP increases. A linear relation was found between i_p and v that can be represented as:

$$i_p = 0.1608 \, v + 0.9784, \, R^2 = 0.9959$$

where, i_p is the anodic peak current in µA and v is the sweep rate in mVs^{-1}. The linear plot of i_p vs v demonstrates the fact that oxidation of 5-HTP at PdNPs:MWCNT/GCE is adsorption controlled which is further confirmed by the linear plot between log i_p vs. log v as shown in inset of **Fig. 3.16**. The linear relation can be represented by the following equation:

$$\text{lop } i_p = 0.8464 \log v - 0.4554, \, R^2 = 0.9905$$

The slope value ($\sim$ 1 and > 0.5) for log i_p vs. log v plot further confirmed that the electron transfer in oxidation of 5-HTP proceeded by an adsorption controlled path [78].
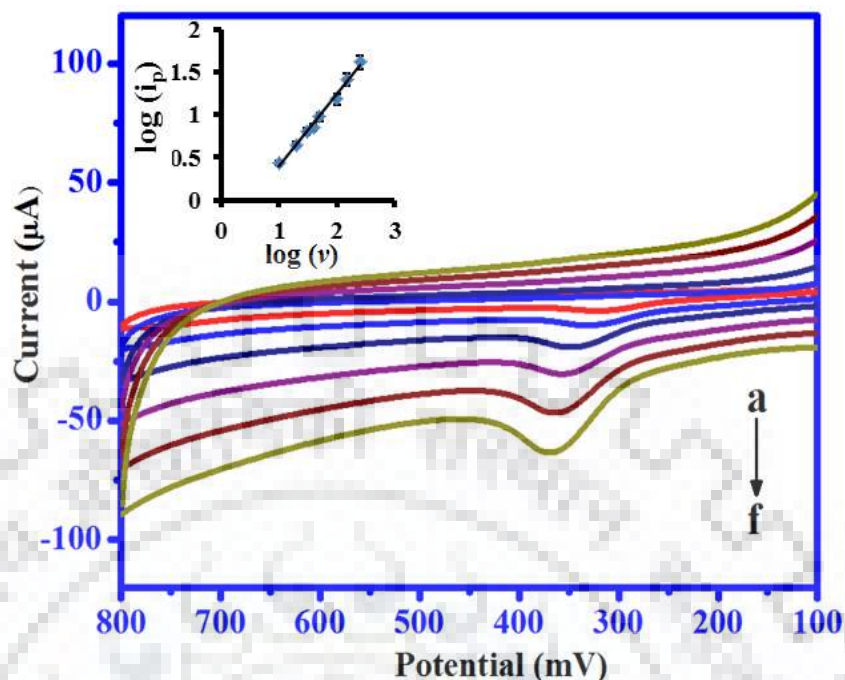
Fig. 3.16: Cyclic Voltammograms observed for 50 μM 5- HTP recorded at (a) 10, (b) 20, (c) 40, (d) 50, (e) 100 and (f) 150 mVs^{-1} scan rates using PdNP:MWCNT/GCE. Inset is the variation of log (i_p) with log (v).

3.6.3 Square wave voltammetry

The square wave voltammetric technique (SWV) was used for the detailed electrochemical analysis of the 5-HTP due to its several advantages, including high sensitivity, low background currents and better peak resolution. For examining the extent of electro-catalytic tendency of PdNP:MWCNT, square wave voltammograms were recorded for 10 μM 5-HTP in pH 7.2 phosphate buffer using unmodified GCE, MWCNT/GCE and PdNP:MWCNT/GCE **(Fig.3.17)**. At unmodified electrode a weak oxidation peak was observed for 5-HTP. While in the case of PdNP:MWCNT/GCE, a sharp anodic peak at ~338 mV was observed with several fold high peak current (i_p) response in comparison to the unmodified sensor as shown in **Fig. 3.17**. As, the oxidation of the 5-HTP exhibited best results at PdNP:MWCNT/GCE, further studies were performed using PdNP:MWCNT modified glassy carbon electrode.
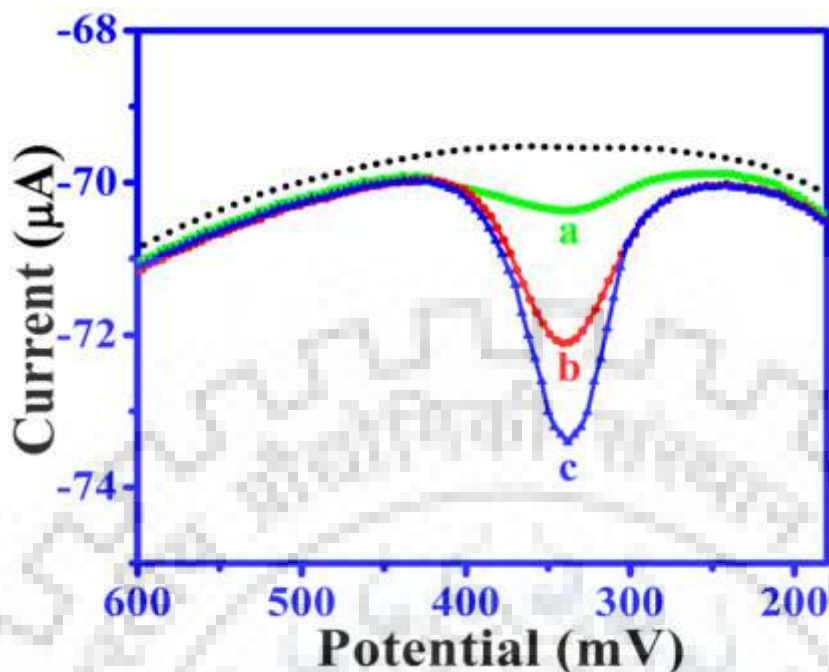
Fig. 3.17: Comparative square wave voltammograms recorded for 10 μM 5-HTP in pH 7.2 phosphate buffer using (a) unmodified GCE, (b) MWCNT/GCE and (c) PdNP:MWCNT/GCE.

3.6.3.1 Concentration study

Concentration study has been carried out in order to prepare a calibration plot for the quantification of 5-HTP as well as for calculating the limit of detection. The SWV technique has been used for the quantitative analysis of 5-HTP and the voltammograms obtained are shown in **Fig. 3.18**. A calibration curve was plotted in the concentration range 2–400 μM. The peak current versus concentration plot exhibited a break at around 100 μM. A linear relation was found between peak current and the 5-HTP concentration in the range of 2–100 μM. However, at higher 5-HTP concentration, a different linear relation was noticed as demonstrated in the inset of **Fig. 3.18**. The dependence can be documented using following equations:

$$i_p = 0.032 \, [C_{\text{5-80 μM}}] - 0.0045, \, R^2 = 0.9891 \, \text{- - - - - - -} \, \textbf{bare electrode}$$

$$i_p = 0.212 \, [C_{\text{2-100 μM}}] + 4.2994, \, R^2 = 0.9889 \, \text{- - - - - -}\textbf{PdNP:MWCNT/GCE}$$

$$i_p = 0.072 \, [C_{\text{150-400 μM}}] + 17.76, \, R^2 = 0.9805 \, \text{- - - - -} \, \textbf{PdNP:MWCNT/GCE}$$

where, C is the 5-HTP concentration in μM and R^2 is the regression coefficient.
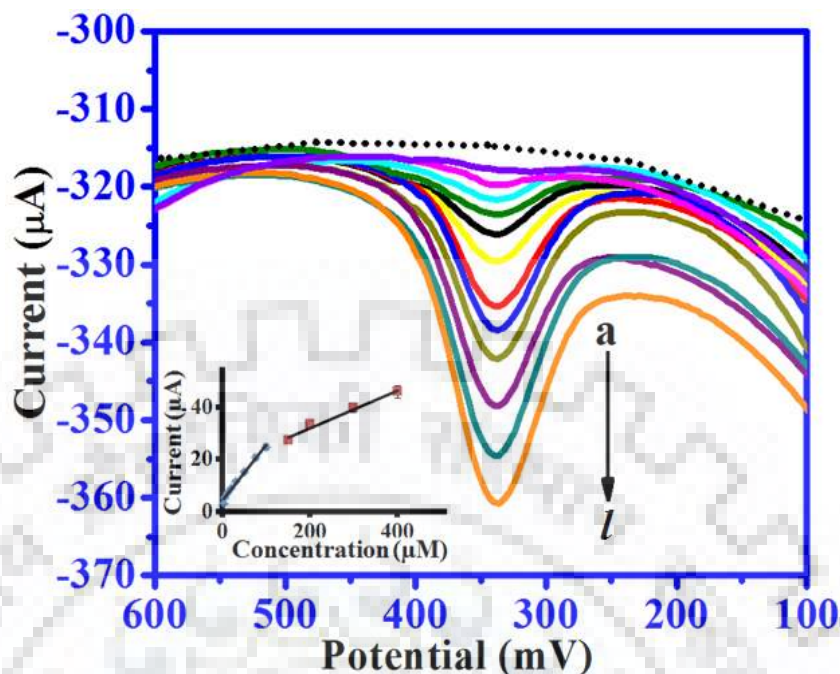
Fig. 3.18: Square wave voltammograms recorded for (a) 2 μM (b) 5 μM, (c) 10 μM, (d) 20 μM, (e) 30 μM, (f) 50 μM, (g) 75 μM, (h) 100 μM, (i) 150 μM, (j) 200 μM, (k) 300 μM and (l) 400 μM 5-HTP concentrations using PdNP:MWCNT/GCE. The dotted line demonstrates the background current. Inset is the calibration plot in the 5-HTP concentration range of 2–400 μM.

The statistical parameters obtained for the quantitative analysis of 5-HTP at PdNP:MWCNT/GCE and bare GCE have been tabulated in **Table 3.6**. From the above equations, it can be seen that modified sensor is ~7 fold more sensitive to 5-HTP in comparison to the unmodified sensor.

Table 3.6: Statistical parameters obtained for the quantitative analysis of 5-HTP at PdNP:MWCNT/GCE and Bare GCE.

Validation Parameters	PdNP:MWCNT/GCE		Bare
	I	**II**	
Concentration range (μM)	2–100 μM	150–400 μM	5–80
Correlation coefficient (R^2)	0.989	0.980	0.989
Sensitivity (μA/μM)	0.212	0.072	0.032
Standard error of slope	0.009	0.007	0.002
Standard error of intercept	0.454	2.007	0.070

The limit of detection (L.O.D.) was calculated by using the formula $3\sigma/b$, where σ is the standard deviation of the three consecutive blank readings and b is the slope of the calibration plot. L.O.D. as low as 77 nM was obtained at PdNP:MWCNT/GCE for concentration range 2–100 µM of 5-HTP. This detection limit is much lower in comparison to the many recently reported investigations on 5-HTP as shown in the **Table 3.7**.

Table 3.7: Comparison of Limit of Detection (L.O.D.) obtained for 5-HTP at PdNP:MWCNT/GCE with previously reported electroanalytical methods.

S.No.	Modification/electrode	LOD (µM)	Linear range	Reference
1	Capillary electrophoresis	0.091	0.18–6 µM	[56]
2	ITO/npSG/CoHCF (LSV)	2.1	10–1000 µM	[58]
3	RuOx/GCE (Amperometric)	0.16	5–50 µM	[59]
4	Carbon disk electrode (CE-ED)	0.097	0.1–200 µM	[60]
5	Gold modified pencil graphite electrode (DPV)	---	10–60 µM	[61]
6	PdNP:MWCNT/GCE (SWV)	0.077	2–100 µM	**Present work**

LSV: Linear sweep voltammetry, SWV: square wave voltammetry, DPV: Differential pulse voltammetry, CE-ED: Capillary electrophoresis with electrochemical detection

3.6.3.2 Effects of pH

To investigate the influence of pH on the electrochemical behavior of 5-HTP, the pH study was carried out using SWV in the pH range 2.4 to 10.0. It was found that both the oxidation peak current and the peak potential of 30 µM 5-HTP were affected by the pH of the phosphate buffer solution and it was found that with increasing pH, a negative shift in the anodic peak potential was observed. A linear relation was found between E_p and pH, which is presented in **Fig. 3.19** and can be expressed by the equation;

$$E_p(mV) = -46.813 \, pH[2.0–10.0] + 664.45, \, R^2 = 0.9988$$

where, R^2 is the correlation coefficient. The slope (dE_P/dpH) value of 46.813 mV/pH suggests that the electro-oxidation of 5-HTP proceeds with a mechanism involving equal number of electrons and protons as shown in **Scheme 3.2** [78-79].
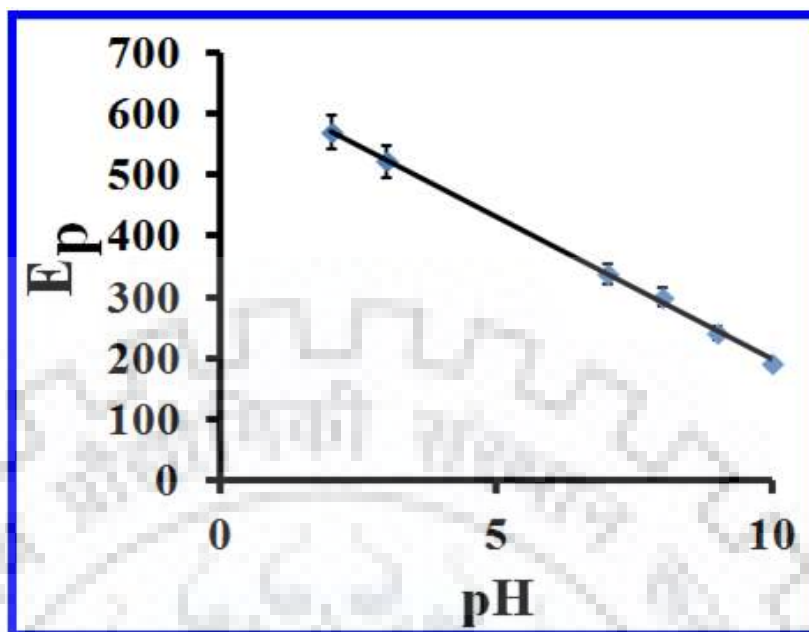
Fig. 3.19: Dependence of peak potential on the pH of the supporting electrolyte.
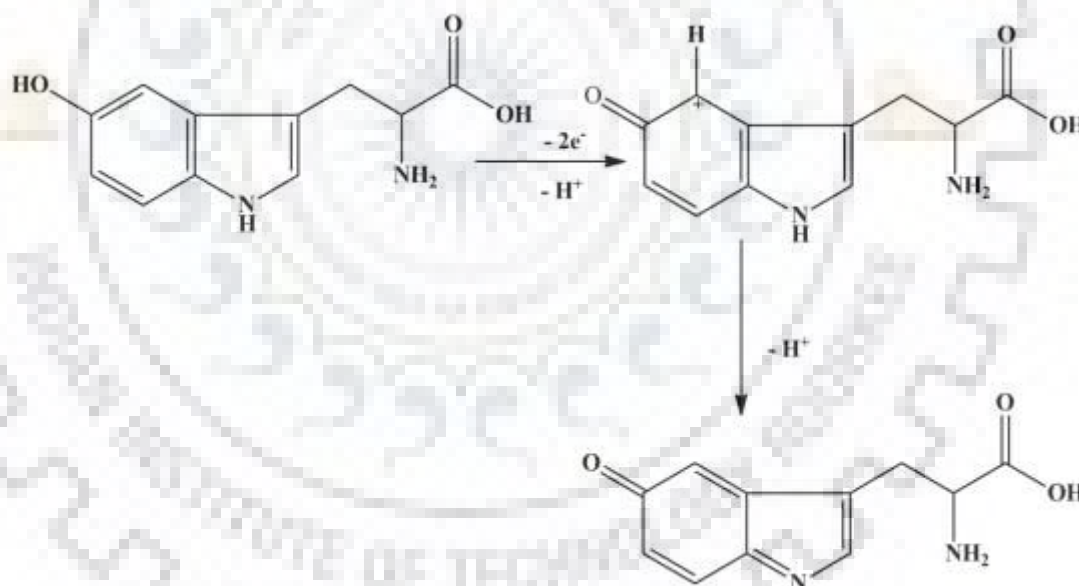
Scheme 3.2. Proposed mechanism for the oxidation of 5-HTP.

3.6.3.3 Frequency study

The effect of the frequency on the peak current (i_p) of 5-HTP was studied in the frequency range 5–15 Hz. The peak current of 5-HTP was found to increase with increasing frequency and showed a linear variation with square wave frequency **(Fig. 3.20 (A))** indicating the involvement

of adsorption controlled electron transfer process on the surface of PdNP:MWCNT/GCE. The dependency of i_p on the frequency (f) can be expressed as:

$$i_p \text{ (µA)} = 0.5022\, f - 1.192, \ldots \ldots R^2 = 0.9918$$

$$\log i_p = 1.327 \log f - 0.7558, \ldots \ldots R^2 = 0.9979$$

Where, i_p is the peak current in µA, f is the square wave frequency in Hz and R^2 is the correlation coefficient. The slope value > 0.5 of $\log i_p$ versus $\log f$ (**Fig. 3.20(B)**) confirmed that the electro-oxidation of the 5-HTP was adsorption controlled and supported the results obtained from the scan rate study [78].
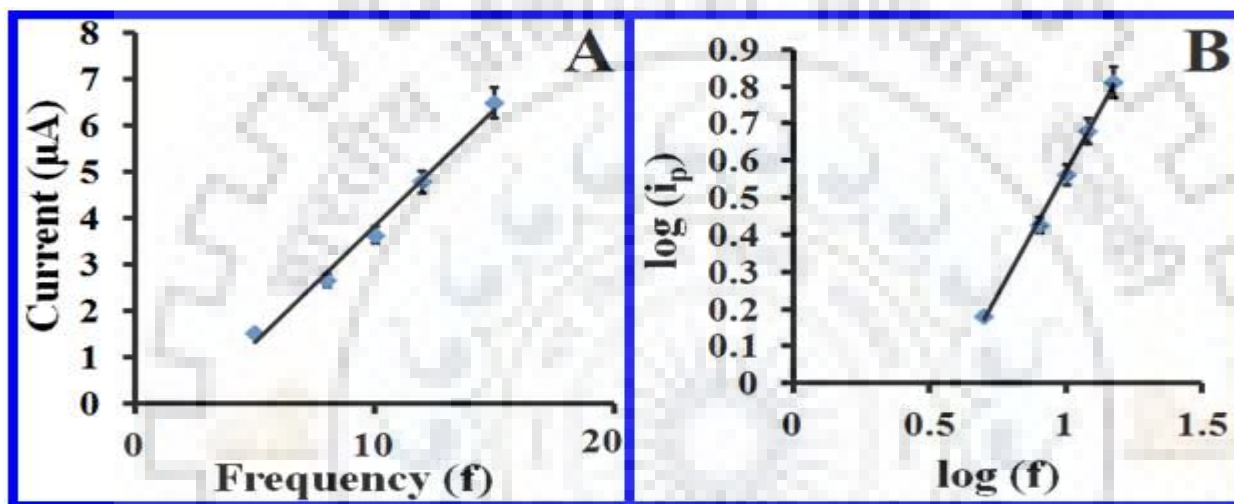
Fig. 3.20: Variation of (A) i_p with the square wave frequency (f) and (B) $\log (i_p)$ with $\log (f)$ for 10 µM 5-HTP.

3.6.4 Interference study

The presence of several metabolites such as uric acid (UA), ascorbic acid (AA), hypoxanthine (HX), xanthine (X) etc. in the human biological fluids can interfere in the selective determination of the 5-HTP, hence, it is considered desirable to check the ability of the developed sensor to analyze 5-HTP in the presence of such metabolites. For this purpose, SW voltammograms were recorded in the solutions having fixed 5-HTP concentration (10 µM) and increasing amount of interfering metabolites. The voltammograms thus obtained are shown in **Fig. 3.21**. From the figure, it can be seen that well defined, separated peaks were observed at 258, 343, 631 and 976 mV corresponding to the oxidation of UA, 5-HTP, X and HX respectively. From **Fig. 3.21**, it can be clearly seen that neither the anodic peak potential nor the peak current of the 5-HTP gets affected by the oxidation of interfering molecules. Hence, the developed sensor can be

successfully employed for the selective investigation of 5-HTP in biological samples such as blood and urine.
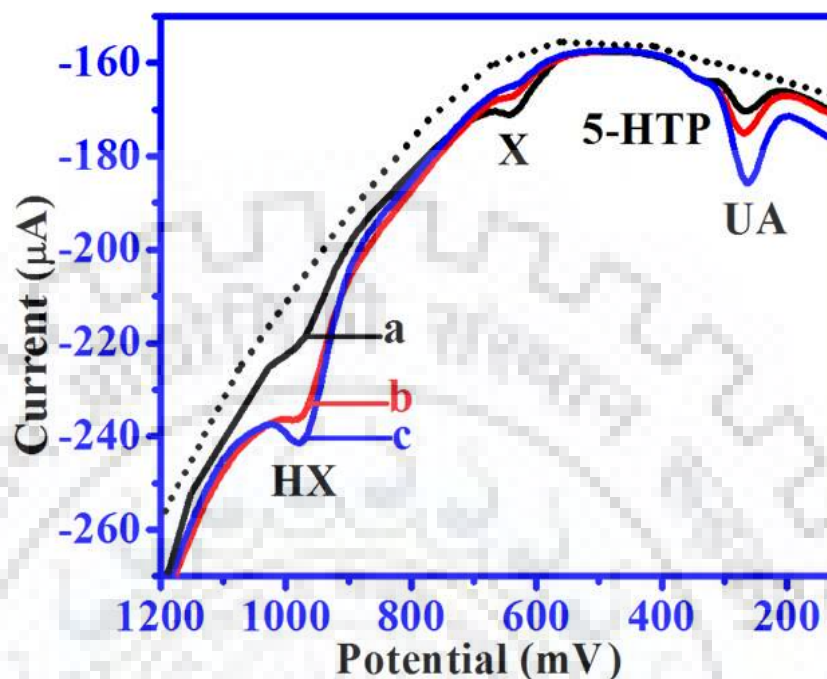
Fig. 3.21: Square wave voltammograms observed for a solution containing 10 μM 5-HTP (a) 50 μM UA + 400 μM X + 100 μM HX, (b) 100 μM UA + 200 μM X + 150 μM HX and (c) 150 μM UA + 125 μM X + 50 μM HX. Background is represented by the dotted line.

3.6.5. ANALYTICAL APPLICATION

3.6.5.1 Urine sample assay

To examine the practical application of the developed analytical method, the PdNP:MWCNT/GCE was applied for the analysis of 5-HTP in the complex matrix like urine sample. In human systems 5-HTP is converted to serotonin in nervous tissues as well as in liver and excess 5-HTP is believed to be excreted. The normal urinary excretion of 5-HTP in the healthy adults is less than 0.3 to 0.7 μmol/24h [80]. Despite of our best efforts, we were not able to find patients on medication of 5-HTP, hence, only recovery studies were carried out. For the recovery measurements, the urine samples of the two healthy volunteers were collected, filtered and diluted 2 folds with pH 7.2 phosphate buffer in order to reduce the complexity of the urine sample. Since the urine samples were taken from healthy person, no peak corresponding to the oxidation of 5-HTP was observed. Thus, in order to carry out the recovery studies, test samples were prepared by spiking the urine samples with the known concentration of the 5-HTP stock solution and SW

voltammograms were recorded. The oxidation peak of 5-HTP was observed at 338 mV with an additional oxidation peak corresponding to uric acid at 258 mV as shown in **Fig. 3.22**.
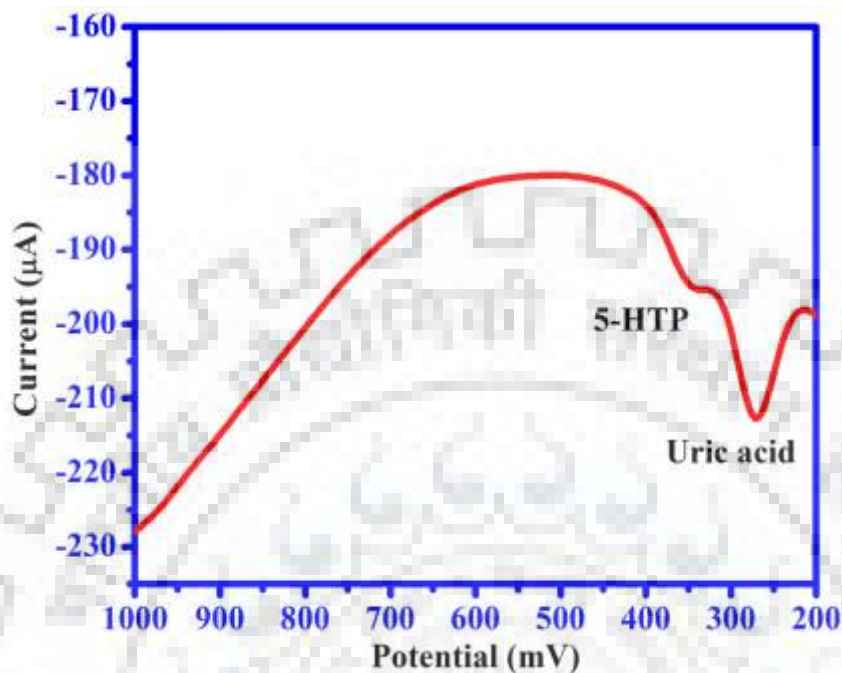
Fig. 3.22: Square wave voltammogram corresponding to the oxidation of 20 µM 5-HTP in urine sample.

The concentration of the 5-HTP was then back calculated by putting the peak current value in the calibration plot equation and results thus obtained are tabulated in **Table 3.8**. The results demonstrated a recovery > 99%, indicating the excellent application of the developed method for the quantification of 5-HTP in complex matrix like human physiological fluids.

Table 3.8: Recovery data of 5-HTP determination in human urine samples

S.No.	Spiked amount (µM)	Detected amount (µM)[*]	Recovery %	Error %
Sample 1				
1	5	4.960	99.20	-0.80
2	10	9.970	99.70	-0.30
3	20	19.90	99.50	-0.50
Sample 1				
1	30	29.97	99.90	-0.10
2	50	49.89	99.78	-0.22
3	100	99.81	99.81	-0.19

*RSD for the determination was 1.23% for n=3

The robustness of the results obtained during recovery studies has also been investigated by studying the effect of pH on the electrochemical determination of the analyte. From the studies, it was found that the results of the recovery studies were not significantly affected by deliberately altering the pH from pH 7.2 to 5.0.

3.6.6 Stability and Intermediate Precision

To investigate the stability of the PdNP:MWCNT/GCE, the oxidation response of 5-HTP at a fixed concentration was examined in pH 7.2 phosphate buffer solution over a period of 30 days. The SW voltammograms were recorded daily. For the first 20 days the peak current response shows a fluctuation of ±4.0%, while after 20 days, a decrement up to 6.5% of the peak current was noticed. Thus, sensor can be safely used for first 20 days after its preparation.

3.6.7 Ruggedness Studies

To further ensure the accuracy of the results, ruggedness was also examined by carrying out the same studies at different voltammetric instruments and by different analysts. To investigate the equipment related variations, voltammetric studies have been carried out using two voltammetric analyzers viz., CV-50 and Epsilon EC-USB (BAS, West Lafayette, USA). In order to examine the intermediate precision of the modified sensor, its performance has been examined at different electrodes on different days. When the results from the two instruments were compared, the electrochemical response of the sensor was found to exhibit a deviation of ±1.18%

demonstrating excellent precision of the protocol followed. The results obtained have been tabulated in **Table 3.9**, which demonstrates that there is no substantial difference between the observed recovery results. Hence, it is concluded that the proposed method presents a reliable, robust and rugged approach for assaying 5-HTP in the complex matrix like urine and other biological fluids.

Table 3.9: The Robustness and ruggedness of the proposed method for the recovery data of 5-HTP determination in human urine samples.

Variables	Recovery % ± R.S.D
Robustness at pH=5	98.70 ± 1.45
Ruggedness Analyst 1	
Instrument: CV 50W	98.48 ± 1.12
Instrument: Epsilon EC-USB	99.19 ± 1.07
Ruggedness Analyst 2	
Instrument: CV 50W	99.26 ± 1.18
Instrument: Epsilon EC-USB	99.64 ± 1.03

To check the electrode to electrode variation and the associated precision, four GCE were modified independently by following the same modification protocol. By using each of the modified GCE, voltammograms were recorded in 10 µM 5-HTP solution and RSD was found to be 2.89%. For calculating the intermediate precision of the protocol at different days, five consecutive voltammograms were recorded for 10 µM 5-HTP and a R.S.D value of 2.13% for n=5 was found. Hence, it is concluded that the developed sensor shows excellent stability and reproducibility.

3.7. CONCLUSION

A simple, rapid and single step modification of GCE with PdNP:MWCNT has been presented in the current section. The sensing surface of the modified sensor has been characterized by using Voltammetry, FE-SEM, EDX, EIS and XRD. The electro-catalytic ability of PdNP:MWCNT has been investigated by employing the modified sensor for the qualitative as well as quantitative analysis of 5-HTP. A linear dependency of the peak current on 5-HTP concentration was obtained in the concentration range of 2 to 400 µM with a sensitivity and L.O.D.

of 0.212 µA/µM and 77 nM respectively. The fabricated sensor also showed successful estimation of 5-HTP in the presence of potential interfering substances like uric acid, hypoxanthine and xanthine. The developed sensor also demonstrated excellent recovery of 5-HTP in the complex matrix like human urine samples and thus creates a interest in extending its application as a analytical tool for the quantification of 5-HTP in pharmaceutical, and medicinal fields.

SECTION C: GRAPHENE NANORIBBONS–SILVER NANOPARTICLES (GNRs-AgNPs) COMPOSITE MODIFIED SENSOR FOR ESTIMATION OF HISTAMINE; AN IMPORTANT BIOGENIC AMINE

Histamine (2-(1*H*-Imidazol-4-yl)ethanamine, HTM) is known as an important biogenic amine present in many food products and acts as chemical messenger in biological systems. HTM is known as a neurotransmitter, which is a product of microbial degradation of histidine (α-amino acid) in the presence of *histidine decarboxylase* [81-82]. It plays an important role in regulating the biological circadian rhythm and wakefulness in mammals and flies [83-84]. The concentration of histamine is associated with food quality index and the level of the HTM in food samples depends upon the hygienic conditions of food processing and storage. Due to the bacterial action HTM is usually present in vegetables, certain fish species such as tuna fish, fermented foodstuffs and beverages. The biogenic amines are responsible for the human foodborne intoxications caused by the histamine. The presence of the secondary amines, like cadaverine or putrescine in tuna fish can increase the toxicity of HTM [82, 85-86]. The intoxication of HTM is associated with headaches, itching, vomiting, diarrhea, red rash, nausea and hypertension [87-88]. Histamine is also involved in regulations of numerous pathological and physiological functions, like secretion of some hormones, regeneration, differentiation, cell proliferation, wound healing, hematopoiesis, regulation of gastrointestinal, inflammatory reactions and circulatory functions [89-90]. Different methods have been reported for the determination of histamine, such as thin-layer chromatography (TLC) [91], colorimetry [92], gas chromatography [93], HPLC [94-96], and capillary zone electrophoresis [97] etc. However, most of these methods are having disadvantages, like expensive and sophisticated instrumental setup, require time consuming process, large solvent requirement, hectic pre cleaning process, slow sample throughput etc. Hence, attempts were made to find the simple, sensitive, accurate and fast analytical method for the determination of HTM. A number of unmodified [98] and modified sensors have been reported for sensing of histamine [82, 86, 99-102]. However, most of these sensors involve complex modification protocol and the detection limit was high and hence, a simple, sensitive and cost effective sensor is still needed to monitor HTM.

Last few years have seen the important role of metal nanoparticles in the preparations of the energy storages devices, super-capacitors, and chemical and biological sensing due to their extensive optical, electric and catalytic properties [103-104]. Silver nanoparticles have unique properties, such as chemical stability, high electrical and thermal conductivity, excellent catalytic

activity and antimicrobial activity. The isolated silver nanoparticles are unstable because of the small particles size, hence, they easily undergo agglomeration [105-107]. To avoid agglomeration and increase the growth of the nanoparticles, carbon nanotubes and graphene nano ribbons (GNRs) have been found useful, which leads to a new hybrid material. In recent years, carbon nanotubes and graphene related materials have been found to play an important role in academia and industry, due to their unique electronics, thermal and mechanical properties [108-110]. GNRs is a class of graphene nano-materials with sp^2-hybridized carbon and is proved as a promising material in the energy storage devices [111-113], electrical and optical devices [113-114], sensors and biosensors [115-117] etc. GNRs can be prepared by variety of methods, however, unzipping of single/multi-walled carbon nanotubes has been extensively used [118-121]. In the present studies GNRs has been chosen as supporting material to grow the silver nano-particles to get superior properties.

The objective of the present studies was to combine the properties of GNRs and AgNPs to fabricate a nano hybrid material, which was then casted on the sensing surface to investigate a sensitive and selective analysis of HTM. The fabricated sensor exhibited good performance with excellent selectivity and sensitivity for the detection of HTM.

3.8. EXPERIMENTAL

3.8.1 Materials and Instrumentation

HTM, xanthine (XT), ascorbic acid (AA), uric acid (UA) and silver nitrate were obtained from Sigma-Aldrich (USA). Potassium chloride (KCl), and potassium ferricyanide ($K_3[Fe(CN)_6]$) were bought from E. Merck (India). Single wall carbon nanotubes (SWCNT; code 519308-250MG) was purchased from Bucky, USA. Red wine (Yvon Man, France) was purchased from the local market of Roorkee. Phosphate buffers (1.0 M) in the pH range of 5.0–9.40 were prepared by the previously reported method [36]. The voltammetric analyzer Epsilon EC-USB (BAS, West Lafayette, USA) was used to carry out electrochemical studies. A glass cell having three electrodes namely, an edge plane pyrolytic graphite (EPPG) as a working electrode, Ag/AgCl (Model; BAS MF-2052RB-5B, 3M NaCl) as a reference electrode and a platinum wire as an auxiliary electrode were used. The EPPG pieces ($15 \times 3 \times 3$ mm^3) were obtained from Pfizer (USA) as a gift. The details of the equipment used for EDX and FE-SEM studies are already described in the section A. Raman Spectroscopy experiments were executed by using Renishaw Invia Raman microscopy at 540 nm. Transmission Electron Microscopy (TEM, model; Technai G^2 20S-TWIN) and High Resolution Transmission Electron Microscopy (HRTEM, model; JEOL, JEM-300FS Field Emission electron

microscope) were used for recording the TEM and HRTEM images. Electrochemical Impedance Spectroscopy (EIS), using VersaSTAT 3 Galvanostat (PAR, USA), was used to evaluate the charge transfer resistance of the modified surface. The X-ray diffraction (XRD) patterns of the composite thin film were characterized by using X-Ray diffractometer (Bruker AXS, D8-advance).

3.8.2 Synthesis of Graphene nano-ribbons (GNRs)

Graphene nanoribbons were prepared from the SWCNT according to the method described in literature [120]. Briefly, 50 mg of SWCNT were added into the mixture of 50 mL of concentrated H_2SO_4 and HNO_3 (3:1) and the mixture was kept in ultrasonic cleaner for 8 h at 45 ^oC. Finally GNR's obtained were washed with water until the filtrate obtained was neutral. The GNRs obtained were then dried in an oven at 100 ^oC.

3.8.3 Composite of GNRs-AgNPs

To prepare the composite of silver nano-particles (AgNPs) and GNRs, the 100 µL of GNRs (1mg/1mL) in double distilled water and 50 µL of 10 mM $AgNO_3$ (aq) solution were mixed. To reduce silver nitrate freshly prepared 50 µL of sodium borohydride solution (1.2 mg in 200 µL) was added drop wise to reduce silver on GNRs surface and the mixture was sonicated for 120s at room temperature 25 ± 3 ^oC. Some oxygen containing groups on GNRs also reduced by using sodium borohydride and helped to grow the Ag nano-particles [122-123].

3.8.4 Fabrication of GNRs−AgNPs composite sensor

Firstly, the EPPG sensor was mechanically scratched using an emery paper (P-400) to get the fresh surface and washed well with double distilled water to remove adhered particles. The prepared GNRs-AgNPs composite material was then drop casted in different volumes (2–20 µL) on the sensor surface and after completely drying voltammetric response of HTM was recorded. The best results were found, when 5 µL was drop casted on the sensor surface, hence, 5 µL optimized composite materials was used for subsequent studies. When lower than 5 µL was used, the peak response for HTM was very small due to the limited binding sites available at the electrode surface. At volume 5 µL, the thickness of the composite increased (optimal) at the electrode surface. The results of optimization studies are presented in **Fig. 3.23**.
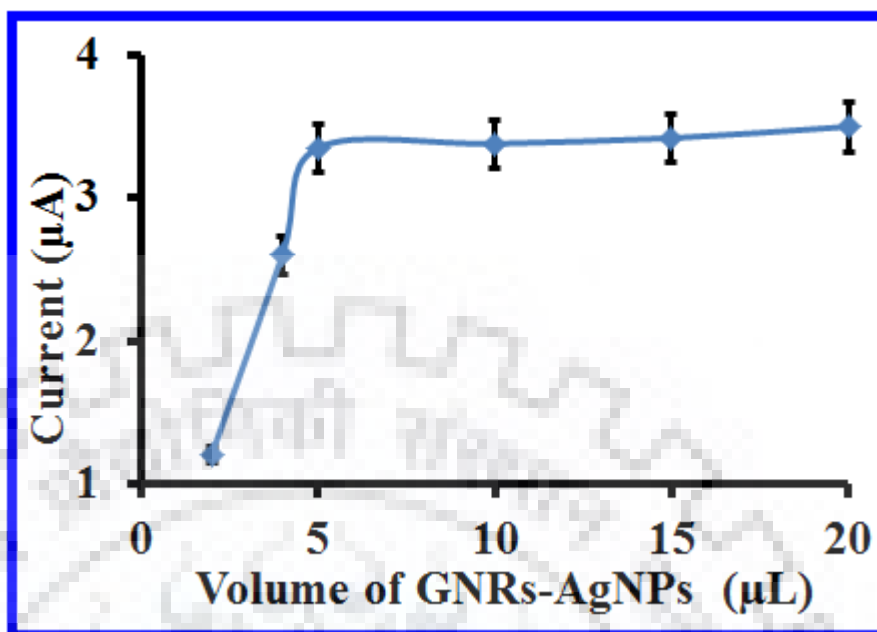
Fig. 3.23: Optimization of the volume of the GNRs-AgNPs (2–20 µL) drop casted by studying the variation of peak current of HTM (10 µM).

3.8.5 Sample preparation and voltammetric procedures

HTM stock solution (1.0 mM) was prepared by dissolving the required amount in deionized water. To prepare the solution for analysis, the required volume of stock solution was added in a cell having 2 mL of phosphate buffer (pH 7.2) and the total volume was made to 4 mL using deionized water. For SWV studies the parameters used were; initial potential (E_i): -100 mV, final potential (E_f): 1200 mV, potential step (E): 4 mV, square wave frequency (f): 15 Hz, square wave amplitude (E_{sw}): 25 mV and for CV studies scan rate 100 mV/s, initial potential (E_i): 200 mV, switching potential (E): 1400 mV and the final potential (E_f): 0 mV were used. The GNRs-AgNPs/EPPG sensor surface was renewed each time by applying the controlled potential at -800 mV for 100 s in pH 7.2 phosphate buffer. At -800 mV, the response of EPPG and GNRs-AgNPs/EPPG sensors was essentially similar and no reduction peak was noticed in both the cases. The samples for TEM and HRTEM were prepared by drop casting of suspension of GNRs in double distilled water onto the copper grid (coated with carbon). The grid was dried in an oven for 30 min. and then used for TEM and HRTEM analysis

The blood plasma samples of three healthy volunteers were collected from the Institute Hospital of I. I. T. Roorkee and filtered through the Whatman 42 filter paper. The filtered samples

were diluted 2 times with the pH 7.2 phosphate buffer. The samples were spiked with required amount of the HTM and recovery studies were carried out.

3.8.6 HPLC studies

HPLC studies for validation were carried out using Shimadzu LC-2010A HT system equipped with C_{18} Bondpack 125 Å, 10 µm) reverse phase column. HPLC grade acetonitrile was used as the solvent at the flow rate of 0.8 mL/min. The injection volume was 40 µL and the wavelength of eluent was monitored at 254 nm.

3.9. RESULTS AND DISCUSSION

3.9.1 Characteristics of GNRs−AgNPs

Fig. 3.24(A) represent the TEM image observed for the GNRs. TEM measurements provided the evidence for GNRs produced by unzipping of SWCNT in the presence of strong acid. **Fig. 3.24(A)** indicates the multi-layered graphene sheet nanoribbons, a part of which is normally aggregated to form wide platelets as described by Valentini et. al [124]. **Fig. 3.24(B)** presents the HRTEM image of GNRs and it is observed that the SWCNT were opened due to the effect of the strong acid and long and thin graphene sheets like structure (GNRs) were formed. **Fig. 3.24**, shows FE-SEM images observed at different stages of modification. **Fig. 3.24 (C)** shows flat and smooth sensor surface before the modification. **Fig. 3.24 (D)** presents the composite of GNRs and silver nanoparticles at the sensor surface, which gives different topology in comparison to other stage of modifications. The atomic percentage of the different elements observed by using the EDX is presented in **Fig. 3.24(E)** and the presence of C, O and Ag atoms was clearly visible.
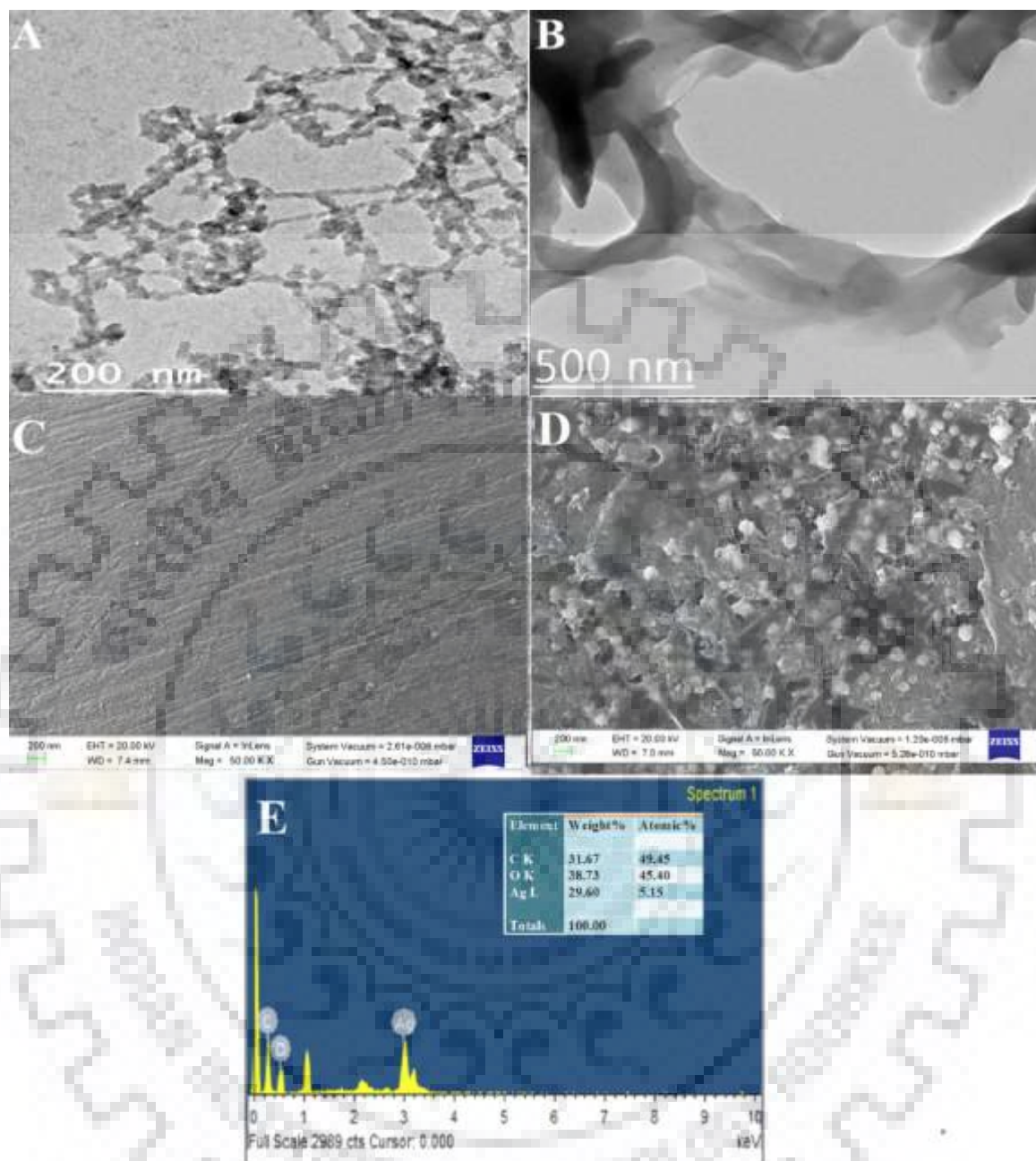
Fig. 3.24: (A) and (B) TEM images observed for GNRs. FE-SEM images demonstrating surface morphology of (C) bare/EPPG, (D) GNRs-AgNPs/EPPG and (E) EDX data of the GNRs-AgNPs nanocomposite at modified sensor surface.

Raman spectroscopy has been applied to characterize the GNRs prepared by using SWCNT. **Fig. 3.25 (A)** presents the Raman spectrum of pure SWCNT and a characteristic peak of SWCNT due to the sp^2 symmetry is observed as G band at 1590 cm^{-1} **(curve b)**. The curve a demonstrates the spectrum observed for GNRs prepared and a broad D band **(in curve a)** is

observed at 1358 cm⁻¹, due to the formation of GNRs and presence of defects in nanoribbons and edges of SWCNT. The increment in the intensity ratio of the I_D/I_G, indicates that formation of GNRs as earlier reported [120, 125]. X-ray diffraction (XRD) analysis of the GNRs-AgNPs shown in **Fig. 3.25 (B)** indicated the crystalline nature of the particles. A peak was observed for GNRs at $2\theta = 25.94^o$, which corresponded to the (0 0 2) plane lattice [126]. The diffraction spectrum of GNRs-AgNPs displayed the major peaks of Ag in the form of nanocrystal at 38.25°, 44.42°, 64.55° and 77.30°, corresponding to the (1 1 1), (2 0 0), (2 2 0) and (3 1 1) planes respectively [127].
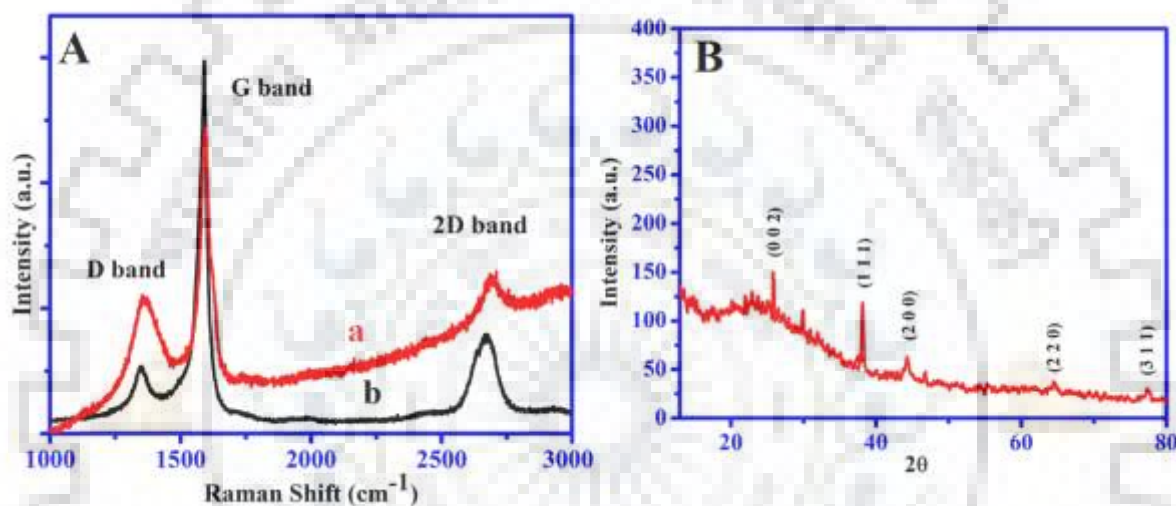
Fig. 3.25: (A) Raman spectrum observed for GNRs (a) and SWCNTs (b), and (B) XRD pattern observed for GNRs-AgNPs nanocomposite at modified surface.

The EIS studies were carried out in 0.01 M KCl and 5 mM $K_3[Fe(CN)_6]$ solution (1:1) over the 1000 kHz to 0.001 Hz frequency range. To evaluate the Rct value, Randle's circuit **(inset Fig. 3.26)** has been used. The typical Nyquist plots observed consisted two portions, one is the semi-circular indicating the charge transfer resistance (Rct) and the linear portion indicating the mass transfer effect at lower frequency [128]. The Nyquist plots observed corresponding to the unmodified/EPPG, GNRs/EPPG and GNRs-AgNPs/EPPG sensors are presented in **Fig. 3.26**. The R_{CT} values for unmodified/EPPG, GNRs/EPPG and GNRs-AgNPs/EPPG were observed as 1172 Ω **(curve a)**, 768.1 Ω **(curve b)** and 597 Ω **(curve c)** respectively. The decrease of the Rct value of GNRs-AgNPs/EPPG in comparison to GNRs/EPPG and bare/EPPG indicated that the GNRs-AgNP/EPPG modified sensor has high electrocatalytic activity and facilitated the electron

transfer reaction. Thus, the GNRs-AgNP/EPPG modified sensor was used for further electrochemical investigations.
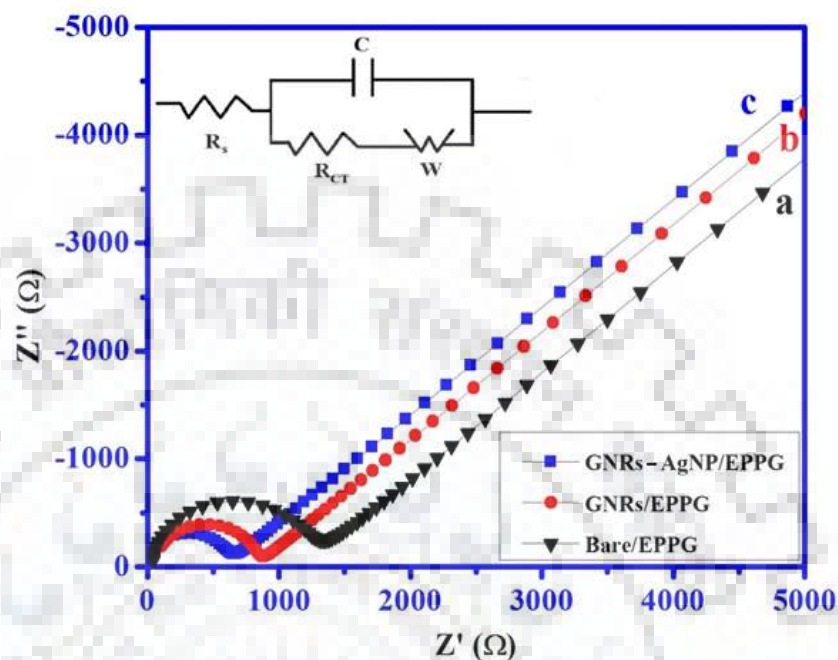
Fig. 3.26: Typical Nyquist plots observed for (a) bare/EPPG, (b) GNRs/EPPG and (c) GNRs-AgNPs/EPPG in 1:1 mixture of 5 mM $K_3Fe(CN)_6$ and 1 mM KCl solution over the frequency range 1000 kHz to 0.001Hz.

3.9.2 Cyclic voltammetry

The redox behavior of HTM was initially studied using cyclic voltammetry (CV). The voltammograms were recorded for 75 µM HTM at the unmodified, GNRs modified and GNRs-AgNPs modified EPPG sensor at 100 mV/s scan rate in pH 7.2 phosphate buffer. A small broad bump at 1000 mV was observed for oxidation of HTM at bare/EPPG as shown in **Fig 3.27 (a)**. The anodic response of HTM at GNRs/EPPG is demonstrated in **Fig 3.27 (b)**, and almost similar peak is observed, whereas for GNRs-AgNPs/EPPG a well defined peak is observed at 952 mV as shown in **Fig 3.27 (c)**. No reduction peak was observed in the reverse scan, indicating that oxidation of HTM is irreversible. Thus, the best result was noticed at GNRs-AgNPs modified sensor, hence further study of the HTM was carried out by using the GNRs-AgNPs/EPPG sensor. Ikhsan et. al., Shin et al. and Donini et al. used composite of graphene oxide and AgNPs modified ITO and GCE electrode for determination of nitric oxide, dopamine and estriol but no oxidation peak was

observed for Ag^0/Ag^{+1} in phosphate buffer (pH 2.5, 7.4 and 9.0). Graphene oxide is suggested to play an important role in protecting the surface oxidation of AgNPs [129-131].
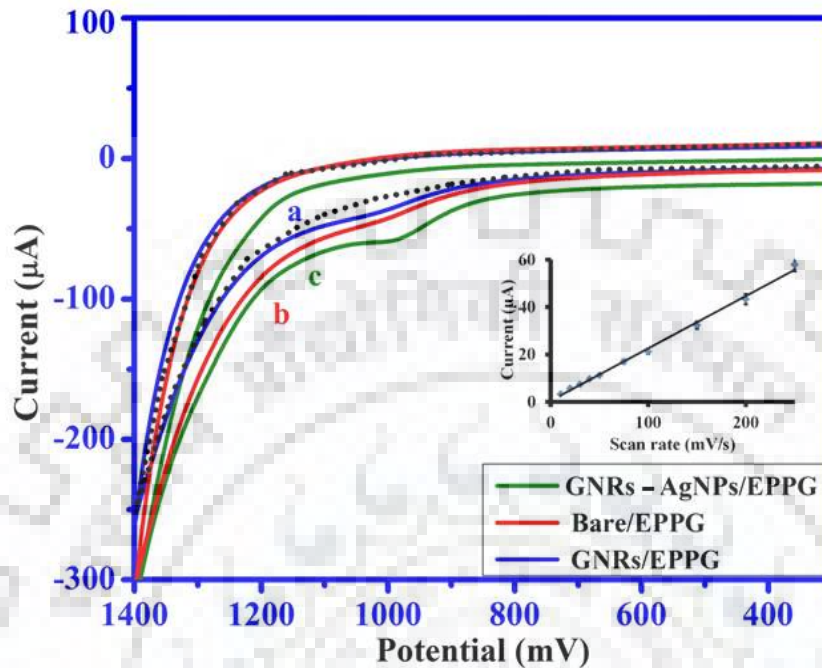
Fig. 3.27: A comparison of cyclic voltammograms observed for 75 μM HTM in phosphate buffer of pH 7.4 using at 100 mV/s (a) bare/EPPG, (b) GNRs/EPPG and (c) GNRs-AgNPs /EPPG.

To determine the information about the nature of the redox reaction involved in the electro-oxidation of HTM, the scan rate studies were performed. The effect of sweep rate on the electro-oxidation of HTM was studied at different scan rates (10–250 mV/s) as shown in insert of **Fig 3.27**. The peak current (i_p) increased with increasing scan rate (v) and a linear relation was observed between the peak current and scan rate. Such behaviour clearly indicated that the electro-oxidation of HTM followed adsorption controlled pathway, which was further supported by the linear log plot between i_p vs. v. The linear relations observed between i_p vs v and log (i_p) vs log (v) are as follows:

$$i_p = 0.221\ v + 0.508, \ldots\ldots\ldots R^2 = 0.996$$

$$\log (i_p) = 0.885 \log v - 0.413, \ldots\ldots\ldots R^2 = 0.994$$

The slope value (dlog i_p/dlog v) was > 0.5 and hence, further confirmed the adsorption controlled pathway for the electro-oxidation of HTM [128].

3.9.3 Square wave voltammetry

The SWV technique was applied for the detailed examination of HTM due to high sensitivity, high peak resolution, and low background current. A comparison of SW voltammograms for 75 µM HTM recorded at unmodified/EPPG, SWCNT/EPPG, GNRs/EPPG, GNRS-AgNPs/EPPG and AgNPs-SWCNT/EPPG at optimised conditions is presented in **Fig. 3.28**. The GNRS-AgNPs modified sensor exhibited a sharp oxidation peak (E_p ~940 mV) in comparison to the small peak at bare/EPPG (Ep ~1000 mV), SWCNT/EPPG (E_p ~1004 mV), GNRs/EPPG (E_p ~996 mV) and AgNPs-SWCNT/EPPG (Ep ~998 mV). The experiments were also performed at AgNPs-SWCNT modified EPPG and only AgNPs modified electrode (Control) to find out the utility of GNRs. An oxidation peak of silver at around 790 mV was observed at only AgNPs modified electrode, however, when AgNPs-SWCNT or GNRs-AgNPs modified sensor was used, no peak of silver oxidation was observed upto +1.0 V. This indicated that SWCNT and GNRs stabilize the AgNPs. This is common and has been reported earlier [106]. In the case of SWCNT, the peak current is increased in comparison to bare and GNR modified sensors, but when GNRs and AgNPs are used a shift in the peak potential to less positive potentials was also noticed. Hence, all the subsequent studies of the HTM were carried out by using the GNRs-AgNPs/EPPG sensor.
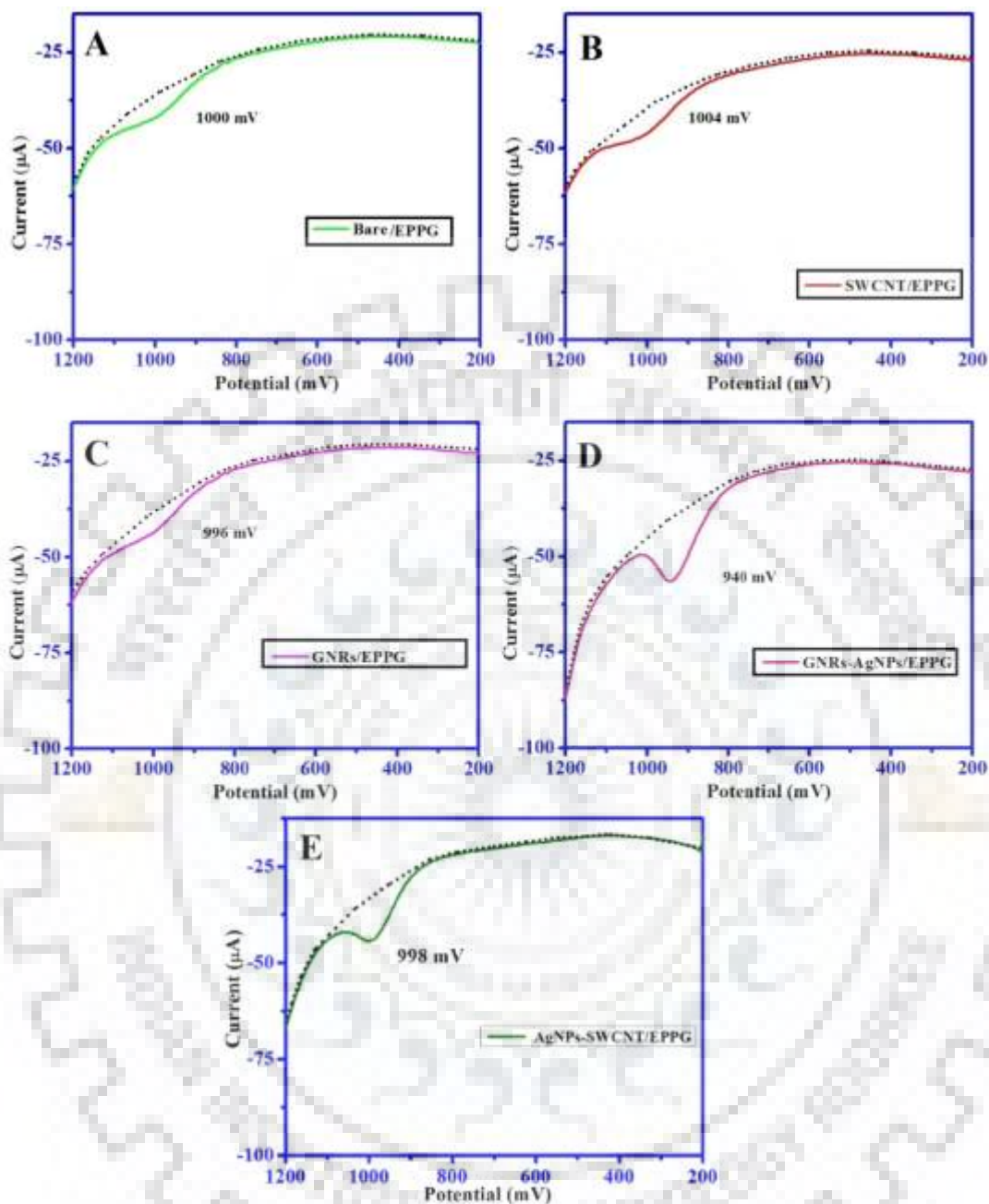
Fig. 3.28: A comparison of SW voltammograms recorded for 75 μM HTM in pH 7.4 phosphate buffer at (A) bare EPPG, (B) SWCNT/EPPG, (C) GNRs/EPPG, (D) GNRs-AgNPs/EPPG and (E) AgNPs-SWCNT/EPPG.

3.9.3.1. Effect of Frequency

The effect of the square wave frequency on the oxidation peak current of HTM (75μM) at GNRs-AgNPs/EPPG was examined in the range 5–30 Hz. The peak current response was recorded at pH 7.2 and the peak current increased with increase in the frequency **(Fig. 3.29)**. A linear

125

relation was observed between frequency (f) and anodic peak current (i_p) and the dependency of i_p on f can be represented by the relation;

$$i_p = 0.603\,f + 5.933, \ldots\ldots.. \ R^2 = 0.997$$

where, R^2 is the correlation coefficient. The log plot between i_p vs. f was also found linear and can be presented as

$$\log i_p = 0.568 \log f + 0.525, \ldots\ldots. \ R^2 = 0.996$$

As the value of dlog i_p/dlog f was > 0.5, it further confirmed that electro-oxidation of HTM at GNRs-AgNPs/EPPG sensor was adsorption controlled [128].
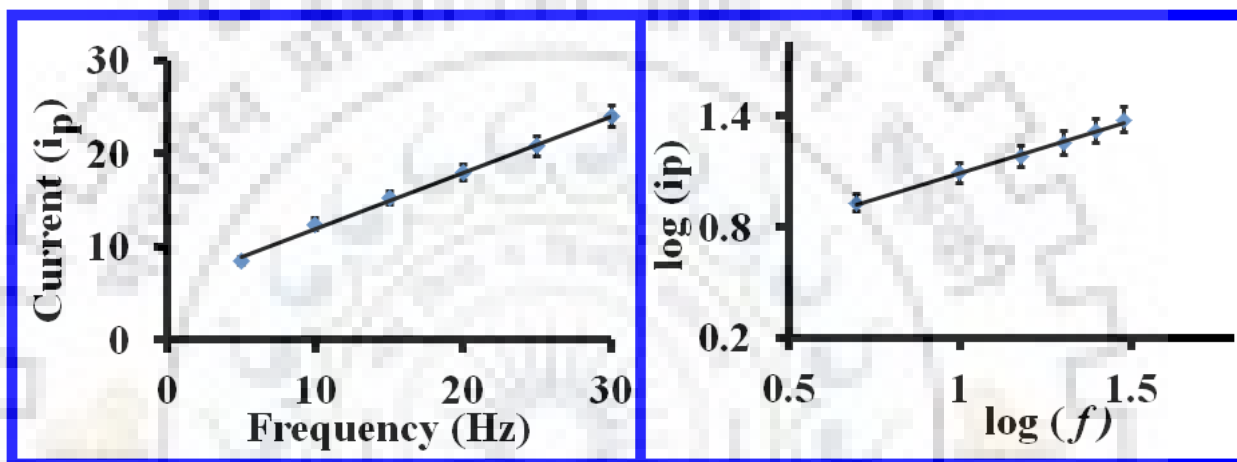
Fig. 3.29: Variation of (A) oxidation peak current (i_p) with the square wave frequency (f) and (B) log (i_p) with log (f) for 75 µM HTM using GNRs-AgNPs /EPPG sensor.

3.9.3.2 Effect of concentration

To study the effect of concentration on the peak current of HTM, SW voltammograms were recorded at pH 7.2 in the range of 1–500 µM at GNRs-AgNPs/EPPG sensor as depicted in **Fig. 3.30**. The peak current increased with the increase in the HTM concentration. The background current was subtracted to calculate the oxidation peak current (i_p) values and the plot of i_p vs concentration displayed a break between 50–60 µM. The dependence of i_p vs. concentration in the two linear ranges can be expressed by the relations:

$$i_p = 0.158\,[C, 1\text{–}50] + 1.370, \ldots\ldots.. \ R^2 = 0.993$$

$$i_p = 0.083\,[C, 60\text{–}500] + 13.84, \ldots\ldots. \ R^2 = 0.990$$

where, R^2 is the correlation coefficient and [C] is HTM concentration in µM. The sensitivity of GNRs-AgNPs/EPPG sensor was found to be 0.158 and 0.083 µA/µM. In the quantitative determination of HTM, the analytical parameters observed are documented in **Table 3.10**.
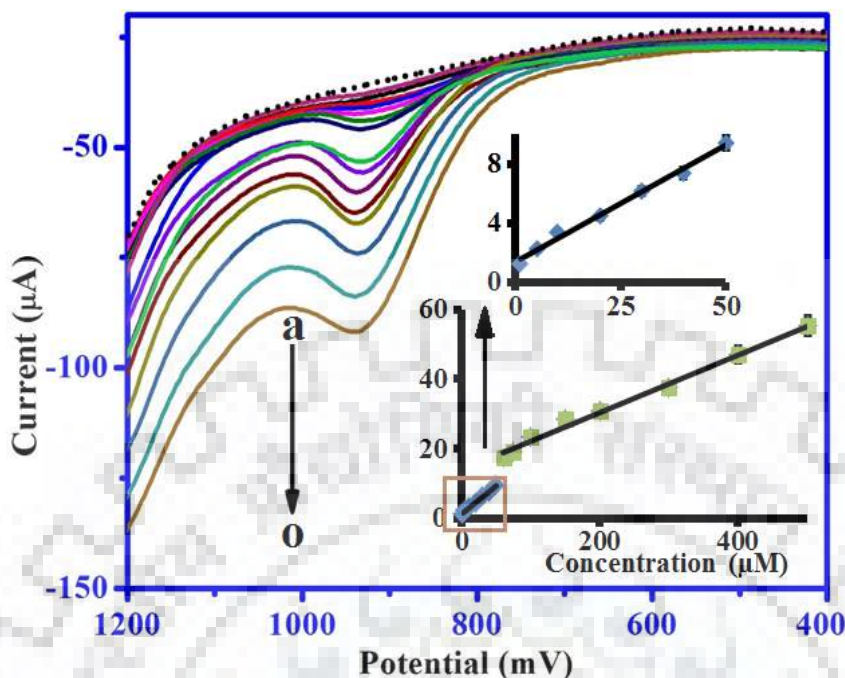
Fig. 3.30: Square wave voltammograms recorded for (a)1 µM, (b) 5 µM, (c) 10 µM, (d) 20 µM, (e) 30 µM, (f) 40 µM, (g) 50 µM, (h) 60, (i) 75 µM, (j) 100 µM, (k) 150 µM, (l) 200 µM, (m) 300 µM, (n) 400 µM and (o) 500 µM HTM concentrations using GNRs-AgNPs/EPPG. The background current is represented by the dotted line. A calibration plot of HTM is presented in the inset.

The formula 3σ/b was used to calculate the limit of detection of HTM at GNRs-AgNPs/EPPG sensor, where σ is the standard deviation of the peak current of five repeated blank readings and b is the slope of the calibration plot. The limit of detection (L.O.D.) was observed as 0.049 µM in the linear range.

Table 3.10: Statistical parameters obtained for quantitative analysis of HTM by using SWV.

Validation Parameters	Determination of HTM	
Concentration (µM)	5–50	60–500
Sensitivity (µA/µM)	0.152	0.083
Correlation coefficient (R^2)	0.994	0.990
Standard error of slope (α, 0.05)	0.006	0.003
Intercept	1.563	13.840
Standard error of intercept (α, 0.05)	0.178	0.901

A comparison of the L.O.D. observed with recently reported by electrochemical methods for HTM are tabulated in **Table 3.11** and it can be clearly seen that the present sensor is highly sensitive in comparison to the ones reported.

Table 3.11: A comparison of Limit of Detection (LOD) obtained for HTM using the proposed method with the previously reported sensors

S.No.	Electrode/Technique	LOD (µM)	Concentration range (µM)	Reference
1.	nAu-GCE, PAD	0.60	2–100	[82]
2.	MWCNTs/p-(AHNSA)/GCE, DPV	0.076	0.1–100	[86]
3.	Diamond electrode, FIA	0.50	0.5–100	[98]
4.	Lignin/GCE, SWV	0.28	5–200	[99]
5.	SPCE with ReO2, Amperometry	1.80	4.5–90	[100]
6.	SWCNT/CPE, DPV	1.26	4.5–180	[101]
7.	DAO-MBs/ carbon electrode, Amperometry	8.25	4.5–5.3	[102]
8.	GNRs-AgNPs/EPPG, SWV	0.049	1–50, 60–500	**Present work**

PAD: pulsed amperometric detection, DPV: differential pulse voltammetric: diamine oxidase (DAO) conjugated to magnetic beads (MBs), CPE: carbon paste electrodes, p-AHNSA: poly (a-amino-3-hydroxynapthalene sulfonic acid), FIA: flow injection analysis

To demonstrate the utility of GNRs over SWCNT at the sensor surface with AgNPs, SWCNT-AgNPs/EPPG modified sensor was similarly prepared. Voltammograms were then recorded for different concentrations of HTM under identical conditions. A linear calibration curve was observed in the concentration range 10–60 µM. The LOD was observed as 0.112 µM, which was higher than the LOD observed at GNRs-AgNPs/EPPG. Thus, it is concluded that GNRs-AgNPs/EPPG sensor is more sensitive than SWCNT-AgNPs /EPPG.

3.9.3.3. Effect of pH

The effect of pH on the E_p of 75 µM HTM was studied in the pH range 4.19 to 9.41. A well-defined oxidation peak was observed in the entire pH range studied. The oxidation potential

of HTM was shifted towards the less positive values with the increase of pH **(Fig. 3.31)**. The plot of E_p versus pH was linear and can be expressed by the relation:

$$E_p = -65.213 \text{ pH } (4.19–9.41) + 1419.9, …….. R^2 = 0.993$$

where, R^2 is the correlation coefficient and E_p is the peak potential in mV. The slope (dE_p/dpH) value of the plot was 65.213 mV/pH and suggested the involvement of equal numbers of protons and electrons in the oxidation of HTM. A mechanism involving 4e, 4 H^+ for the oxidation of HTM has already been proposed by Degefu et. al [99].
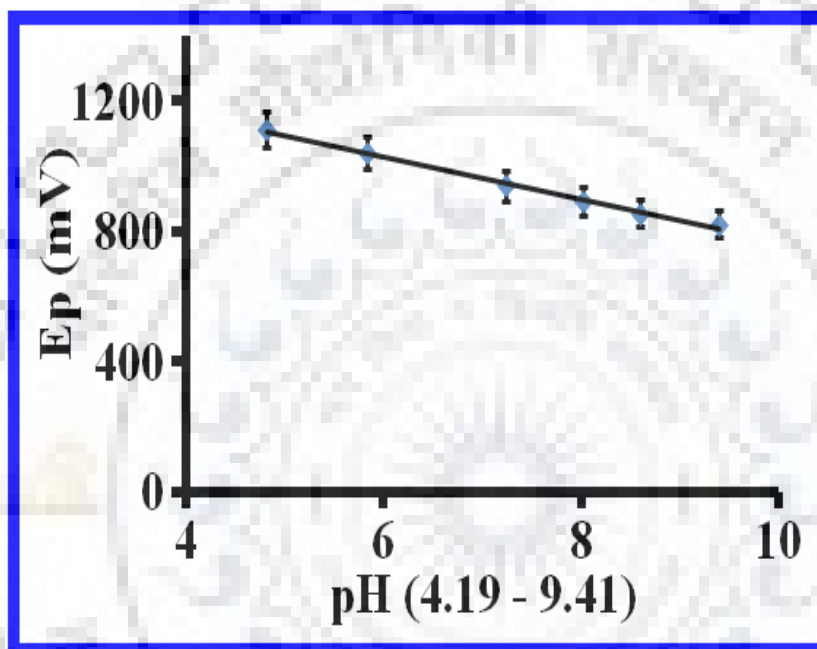
Fig. 3.31: Dependence of peak potential of HTM observed on pH.

3.9.4 Interference study

Under the optimized experimental conditions selectivity of GNRs-AgNPs/EPPG sensor was examined with commonly present interfering substance like UA, XT and AA on the voltammetric response of a fixed concentration of analytes. The SW voltammograms were recorded at different concentration of interferents having a fixed concentration of 30 μM HTM. The anodic peaks for AA and XT were found at -10 and 650 mV respectively, whereas, UA exhibited two oxidation peaks at 300 and 1025 mV as reported by Dryhurst et. al [132]. The second oxidation peak of the uric acid at higher potentials at concentration > 5 μM interfered in the determination of HTM because of close oxidation potential **(Fig. 3.32)**, whereas AA and XT did not interfere in the determination even upto 250 and 300 μM concentration respectively.
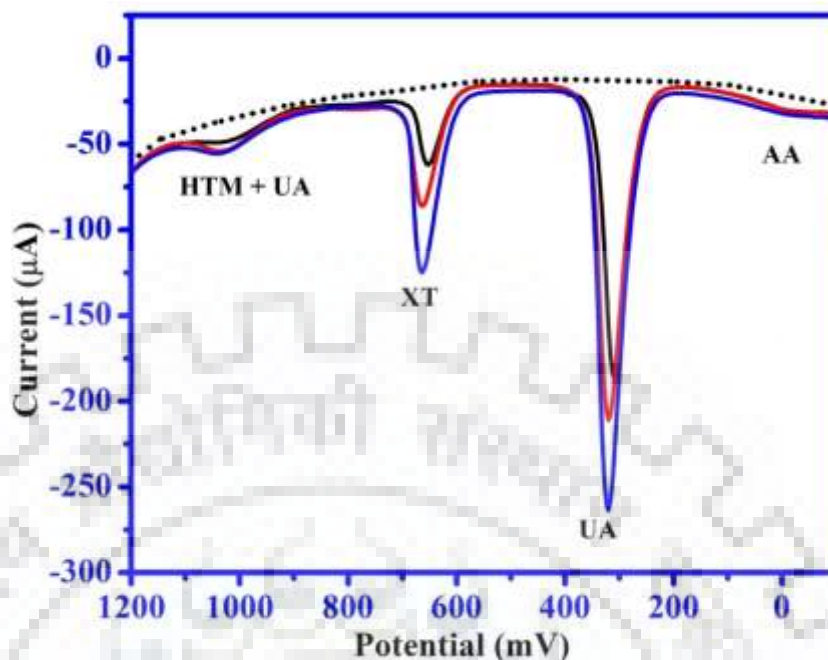
Fig. 3.32: Square wave voltammograms recorded in the presence of 30 µM HTM with (a) 150 µM UA + 100 µM XT + 100 µM AA, (b) 300 µM UA + 200 µM XT + 200 µM AA and (c) 400 µM UA + 300 µM XT + 250 µM AA at pH 7.4. Background current is represented by the dotted line.

3.9.5 ANALYTICAL APPLICATION

3.9.5.1 Recovery study

The applicability of the proposed voltammetric GNRs-AgNPs/EPPG sensor for the determination of HTM in spiked plasma samples was examined. The plasma samples were diluted two times by using the phosphate buffer (pH 7.2) to reduce the complex behaviour of the samples. The diluted plasma samples were spiked with known amount of histamine and used for further studies. The obtained results are shown in **Table 3.12**, indicating the good recovery in human blood plasma samples with low RSD (2.46%). The observed results indicated the good recovery and practical applicability of the GNRs-AgNPs/EPPG sensor for quantification of HTM in biological samples.

Table 3.12: Recovery data observed for HTM in human blood plasma samples

S.No.	Spiked amount (μM)	Detected amount (μM)[*]	Recovery %	Error %
Sample 1				
1	10	9.96	99.60	-0.40
2	20	19.86	99.30	-0.70
3	30	29.65	98.83	-1.17
Sample 2				
1	10	9.98	99.80	-0.20
2	20	20.06	100.30	+0.30
3	40	39.86	99.65	-0.35

*RSD for the determination was 1.57% for n=3

3.9.5.2 Analysis of HTM in red wine

The concentration of the biogenesis HTM has been found to be present in red wines (11.1 mg/L), which is higher than any fruits wines, ice-wine and white wines [133]. Hence, the applicability of the proposed voltammetric sensor was examined for the determination of HTM in wine sample. The standard addition method was applied to investigate the HTM concentration in red wine sample. For this purpose, the wine sample was filtered and the different concentrations of the HTM were spiked in the diluted wine sample and the square wave voltammetric response was recorded. A standard addition, curve was plotted in between the observed peak current and spiked concentration of HTM **(Fig. 3.33)**. The negative intercept on x-axis demonstrated the presence of the HTM concentration in the wine sample. The amount of the HTM was observed as 12.8 μM in the red wine sample. The lower value of RSD (±1.73%) shows the good reliability and accuracy of the developed sensor.
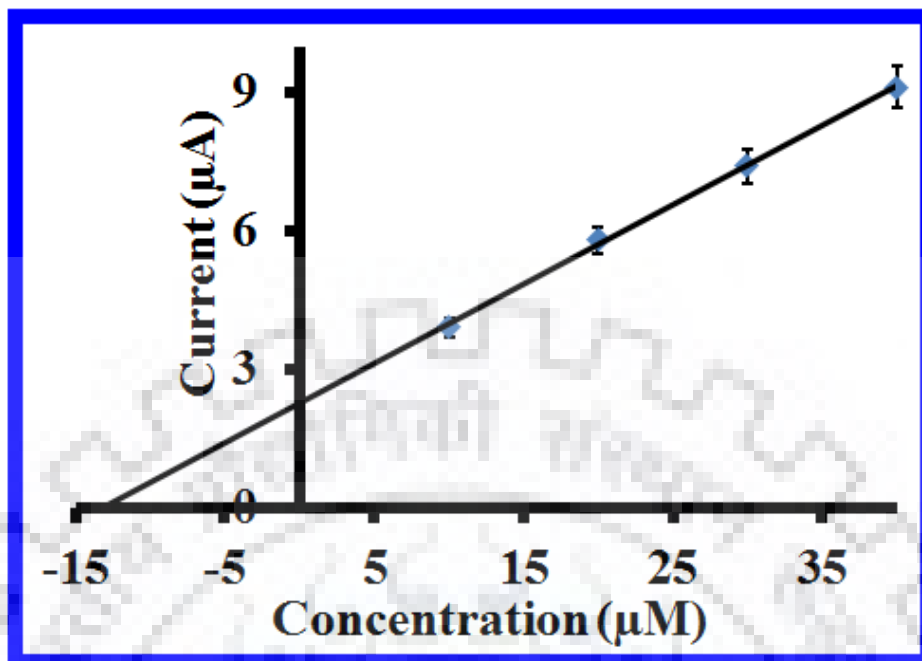
Fig. 3.33: The standard addition plot observed for HTM concentration in red wine sample.

The results of analysis were validated using HPLC. A sharp peak at 16.721 min was observed in HPLC chromatogram for HTM **(Fig. 3.34)**. Different concentrations of HTM were then analyzed and the area under the peaks was plotted against concentration. The red wine sample was then injected in HPLC and the area of the peak observed at 16.741 min was determined. The concentration of HTM calculated from the calibration plot was determined and found to be 12.7 µM. Thus, the practically similar values of HTM by the two methods indicated that the sensor is sufficiently sensitive.
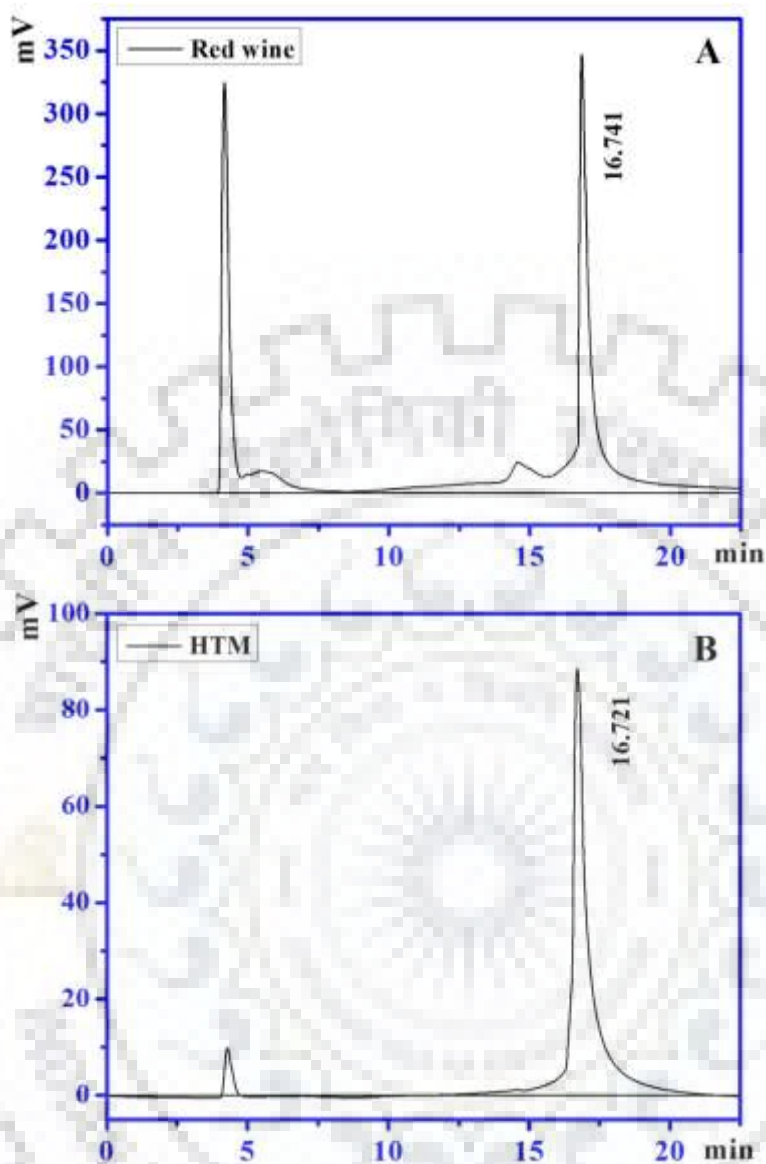
Fig. 3.34: A comparison of HPLC chromatogram observed for (A) red wine and (B) 5 µM HTM.

3.9.6. Stability and reproducibility of the sensor

The stability of GNRs-AgNPs/EPPG sensor was investigated under optimized SWV parameters. The current response at a fixed HTM concentration (10 µM) was recorded once daily for 30 days. The results demonstrated that current deviated $< \pm 3.8\%$ for first 24 days, after which a drop in the current up to 5.8% was noticed. Therefore, the developed GNRs-AgNPs/EPPG sensor can be employed safely for 24 days after its modification. The developed sensor can be used for 30 scans. The results indicate that after the 30 scans the response deviate up to 6.8%. So the developed sensor successfully works till 30 scans.

Similarly for intra molecular stability, voltammograms were recorded at an interval of 1 h within a day. The R.S.D. was found to be ±2.16% for n=8 measurements, which suggested good stability and reproducibility of the developed sensor. To investigate the sensor to sensor deviation, three GNRs-AgNPs/EPPG sensors were fabricated under the same protocol used for the modification. The voltammetric experiments were performed at pH 7.2 in 10 μM HTM solutions for each sensor individually. A small deviation was noticed in the current response of HTM having RSD as ±2.48%. Hence, it is concluded that the proposed sensor has high reproducibility and stability.

3.9.7. Ruggedness studies

To avoid the variation during interlaboratory studies of GNRs@AgNPs/EPPG sensor, ruggedness study has been executed under the identical parameter. To investigate the instruments related problems in the term of voltammetric response, two voltammetric analyzers viz., CV-50W and Epsilon (Bioanalytical system, WL, USA) were applied. The intermediate precision of GNRs@AgNPs/EPPG sensor was executed on different days by using two different analysts. The results observed at different instruments and sensor showed a deviation of ±1.68% in the current response of HTM and the observed results are summarized in **Table 3.13**. Thus, presented GNRs@AgNPs/EPPG sensor shows the robust, reliable and rugged system for the analysis the HTM.

Table 3.13: The robustness and ruggedness of the proposed method for the recovery data of HTM determination in blood plasma samples

Variables	Recovery % ± R.S.D
Robustness at pH=7.2	99.23 ± 1.47
Ruggedness Analyst 1	
Instrument: CV 50W	98.57 ± 1.67
Instrument: Epsilon EC-USB	99.43 ± 1.53
Ruggedness Analyst 2	
Instrument: CV 50W	99.32 ± 1.61
Instrument: Epsilon EC-USB	98.43 ± 1.34

3.10 CONCLUSION

GNRs and composite of GNRs-AgNPs were synthesized and characterized by using the FE-SEM, EDX, TEM, HRTEM, film XRD and EIS. The electrochemical investigation of HTM at the surface of GNRs-AgNPs fabricated edge plane pyrolytic graphite sensor were carried out using SWV. The observed oxidation of HTM was adsorption controlled and involved equal number of electrons and protons. Linear calibration curves between peak current and HTM concentration were noticed in the range 1–50 μM and 60–500 μM. The GNRs-AgNPs/EPPG sensor exhibited superiority in the term of high sensitivity and low limit of detection in comparison to sensor reported in recent years. The low Rct value at GNRs-AgNPs/EPPG sensor has shown the high catalytic ability of the developed protocol. The sensitive response of GNRs-AgNPs/EPPG sensor to HTM is most likely due to the increase of effective surface area and catalytic activity of AgNPs and GNRs. The analysis of HTM in blood plasma samples indicated the good recovery and the HTM observed in red wine was validated using HPLC and the values were practically similar. Thus, the proposed sensor can be successfully used for the determination of HTM in real samples.

3.11 REFERENCES

[1]   M. Jia, S. Li, L. Zang, X. Lu, H. Zhang, "Analysis of biomolecules based on the surface enhanced Raman spectroscopy", Nanomaterials 8 (2018) 730.

[2]   M. Labib, E.H. Sargent, S.O. Kelley, "Electrochemical methods for the analysis of clinically relevant biomolecules", Chem. Rev. 116 (2016) 9001–9090.

[3]   C.B. Jacobs, M.J. Peairs, B.J. Venton, "Review: Carbon nanotube based electrochemical sensors for biomolecules", Anal. Chim. Acta 662 (2010) 105–127.

[4]   R.A. Webster, "Neurotransmitter, drugs and brain function", John Wiley & Sons Ltd, UK, (2001).

[5]   Y. Chen, Y. Zheng, N. Wang, S. Lu, T. Pang, Q. Yang and G. Xu, "Significant of urinary nucleosides detection in diagnosis of gastric carcinoma", Aizheng 22 (2003) 537–539.

[6]   P. Gupta, R.N. Goyal, "Graphene and co-polymer composite based molecularly imprinted sensor for ultratrace determination of melatonin in human biological fluids", RSC Adv. 5 (2015) 40444–40454.

[7]   D. Kriz, O. Ramstrom, K. Mosbach, "Peer reviewed: Molecular imprinting: New possibilities for sensor technology", Anal. Chemi. 69(11) (1997) 345A–349A.

[8]   L.M. Kindschy, E.C. Alocilja, "Development of a molecularly imprinted biomimetic electrode", Sensors 7 (2007) 1630–1642.

[9]   D. Lakshmi, B.B. Prasad, P.S. Sharma, "Creatinine sensor based on a molecularly imprinted polymer-modified hanging mercury drop electrode", Talanta 70 (2006) 272–280.

[10]   D.C. Apodaca, R.B. Pernites, R. Ponnapati, F.R.D. Mundo, R.C. Advincula, "Electropolymerized molecularly imprinted polymer film: EIS sensing of bisphenol A", Macromolecules 44 (2011) 6669–6682.

[11]   X. Wang, L. Wang, X. He, Y. Zhang, L. Chen, "A molecularly imprinted polymer-coated nanocomposite of magnetic nanoparticles for estrone recognition", Talanta 78 (2009) 327–332.

[12]   R. Schirhagl, "Bioapplications for molecularly imprinted polymers", Anal. Chem. 86 (2014) 250−261.

[13]   Rosy, H. Chasta, R.N. Goyal, "Molecularly imprinted sensor based on o-aminophenol for the selective determination of norepinephrine in pharmaceutical and biological samples", Talanta 125 (2014) 167–173.

[14]   A.A. Abdelwahab, H.M. Lee, Y.B. Shim, "Selective determination of dopamine with a cibacron blue/poly-1,5-diaminonaphthalene composite film", Anal. Chim. Acta 650 (2009) 247–253.

[15]   J. Zhang, S. Yang, H. Wang, S. Wang, "Enhanced sensitivity for biosensors: Functionalized P1,5-diaminonaphthalene-multiwall carbon nanotube composite film-modified electrode", Electrochim. Acta 85 (2012) 467–474.

[16]   I. Migneault, C. Dartiguenave, M.J. Bertrand, K.C. Waldron, "Glutaraldehyde: Behavior in aqueous solution, reaction with proteins, and application to enzyme crosslinking", BioTechniques 37 (2004) 790–802.

[17]   R. Pauliukaite, M.E. Ghica, O.F. Filho, C.M.A. Brett, "Comparative study of different cross-linking agents for the immobilization of functionalized carbon nanotubes within a chitosan film supported on a graphite-epoxy composite electrode", Anal. Chem. 81 (2009) 5364–5372.

[18]   S. Zhang, X. Song, W. Zhang, N. Luo, L. Cai, "Determination of low urinary 8-hydroxy-2`-deoxyguanosine excretion with capillary electrophoresis and molecularly imprinted monolith solid phase microextraction", Sci. Total Environ. 450–451 (2013) 266–270.

[19]   R. Arunachalam, A.P. Reshma, V. Rajeev, S.B. Kurra, M.J. Prince, N. Syam, "Salivary 8-hydroxydeoxyguanosine – a valuable indicator for oxidative DNA damage in periodontal disease", The Saudi J. Dental Res. 6 (2015) 15–20.

[20]   S. Mei, Q. Yao, C. Wu, G. Xu, "Determination of urinary 8-hydroxy-2-deoxyguanosine by two approaches-capillary electrophoresis and GC/MS: An assay for in vivo oxidative DNA damage in cancer patients", J. Chromatogr. B 827 (2005) 83–87.

[21]   A. Pilger, S. Ivancsits, D. Germadnik, H.W. Rudiger, "Urinary excretion of 8-hydroxy-2-deoxyguanosine measured by high-performance liquid chromatography with electrochemical detection", J. Chromatogr. B 778 (2002) 393–401.

[22]   D. Nakae, Y. Kobayashi, H. Akai, N. Andoh, H. Satoh, K. Ohashi, M. Tsutsumi, Y. Konishi, "Involvement of 8-hydroxyguanine formation in the initiation of rat liver carcinogenesis by low dose levels of N-nitrosodiethylamme", Cancer Res. 57 (1997) 1281–1287.

[23]   M. Shi, H. Takeshita, M. Komatsu, B. Xu, K. Aoyama, T. Takeuchi, "Generation of 8-hydroxydeoxyguanosine from DNA using rat liver homogenates", Cancer Sci. 96 (2005) 13–18.

[24]   D. Kato, M. Komoriya, K. Nakamoto, R. Kurita, S. Hirono, O. Niwa, "Electrochemical determination of oxidative damaged DNA with high sensitivity and stability using a nanocarbon film", Anal. Sci. 27 (2011) 703–707.

[25]   L.J. Kroese, P.G. Scheffer, "8-Hydroxy-2′-deoxyguanosine and cardiovascular disease: A Systematic Review", Curr Atheroscler Rep 16(452) (2014) 1–8.

[26]   T. Akimoto, Y. Morishita, C. Ito, O. Limura, S. Tsunematsu, Y. Watnabe, E. Kusano, D. Nagata, "Febuxostat for hyperuricimia in patients with advanced chronic kidney disease", Drug Target Insights 8 (2014) 39–43.

[27]   S. Mei, G. Xu, J. Xing, C. Wu, "Method for the analysis of 8-hydroxy-2′-deoxyguanosine in urine by gas chromatography", Anal. Sci. 17 (2001) 779–781.

[28]   C. Wan, T. Liu, S. Wei, S. Zhang, "Electrochemical determination of 8-Hydroxydeoxyguanosine using a carbon nanotube modified electrode", Russ. J. Electrochem. 44(3) (2008) 351–356.

[29]   A. Gutierrez, S. Gutierrez, G. Garcia, L. Galicia, G.A. Rivas, "Determination of 8-hydroxy 2'-deoxyguanosine using electrodes modified with a dispersion of carbon nanotubes in polyethylenimine", Electroanalysis 23(5) (2011) 1221–1228.

[30]   Y.H. Wang, J. Li, Y. Liu, R.N. Ma, W. L. Jia, H. Cui, H.S. Wang, "Fabrication of the DNA/poly(3-methylthiophene) composite film modified electrode and its application for the study on the voltammetric behavior and determination of 8-hydroxy-2'-deoxyguanosine", Sci China Ser B-Chem 52(11) (2009) 2006–2012.

[31]   T.H. Li, W.L. Jia, H.S. Wang, R.M. Liu, "Electrochemical performance of 8-hydroxy-2-deoxyguanosine and its detection at poly(3-methylthiophene) modified glassy carbon electrode", Biosens. Bioelectron. 22 (2007) 1245–1250.

[32]   L. Yang, B. Wang, H. Qi, Q. Gao, C.Z. Li, C. Zhang, "Highly sensitive electrochemical sensor for the determination of 8-Hydroxy-2-deoxyguanosine incorporating SWCNTs-nafion composite film", Journal of Sensors 2015 (2015), 1–11. (http://dx.doi.org/10.1155/2015/504869).

[33]   A. Gutierrez, F.A. Gutierrez, M. Eguilaz, J.M.G. Dominguez, J.H. Ferrer, A. Anson-Casaos, M.T. Martinez, G.A. Rivas, "Electrochemical sensing of guanine, adenine and 8-hydroxy-2-deoxyguanosine at glassy carbon modified with single-walled carbon nanotubes covalently functionalized with lysine", RSC Adv. 6 (2016) 13469-13477.

[34]   P.   Gupta, M.   Oyama, R.N.   Goyal,   "Electrochemical   investigations   of   8-hydroxydeoxyguanosine and its determination at an edge plane pyrolytic graphite electrode", RSC Adv. 6 (2016) 1722–1728.

[35]   Rosy, R.N. Goyal, "Determination of 8-hydroxydeoxyguanosine: A potential biomarker of oxidative stress, using carbon-allotropic nanomaterials modified glassy carbon sensor", Talanta 161 (2016) 735–742.

[36]   G.D. Christian, W.C. Purdy, "The residual current in orthophosphate medium", J. Electroanal. Chem. 3(6) (1962) 363–367.

[37]   S. Baskar, C.W. Liao, J.L. Chang, J.M. Zen, "Electrochemical synthesis of electroactive poly(melamine) with mechanistic explanation and its applicability to functionalize carbon surface to prepare nanotube–nanoparticles hybrid", Electrochim. Acta 88 (2013) 1–5.

[38]   E. Barsoukov, J.R. Macdonald, "Impedance spectroscopy, theory, experiment and applications", 2nd Edition, Wiley Interscience, New Jersey, (2005).

[39]   R. H. Wopschall, I. Shain, "Effects of adsorption of electroactive species in stationary electrode polarography", Anal. Chem. 39 (1967) 1527–1534.

[40]   E. Laviron, "General expression of the linear potential sweep voltammogram in the case of diffusionless electrochemical systems", J. Electroanal. Chem. 101 (1979) 19–28.

[41]   L. Fotouhi, M. Fatollahzadeh, M.M. Heravi, "Electrochemical behavior and voltammetric determination of sulfaguanidine at a glassy carbon electrode modified with a multi-walled carbon nanotube", Int. J. Electrochem. Sci. 7 (2012) 3919–3928.

[42]   E.H. Turner, J.M. Loftis, A.D. Blackwell, "Serotonin a la carte: Supplementation with the serotonin precursor 5-hydroxytryptophan", Pharmacol. Ther. 109 (2006) 325–338.

[43]   C.P.L. Bullock, K. Welshhans, S.L. Pallas, P.S. Katz, "The effect of oral 5-HTP administration on 5-HTP and 5-HT immunoreactivity in monoaminergic brain regions of rats", J. Chem. Neuroanat. 27 (2004) 129–138.

[44]   K.A. Shaw, J. Turner, C.D. Mar, "Tryptophan and 5-hydroxytryptophan for depression", Cochrane Database Syst. Rev. (2002) Issue 1, Art. No.: CD003198.
(DOI: 10.1002/14651858.CD003198).

[45]   Y. Chen, G. Li, Y. Hu, "A sensitive electrochemical method for the determination of 5-hydroxytryptophan in rats brain tissue based on a carbon nano sheets modified electrode", Anal. Methods 7 (2015) 1971–1976.

[46]   Y.T. Das, M. Bagchi, D. Bagchi, H.G. Preuss, "Safety of 5-hydroxy-L-tryptophan", Toxicol. Lett. 150 (2004) 111–122.

[47]   T.C. Birdsall, "5-Hydroxytryptophan: A clinically-effective serotonin precursor", Altern. Med. Rev. 3(4) (1998) 271–280.

[48]   I. Caruso, P.S. Puttini, M. Cazzola, V. Azzolini, "Double-blind study of 5-hydroxytryptophan versus placebo in the treatment of primary fibromyalgia syndrome", J. Int. Med. Res. 18 (1990) 201–209.

[49]   C. Cangiano, F. Ceci, A. Cascino, M.D. Ben, A. Laviano, M. Muscaritoli, F. Antonucci, F.R. Fanell, "Eating behavior and adherence to dietary prescriptions in obese adult subjects treated with 5-hydroxytryptophan", Am. J. Clin. Nutr. 56 (1992) 863–867.

[50]   G. Koppisetti, A. Siriki, K. Sukala, G.V. Subbaraju, "Estimation of L-5-hydroxytryptophan in rat serum and griffoniaseed extracts by liquid chromatography–mass spectrometry", Anal. Chim. Acta 549 (2005) 129–133.

[51]   J.L. Meek, "Application of inexpensive equipment for high pressure liquid chromatography to assays for taurine, ϒ-amino butyric acid, and 5-hydroxytryptophan", Anal. Chem. 48(2) (1976) 375–379.

[52]   S.P. Arneric, D.B. Goodale, J.R. Flynn, J.P. Long, "Rapid and simple analysis of DOPA and 5-HTP using high performance liquid chromatography with electrochemical detection", Brain Res. Bull. 6(4–6) (1981) 407–411.

[53]   G.V. Subbarajua, S. Kannababua, K. Vijayakumara, P.B.S. Murthya, M. Vanisreeb, H.S Tsay, "Spectrophotometric estimation of L- 5-hydroxytryptophan in griffonia simplicifolia extracts and dosage forms", Int. J. Appl. Sci. Eng. 3(2) (2005) 111–116.

[54]   K.H. Tachiki, M.H. Aprison, "Fluorometric assay for 5-hydroxytryptophan with sensitivity in the picomole range", Anal. Chem. 47(1) (1975) 7–11.

[55]   K. Petritis, A. Valleix, C. Elfakir, M. Dreux, "Simultaneous analysis of underivatized chiral amino acids by liquid chromatography–ionspray tandem mass spectrometry using a teicoplanin chiral stationary phase", J. Chromatogr. A 913 (2001) 331–340.

[56]   Y. Takagai, S. Igarashi, "Determination of ppb levels of tryptophan derivatives by capillary electrophoresis with homogeneous liquid–liquid extraction and sweeping method", Chem. Pharm. Bull. 51(4) (2003) 373–377.

[57]   B. Agrawal, P. Chandra, R.N. Goyal, Y.B. Shim, "Detection of norfloxacin and monitoring its effect on caffeine catabolism in urine samples", Biosens. Bioelectron. 47 (2013) 307–312.

[58]   D. Ranganathana, S. Zamponi, M. Berrettoni, B.L. Mehdi, J.A. Cox, "Oxidation and flow-injection amperometric determination of 5-hydroxytryptophan at an electrode modified by electrochemically assisted deposition of a sol–gel film with templated nanoscale pores", Talanta 82 (2010) 1149–1155.

[59]   J.L. Cohen, J. Widera, J.A. Cox, "Electrocatalytic oxidation and flow injection amperometric determination of 5-hydroxytryptophan", Electroanalysis 14(3) (2002) 231–234.

[60]   G. Chen, J. Cheng, J. Ye, "Application of a novel micro-injector in the determination of indole derivatives in the rat pineal gland by capillary electrophoresis with electrochemical detection", Fresenius J. Anal. Chem. 370 (2001) 930–934.

[61]   H.C.B. Kalachar, Y.A. Naik, S. Basavanna, R. Viswanatha, T.G. Venkatesha, T. Sheela, "Amperometric and differential pulse voltammetric determination of 5-hydroxy-L-tryptophan in pharmaceutical samples using gold modified pencil graphite electrode", J. Chem. Pharm. Res. 3(3) (2011) 530–539.

[62]   Rosy, S.K. Yadav, B. Agrawal, M. Oyama, R.N. Goyal, "Graphene modified palladium sensor for electrochemical analysis of norepinephrine in pharmaceuticals and biological fluids", Electrochim. Acta 125 (2014) 622–629.

[63]   X.M. Chen, Z.X. Cai, Z.Y. Huang, M. Oyama, Y.Q. Jiang, X. Chen, "Ultrafine palladium nanoparticles grown on graphene nanosheets for enhanced electrochemical sensing of hydrogen peroxide", Electrochim. Acta 97 (2013) 398–403.

[64]   Q. Wang, X. Cui, J. Chen, X. Zheng, C. Liu, T. Xue, H. Wang, Z. Jin, L. Qiao,W. Zheng, "Well-dispersed palladium nanoparticles on graphene oxide as a non-enzymatic glucose sensor", RSC Adv. 2 (2012) 6245–6249.

[65]   D.J Guo, H.L. Li, "Electrochemical synthesis of Pd nanoparticles on functional MWNT surfaces", Electrochem. Commun. 6 (2004) 999–1003.

[66]   G.G. Wildgoose, C.E. Banks, R.G. Compton, "Metal nanoparticles and related materials supported on carbon nanotubes : Methods and applications", Small 2(2) (2006) 182–193.

[67]   Z. Jiang, Z.J. Jiang, "Carbon nanotubes supported metal nanoparticles for the applications in proton exchange membrane fuel cells (PEMFCs)", in: "carbon nanotubes - growth and applications", M. Naraghi (Ed.), InTech Inc. (2011) 567–604.

[68]   C. Gao, Z. Guo, J.H. Liu, X.J. Huang, "The new age of carbon nanotubes: An updated review of functionalized carbon nanotubes in electrochemical sensors", Nanoscale 4 (2012) 1948–1963.

[69]   W.D. Zhang, B. Xu, L.C. Jiang, "Functional hybrid materials based on carbon nanotubes and metal oxides", J. Mater. Chem. 20 (2010) 6383–6391.

[70]   J.I. Gowda, D.G. Gunjiganvi, N.B. Sunagar, M.N. Bhat, S.T. Nandibewoor, "MWCNT–CTAB modified glassy carbon electrode as a sensor for the determination of paracetamol", RSC Adv. 5 (2015) 49045–49053.

[71]   R. Jain, S. Sharma, "Glassy carbon electrode modified with multi-walled carbon nanotubes sensor for the quantification of antihistamine drug pheniramine in solubilized systems", J. Pharm. Anal. 2(1) (2012) 56–61.

[72]   B. Yoon, C.M. Wai, "Microemulsion-templated synthesis of carbon nanotube-supported Pd and Rh nanoparticles for catalytic applications", J. Am. Chem. Soc. 127 (2005) 17174–17175.

[73]   H.C. Choi, M. Shim, S. Bangsaruntip, H. Dai, "Spontaneous reduction of metal ions on the sidewalls of carbon nanotubes", J. Am. Chem. Soc. 124 (2002) 9058–9059.

[74]   N. Karousis, G.E. Tsotsou, F. Evangelista, P. Rudolf, N. Ragoussis, N. Tagmatarchis, "Carbon nanotubes decorated with palladium nanoparticles: Synthesis, characterization, and catalytic activity", J. Phys. Chem. C 112 (2008) 13463–13469.

[75]   D. Bera, S.C. Kuiry, M. McCutchen, A. Kruize, H. Heinrich, M. Meyyappan, S. Seal, "In-situ synthesis of palladium nanoparticles-filled carbon nanotubes using arc-discharge in solution", Chem. Phys. Lett. 386 (2004) 364–368.

[76]   L. Chen, K. Yang, H. Liu, X. Wang, "Carbon nanotube supported Pd catalyst for liquid-phase hydrodehalogenation of bromobenzene", Carbon 46 (2008) 2137–2143.

[77]   X. Chen, Y. Hou, H. Wang, Y. Cao, J. He, "Facile deposition of Pd nanoparticles on carbon nanotube microparticles and their catalytic activity for Suzuki coupling reactions", J. Phys. Chem. C 112 (2008) 8172–8176.

[78]   P. Gupta, S.K. Yadav, R.N. Goyal, "A sensitive polymelamine modified sensor for the determination of lomefloxacin in biological fluids", J. Electrochem. Soc. 162(1) (2015) H86–H92.

[79]   X. Lin, Y. Li, "Monolayer covalent modification of 5-hydroxytryptophan on glassy carbon electrodes for simultaneous determination of uric acid and ascorbic acid", Electrochim. Acta 51 (2006) 5794–5801.

[80]   J.M. Feldman, "Urinary serotonin in the diagnosis of carcinoid tumors", Clin. Chem. 32(5) (1986) 840–844.

[81]   B.A. Adergani, P. Norouzi, M.R. Ganjali, R. Dinarvand, "Ultrasensitive flow-injection electrochemical method for determination of histamine in tuna fish samples", Food Res. Int. 43 (2010) 1116–1122.

[82]   V. Carralero, A.G. Cortes, P.Y. Sedeno, J.M. Pingarron, "Pulsed amperometric detection of histamine at glassy carbon electrodes modified with gold nanoparticles", Electroanalysis 17 (4) (2005) 289–297.

[83]   M.E. Denno, E. Privman, R.P. Borman, D.C. Wolin, B.J. Venton, "Quantification of histamine and carcinine in drosophila melanogaster tissues", ACS Chem. Neurosci. 7(2016) 407−414.

[84]   H.L. Haas, O.A. Sergeeva, O. Selbach, "Histamine in the nervous system", Physiol. Rev. 88 (2008) 1183–1241.

[85]   F.M. Colombo, P. Cattaneo, E. Confalonieri, C. Bernardi, "Histamine food poisonings: A systematic review and meta-analysis", Crit. Rev. Food Sci. Nutr. (2016) 1–22.

[86]   A. Geto, M. Tessema, S. Admassie, "Determination of histamine in fish muscle at multi-walled carbon nanotubes coated conducting polymer modified glassy carbon electrode", Synth. Met. 191 (2014) 135–140.

[87]   M.L.L. Moratalla, O.C. Baste, S.B. Cid, M.C.V. Carou, "Tyramine and histamine risk assessment related to consumption of dry fermented sausages by the Spanish population", Food Chem. Toxicol. 99 (2017) 78–85.

[88]   L. Maintz, N. Novak, "Histamine and histamine intolerance", Am. J. Clin. Nutr. 85 (2007) 1185–1196.

[89]   C. Teuscher, M.E. Poynter, H. Offner, A. Zamora, T. Watanabe, P.D. Fillmore, J.F. Zachary, E.P. Blankenhorn, "Attenuation of Th1 effector cell responses and susceptibility to experimental allergic encephalomyelitis in histamine H_2 receptor knockout mice is due
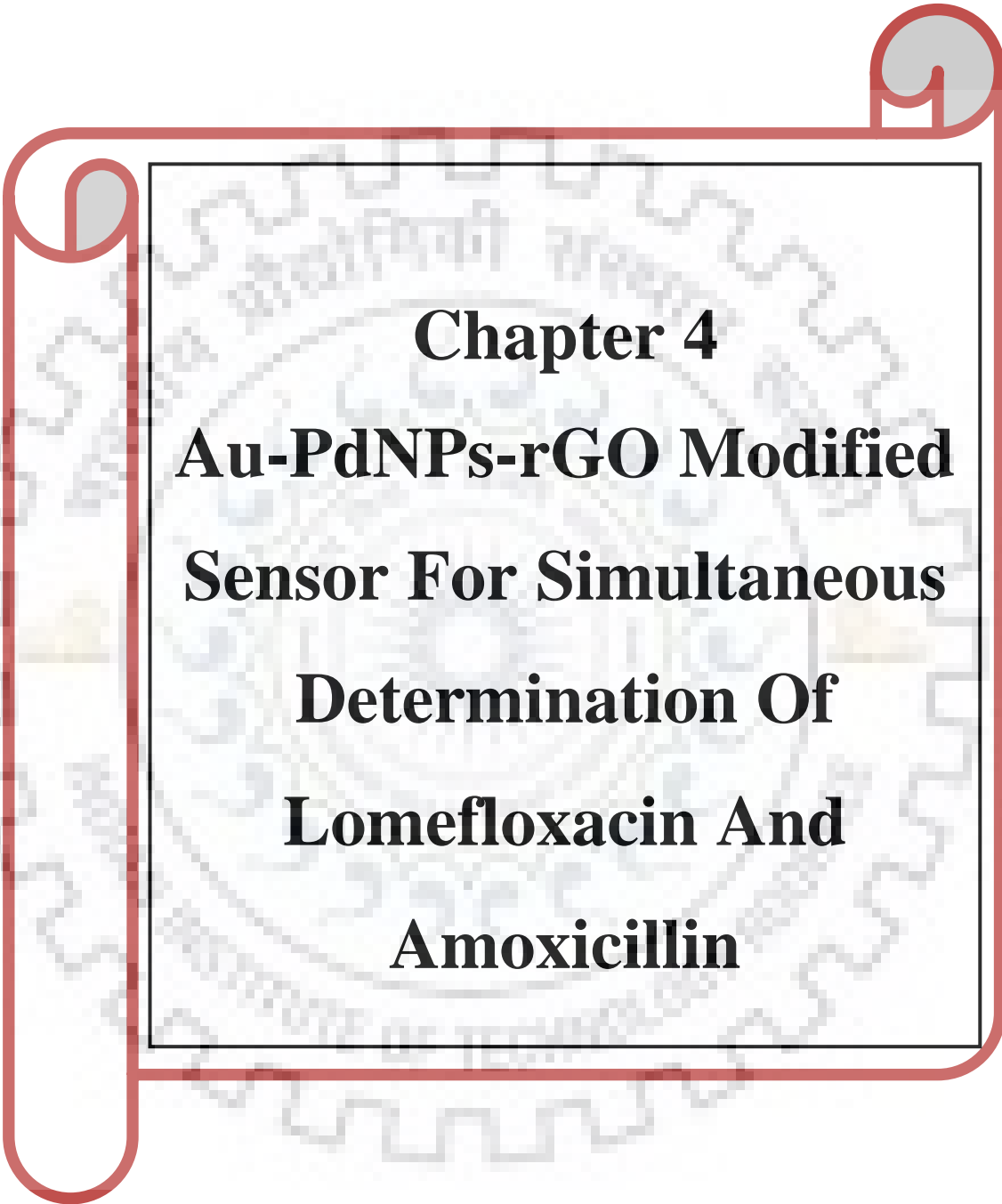
to dysregulation of cytokine production by antigen-presenting cells", Am. J. Pathol. 164 (2004) 883–891.

[90] M. Jutel, T. Watanabe, M. Akdis, K. Blaser, C.A Akdis, "Immune regulation by histamine opinion", Curr. Opin. Immunol. 14 (2002) 735–740.

[91] Z. Tao, M. Sato, Y. Han, Z. Tan, T. Yamaguchi, T. Nakano, "A simple and rapid method for histamine analysis in fish and fishery products by TLC determination", Food Control 22 (2011) 1154–1157.

[92] S.B. Patange, M.K. Mukundan, K.A. Kumar, "A simple and rapid method for colorimetric determination of histamine in fish flesh", Food Control 16 (2005) 465–472.

[93] B.S. Hwang, J.T. Wang, Y.M. Choong, "A rapid gas chromatographic method for the determination of histamine in fish and fish products", Food Chem. 82 (2003) 329–334.

[94] S. Tahmouzi, R. Khaksar, M. Ghasemlou, "Development and validation of an HPLC-FLD method for rapid determination of histamine in skipjack tuna fish (Katsuwonus pelamis)", Food Chem. 126 (2011) 756–761.

[95] J.H. Kim, I.S. Shin, Y.K. Lee, H.J. Oh, S.J. Ban, "Improved HPLC method using 2,3-naphthalenedicarboxaldehyde as fluorescent labeling agent for quantification of histamine in human immunoglobulin preparations", Public Health Res Perspect 2(2) (2011) 127–134.

[96] V. Simat, P. Dalgaard, "Use of small diameter column particles to enhance HPLC determination of histamine and other biogenic amines in seafood", LWT - Food Sci. Technol. 44 (2011) 399–406.

[97] L.Y. Zhang, M.X. Sun, "Determination of histamine and histidine by capillary zone electrophoresis with pre-column naphthalene-2,3-dicarboxaldehyde derivatization and fluorescence detection", J. Chromatogr. A 1040 (2004) 133–140.

[98] B.V. Sarada, T.N. Rao, D.A. Tryk, A. Fujishima, "Electrochemical oxidation of histamine and serotonin at highly boron-doped diamond electrodes", Anal. Chem. 72 (2000) 1632–1638.

[99] H. Degefu, M. Amare, M. Tessemaa, S. Admassie, "Lignin modified glassy carbon electrode for the electrochemical determination of histamine in human urine and wine samples", Electrochim. Acta 121 (2014) 307–314.

[100] A. Veseli, M. Vasjari, T. Arbneshi, A. Hajrizi, L. Svorc, A. Samphao, K. Kalcher, "Electrochemical determination of histamine in fish sauce using heterogeneous carbon electrodes modified with rhenium(IV) oxide", Sens. Actuator B-chem 228 (2016) 774–781.

[101] Z.S. Stojanovic, E. Mehmeti, K. Kalcher, V. Guzsvany, D.M. Stankovic, "SWCNT-modified carbon paste electrode as an electrochemical sensor for histamine determination in alcoholic beverages", Food Anal. Methods 9 (2016) 2701–2710.

[102] S. Leonardo, M. Campas, "Electrochemical enzyme sensor arrays for the detection of the biogenic amines histamine, putrescine and cadaverine using magnetic beads as immobilisation supports", Microchim. Acta 183 (2016) 1881–1890.

[103] X. Luo, A. Morrin, A.J. Killard, M.R. Smyth, "Application of nanoparticles in electrochemical sensors and biosensors", Electroanalysis 18 (2006) 319–326.

[104] C. Xu, X. Wang, "Fabrication of flexible metal-nanoparticle films using graphene oxide sheets as substrates", Small 5 (2009) 2212–2217.

[105] M. Rai, A. Yadav, A. Gade, "Silver nanoparticles as a new generation of antimicrobials", Biotechnol. Adv. 27 (2009) 76–83.

[106] P. Raveendran, J. Fu, S.L. Wallen, "Completely "Green" synthesis and stabilization of metal nanoparticles", J. Am. Chem. Soc. 125 (2003) 13940–13941.

[107] B. Swathy, "A review on metallic silver nanoparticles", J. Pharm. 4(7) (2014) 38–44.

[108] L. Han, P. Krstic, I. Kaganovich, R. Car, "Migration of a carbon adatom on a charged single-walled carbon Nanotube", Carbon 116 (2017) 174–180.

[109] R.H. Baughman, A.A. Zakhidov, W.A. de Heer, "Carbon nanotubes—the route toward applications", Science 297 (5582) (2002) 787–792.

[110] H. Chen, M.B. Muller, K.J. Gilmore, G.G. Wallace, Dan Li, "Mechanically strong, electrically conductive, and biocompatible graphene paper", Adv. Mater. 20 (2008) 3557–3561.

[111] J. Che, K. Wu, Y. Lin, K. Wang, Q. Fu, "Largely improved thermal conductivity of HDPE/expanded graphite/carbon nanotubes ternary composites via filler network-network synergy", Composites: Part A 99 (2017) 32–40.

[112] M. Pumera, "Graphene-based nanomaterials for energy storage", Energy Environ. Sci. 4 (2011) 668–674.

[113] G. Jo, M. Choe, S. Lee, W. Park, Y.H. Kahng, T. Lee, "The application of graphene as electrodes in electrical and optical devices", Nanotechnology 23 (2012) 112001 (19pp).

[114] N. Kumar, Rosy, R.N. Goyal, "Nanopalladium grained polymer nanocomposite based sensor for the sensitive determination of melatonin", Electrochim. Acta 211 (2016) 18–26.

[115] Y. Shao, J. Wang, H. Wu, J. Liu, I.A. Aksay, Y. Lin, "Graphene based electrochemical sensors and biosensors: A review", Electroanalysis 22 (2010) 1027–1036.

[116] Z. Zhu, L.G. Gancedo, A.J. Flewitt, H. Xie, F. Moussy, W.I. Milne, "A critical review of glucose biosensors based on carbon nanomaterials: carbon nanotubes and graphene", Sensors 12 (2012) 5996–6022.

[117] C.M. Tilmaciu, M.C. Morris, "Carbon nanotube biosensors", Front. Chem. 3 (2015) 59.

[118] M. Sprinkle, M. Ruan, Y. Hu, J. Hankinson, M.R. Roy, B. Zhang, X. Wu, C. Berger, W.A. de Heer, "Scalable templated growth of graphene nanoribbons on SiC", Nat. Nanotechnol. 5 (2010) 727–731.

[119] D.V. Kosynkin, A.L. Higginbotham, A. Sinitskii, J.R. Lomeda, A. Dimiev, B.K. Price, J.M. Tour, "Longitudinal unzipping of carbon nanotubes to form graphene nanoribbons", Nature 458 (2009) 872–876.

[120] F. Cataldo, G. Compagnini, G. Patane, O. Ursini, G. Angelini, P.R. Ribic, G. Margaritondo, A. Cricenti, G. Palleschi, F. Valentini, "Graphene nanoribbons produced by the oxidative unzipping of single-wall carbon nanotubes", Carbon 48 (2010) 2596–2602.

[121] A. Sinitskii, A. Dimiev, D.V. Kosynkin, J.M. Tour, "Graphene nanoribbon devices produced by oxidative unzipping of carbon nanotubes", ACS Nano 4 (9) (2010) 5405–5413.

[122] K. Mavani, M. Shah, "Synthesis of silver nanoparticles by using sodium borohydride as a reducing agent", Int. J. Eng. Res. Technol. 2 (3) (2013) 1–5.

[123] S. Murphy, L. Huang, P.V. Kamat, "Reduced graphene oxide−silver nanoparticle composite as an active SERS material", J. Phys. Chem. C 117 (2013) 4740−4747.

[124] F. Valentini, L. Persichetti, A. Sgarlata, A. Balzarotti, G. Palleschi, "Morphological and electronic characterization of functionalized graphene nanoribbons obtained by the unzipping of single-wall carbon nanotubes: A scanning tunneling microscopy study", Fuller. Nanotub. Carbon Nanostruct. 21 (2013) 302–310.

[125] D. Wei, Y. Liu, H. Zhang, L. Huang, B. Wu, J. Chen, G. Yu, "Scalable synthesis of few-layer graphene ribbons with controlled morphologies by a template method and their applications in nanoelectromechanical switches", J. Am. Chem. Soc. 131 (2009) 11147–11154.

[126] M. Liu, Y. Miao, C. Zhang, W.W. Tjiu, Z. Yang, H. Penga, T. Liu, "Hierarchical composites of polyaniline–graphene nanoribbons–carbon nanotubes as electrode materials in all-solid-state supercapacitors", Nanoscale 5 (2013) 7312–7320.

[127] A.M. Awwad, N.M. Salem, A.O. Abdeen, "Biosynthesis of silver nanoparticles using olea europaea leaves extract and its antibacterial activity", Nanosci. Nanotechnol. 2(6) (2012) 164–170.

[128] N. Kumar, Rosy, R.N. Goyal, "Palladium nano particles decorated multi-walled carbon nanotubes modified sensor for the determination of 5-hydroxytryptophan in biological fluids", Sens. Actuators B-chem 239 (2017) 1060–1068.

[129] J.W. Shin, K.J. Kim, J. Yoon, J. Jo, W.A. El-Said, J.W. Choi, "Silver nanoparticle modified electrode covered by graphene oxide for the enhanced electrochemical detection of dopamine", Sensors 17 (2017) 2771.

[130] C.A. Donini, M.K.L. da Silva, R.P. Simoes, I. Cesarino, "Reduced graphene oxide modified with silver nanoparticles for the electrochemical detection of estriol", J. Electroanal. Chem. 809 (2018) 67–73.

[131] N.I. Ikhsan, P. Rameshkumar, N.M. Huang, "Electrochemical properties of silver nanoparticle-supported reduced graphene oxide in nitric oxide oxidation and detection", RSC Adv. 6 (2016) 107141–107150.

[132] G. Dryhurst, "Electrochemical oxidation of uric acid and xanthine at the pyrolytic graphite electrode mechanistic interpretation of electrochemistry", J. Electrochem. Soc. (1972) 1659–1665.

[133] H.P.V. Rupasinghe, S. Clegg, "Total antioxidant capacity, total phenolic content, mineral elements, and histamine concentrations in wines of different fruit sources", J. Food Comp. Anal. 20 (2007) 133–137.

Chapter 4

Au-PdNPs-rGO Modified Sensor For Simultaneous Determination Of Lomefloxacin And Amoxicillin

4.1 INTRODUCTION

Graphene and related materials are attracting the interest of scientific community from more than a decade because of their exceptional properties like 2D morphology, high electronic conductivity, large surface area [1,2] and their ability to interact strongly with different materials such as metals, π- conjugated system etc. [3,4]. Amongst the graphene like carbon materials, ideal defect free graphene is difficult to prepare, bears high cost and suffers from many processability issues like, poor solubility, absence of groups that facilitate chemical interactions and limited number of active sites [3,5,6]. Thus, electrochemically reduced graphene oxide (ErGO) is used for the electrochemical purposes [2] because of its easy synthesis [7], comparatively more dispersability, and presence of number of surface defects and oxygen functionalities like epoxides, hydroxides and carboxylates, which endow ErGO the ability to strongly interact with other materials [3,6]. The combination of rGO and metallic nanoparticles can lead to the development of rGO based nanohybrids exhibiting enhanced sensitivity and catalytic properties. Such nanohybrid assemblies are known to have larger electrochemically active surface area, and functional sites for the adsorption of analytes and thus results in more rapid and effective electron transfer processes [3,8]. Hence, in the last few years, the number of investigations reporting the use of noble metal nanoparticles in combination with reduced graphene oxide (rGO) in electrochemistry has exponentially increased. The presence of the extended π- orbitals further supports the metal-rGO interaction as it provides the possibility of overlap between the π- orbitals of rGO and the d orbitals of metallic substrates. Such metal-rGO interactions results in stable graphene based metal nanohybrid assemblies and facilitate the charge transfer which is reflected by the enhanced performance of such modifications in sensing. Among the noble metals, gold (Au) interacts weakly with rGO and only gets physisorbed on the rGO surface, which is attributed to its completely filled d orbitals [3] but the oxygen functional groups present on rGO helps in the nucleation and growth of gold nanoparticles (AuNPs) [9]. AuNPs also acts as seeds for the growth of other metal clusters and is also known to improve the electronic conductivity tremendously [9,6]. On the other hand, palladium (Pd) forms strong bonds with rGO, which results in altered electronic configuration and band structures near the dirac points [10]. The strong interaction between the rGO and Pd nanoparticles prevents metal leaching and thus imparts stability in the configuration as well as size distribution [3]. Thus, both the metals are chosen for constructing a stable rGO based bimetallic nanohybrid assembly as the electrochemical sensing platform in which AuNP contributes

enhanced electronic conductivity and Pd provides the required stability for the fabrication of a stable, rapid and efficient voltammetric sensor [11]. The AuNP-PdNP decorated rGO films and related composite material have also been reported with several different synthetic strategies in the recent literature, but all these involve the use of toxic chemicals and reducing agents [12,13]. In this chapter, we are proposing a single step, green electrochemical method for the preparation of Au-PdNP decorated rGO sheets, which does not require any reducing agent.

Lomefloxacin (LMF) and amoxicillin (AMX) are the broad range antibiotics effective against large number of gram positive and gram negative bacteria [14, 15]. Both are frequently administered for the treatment of urinary tract infections, bronchitis and other infections of the nose, throat, eye etc. [14- 18]. Inspite of their frequent use both the drugs are known to pose severe harmful effects to humans. LMF, a fluoroquinolone not only results in some mild side effects like nausea, diarrhea, headache, dizziness etc., but it also undergoes serious phototoxic reactions in melanin containing tissues resulting in severe allergies, retinal degeneration, and toxic dermatitis and in some adverse conditions may end up in mitochondrial and DNA damage [19-22]. LMF has also been reported to induce cardiotoxicity [20], Central nervous system (CNS) disorders [21] etc. Similarly, AMX results in CNS related disorders, spermatogenesis and many more side effects like nausea, diarrhea etc. [17, 23]. Flouroquinone antibiotics have been used in combination with AMX and rabeprazole as triple therapy for the eradication of helicobacter pylori infection [24, 25]. The LMF-AMX combination has also been found effective in the patients infected with Chlamydia trachomatis infections [26]. However, in many cases drug-drug interaction has been found harmful particularly in the elderly patients [27]. In view of this it is necessary to develop methods for the simultaneous determination of drugs in biological fluids. Thus, techniques for the analysis of these two antibiotics in food samples, biological fluids and pharmaceutical samples require an investigation. Enzyme-linked immuno sorbent assay (ELISA) has been proposed for the determination of some flouroquinones and β–lactam antibiotics in milk samples, however, the method requires tedious preparation of protein conjugates and anti serum of flouroquinones and sulfonamides [28]. The adsorption spectroscopy has been the most commonly and widely used technique for the analysis of such drugs but both LMF and AMX exhibits overlapping bands and show an absorption maximum at ~280 nm [15, 29,30] thus, limits the application of UV spectroscopy for the quantification of AMX and LMF together. Other techniques like capillary electrophoresis [31], HPLC [32], differential pulse anodic stripping voltammetry [33-35], linear sweep voltammetry [36], cyclic voltammetry [34, 36, 37], potentiometry [38], square wave

voltammetry [39], spectrophotometry [40] etc. have been used for the analysis of LMF and AMX individually. But, no attempt for the simultaneous determination of LMF and AMX has been made within the limits of our knowledge. Hence, in the present chapter, the application of enhanced electronic and sensing properties of AuNP-PdNP-ErGO modified GCE have been explored for the quantitative and qualitative determination of both LMF and AMX in the presence of each other using square wave voltammetry.

4.2 EXPERIMENTAL

4.2.1 Instrumentation

AMX, LMF, uric acid (UA), hypoxanthine (HX), ascorbic acid (AA), graphite powder (< 20 μm), sulphuric acid, phosphoric acid, $KMnO_4$, $PdCl_2$, $HAuCl_4$ were purchased from Sigma Aldrich Inc. (USA). Phosphate buffers (from pH 2.4–10.0) were used as the supporting electrolyte and were prepared following the previously reported paper of Christian and Purdy [41]. Double distilled water was used throughout the experimental procedure for making up the stock solutions.

The details of the instruments used for electrochemical studies, FE-SEM, EDX and EIS were same as reported in chapter 2. Transmission electron microscopic images were recorded using Technai G^2 20S-TWIN microscope. Raman Spectra were obtained using Renishaw Invia Raman microscope with an excitation laser wavelength of 540 nm and *X-ray diffraction (XRD)* was performed by using *Bruker* D8-advance X-ray diffractometer.

4.2.2 Synthesis of graphite oxide

Graphite oxide was synthesized using graphite powder (>20 μm) by adopting improved Hummers method as reported previously [42]. Briefly, 1.5 g of the graphite powder was suspended in 20: 180 mixture of H_3PO_4 and H_2SO_4 and stirred for 2 h. After 2 h, 9 g of $KMnO_4$ was slowly added to the graphite suspension and the final mixture so obtained was then stirred and heated at 50 °C for 12 h, which resulted in a dark brown mixture. The mixture was allowed to cool down and 100 mL of water was added followed by the drop by drop addition of H_2O_2 (1.5 mL, 30%), which resulted in a colour change from dark brown to yellow. The yellow solution was then centrifuged and the sediment so obtained was washed with 200 mL of water, 100 mL of 30% HCl and finally with 200 mL of ethanol. The final sediment so obtained was dried and characterized to finally label it as GO.

4.2.3 Preparation of metallic nano particles decorated ErGO sheets

For carrying out the surface modification, a dispersion was prepared by suspending 1 mg of GO in 2 mL of 1 mM $HAuCl_4$ and 2 mL $PdCl_2$ aqueous solution followed by ultrasonic agitation for 300 s. AuNP-PdNP-ErGO nanocomposite was directly electrodeposited on the precleaned surface of GCE by cycling the potential between - 800 to 1500 mV at a scan rate of 100 mVs^{-1} in the above prepared suspension [43]. After the completion of optimized number of cyclic voltammetric runs the GCE was taken out, rinsed with double distilled water and dried at room temperature to get the final sensing surface for the characterization as well as analysis.

4.2.4 Fabrication of different surface modified sensors for comparing the electrocatalytic activity

To compare the properties of AuNP-PdNP-ErGO/GCE, electrodes modified individually with the components of the composite that is ErGO, PdNP and AuNP were also prepared. For the preparation of ErGO/GCE, 1mg GO was suspended in 4 mL pH 7.2 phosphate buffer and placed under ultrasonic agitation for 300 s. In the above suspension, 15 cyclic voltammograms were recorded in the potential window of -800 to 1500 mV at 100 mVs^{-1} scan rate, which resulted in electrochemical reduction of GO and finally to the ErGO/GCE. Similarly PdNP modified GCE (PdNP/GCE) and AuNP modified GCE (AuNP/GCE) were prepared by scanning 15 runs of cyclic voltammetry in 1mM $PdCl_2$ and 1 mM $HAuCl_4$ solution respectively by applying the same potential window.

4.2.5 Preparation of Stock Solution

2 mM stock solutions of LMF and AMX each were prepared by dissolving the required amount in the double distilled water. Test solutions (4 mL) of different concentrations were prepared by transferring the required volume of the stock solution in a voltammetric glass cell already holding 2 mL of phosphate buffer as supporting electrolyte. The sensing surface was cleaned after every run by applying a potential of -600 mV for 180 s in blank solution.

For the analysis of pharmaceutical formulations different commercially available tablets containing 400 mg of LMF (**Lomaday and Floxaday**) and 500 mg of AMX (**Sensiclav-625 and Erox 500**) were purchased from the local market of Roorkee. The tablets were grounded individually to a fine powder in a mortar and pestle, weighed and dissolved in the double distilled

water to prepare a stock solution of 2 mM. This stock solution has been further used to prepare test samples lying in a defined concentration range.

For the determination of LMF and AMX in the biological samples, human urine samples from two healthy volunteers (1 Male; age 27 yrs and 1 Female; age 25 yrs) were collected and filtered using whatman 42 filter paper. The supernatant was further diluted two folds using pH 7.2 phosphate buffer in order to reduce the complex matrix. The diluted urine samples were then used to prepare solutions of different concentration by spiking it with a known amount of the analyte.

4.3. RESULTS AND DISCUSSION

4.3.1 Optimization of number of scans required for AuNP-PdNP-ErGO fabrication

The number of cycles for electrodepositing AuNP-PdNP-ErGO nanocomposite directly on the precleaned surface of GCE were optimized in the range of 1–30 (**Fig 4.1**) and it was found that best electrochemical response for the oxidation of 30 μM LMF was obtained when 15 number of scans were used as higher number of scans resulted in the agglomeration of GO, whereas, lower number resulted in the inhomogeneous dispersion of nanoparticles on the ErGO film. Thus, the best results in terms of electrochemical response as well as surface characteristics were observed when 15 scans were carried out for the fabrication of AuNP-PdNP-ErGO nanocomposite modified GC sensor. Hence, throughout the fabrication protocol the potential was scanned 15 times for the electrodeposition of the nanocomposite on the surface of GCE.
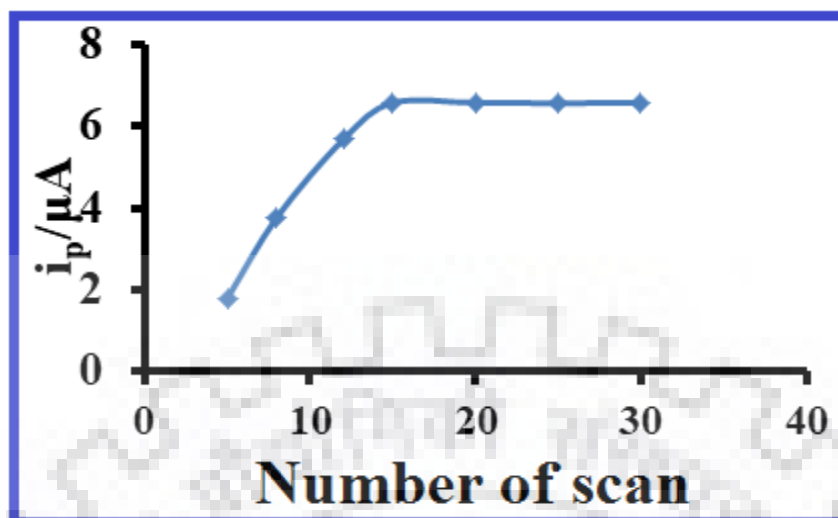
Fig. 4.1: The optimization of the experimental parameter; variation of peak current of LMF (30µM) with the number of scans used to carry out electrochemical modification of AuNP-PdNP-ErGO on the surface of GCE.

4.3.2 Characterization of composite

Exploiting the concept of electrochemical deposition, an ErGO based nanocomposite modified GCE has been generated. The one step synthesis of nanocomposite involving electrochemical reduction of GO to ErGO and the decoration of ErGO sheets with the AuNP and PdNP has been achieved. **Fig. 4.2** indicates the consecutive cyclic voltammograms observed during the electrochemical deposition of AuNP-PdNP-ErGO at the GCE. The peak I around ~ -500 mV corresponds to the electrochemical reduction of GO to ErGO as can be seen in the inset of **Fig. 4.2** and was similar to the ones reported earlier [43,44]. While, the other three peaks II, III and IV were observed due to the deposition of PdNP in accordance to earlier studies [45]. The peak V at around ~800 mV corresponds to the reduction of Au(III) to Au(0) at the surface of electrode, which is attributed to the reduction of absorbed $AuCl_4^-$ to Au (0) [46].
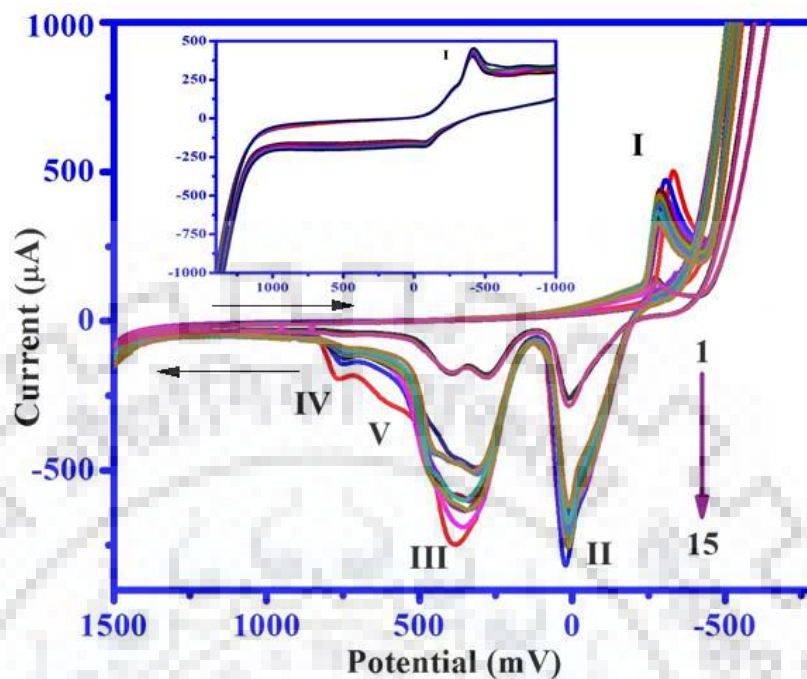
Fig. 4.2: Cyclic voltammograms observed during electrochemical fabrication of AuNP-PdNP-ErGO nanocomposite modified GCE at a sweep rate of $100\ \text{mV s}^{-1}$. Inset represents the consecutive cyclic voltammograms observed during electrochemical reduction of GO to ErGO.

In order to investigate the efficacy of the surface modification, surface area of unmodified GCE, AuNP-PdNP/GCE and AuNP-PdNP–ErGO/GCE sensors were calculated. For this purpose, cyclic voltammograms were recorded in the mixture of 2 mL of 2 mM $K_3[Fe(CN)_6]$ and 2 mL of 0.1M KCl at different scan rate. At the surface of the bare and modified electrode, a well defined redox couple was observed due to the presence of Fe^{+3}/Fe^{+2}, however, enhancement in the peak current of both the peaks was noticed at AuNP-PdNP–ErGO/GCE in comparison to the bare and AuNP-PdNP/GCE. The surface area was calculated by using the Randles–Sevcik equation. The slope of plot i_p vs. $v^{1/2}$ was used for calculating the surface area of bare, AuNP-PdNP/GCE and AuNP-PdNP–ErGO/GCE and the effective surface area for the three electrodes was found to be 0.10, 0.13 and 0.15 cm^2 respectively.

The changes produced on the surface of GCE after modification have been witnessed using FE-SEM and are presented in **Fig. 4.3**. From the figure, it can be concluded that the proposed protocol has successfully altered the GCE surface and resulted in small spherical structures

uniformly distributed all over the surface. On carefully analyzing **Fig. 4.3(B)**, the presence of wrinkled, crumbled thin films encapsulating the nanoparticles can be seen, which indicates the interaction of metallic nanoparticles with the reduced GO films. Elemental mapping was also done to check the distribution of Au and Pd nanoparticles on the modified surface. **Fig.4.3**, shows four distinguished colours corresponding to the Au, Pd, C and O. From the images a uniform distribution of red and green colour corresponding to Pd and Au respectively ensures the homogenous deposition of nanoparticles on the surface. Because of the homogenous distribution, similar sized nanoparticles are evenly placed on the sensing surface which results in much enhanced surface area that has also been concluded from the surface area calculations as discussed in the above text. The increased surface area is expected to result in substantially enhanced electrochemical sensitivity and is also expected to influence the electron transfer kinetics positively.
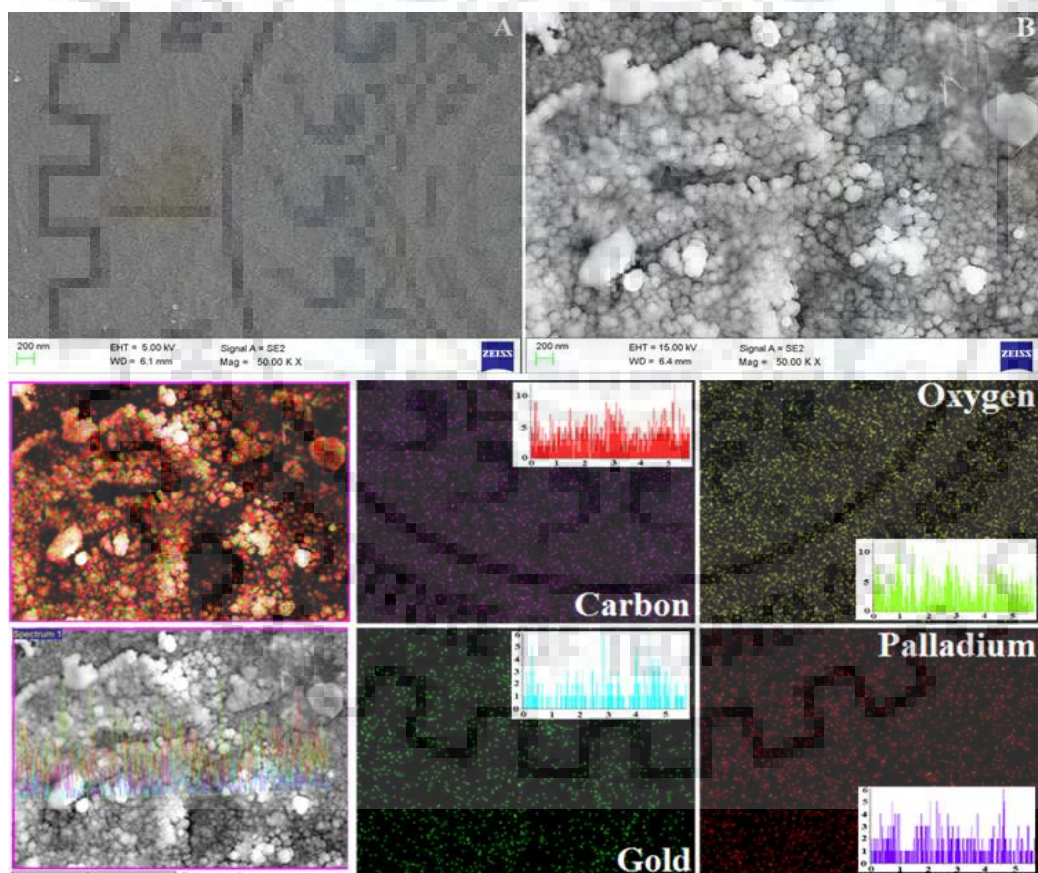
Fig. 4.3: FE-SEM images of (A) bare GCE and (B) AuNP-PdNP-ErGO/GCE. Elemental mapping images corresponding to different elements on modified GC substrate.

The corresponding Energy dispersive X-ray spectroscopy (EDX) for AuNP-PdNP-ErGO/GCE surface further shows the peaks attributed to C, O, Pd, and Au elements as presented in **Fig. 4.4(A)** and thus confirms the presence of Pd and Au on the GC surface. From the results obtained, the atomic percentage of Pd and Au is found to be almost similar (0.62 and 0.57 % respectively), resulting in an atomic ratio of 1:1 which is in accordance to the molar ratio of metal precursors used. From the low magnification TEM image **(Fig. 4.4 B)**, transparent, wrinkled thin film of ErGO can be seen on which many small spherical structures are uniformly distributed. Further, the absence of free nanoparticles (without ErGO) reveals that the metal NPs interact strongly with the ErGO as also concluded from the FE-SEM images.

Element	Weight%	Atomic%
C	63.58	76.86
O	24.20	21.96
Pd	4.53	0.62
Au	7.69	0.57
Totals	100.00	
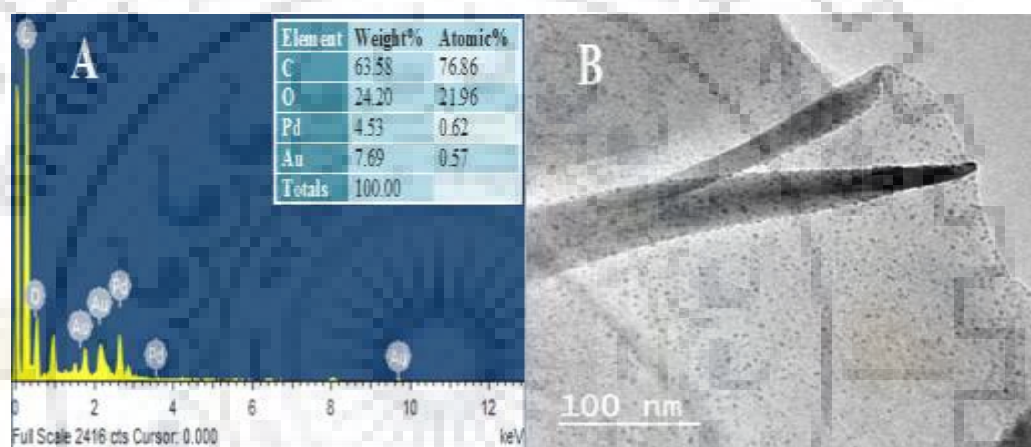
Fig. 4.4 (A): EDX data obtained for AuNP-PdNP-ErGO nanocomposite modified GCE and (B) Low magnification TEM image of AuNP-PdNP-ErGO nanocomposite modified GCE.

Raman spectroscopy was further used to characterize the carbonaceous material i.e GO and AuNP-PdNP-ErGO. **Fig. 4.5(A)** presents the Raman spectra of AuNP-PdNP-ErGO and GO. The frequencies at which the G and D band appears in AuNP-PdNP-ErGO are similar to those observed for GO. But, the intensity of D band is greater than G band in AuNP-PdNP-ErGO, whereas reverse was the case observed for GO which symbolizes the effective reduction of GO as a result of which AuNP-PdNP-ErGO exhibits higher I_D/I_G ratio. This change suggests the decrease in the average size of in-plane sp^2 domain and also indicates the interaction between the nanoparticles and ErGO film as reported earlier [8,47]. To know the plane lattice and interlayer spacing of the ErGO, the X-ray diffraction (XRD) was performed and spectrum of ErGO is presented in **Fig. 4.5(B)**. A broad peak at $2\theta = 24.3°$ corresponding to the (0 0 2) plane lattice of

the ErGO along with a d-spacing value 0.37 nm was observed, which indicated the successful electrochemical reduction of GO at the surface of GCE [48].
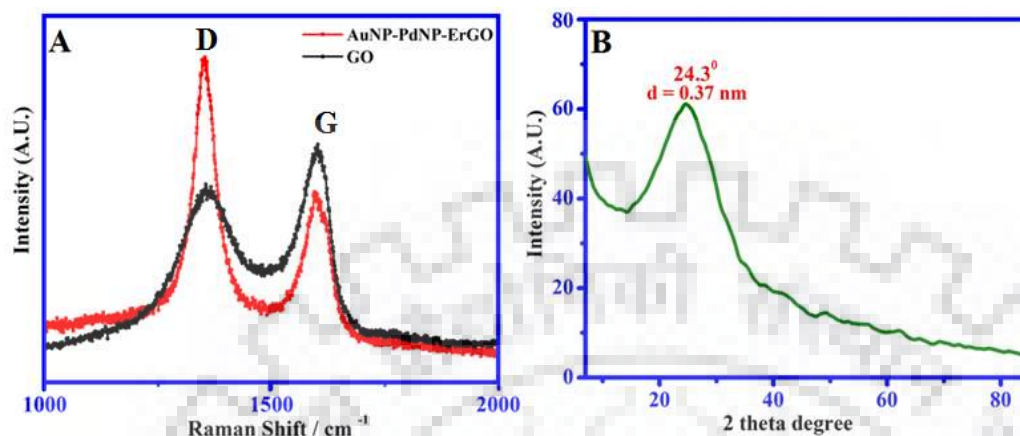
Fig. 4.5: (A) A comparison of Raman spectrum observed for GO and AuNP-PdNP-ErGO nanocomposite and (**B**) XRD pattern for ErGO.

The effect of surface modification on the electrochemical behavior of the developed sensor has also been investigated using EIS. The experiment was performed using 1:1 mixture of 5 mM $K_3[Fe(CN)_6]$ and 0.1 M KCl solution over 1000 kHz to 1 mHz frequency range. The impedance data were normalized to the electrode area. **Fig. 4.6** presents the comparative EIS plots corresponding to AuNP-PdNP-ErGO/GCE (**A**), AuNP-PdNP/GCE (**B**) and bare GCE (**C**). The normalized value of charge transfer resistance (R_{CT}) was calculated by fitting the Randle's circuit and was found to be 115 Ω cm^2, 162 Ω cm^2 and 200 Ω cm^2 for AuNP-PdNP-ErGO/GCE, AuNP-PdNP/GCE and bare GCE sensor respectively. A significantly reduced diameter of the circular portion for the AuNP-PdNP-ErGO indicates the decreased charge transfer resistance (R_{CT}), which may be attributed to the improved conductivity of the reduced GO in comparison to GO as well as the electrocatalytic effect of the surface modification. Thus, the results obtained from FE-SEM, EDX, TEM, Raman and EIS studies clearly demonstrated that GO was successfully reduced by the electrochemical means and was uniformly decorated by the AuNPs and PdNPs.
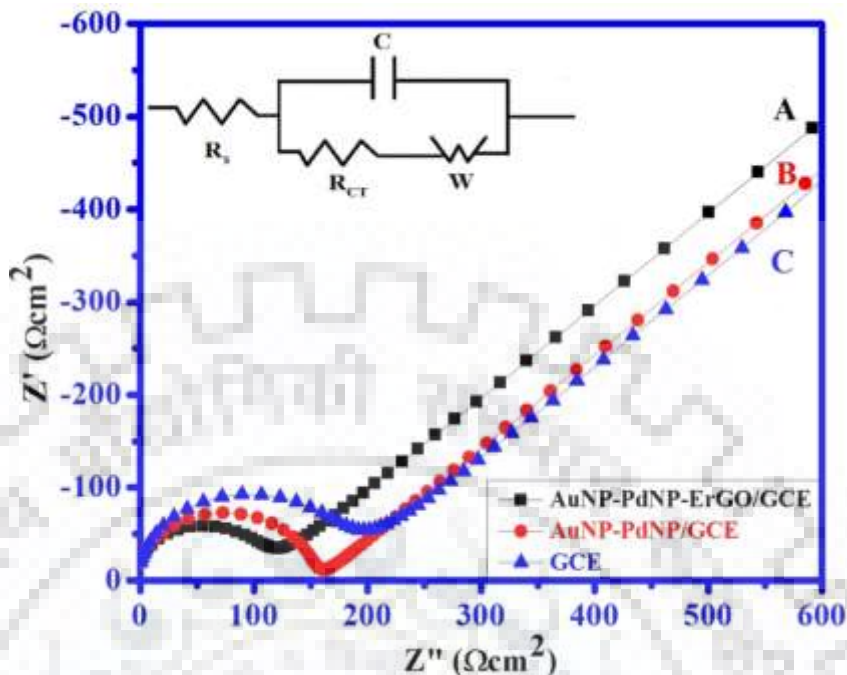
Fig. 4.6: Typical EIS plot obtained for (A) AuNP-PdNP-ErGO/GCE, (B) AuNP-PdNP/GCE and (C) unmodified GCE in 1:1 mixture of 5 mM $K_3Fe(CN)_6$ and 0.1 M KCl solution over the frequency range 1000 kHz to 1 mHz. Inset is the Randles circuit.

4.3.3 Electrochemical behavior of AuNP-PdNP-ErGO composite

To compare the electrochemical behavior of the AuNP-PdNP-ErGO composite with the individual constituents, square wave voltammograms for 100 µM LMF were recorded in pH 7.2 phosphate buffer using bare GCE, AuNP/GCE, PdNP/GCE, PdNP-ErGO/GCE and AuNP-PdNP-ErGO/GCE. A comparison of the observed voltammograms is presented in **Fig. 4.7**. Small oxidation peak corresponding to LMF was observed at ~990 mV for bare GCE. In the presence of AuNP the current signal was enhanced, but no significant change in peak potential was observed. Whereas, PdNP resulted in both substantially increased peak current as well as a shift of ~30 mV in the peak potential. However, the incorporation of AuNP and PdNP on the ErGO sheets showed the best response in the terms of sensitivity as significantly enhanced peak current for LMF was observed for the composite in comparison to the individual modifications by Au or PdNP. Moreover, the oxidation of LMF was witnessed at much lower potential (~880 mV), when AuNP-PdNP-ErGO/GCE was used as the working electrode in comparison to the bare GCE (~990 mV). This shift in the peak potential of LMF towards less positive potentials clearly indicated the

158

efficient electrocatalytic activity of the composite that facilitated the electron transfer. Thus, AuNP-PdNP-ErGO/GCE has been chosen as the final sensing surface and is used for the further investigations.
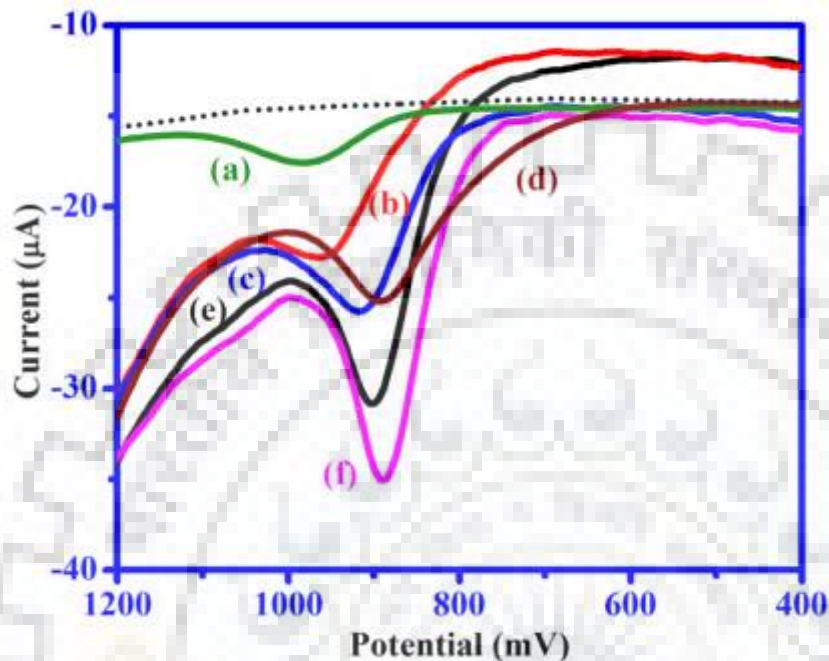
Fig. 4.7: A comparison of square wave voltammograms observed for 100 μM LMF in pH 7.2 phosphate buffer at (a) unmodified GCE, (b) AuNP/GCE, (c) PdNP/GCE, (d) AuNP-PdNP/GCE, (e) PdNP-ErGO/GCE and (f) AuNP-PdNP-ErGO/GCE. Background of bare GCE is presented by dotted line.

4.3.3.1 Effect of pH

The effect of pH on the electrochemical oxidation of LMF and AMX has been evaluated by varying the pH of the supporting electrolyte i.e. phosphate buffer in the range of 2.4–10.0. On analyzing the oxidation peak in the square wave voltammograms, it was observed that as the pH value increased the oxidation potential of both LMF and AMX shifted towards less positive potentials. The plot of Ep versus pH was linear for LMF and AMX as represented in **Fig. 4.8 (A)** and **4.8 (B)** respectively.

$$E_p \, (mV) = -63.52 \, pH + 1358, \quad R^2 = 0.98 \, \text{..............for LMF}$$
$$E_p \, (mV) = -65.45 \, pH + 1212; \quad R^2 = 0.98 \, \text{..............for AMX}$$

The slope of the following linear relations between the peak potential and the pH of the supporting electrolyte signifies the nernstian behavior of the oxidation process involving equal number of electron and proton transfer.
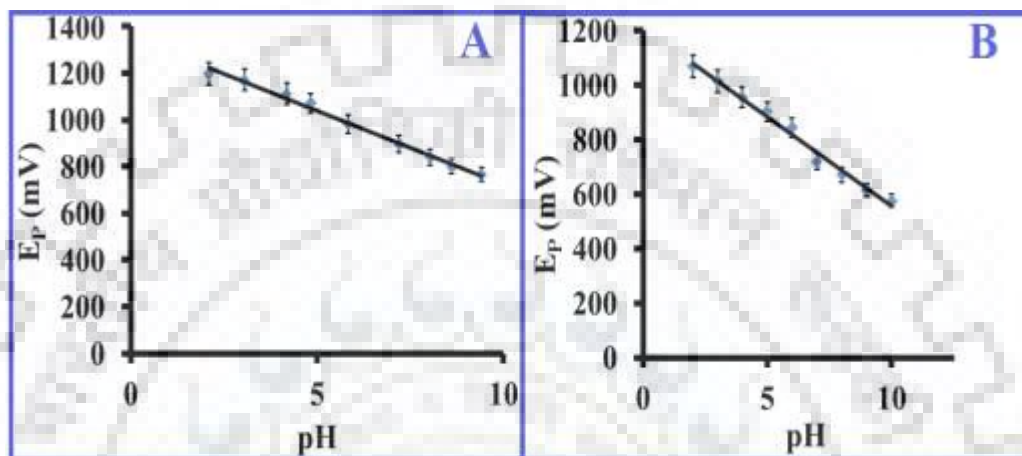
Fig. 4.8: The dependence of peak potential over the pH of the supporting electrolyte for (A) 25 µM LMF and (B) 25 µM AMX.

To further calculate the exact number of electrons involved in the oxidation of analytes, Laviron's equation has been used [49]. For this purpose, the oxidation of LMF and AMX were investigated using cyclic voltammetry. The voltammograms were recorded for 50 µM LMF and 100 µM AMX at scan rates (v) ranging between 10–250 mVs^{-1} and 20–250 mVs^{-1} respectively. The peak potential (E_p) was found to increase with the increasing scan rate for both the analytes and the variation can be expressed using following expressions:

$$E_p = 53.496 \log v + 832.95, R^2 = 0.99 \ldots\ldots\ldots\ldots \text{ For LMF}$$
$$E_p = 58.556 \log v + 667.92, R^2 = 0.99 \ldots\ldots\ldots.. \text{ For AMX}$$

According to the Laviron's equation, the slope of the plot E_p vs. $\log v$ gives the value of αn. Assuming $\alpha = 0.5$ (as for a totally irreversible electron transfer, the value of α is usually assumed as 0.5 [50]), the number of electrons involved in the oxidation of LMF and AMX were found to be 2.21 and 2.01 respectively. The results indicates that two electrons were involved in the electro-oxidation of both the analytes following the mechanism shown in **Scheme 4.1**, which is in accordance with the previous literature [17, 39].
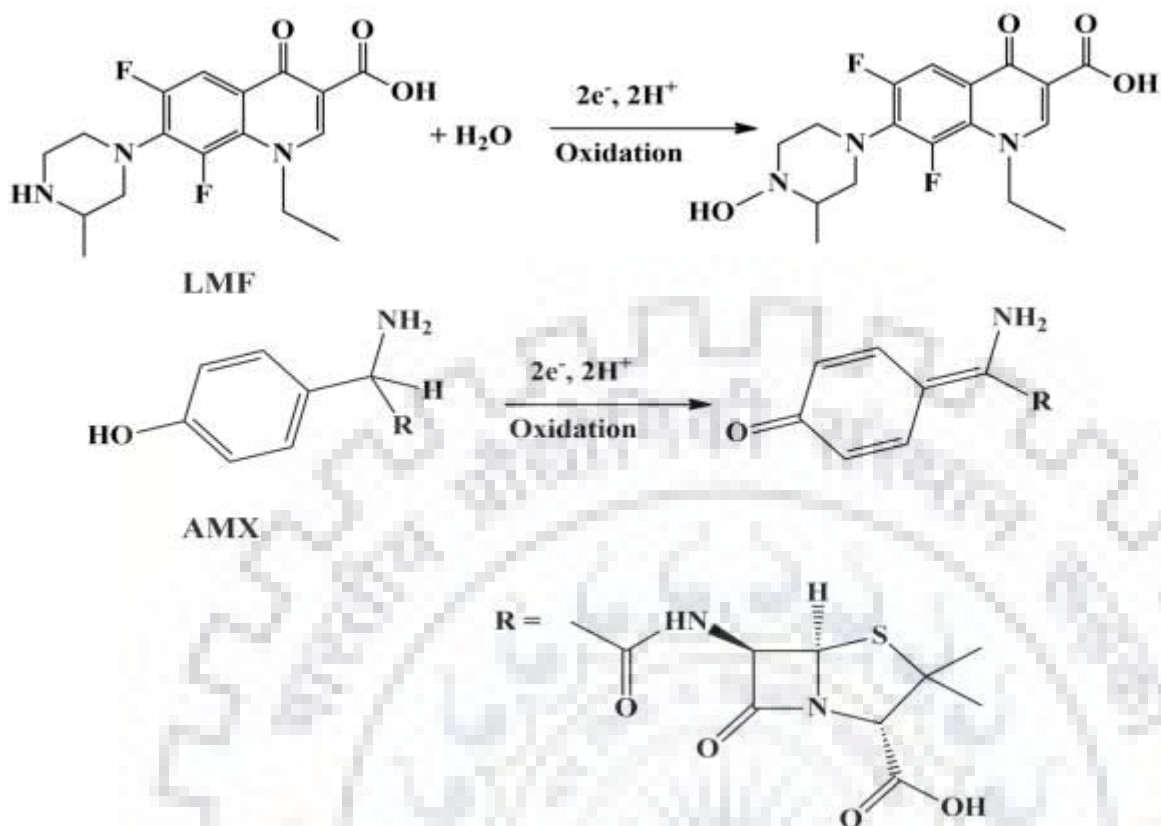
Scheme 4.1. Proposed mechanism for the oxidation of LMF and AMX.

4.3.3.2 Effect of frequency

The variation of the peak parameters (like current and potential) with the square wave frequency is known to be an indicator of the nature of electron transfer involved. Thus, change in the peak current with the change in frequency of the square wave has been investigated for LMF and AMX.

For LMF, the peak current was found to increase linearly with the increasing frequency **(Fig. 4.9 (A1))** and the dependence of i_p on frequency can be documented by following regression equation:

$$i_p \, (\mu A) = 0.2896 \, f \, (5\text{-}50 \text{ Hz}) - 0.7128, \, R^2 = 0.99$$

The linearity of the i_p with f clearly indicates the involvement of adsorption controlled electron transfer, which was further confirmed from the slope value of ~1 in linear $\log i_p$ versus $\log f$ plots **(Fig. 4.9 (A2))**. The dependence of $\log i_p$ on $\log f$ can be represented by the following equation:

$$\log i_p = 1.3501 \log f - 1.0818, \, R^2 = 0.98$$

161
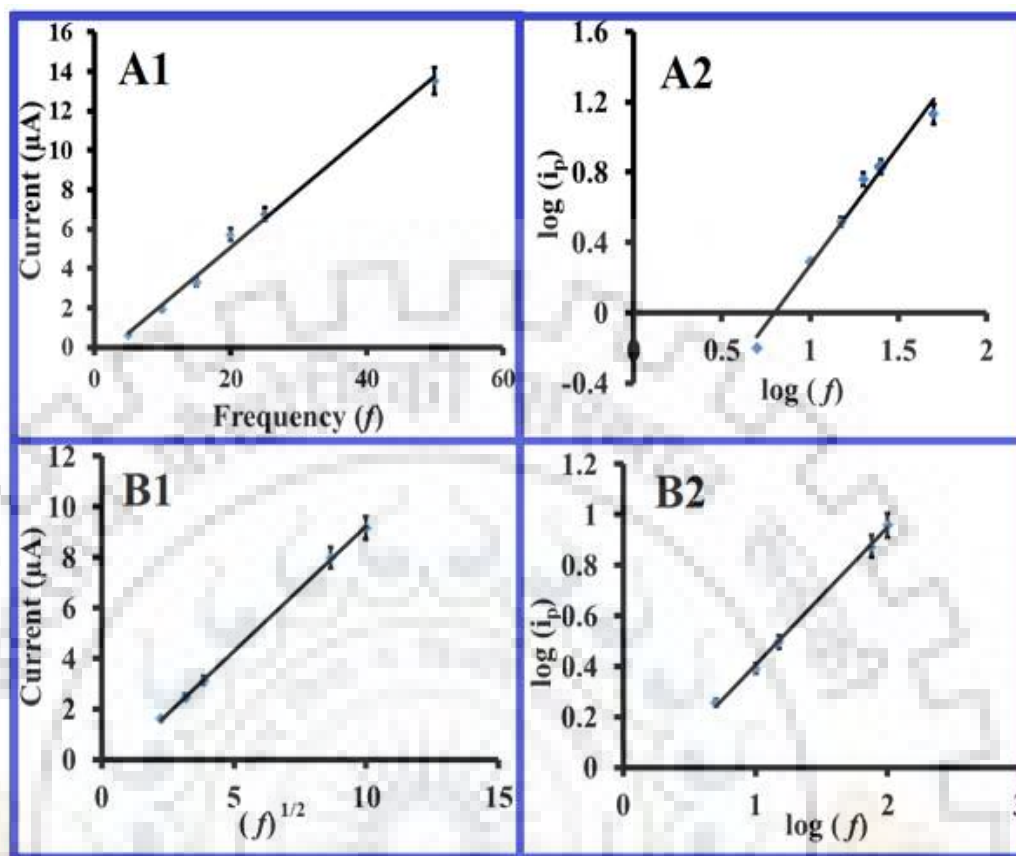
Fig. 4.9: Variation of (A1) current (i_p) with the frequency (f), (A2) log (i_p) with log (f) for 10 µM LMF and variation of (B1) current (i_p) with the square root of frequency ($f^{1/2}$), (B2) log (i_p) with log (f) for 60 µM AMX.

For AMX, the peak current was found to increase linearly with the square root of frequency, which demonstrated the diffusion controlled electron transfer process. The relation between i_p and $f^{1/2}$ can be given by the following regression equation **(Fig. 4.9 (B))**.

$$i_p \ (\mu A) = 0.9861 \, f^{1/2} \ (5–100 \ Hz) - 0.6394, \ \dots. \ R^2 = 0.99$$

$$\log i_p = 0.5428 \log f - 0.1376, \ \dots\dots\dots\dots. \ R^2 = 0.99$$

A gradient of ~ 0.5 for log i_p versus log f plot for AMX further supports the involvement of diffusion controlled electron transfer process and absence of any thin layer effect as governed by the Randles Sevick equation [51].

4.3.3.3 Effect of Concentration

The variation of the peak current with the analyte concentration is important for the quantitative estimation of the analyte as well as for the calculation of limit of detection (LOD). Thus, the concentration study has been carried out by recording the square wave voltammograms for the increasing concentration of LMF under same optimized parameters and experimental conditions. The peak current for LMF oxidation was found to increase with the increasing concentration using both bare GCE and AuNP-PdNP-ErGO/GCE **(Fig. 4.10 (A))** and can be given by the following linear equations:

i_p (μA) = 0.0759 [C_{LMF}, 4–500 μM] + 3.5291, R^2 = 0.99: AuNP-PdNP-ErGO/GCE.

i_p (μA) = 0.0259 [C_{LMF}, 15–200 μM] + 1.5126, R^2 = 0.99: Bare GCE

From the regression equations, it can be seen that the surface modification of GCE with the AuNP-PdNP-ErGO nanocomposite resulted in approximately 3 folds enhanced sensitivity in comparison to the bare GCE. The LOD calculated using 3σ/b, where σ stands for the standard deviation of 'n' background voltammograms and b is the slope of the calibration equation, was 81 nM (for n=3).

The effect of AMX concentration on the peak current has also been investigated using AuNP-PdNP-ErGO/GCE and analytical curve was prepared. The peak current of AMX was found to increase with the increasing concentration of the AMX **(Fig. 4.10)**. The dependence of the peak current on the concentration can be represented by the following linear relation **(Inset of Fig. 4.10(B))**:

i_p (μA) = 0.0376 [C_{AMX}, 30–350 μM] + 0.4733, R^2 = 0.98

The value of LOD calculated by using relation 3σ/b was found to be 9 μM (n=3).
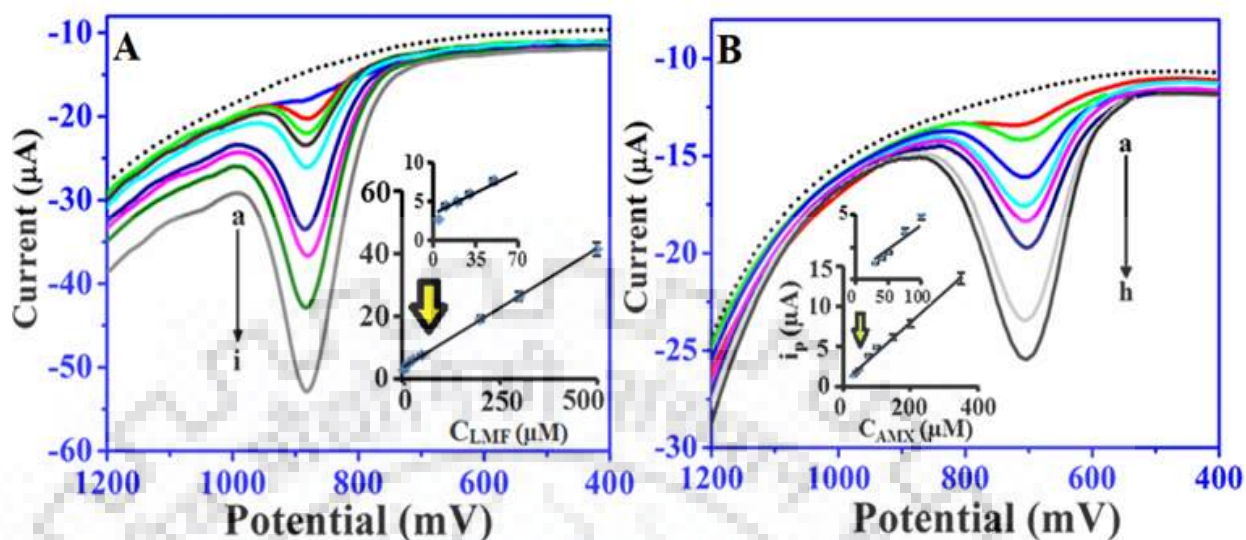
Fig. 4.10(A): Square wave voltammograms recorded for (a) 4, (b) 10, (c) 20, (d) 30, (e) 50, (f) 100, (g) 200, (h) 300 and (i) 500 µM LMF using AuNP-PdNP-ErGO/GCE. The dotted line demonstrates the background current. Inset is the calibration plot of the LMF in the concentration range of 4–500 µM. **(B):** Square wave voltammograms recorded for (a) 30, (b) 40, (c) 50, (d) 75, (e) 100, (f) 150, (g) 200 and (h) 350 µM AMX using AuNP-PdNP-ErGO/GCE. Inset is the calibration plot of the AMX in the concentration range 30–350 µM.

A comparison of the linear concentration range and LOD values obtained by using other techniques and at other electrodes and our developed sensor has been listed in **Table 4.1**. From the Table, it can be seen that the proposed method showed improved results in the terms of LOD and the linear dynamic range from most of the senors reported in recent years. The enhanced sensing properties and the improved performance of the sensor is attributed to the synergistic interaction of the Au and Pd nanoparticles on rGO that leads to the improved charge transfer and large number of adsorption sites on the modified surface of GCE [3,8].

Table 4.1: Comparison of Limit of Detection (LOD) obtained for LMF and AMX using the proposed method with the previously reported techniques

S.No	Method/electrode	LOD (μM)	Concentration range (μM)	Reference
LMF				
1	UV-Spectrophotometric	3.6	5.0–30	**[30]**
2	Capillary electrophoretic (CE)	0.09	0.5–130	**[31]**
3	HPLC	0.438	10–62	**[32]**
4	Dropping mercury electrode (DPV)	1	7–70	**[33]**
5	Carbon paste electrode (DPV)	0.42	0.2–40	**[34]**
6	PVC membrane Potentiometric sensors LO_{M8}	52.3	50–10000	**[38]**
7	p-(melamine)/GCE (SWV)	16 nM	0.1–500	**[39]**
8	Two phase floatation system/HPLC	0.017	---	**[52]**
	AuNP-PdNP-ErGO/GCE	0.081	4–500	**Present work**
AMX				
9	[VO(Salen)]/CPE (LSV)	24.8	28.5–82.6	**[35]**
10	[VO(Salen)]/CPE (DPV)	16.6	18.3–35.5	**[35]**
11	[VO(Salen)]/CPE (SWV)	8.49	18.9–91.9	**[35]**
12	AuNP/ITO (SWV)	0.005	0.01–1	**[36]**
13	ZnO NRs/gold/glass electrode	19	50–250	**[37]**
14	Spectrophotometry	15.47	0–490	**[40]**
	AuNP-PdNP-ErGO/GCE	9	30–350	**Present work**

CPE: Carbon Paste Electrode, LSV: Linear sweep voltammetry, CV: Cyclic voltammetry, DPV: differential pulse voltammetry, LOM – MPA (molybdophosphoric acid) ion association (LO_{M8}), [VO(Salen)]: N,N-ethylenebis(salicylideneaminato)] oxovanadium(IV)

4.3.3.4 Simultaneous voltammetric determination of LMF and AMX

The simultaneous analysis of LMF and AMX was done using AuNP-PdNP-ErGO/GCE. Firstly, analytical curve was constructed by varying the LMF concentration from 10–150 µM while keeping the AMX concentration fixed at 40 µM. In the second set of experiments the AMX concentration was increased from 50–100 µM and the LMF concentration was maintained constant at 20 µM. From the voltammograms as shown in **Fig. 4.11 (A and B)**, it can be seen that the oxidation peak currents increased linearly with the increase in concentrations, while the peak current for the analyte having fixed concentration remained fairly constant. This behaviour demonstrated that LMF and AMX do not interfere with each other and can be successfully determined in the presence of each other.
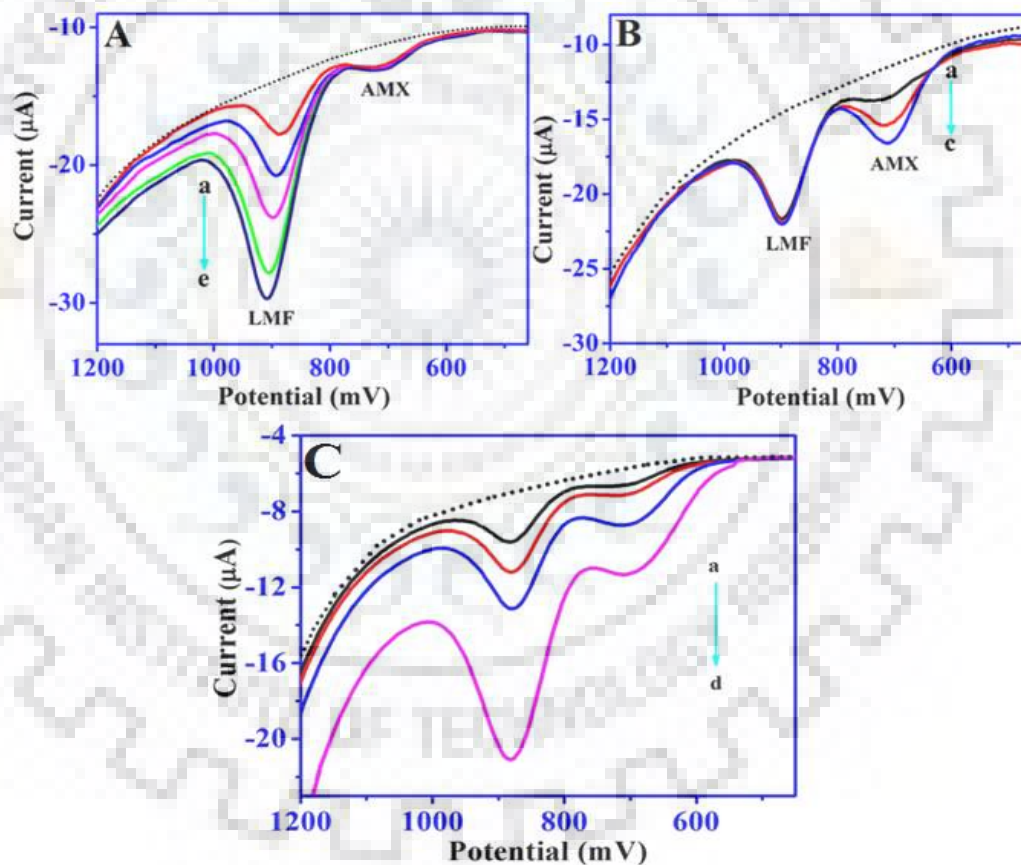
Fig. 4.11: Square wave voltammograms observed for a solution containing (A) fixed concentration of AMX (40 µM) with increasing concentration of LMF (10–150 µM), (B) fixed concentration of LMF (20 µM) and increasing concentration of AMX (50–150 µM) and (C) different concentrations of LMF and AMX in the range of 5–150 µM and 30–200 µM respectively at pH 7.2.

To investigate the simultaneous study of LMF and AMX at the surface of AuNP-PdNP-ErGO/GCE, the experiment was performed by using SWV in phosphate buffer (pH 7.2) solution. The concentrations of LMF and AMX were increased simultaneously and SW voltammograms were recorded in the range of 5–150 μM and 30–200 μM respectively as shown in **Fig. 4.11 (C)**. It can be seen that the oxidation peak currents of both the analytes increase consecutively with the increasing concentration of LMF and AMX. This behaviour shows that LMF and AMX can be determined successfully in the mixture of both analytes. Statistical parameters obtained for the quantitative investigations of LMF and AMX at AuNP-PdNP-ErGO/GCE for individual and co-existence in the reaction mixture have been tabulated in **Table 4.2**.

Table 4.2: Statistical parameters obtained for individual and simultaneous quantitative analysis of LMF and AMX.

Validation Parameters	Individual determination of LMF	LMF determination in presence of AMX	Individual determination of AMX	AMX determination in presence of LMF
Concentration			4–500 μM	5–150 μM
Sensitivity (μA/μM)	0.0773	0.0776	0.0376	0.0320
Correlation coefficient (R^2)	0.99	0.99	0.98	0.99
Standard error of slope	0.0013	0.0005	0.0013	0.0004
Intercept	3.5291	2.285	1.5126	- 0.205
Standard error of intercept	0.2714	0.0414	0.2159	0.0405

The paired t-test has been performed for anlaysing the results of LMF and AMX quantification in the presence and absence of each other. The calculated and tabulated paired t values for the individual LMF determination and its quantification in the presence of AMX were - 0.8758 and 2.920 respectively. Whereas, for the AMX investigations, the calculated and tabulated

paired t-values under a confidence limit of 95% were 1.257 and 2.353 respectively. As the calculated values are less than tabulated t-values, it was concluded that the results obtained for the individual concentration studies are not significantly different from the results obtained when both the analytes are varied simultaneously.

4.3.4 Interference study

The key problem with the simultaneous determination of drugs is the overlapping voltammetric signals because of the presence of large excess of coexisting biological molecules present in human urine, like uric acid, ascorbic acid, hypoxanthine etc. Thus, it is of prime importance to check the selectivity of the developed sensor for the determination of LMF and AMX. Hence, the analysis of LMF and AMX was done by increasing the concentration of interfering molecules and keeping the analyte concentration fixed. From the **Fig. 4.12**, it can be seen firstly, that the peak corresponding to AMX and LMF oxidation are well separated from AA, UA and HX and secondly, even in the presence of excess of potentially interfering molecules, the voltammetric signal for LMF or AMX showed no significant deviation. Hence, the fabricated sensor is selective for the chosen analyte and can be extended for the determination of LMF or AMX in biological samples.
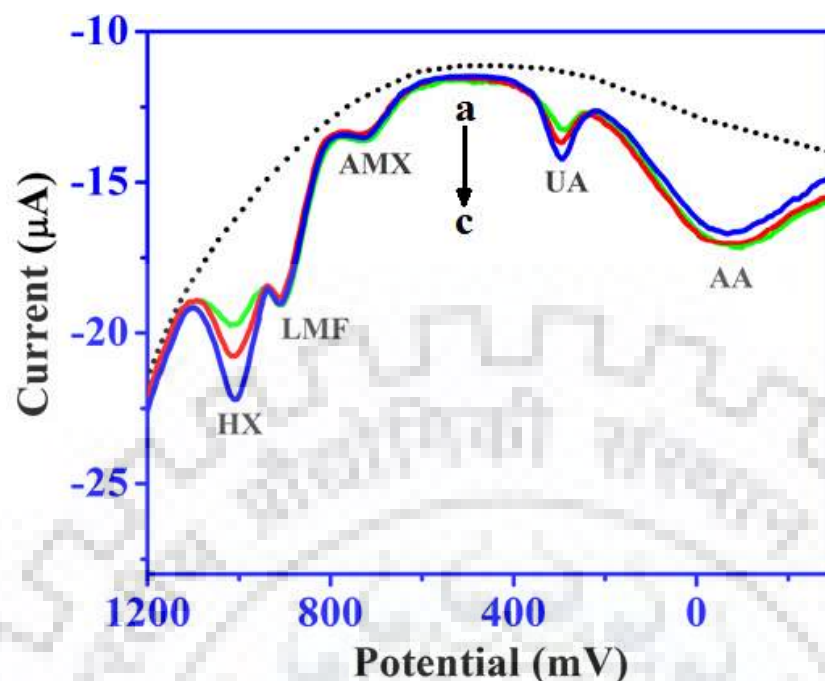
Fig. 4.12: Square wave voltammograms observed for a solution containing (a) 25 µM AA + 10 µM UA + 30 µM AMX + 10 µM LMF + 10 µM HX, (b) 50 µM AA + 25 µM UA+ 30 µM AMX + 10 µM LMF + 25 µM HX and (c) 100 µM AA + 50 µM UA+ 30 µM AMX + 10 µM LMF + 50 µM HX. Background is represented by the dotted line.

4.3.5 ANALYTICAL APPLICATION

4.3.5.1 Pharmaceutical sample analysis

In order to check the analytical feasibility of the developed sensor, the content of the LMF and AMX in some commercially available pharmaceutical formulations was estimated. The samples were prepared as described in section 2.5 and the SW voltammograms were recorded under the optimized parameters. The results obtained are tabulated in **Table 4.3**. In all the cases, an error of less than 3.5% has been observed, which clearly indicated an excellent agreement between the calculated values with the stated ones.

Table 4.3: Determinations of LMF and AMX content in pharmaceutical drug formulations using an AuNP-PdNP-ErGO/GCE.

Tablet	Added (µM)	Detected (µM)	Error %
LMF Tablets			
Lomaday	100	97.96	2.04
	125	122.94	1.65
	150	151.67	1.13
Floxaday	50	48.43	3.14
	75	77.29	3.05
	100	98.58	1.42
AMX Tablets			
Sensiclav-625	50	49.07	1.86
	75	73.98	1.36
	100	102.72	2.72
Erox 500	125	123.45	1.24
	150	148.34	1.11
	200	203.79	1.89

The R.S.D. value for the determination was less than 1.79% for n = 3.

4.3.5.2 Recovery study

To investigate the performance of the fabricated sensor in the complex matrix, urine samples were spiked with different levels of LMF and AMX concentrations and analyzed by the proposed method. The results obtained for the urine analysis with respect to both LMF and AMX in individual **(Table 4.4)** and simultaneous recovery study are shown in **Table 4.5**. As can be seen from these Tables, excellent recovery was obtained for both the analytes and thus it can be concluded that SWV using the AuNP-PdNP-ErGO/GCE did not suffer interference with the complex matrix and can be efficiently applied for the simultaneous determination of LMF and AMX in real biological samples. The reliability of the results obtained in recovery study were confirmed by using the paired *t*-test for LMF and AMX recovery study. Since, the calculated *t*-test values for LMF and AMX (0.9052, 0.3265) were less than the tabulated t-values under a confidence limit of 95%, it was concluded that there is no significant difference between the

investigated data of individuals and simultaneous recovery study which indicates the validity of the proposed methods.

Table 4.4: Recovery data of LMF and AMX determination in human urine sample

S.No.	Spiked amount (µM)	Detected amount (µM)[*]	Recovery %
LMF			
1	75	76.32	101.76
2	125	123.89	99.11
3	200	196.57	98.28
Sample 2			
1	25	23.96	95.84
2	50	51.04	102.08
3	75	73.75	98.33
AMX			
1	50	49.87	99.74
2	150	154.69	101.13
3	300	297.41	99.13
Sample 2			
1	75	73.47	97.96
2	125	126.54	101.23
3	350	347.85	99.38

The R.S.D. value for the determination was less than 2.38% for n = 3.

Table 4.5: Recovery data for simultaneous determination of LMF and AMX in human urine sample

S.No.	Spiked amount (μM) LMF	Spiked amount (μM) AMX	Detected amount (μM)* LMF	Detected amount (μM)* AMX	Recovery%	Recovery%
1.	25	30	24.84	29.80	99.36	99.33
2.	50	50	50.5	49.90	101.10	99.80
3.	75	75	74.10	75.10	98.80	100.10
4.	200	125	199.40	124.70	99.70	99.76

The R.S.D. value for the determination was less than 2.43% for n = 3.

4.3.6 Stability and reproducibility studies

The intraday reproducibility of the fabricated sensor was checked by recording five voltammograms in pH 7.2 phosphate buffer containing 50 μM of LMF and the calculated RSD value was found to be 1.97% for n=3 and 2.18% for n=5. Inter-day reproducibility was also examined by checking the voltammetric signals obtained for 50 μM LMF oxidation for 30 days. The current response showed a deviation of 4.7% for the first 15 days, however, after 15 days the voltammetric signal fluctuated by upto ~7.0%. Thus, the results obtained showed that the proposed sensor bears appreciable stability and reproducibility.

4.3.7 Ruggedness studies

To further confirm the accuracy of the obtained results, the ruggedness of the developed method was evaluated by using the different voltammetric instruments and by different analysts. The voltammetric studies were performed by using two voltammetric analyzers viz., Epsilon EC-USB and CV-50 (BAS, West Lafayette, USA) to examine the instruments related variation. In order to investigate the intermediate precision of the developed sensor, its performance has been evaluated at different electrodes on different days. On comparing the results obtained at different sensors and different instruments, the ±1.48% fluctuation was found in the electrochemical response. The obtained results are summarized in **Table 4.6** which showed that there is no significant difference observed between the recovery results. Hence, the proposed method shows

the reliable, robust and rugged approach for assaying LMF and AMX in the complex matrix such as urine and other biological fluids.

Table 4.6: The Robustness and ruggedness of the developed method for the recovery data of LMF and AMX determination in human urine samples.

Variables	Recovery % ± R.S.D	
	For LMF	**For AMX**
Robustness at pH=5	97.70 ± 1.45	97.65 ± 1.23
Ruggedness Analyst 1		
Instrument: Epsilon EC-USB	98.18 ± 1.12	97.52 ± 1.34
Instrument: CV 50W	98.29 ± 1.47	97.68 ± 1.27
Ruggedness Analyst 2		
Instrument: Epsilon EC-USB	98.26 ± 1.58	98.26 ± 1.14
Instrument: CV 50W	98.34 ± 1.43	97.84 ± 1.18

4.4. CONCLUSION

A facile synthesis of AuNP-PdNP-ErGO nanocomposite based sensing platform has been developed for the single or simultaneous determination of LMF and AMX using SWV method. The proposed method showed homogenous and uniform distribution of AuNP and PdNP on the ErGO sheets. The beneficial interaction between noble metals and rGO allows improved charge transfer and provides effective catalytic effects that result in enhanced sensitivity and significant shift in peak potential enabling the simultaneous determination of LMF and AMX. The quantitative determination of LMF and AMX has been done using SWV and a linear calibration curve has been developed in the concentration range of 4–500 µM and 30–350 µM respectively. The application of the developed sensor for LMF and AMX analysis has also been demonstrated in the presence of excess of potentially interfering compounds commonly found in biological fluids. Moreover, recovery studies in the urine samples indicated no significant interference by the complex matrix. The excellent stability and reproducibility of the technique further proves the worth of the developed sensor in real sample analysis as well as in routine pharmaceutical investigations.

4.5 REFERENCES

[1]   Y. Zhao, X.G. Li, X. Zhou, Y.N. Zhang, "Review on graphene based optical fiber chemical and biological sensors", Sens. Actuators B-chem 231 (2016) 324–340.

[2]   Rosy, F. Singh, R.N. Goyal, "Structural and electrochemical characterization of carbon ion beam irradiated reduced graphene oxide and its application in voltammetric determination of norepinephrine", RSC Adv. 5 (2015) 87504–87510.

[3]   S. Navalon, A. Dhakshinamoorthy, M. Alvaro, H. Garcia, "Metal nanoparticles supported on two-dimensional graphenes as heterogeneous catalysts", Coord. Chem. Rev. 312 (2016) 99–148.

[4]   D.H. Shin, J.S. Lee, J. Jun, Ji Hyun An, S.G. Kim, K.H. Cho, J. Jang, "Flower-like palladium nanoclusters decorated graphene electrodes for ultrasensitive and flexible hydrogen gas sensing", Sci. Rep. 5 (2015) 12294 (DOI: 10.1038/srep12294).

[5]   B. Silwana, C. van der Horst, E. Iwuoha, V. Somerset, "Synthesis, characterisation and electrochemical evaluation of reduced graphene oxide modified antimony nanoparticles", Thin Solid Films 592 (2015) 124–134.

[6]   M.F. Hossain, J.Y. Park, "Palladium nanoparticles on electrochemically reduced chemically modified graphene oxide for non-enzymatic bimolecular sensing", RSC Adv. 3 (2013) 16109–16115.

[7]   J. Ping, Y. Wang, K. Fan, J. Wu, Y. Ying, "Direct electrochemical reduction of graphene oxide on ionic liquid doped screen-printed electrode and its electrochemical biosensing application", Biosens. Bioelectron. 28 (2011) 204–209.

[8]   S. Guo, D. Wen, Y. Zhai, S. Dong, E. Wang, "Platinum nanoparticle ensemble-on-graphene hybrid nanosheet: one-pot, rapid synthesis, and used as new electrode material for electrochemical sensing", ACS Nano 4 (2010) 3959–3968.

[9]   G. Goncalves, P.A.A.P. Marques, C.M. Granadeiro, H.I.S. Nogueira, M.K. Singh, J. Gracio, "Surface modification of graphene nanosheets with gold nanoparticles: The role of oxygen moieties at graphene surface on gold nucleation and growth", Chem. Mater. 21 (2009) 4796–4802.

[10]   A.A. Sharbaf, S. Ezugwu, M.S. Ahmed, M.G. Cottam, G. Fanchini, "Doping graphene thin films with metallic nanoparticles: experiment and theory", Carbon 95 (2015) 199–207.

[11] K.Y. Cho, H.Y. Seo, Y.S. Yeom, P. Kumar, A.S. Lee, K.Y. Baek, H.G. Yoon, "Stable 2D-structured supports incorporating ionic block copolymer-wrapped carbon nanotubes with graphene oxide toward compact decoration of metal nanoparticles and high-performance nano-catalysis", Carbon 105 (2016) 340–352.

[12] F. Xiao, F. Zhao, L. Deng, B. Zeng, "High electrocatalytic effect of PtAuPd ternary alloy nanoparticles electrodeposited on mercapto ionic liquid film", Electrochem Commun 12 (2010) 620–623.

[13] J. Wang, B. Yang, K. Zhang, D. Bin, Y. Shiraishi, P. Yang, Y. Du, "Highly sensitive electrochemical determination of sunset yellow based on the ultrafine Au-Pd and reduced graphene oxide nanocomposites", J. Colloid Interface Sci. 481 (2016) 229–235.

[14] G. Carlucci, P. Mazzeo, C. Vetuschi, "Development and validation of an HPLC method for determination of lomefloxacin in seminal plasma involving solid-phase extraction (SPE)", J. Liq. Chromatogr. Relat. Technol. 26 (2003) 2053–2063.

[15] P. Patel, P. Varshney, M. Rohit, "Analytical method development and validation for simultaneous estimation of metronidazole and amoxicillin in synthetic mixture by UV-visible spectroscopy", Int. J. Pharm. Pharm. Sci. 6 (2014) 317–319.

[16] A.N. Wadworth, K.L. Goa, "Lomefloxacin. A review of its antibacterial activity, pharmacokinetic properties and therapeutic use", Drugs 42 (1991) 1018–1060.

[17] Rosy, R.N. Goyal, "Estimation of amoxicillin in presence of high concentration of uric acid and other urinary metabolites using an unmodified pyrolytic graphite sensor", J. Electrochem. Soc. 162 (2015) G8–G13.

[18] M.S. Amran, M.R. Hossain, F.M. Amjad, S. Sultana, M.A. Baki, M.A. Hossain, "Development of a simple, sensitive and rapid quantitative analytical method for lomefloxacin by high performance liquid chromatography", S. J. Pharm. Sci. 4 (2011) 69–73.

[19] A. Beberok, M. Otreba, D. Wrzeoeniok, E. Buszman, "Cytotoxic effect of lomefloxacin in culture of human epidermal melanocytes", Pharmacol. Rep. 65 (2013) 689–699.

[20] A.D. Sarro, G.D. Sarro, "Adverse reactions to fluoroquinolones. An overview on mechanistic aspects", Curr. Med. Chem. 8 (2001) 371–384.

[21] W. Christ, "Central nervous system toxicity of quinolones: human and animal findings", J. Antimicrob. Chemother. 26 (suppl B) (1990) 219–225 (doi: 10.1093/jac/26.suppl_B.219).

[22] J. Sousa, G. Alves, A. Fortuna, A. Falcao, "Third and fourth generation fluoroquinolone antibacterials: a systematic review of safety and toxicity profiles", Curr. Drug Saf. 9 (2014) 89–105.

[23] S. Adhikari, K.R. Dhital, K. Paudel, S. Adhikari, S. Parajuli, "Fixed drug eruption resulting from amoxicillin use: a case report", J. Inst. Med. 37 (2016) 122–124.

[24] M.C. Chen, Wei-Yi Lei, J.S. Lin, C.H. Yi, D.C. Wu, C.T. Hu, "Levofloxacin-amoxicillin/clavulanate-rabeprazole versus a standard seven-day triple therapy for eradication of helicobacter pylori Infection", BioMed. Res. Int. (2014) 158520 (doi: 10.1155/2014/158520).

[25] W.C. Tai, C.H. Chiu, C.M. Liang, K.C. Chang, C.M. Kuo, Y.C. Chiu, K.L. Wu, M.L. Hu, Y.P. Chou, S.S. Chiou, K.W. Chiu, C.H. Kuo, T.H. Hu, M.T. Lin, S.K. Chuah, "Ten-day versus 14-day levofloxacin-containing triple therapy for second-line anti-helicobacter pylori eradication in Taiwan", Gastroenterol. Res. Pract. (2013) 932478 (doi: 10.1155/2013/932478).

[26] J. Orfila, F. Haider, "Comparative study of the in vitro activity of lomefloxacin versus lomefloxacin combined with metronidazole versus lomefloxacin in combination with amoxicillin/clavulanic acid against chlamydia trachomatis", Int. J. Antimicro. Agent 2 (1992) 11–13.

[27] L.E. Hines, J.E. Murphy, "Potentially harmful drug–drug interactions in the elderly: a review", Am. J. Geriatr. Pharmacother. 9 (2011) 364–377.

[28] J. Adrian, D.G. Pinacho, B. Granier, J.M. Diserens, F.S. Baeza, M.P. Marco, "A multianalyte ELISA for immunochemical screening of sulfonamide, fluoroquinolone and ß-lactam antibiotics in milk samples using class-selective bioreceptors" Anal. Bioanal. Chem. 391 (2008) 1703–1712.

[29] M.A. Cantarelli, R.G. Pellerano, E.J. Marchevsky, J.M. Camina, "Simultaneous determination of amoxicillin and diclofenac in pharmaceutical formulations using UV spectral data and the PLS chemometric method", Anal. Sci. 27 (2011) 73–78.

[30] S.B. Singh, S. Singh, "Validated UV-spectrophotometric method for quantitative estimation of lomefloxacin HCl in bulk and pharmaceutical dosages forms", World J. Pharm. Sci. 2 (2014) 1520–1525.

[31] J. Tian, J. Hu, F. Yang, T. Tang, J. Guo, W. Qin, "Polyamidoamine dendrimers as off-column binding agent and in-column pseudostationary phase for efficient and sensitive capillary electrophoretic analysis of fluoroquinolones in chicken muscles", Food Chem. 157 (2014) 498–503.

[32] M.I.R.M. Santoro, N.M. Kassab, A.K. Singh, E. R.M.K. Hackmam, "Quantitative determination of gatifloxacin, levofloxacin, lomefloxacin and pefloxacin fluoroquinolonic antibiotics in pharmaceutical preparations by high-performance liquid chromatography", J. Pharm. Biomed. Anal. 40 (2006) 179–184.

[33] A.A. Lueje, C. Lopez, L.J.N. Vergara, J.A. Squella, "Voltammetric behavior and analytical applications of lomefloxacin, an antibacterial fluorquinolone", J. AOAC Int. 84 (2001) 649–658.

[34] M.A. El Ries, A.A. Wassel, N.T.A. Ghani, M.A. El-Shall, "Electrochemical Adsorptive Behavior of some fluoroquinolones at carbon paste electrode", Anal. Sci. 21 (2005) 1249–1254.

[35] M.F. Bergamini, M.F.S. Teixeira, E.R. Dockal, N. Bocchi, E.T.G. Cavalheiro, "Evaluation of different voltammetric techniques in the determination of amoxicillin using a carbon paste electrode modified with [N,N-ethylenebis(salicylideneaminato)] oxovanadium(IV)", J. Electrochem. Soc. 153 (2006) E94–E98.

[36] T.R. Chowdhary, A.A. Shaikh, H. Akter, M.M. Neaz, P.K. Bakshi, A.J.S. Ahammad, "Highly sensitive detection of amoxicillin based on gold nanoparticle-modified ito electrode", ECS Solid State lett. 3 (2014) 14–16.

[37] A. Hatamie, A. Echresh, B. Zargar, O. Nur, M. Willandera, "Fabrication and characterization of highly-ordered zinc oxide nanorods on gold/glass electrode, and its application as a voltammetric sensor", Electrochim. Acta 174 (2015) 1261–1267.

[38] P. Augustine, Dr. K.G. Kumar, "Sensors for the determination of lomefloxacin in "Development of electrochemical sensors for the determination of certain pharmaceuticals" (http://dyuthi.cusat.ac.in/purl/2731).

[39] P. Gupta, S.K. Yadav, R.N. Goyal, "A sensitive polymelamine modified sensor for the determination of lomefloxacin in biological fluids", J. Electrochem. Soc. 162 (1) (2015) H86–H92.

[40]   A.G. Reiriz, P.C. Damiani, A.C. Olivieri, "Different strategies for the direct determination of amoxicillin in human urine by second-order multivariate analysis of kinetic–spectrophotometric data", Talanta 71 (2007) 806–815.

[41]   G.D. Christian, W.C. Purdy, "The residual current in orthophosphate medium", J. Electroanal. Chem. 3 (1962) 363–397.

[42]   W.S. Hummers, R.E. Offeman, "Preparation of graphitic oxide", J. Am. Chem. Soc. 80 (1958) 1339–1339.

[43]   Rosy, M. Raj, R.N. Goyal, "A facile method to anchor reduced graphene oxide polymer nanocomposite on the glassy carbon surface and its application in the voltammetric estimation of tryptophan in presence of 5-hydroxytryptamine", Sens. Actuators B-chem 233 (2016) 445–453.

[44]   M. Yaldagard, N. Seghatoleslami, M. Jahanshahi, "Preparation of Pt-Co nanoparticles by galvanostatic pulse electrochemical codeposition on in situ electrochemical reduced graphene nanoplates based carbon paper electrode for oxygen reduction reaction in proton exchange membrane fuel cell", Appl. Surf. Sci. 315 (2014) 222–234.

[45]   N. Kumar, Rosy, R.N. Goyal, "Nanopalladium grained polymer nanocomposite based sensor for the sensitive determination of melatonin", Electrochim. Acta 211 (2016) 18–26.

[46]   M.O. Finot, G.D. Braybrook, M.T. McDermott, "Characterization of electrochemically deposited gold nanocrystals on glassy carbon electrodes", J. Electroanal. Chem. 466 (1999) 234–241.

[47]   K. Qu, Li Wu, J. Ren, X. Qu, "Natural DNA-modified graphene/Pd nanoparticles as highly active catalyst for formic acid electro-oxidation and for the Suzuki reaction", ACS Appl. Mater. Interfaces 4 (2012) 5001–5009.

[48]   Rosy, S.K. Yadav, B. Agrawal, M. Oyama, R.N. Goyal, "Graphene modified Palladium sensor for electrochemical analysis of norepinephrine in pharmaceuticals and biological fluids", Electrochim. Acta 125 (2014) 622–629.

[49]   E. Laviron, "General expression of the linear potential sweep voltammogram in the case of diffusionless electrochemical systems", J. Electroanal. Chem. 101 (1979) 19–28.

[50]   L. Fotouhi, M. Fatollahzadeh, M.M. Heravi, "Electrochemical behavior and voltammetric determination of sulfaguanidine at a glassy carbon electrode modified with a multi-walled carbon nanotube", Int. J. Electrochem. Sci. 7 (2012) 3919–3928.

[51] L.C.S.F. Filho, T.A. Silva, F.C. Vicentini, O.F. Filho, "Simultaneous voltammetric determination of dopamine and epinephrine in human body fluid samples using a glassy carbon electrode modified with nickel oxide nanoparticles and carbon nanotubes within a dihexadecylphosphate film", Analyst 139 (2014) 2842–2849.

[52] Y. Lu, B. Chen, M. Yu, J. Han, Y. Wang, Z. Tan, Y. Yan, "Simultaneous separation/enrichment and detection of trace ciprofloxacin and lomefloxacin in food samples using thermosensitive smart polymers aqueous two-phase flotation system combined with HPLC", Food Chem. 210 (2016) 1–8.

Chapter 5

Sensors For The Determination Of Antihypertensive Drugs

5.1 INTRODUCTION

High blood pressure commonly known as hypertension is a condition in which the blood pressure in the arteries is increased. It does not show significant symptoms, however, long term hypertension leads to many diseases, such as, stroke, heart failure, coronary artery disease, loss of vision, kidney diseases and so on [1]. Hence, it is advisable to control hypertension by proper medication and changes in the life-style [2]. Antihypertensive drugs are frequently used for the treatment of hypertension. These drugs are used to reduce or lower the blood pressure and prevent the risk of stroke, cardiovascular disease, heart failure and dementia. Antihypertensive drugs are classified on the basis of their action to lower the blood pressure. Most significant and main pharmacological classes of antihypertensive drugs are beta-blockers, thiazide diuretics, calcium channel blockers, angiotensin II receptor antagonists and angiotensin-converting enzyme. The ultimate aim of the treatment is to prevent damage like, heart attack, stroke and heart failure due to abnormally high blood pressure. Hydrochlorothiazide is most commonly used thiazide diutrics and it excretes the extra salt and water from the body. The low dose of diuretics have been shown to decrease the cases of coronary artery disease and total cardiovascular mortality. However, it is well documented that a blood pressure of 140/ 90 mm Hg is achieved only in about 50% patients treated with monotherapy. In many cases combination of the two or more drugs is used and include diuretics-beta blockers; angiotensin II antagonists-diuretics; calcium channel blockers-angiotensin converting enzyme and so on. Telmisartan is an angiotensin II receptor antagonist, selectively inhibits the action of angiotensin type I receptors. Thus, both these drugs are used extensively to lower the blood pressure in human system [3].

This chapter is devoted to the determination of these drugs. The chapter is divided into two sections, **Section A** deals with the fabrication of melamine based Molecularly Imprinted sensor for the analysis of Hydrochlorothiazide, whereas, **Section B** describes the surfactant based sensor for simple and selective estimation of Telmisartan. In both the sections analysis has been carried out in pharmaceutical and urine samples.

SECTION A: Molecularly Imprinted Sensor for Determination of Hydrochlorothiazide

SECTION B: Determination of Telmisartan by using Surfactant Modified Edge Plane Pyrolytic Graphite Electrode

SECTION A: MOLECULARLY IMPRINTED SENSOR FOR DETERMINATION OF HYDROCHLOROTHIAZIDE

Molecular imprinted polymers (MIPs) are a synthetic approach to design an artificial molecular recognition system. In the place of natural receptors, like enzymes and antibody-antigen, MIPs have acquired more interest due to their superior stability, affordability and simple fabrication. They have inherent advantages, including high sensitivity, selectivity, long term stability and high chemical stability. These qualities attract the researchers to establish the artificial and robust recognition materials [4-5]. A permanent molecular memory is imprinted in the polymer film, which is capable to selectively rebinding to template molecules in rebinding step. MIP is fabricated by polymerizing a 'template' molecule recognition monomer complex together with a monomer. In the establishment of molecular imprinted sensor the target molecules act as a template molecule and initially the monomer forms complex with template molecules through the non-covalent or covalent interaction. Later on, removal of template molecules leave a permanent memory or 'mimics' of similar in shape and size on the surface [4, 6-7]. MIPs have several applications in various disciplines, such as purification/separation [8], chemo/biosensor [9], drug delivery [10] etc. Recently, several methods have been employed for the fabrication of molecular imprinted sensors such as, spin coating [11], electrochemical [12], drop casting [13] etc. Among these methods, electrochemical method has some benefits over the other because it leads to the generation of uniform, rigid and stable film, and also the thickness and morphology of the film can be controlled. Hence, electrochemical method has been extensively utilized for the formation of the MIP film. Nano-materials have unique attributes, such as high surface area, high catalytic efficiency and high surface reaction activity [14]. Magnetic nanoparticles have acquired the interest in the last decade as promising materials in drug delivery, biosepration, cell separation, enzymic assays, biosensors etc [15-19]. Iron oxide has interesting magnetic properties and is a very promising candidate for biochemical characteristics due to biodegradability, biocompatibility and non-toxicity [19-21]. Due to the unique properties of magnetic nanoparticles, iron oxide nanoparticles have been used for the preparation of the sensors as a supporting material due to their high surface area and provide the stability to the fabricated imprinted film. Various types of chemical methods have been reported for the preparation of iron oxide nanoparticles. However, an electrochemical method for the preparation of iron oxide nanoparticles in a single step is proposed in this chapter. Recently, conducting polymers gained enormous attention for the modification of electrode surface, due to its unique properties, like chemical stability of thin film, reproducibility,

and reactivity towards the organic compounds. Conducting polymers contain π-back bond, which is responsible for the electronic properties, like electrical conductivity, low ionization potential and high electron affinity [22-24]. Melamine (MM, 1,3,5-triazine-2,4,6-triamine) is a triazine compound and has nitrogen and amino groups, which are capable to prevent its aggregation and provide bio-compatibility and hence it is used for the surface modifications [25-26].

Hydrochlorothiazide (HCTZ or 6-chloro-1,1-dioxo-3,4-dihydro-2*H*-1,2,4-benzothiadiazine-7-sulfonamide, *I*) is an antihypertensive drug and helps to excrete extra salt and water from the human system. It is a benzothiazide diuretic medication that acts directly on the kidney and blocks the renal sodium chloride channel and increases the excretion of sodium chloride and a lesser extent of potassium ions [27-29]. It is widely used in the treatment of edema, cardiovascular diseases, management of diabetes insipidus, and control of essential hypertension [30-31]. The half-life of HCTZ varies between 6 to 15 h and nearly 50 – 60% of the orally administered drug excretes through urine. Greater than 90% of the adsorbed drug also excretes as unchanged drug through urine. The aim of the present studies is to develop easy, selective, sensitive and stable MIP based sensor for the determination of HCTZ in biological fluids, such as plasma and urine. Several analytical methods have been described for the determination of hydrochlorothiazide, such as high performance liquid chromatography [32-33], spectrophotometry [33-34], differential pulse polarography [35] etc. However, some of these methods have disadvantages, like time consuming process for preparing the test samples, expensive instrument and large solvent requirement for processing. Electrochemical methods, especially voltammetry has gained interest in the recent years as it proposes a more workable, high sensitive, cost-effective, environment friendly for the selective determination of electro-active analytes. Various types of unmodified and modified electrodes have been employed for the determination of HCTZ [28-29, 31 37-42]. However, most of the previously reported methods have lower sensitivity and selectivity, higher detection limit and complex modification procedure. Thus, a simple MIP sensor based on melamine has been fabricated for the determination of the trace amount of HCTZ in biological samples in the present chapter. It is expected that the amino groups of MM will form the covalent and non-covalent bonds (e.g. Hydrogen bond) with the functional groups of HCTZ and lead to better sensitivity [43]. The recognition sites of the MIP sensor (MIP/Fe_3O_4/EPPG) are found highly attractive for HCTZ.

5.2 EXPERIMENTAL

5.2.1 Reagents and Instrumentation

HCTZ, MM, ascorbic acid (AA), uric acid (UA), xanthine (X), hypoxanthine (HX), $FeCl_2$, and sulphuric acid were purchased from E. Merck (India). The phosphate buffer solutions of different pH were prepared in the range of 2.4–10.0 by using reported method [44]. All the stock solutions were freshly prepared in double distilled water throughout the experiments. The voltammetric experiments were done by using Bioanalytical voltammetric analyzer (Epsilon, EC-USB, USA). The pH measurements were made by using a digital pH meter (Eutech Instruments, model pH 700). The voltammetric studies were carried out by applying a conventional three electrodes system, having, Ag/AgCl, NaCl(sat) as the reference, molecular imprinted sensor as working and platinum wire was as an auxiliary electrode. Field Emission Scanning Electron Microscopy (FE-SEM) and Energy Dispersive X-ray analysis (EDX) were carried out using (model; Zeiss ultra plus 55) instrument. Electrochemical Impedance Spectroscopy (EIS) experiments were performed by using VersaSTAT 3 Galvanostat (PAR, USA) and X-ray diffraction (XRD) patterns of films were recorded by using Bruker D8-advance X-ray diffractometer.

5.2.2 Fabrication of modified sensor

To fabricate the molecular imprinted sensor, the surface of the edge plane pyrolytic graphite (EPPG) electrode was firstly scratched mechanically on an emery paper (P-400) to renew the surface and then it was washed with double distilled water. The electrode was then dipped in 4 mL of 4 mM $FeCl_2$ solution prepared in water. The electrochemical deposition of iron oxide nanoparticles was then carried out transversing potential in the range -100 to 1500 mV at 100 mV/s for 15 cyclic voltammetric scans (optimized). The obtained film was then carefully rinsed with double distilled water and allowed to dry at room temperature. The sensor was named as Fe_3O_4 nanoparticles modified EPPG. In the second step, the electro-polymerization of melamine with HCTZ as template was carried out. For this purpose, 2 mL of 2 mM HCTZ and 3 mL of 4 mM melamine (prepared in 0.1 M H_2SO_4) were used and then the potential was scanned in the range of 0 to 1600 mV at 100 mV/s using cyclic voltammetry for optimized 20 scans. The obtained film was carefully rinsed with distilled water to remove the unreactive substances [26]. Finally, modified sensor was cycled between -1.0 to 1.5 V at 100 mV/s sweep rate for 25 cycles in 0.25 M H_2SO_4 to release the imprinted HCTZ template molecules. A non-imprinted polymer

(NIP/Fe$_3$O$_4$/EPPG) sensor was also prepared under identical conditions without the template molecules solution. The sensing surface of the developed MIP sensor was characterized by using voltammetry, FE-SEM, EDX, EIS and XRD studies.

5.2.3. Voltammetric procedures

The stock solution of HCTZ (1.0 mM), was prepared by dissolving the required amount in the double distilled water. To prepare the test solution, the required volume of the HCTZ stock solution was added into the electrochemical glass cell, which already contained 2 mL of pH 7.2 phosphate buffer and the total volume was made to 4 mL by using double distilled water. The optimized experimental conditions used for the square wave voltammetry (SWV) were: initial potential (E$_i$): 0 mV, the final potential (E$_f$): 1200 mV, square wave amplitude (Esw): 25 mV, square wave frequency (*f*): 15 Hz, potential step (E): 4 mV, and the optimal operating conditions for the cyclic voltammetry (CV) were initial potential (E$_i$): 0 mV, switching potential (E): 1600 mV, the final potential (E$_f$): 0 mV and sweep rate 100 mV/s. The MIP sensor surface was cleaned after every run by using a potential of -800 mV for 100 s in the phosphate buffer (pH 7.2).

5.2.4 Analysis of Pharmaceutical samples

To test the pharmaceutical samples, three tablets viz., Xstan-H (Blue Cross PVT Ltd, Mumbai), Tazloc-H (USV Ltd, Baddi, Himachal Pradesh) and Tadil 40-H (Zee laboratories, Paonta Sahib, Himachal Pradesh) having HCTZ (12.5 mg) were purchased from the local market of Roorkee (India). The tablets were completely crushed and ~ 1 mg was dissolved in 10 mL volumetric flask by using double distilled water.

5.2.5 Urine sample analysis

For recovery measurements, the urine samples of two healthy volunteers (Female, age 25 and Male, age 28) were obtained from the Institute hospital of I.I.T. Roorkee. The collected urine samples were filtered by using the Whatman 42 filter paper and diluted twice by using phosphate buffer (pH 7.2). The test solutions for the recovery study were prepared by spiking the required volume of HCTZ stock solution (1.0 mM) into the diluted urine sample in the working range.

5.3 RESULTS AND DISCUSSION

5.3.1 Characterization of composite film

The changes occurring on the surface modification of EPPG at different level of modification were visualized by using FE-SEM. **Fig. 5.1** represents a comparison of FE-SEM images and an unmodified EPPG surface **[Fig. 5.1 (a)]** shows a different topography in comparison to the Fe_3O_4 nanoparticles modified/EPPG and MIP/Fe_3O_4/EPPG sensors. **Fig. 5.1 (b)** shows clearly the deposition of Fe_3O_4 nanoparticles at the sensing surface and **Fig. 5.1 (c)** represents the even distribution of cubical, crystalline structures of melamine at the Fe_3O_4 nanoparticles modified EPPG surface. **Fig. 5.1 (d)** shows the EDX of the Fe_3O_4 modified surface and indicates the deposition of Fe.
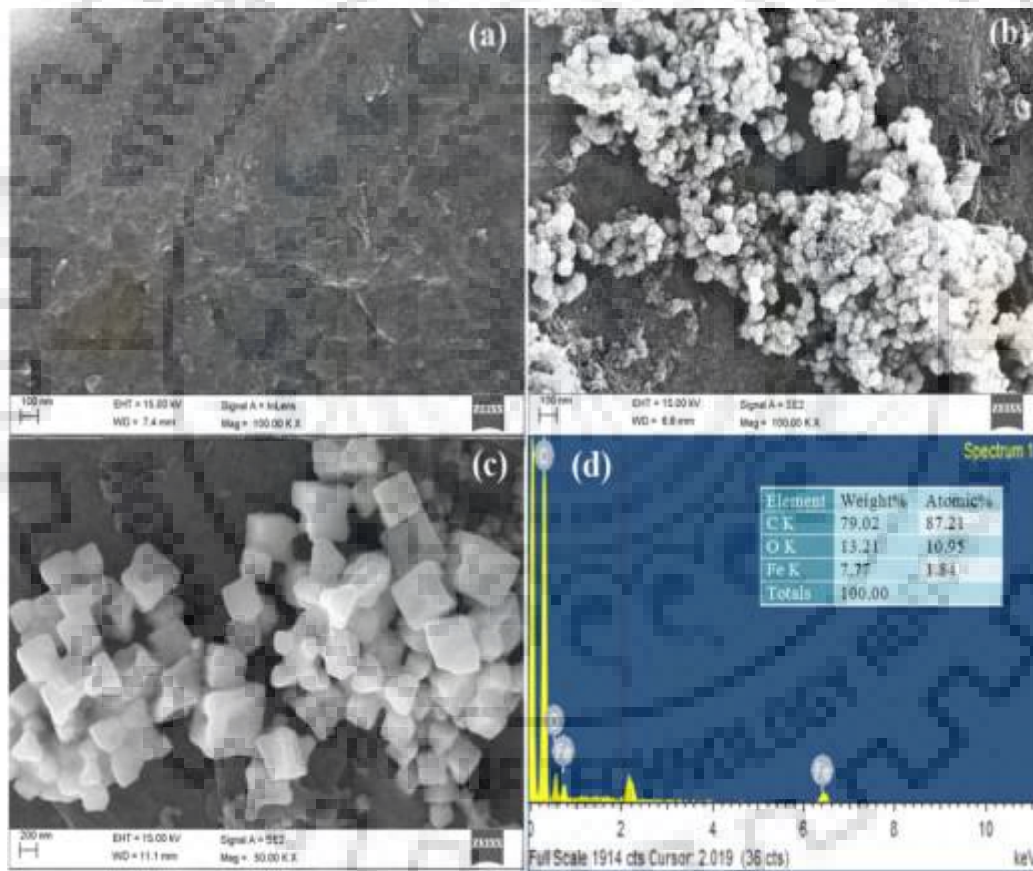

Fig. 5.1: FE-SEM images demonstrating surface morphology of (a) unmodified EPPG, (b) Fe_3O_4/EPPG, (c) MIP/Fe_3O_4/EPPG and (d) EDX data demonstrating presence of Iron at the sensor surface.

The further characterization of the iron oxide nanoparticles deposition at the sensor surface was carried out by using X-ray studies. The X-ray diffraction (XRD) spectrum after deposition of

iron oxide (Fe_3O_4) nanoparticles is presented in **Fig. 5.2**. Five peaks at $2\theta = 21.2°$, $30.5°$, $35.5°$, $51°$, $60.5°$ were observed, which corresponded to the (0 1 2), (2 2 0), (3 1 1), (4 2 2) and (4 4 0) and indicated the successful deposition of iron oxide nanoparticles at the sensing surface [45-46].
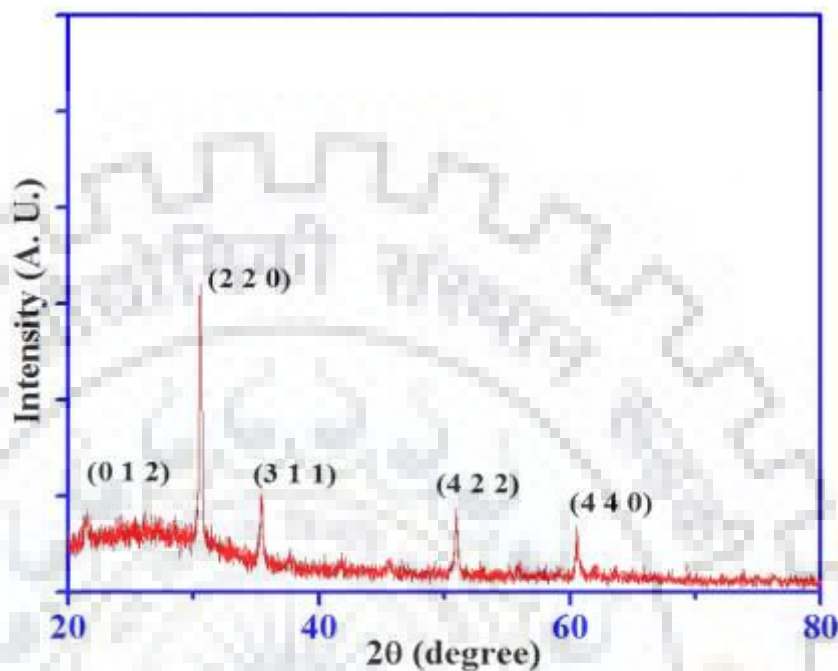
Fig. 5.2: Observed XRD pattern for Iron oxide nanoparticles.

The charge transfer resistance (Rct) corresponding to the unmodified/EPPG, NIP/Fe_3O_4/EPPG, MIP/Fe_3O_4/EPPG and imprinted with template/EPPG surfaces were calculated by using EIS. The experiment was performed in 1:1 mixture of 0.01M KCl and 5 mM $K_3Fe(CN)_6$ solution in the frequency range 1000 kHz to 10 mHz at a potential of 1.0 V. The typical Nyquist plots observed are presented in **Fig. 5.3**. The best fitted results were found by using a simple Randles equivalence circuit. The charge transfer resistance (R_{CT}) values for unmodified/EPPG, NIP/Fe_3O_4/EPPG, Fe_3O_4/EPPG, MIP/Fe_3O_4/EPPG and MIP with template were determined as 1142 Ω **(curve A)**, 901.4 Ω **(curve B)**, 954 Ω **(curve C)**, 1005 Ω **(curve D)**, and 811.8 Ω **(curve E)**, respectively. From **Fig. 5.3**, it can be clearly seen that the lowest R_{CT} value was observed for MIP with template, indicating the special affinity of recognition sites for the template molecules at sensing surface. However, MIP without template molecules has higher Rct value in comparison to the NIP, which may be due to the presence of cavities in MIP film, while NIP is the result of a continuous coating of conducting poly melamine on the sensor surface. While in case of Fe_3O_4 modified sensor the Rct value is greater than MIP and bare due to the presence of the iron

nanoparticles and high surface area. The higher Rct value in the case of imprinted sensor appears to be due to the uneven surface of the conducting melamine and presence of cavities.
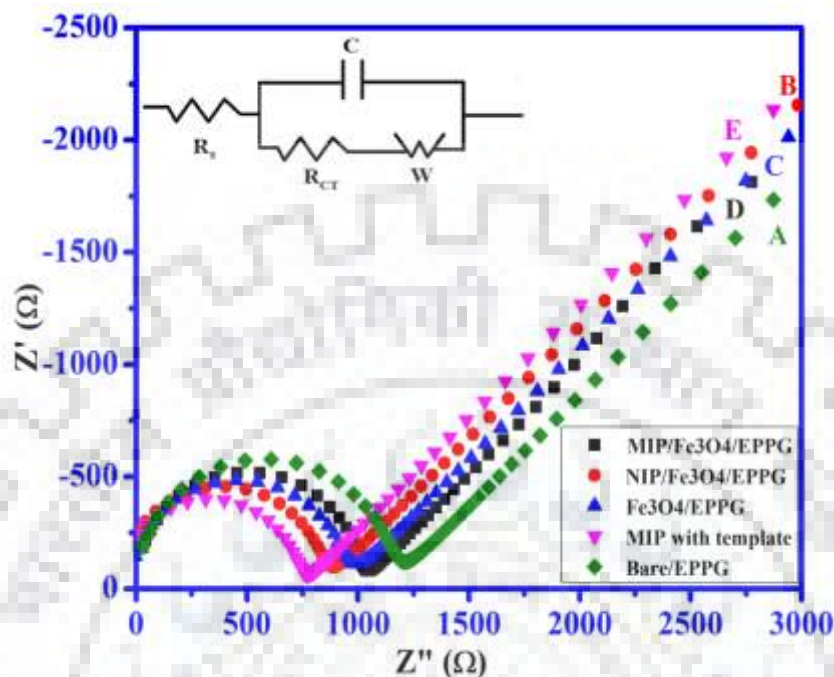
Fig. 5.3: Typical Nyquist plots obtained for (A) unmodified/EPPG, (B) MIP/ Fe_3O_4/EPPG, (C) Fe_3O_4/EPPG, (D) NIP/Fe_3O_4/EPPG and (E) MIP with template at EPPG during EIS in 1:1 mixture of 5 mM $K_3Fe(CN)_6$ and 10 mM KCl solution over the frequency range 1000 kHz to 1 mHz.

5.3.2 Optimization of experimental conditions

The incubation step plays a key role in enhancing the sensitivity of molecular imprinted sensor. The interaction between imprinted molecular recognition cavity and analyte molecules were evaluated by incubating 1 µM concentration of HCTZ in phosphate buffer of pH 7.2 for 1–30 min and current responses were measured each time. It was observed that the anodic peak current increased with increasing the incubation time till 15 min and then became practically constant (as shown in **Fig. 5.4 (A)**). This behaviour can be explained due to the saturation of all active sites due to which the peak current became practically constant. The maximum peak current was found at 15 min and hence was used as optimized incubation time for the subsequent studies.

To construct the imprinted molecular recognition sites on the sensor surface, the concentration ratio of template to monomer plays an important role. Hence, to attain the maximum sensitivity of the MIP sensor, the optimization was performed by varying the concentration of the melamine monomer up to 2 times in comparison to the template. For this purpose, 2 mL of 2 mM

187

HCTZ was taken with the different volume (1–4 mL) of 4 mM MM monomer. It was observed that the largest peak current response at MIP/Fe$_3$O$_4$/EPPG was observed, when MIP film was synthesized by using the solution having 2 mL of HCTZ and 3 mL of MM monomer (2 : 3) in comparison to other template to monomer ratios as represented in **Fig. 5.4 (B)**. When the ratio of the concentration of template and monomer was 2 : 1, the peak current response for HCTZ was very small due to the limited amount of monomer available for binding to the template molecules. At the ratio of 2 : 4 the peak current decreased in comparison to 2 : 3 template monomer ratio, probably because of the increased thickness of the imprinted membrane, due to which the access of the binding sites by template molecules became difficult.
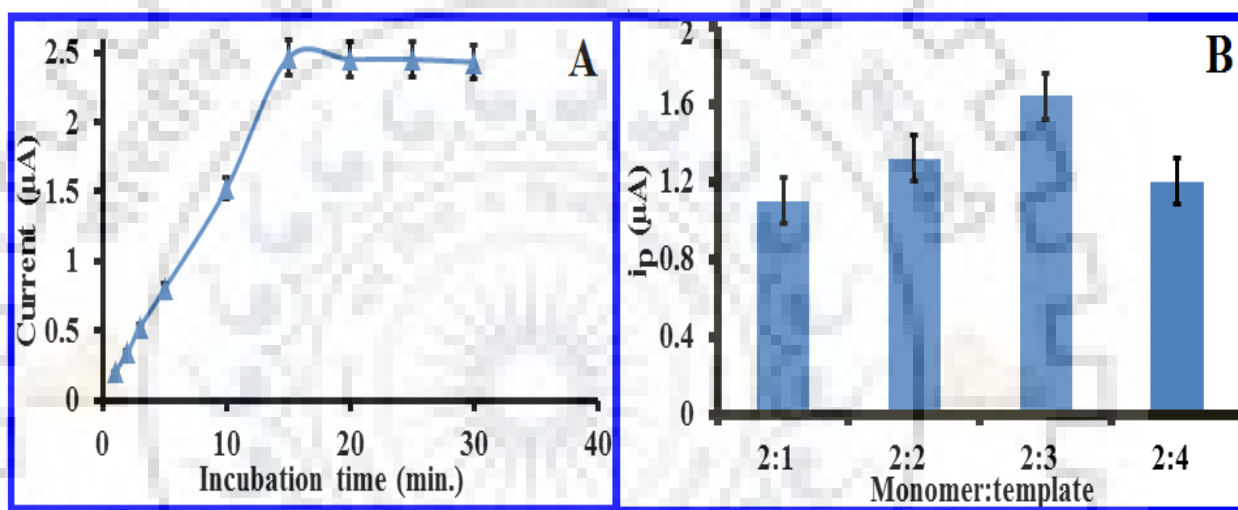
Fig. 5.4: (A) Effect of incubation time and (B) polymer to template ratio on the anodic peak current response of 1 μM HCTZ observed using the imprinted sensor at pH 7.2.

5.3.3 Cyclic voltammetry

The cyclic voltammetric studies were performed for examining the redox behavior of HCTZ at the sensor surface. **Fig. 5.5** represents a comparison of typical cyclic voltammograms for the irreversible anodic oxidation of HCTZ at unmodified EPPG, NIP/Fe$_3$O$_4$/EPPG and MIP/Fe$_3$O$_4$/EPPG surfaces at pH 7.2 at a scan rate of 100 mV s^{-1}. A weak anodic peak of HCTZ was found at ~806 mV at unmodified EPPG **(curve a)** and at ~808 mV at NIP/Fe$_3$O$_4$/EPPG **(curve b)**. Whereas, a sharp and well-defined peak was observed at lower potential (~766 mV) at the MIP/Fe$_3$O$_4$/EPPG **(curve c)**. At all the three sensors a single irreversible oxidation peak was observed for HCTZ. However, the peak current enhancement and the decrement in the peak

potential at the MIP for HCTZ, clearly indicates the electrocatalytic behavior and sensitivity of the $MIP/Fe_3O_4/EPPG$ towards the HCTZ.
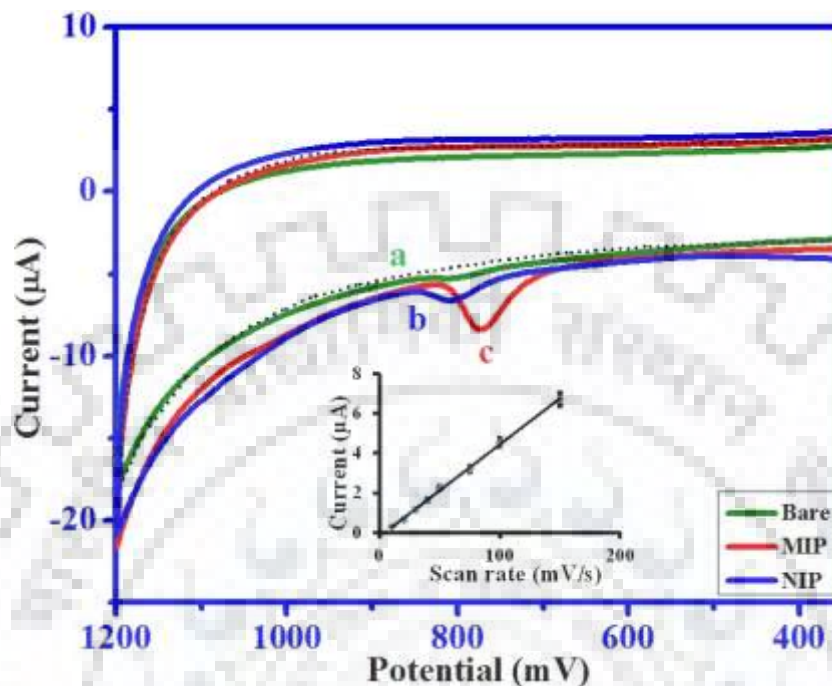
Fig. 5.5: Comparative cyclic voltammograms for 1 µM HCTZ in pH 7.2 phosphate buffer at 100 mV/s using (a) Unmodified EPPG, (b) $NIP/Fe_3O_4/EPPG$ and (c) $MIP/Fe_3O_4/EPPG$.

To elucidate the nature of electron transfer reactions involved in the electrochemical oxidation of HCTZ at $MIP/Fe_3O_4/EPPG$, scan rate study was performed. It was observed that with increasing the scan rate (v), oxidation peak current of HCTZ increased in the range 10-150 mV/s as demonstrated in the inset of **Fig. 5.5**. A linear relation between the scan rate (v) and peak current (i_p) can be represented as:

$$i_p = 0.0464\ v - 0.2036, R^2 = 0.9986$$

$$\log i_p = 1.181 \log v - 1.7041,\ R^2 = 0.9955$$

where, i_p is the oxidation peak current in µA and v is the scan rate in mVs^{-1}. The linear plot of i_p vs v indicates that anodic oxidation of HCTZ at $MIP/Fe_3O_4/EPPG$ follows the adsorption controlled pathway. The adsorption of HCTZ was further confirmed by the linear plot between $\log i_p$ vs. $\log v$. The slope value ($d\log i_p/d\log v$) of 1.181 was greater than 0.5 and thus indicated that the nature of electron transfer processes in the oxidation of HCTZ was adsorption controlled [47].

5.3.4. Square wave voltammetry

For detailed studies SWV technique was used due to its advantages such as low background current and better peak resolution. **Fig. 5.6** represents comparative square wave voltammograms recorded at different stages of surface modification, such as at bare EPPG, Fe_3O_4/EPPG, NIP/ Fe_3O_4/EPPG and MIP/Fe_3O_4/EPPG at 7.2 pH containing 1 µM HCTZ. At bare EPPG, a broad peak is observed at 787 mV which shifted to 782 mV and 785 mV with enhanced peak current at Fe_3O_4/EPPG and NIP/Fe_3O_4/EPPG, respectively. On the other hand, a sharp peak having maximum peak current was observed at the MIP/Fe_3O_4/EPPG (E_p=754 mV). The best result for the oxidation of HCTZ was observed at MIP/Fe_3O_4/EPPG, hence, subsequent voltammetric studies were performed by using MIP/Fe_3O_4/EPPG. To prove that only entrapped molecules of HCTZ at the sensor surface undergo oxidation two scans were recorded. **Fig. 5.6 (E)** shows the anodic response of 1 µM HCTZ at MIP/Fe_3O_4/EPPG in the first and second scans. It can be clearly seen that the oxidation of HCTZ takes place only in the first scan, while in case of second scan no oxidation peak was observed. This behaviour indicated that only entrapped molecules undergo oxidation.
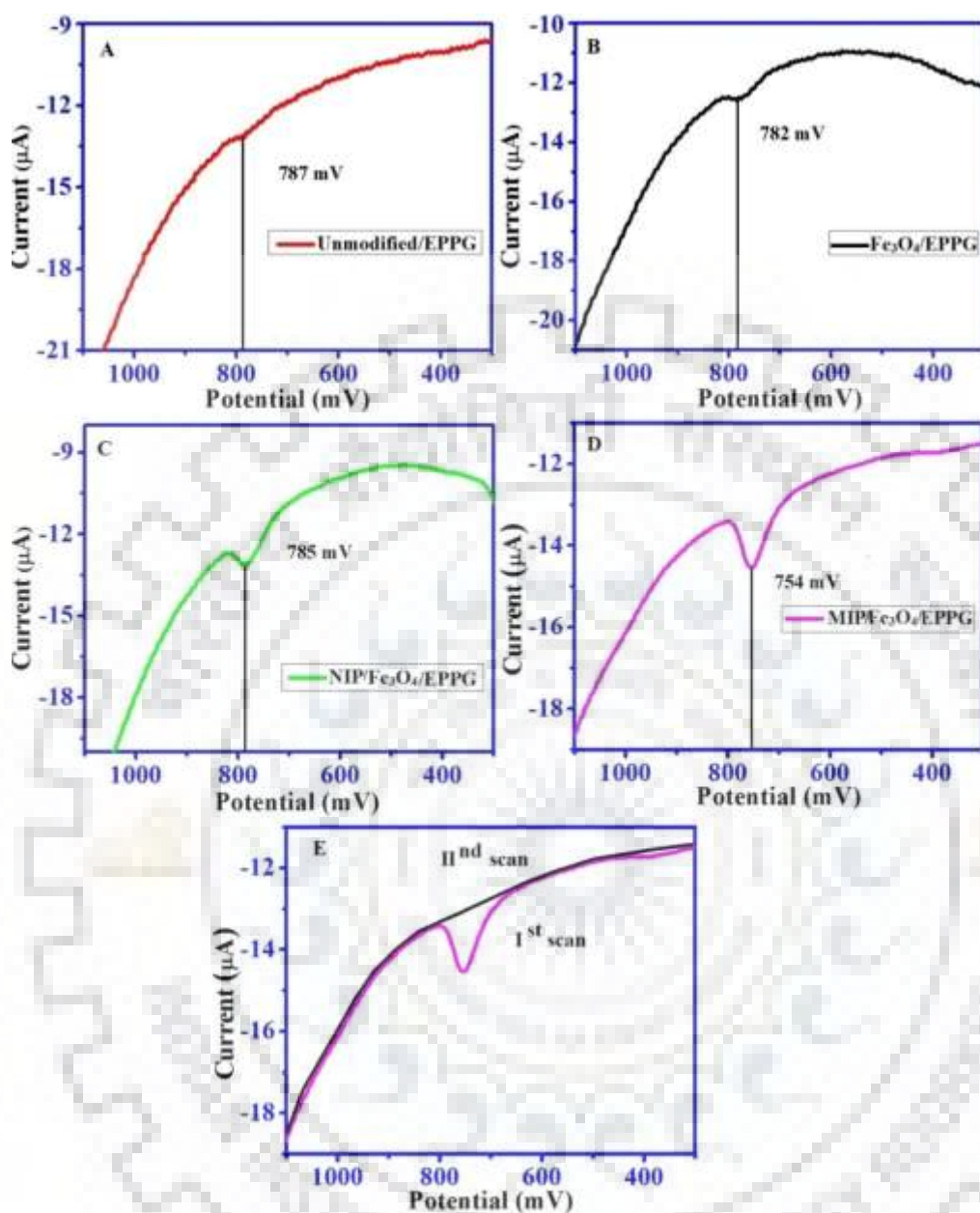
Fig. 5.6: A comparison of square wave voltammograms recorded for 1 μM HCTZ at pH 7.2 phosphate buffer at (A) Unmodified EPPG, (B) Fe$_3$O$_4$/EPPG, (C) NIP/Fe$_3$O$_4$/EPPG, (D) MIP/Fe$_3$O$_4$/EPPG and (E) Effect of number of scans on the oxidation of HCTZ at MIP/Fe$_3$O$_4$/EPPG sensor

5.3.4.1. Frequency study

The influence of the frequency on anodic peak current of HCTZ was studied at MIP/Fe$_3$O$_4$/EPPG by using the SWV. The response of 1 μM HCTZ was recorded at different

frequency (f) in the range of 10 – 150 Hz. The oxidation peak current (i_p) was found to increase linearly with increasing frequency. The dependence between i_p vs. f and log i_p vs. log f can be presented by the relations:

$$i_p = 0.0693\,f + 0.1992, R^2 = 0.9917$$

$$\log i_p = 1.0051 \log f - 1.125, R^2 = 0.9926$$

where, R^2 is the correlation coefficient, and f is square wave frequency in Hz and i_p is anodic peak current in μA. The slope of log i_p vs log f plot being greater than 0.5 again confirmed that the oxidation of HCTZ at the MIP/Fe$_3$O$_4$/EPPG is adsorption controlled and further supported the results obtained using cyclic voltammetry [47].

5.3.4.2. Effect of pH

The influence of pH on the oxidation peak potential of the 1 μM HCTZ was evaluated in the range of 2.4 – 10.0. It was found that the peak potential of the HCTZ shifted to the less positive potentials with increase in pH (**Fig. 5.7**). A linear relation was obtained between the peak potential (E_p) and pH of the HCTZ and can be represented as:

$$E_p = -62\,pH\,[2.0\text{-}10.0] + 1222.8, R^2 = 0.982$$

Where, Ep is the anodic peak potential in mV and R^2 is the correlation coefficient. The slope value (dE_P/dpH) of 62 mV/pH suggests that the equal numbers of electrons and protons are involved in the electro-oxidation of HCTZ [38].
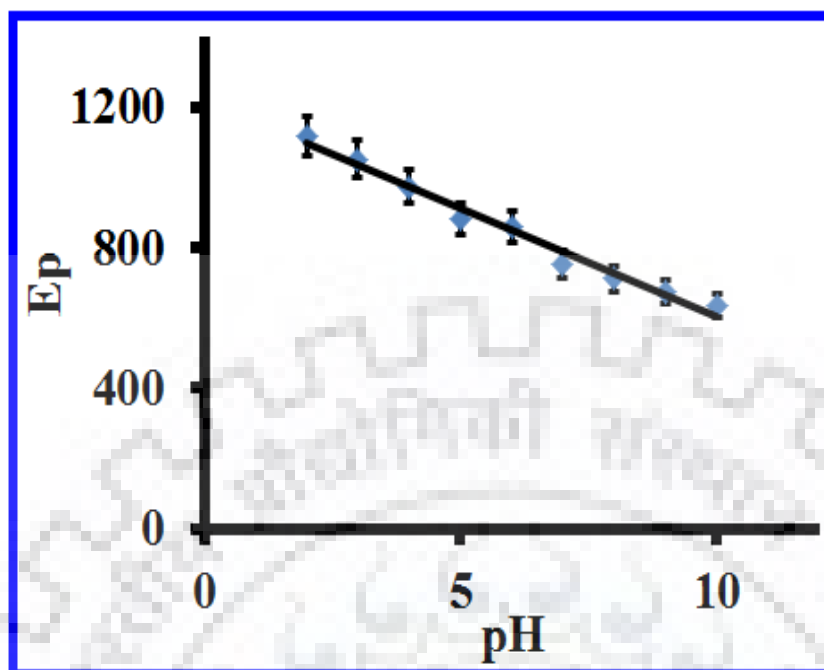
Fig. 5.7: Dependence of peak potential (E_P) on the pH of the supporting electrolyte for 1 μM HCTZ.

Further, to calculate the number of electrons involved in the oxidation of HCTZ, Laviron's equation was used [48]. For this purpose, cyclic voltammograms were recorded for 1 μM HCTZ at different sweep rates (v) between 10–250 mVs^{-1}. It was observed that with increase in the sweep rate (v), the anodic peak potential (E_p) of HCTZ shifted to more positive potentials. The E_p vs. log v plot was linear and dependence of Ep on log v can be expressed by the relation:

$$Ep = 49.831 \log v + 667.62, R^2 = 0.9934$$

Laviron's equation was applied to obtain the value of n, number of electrons involved in the oxidation. The slope ($dE_P/d\log v$) value of E_p vs. log v plot was utilized to calculate the value αn, where n is the number of electrons and α is the transfer coefficient. For an irreversible electron transfer process, the value of α is commonly assumed as 0.5 [49], hence the number of electrons involved in the oxidation of HCTZ was found to be ~2.30. Thus, it was concluded that two electrons are involved in the electro-oxidation of HCTZ. A 2e$^-$, 2H$^+$ mechanism for HCTZ oxidation can be proposed **(Scheme 5.1)** as reported earlier [38].
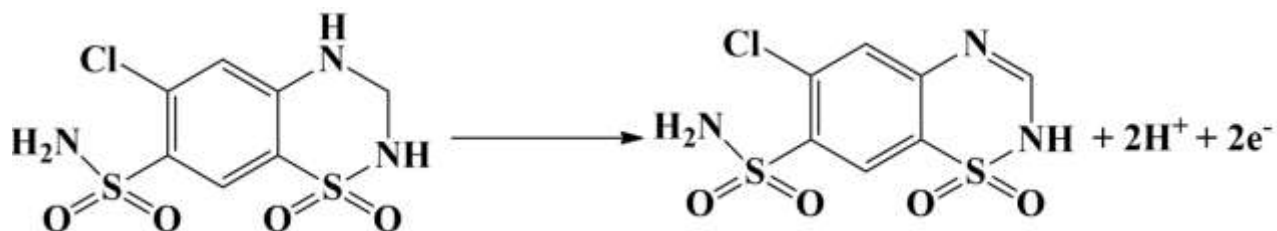
Scheme 5.1: Mechanism suggested for oxidation of Hydrochlorothiazide.

5.3.4.3. Concentration study

The quantitative analysis of the HCTZ is based on the dependence of the anodic peak current on the concentration. The square wave voltammograms were recorded at different concentrations of HCTZ in the range 0.025–10 µM at MIP/Fe$_3$O$_4$/EPPG as depicted in **Fig. 5.8**. It was found that the peak current increases with the increase in the concentration of HCTZ. The peak current values were measured by subtracting the background current. The plot of i_p vs concentration exhibited a break at around 0.25 µM. The dependence of peak current (i_p) on concentration can be expressed as:

i_p = 2.3426 [C, 0.025-0.25] + 0.2061, R² = 0.985 ----------------MIP/Fe$_3$O$_4$/EPPG

i_p = 0.7411 [C, 0.25-10] + 0.7973, R² = 0.996 ------------------- MIP/Fe$_3$O$_4$/EPPG

i_p = 0.2533 [C] - 0.2296, R² = 0.996 ----------------------unmodified EPPG

Where, [C] is the concentration of HCTZ in µM and R^2 is the correlation coefficient. From the regression equations, it is found that the MIP sensor has ~10 fold higher sensitivity towards the HCTZ in the lower concentration range as compared to the unmodified EPPG. In the quantitative analysis of HCTZ, observed analytical parameters at MIP/Fe$_3$O$_4$/EPPG and unmodified EPPG sensors are summarized in **Table 5.1**.
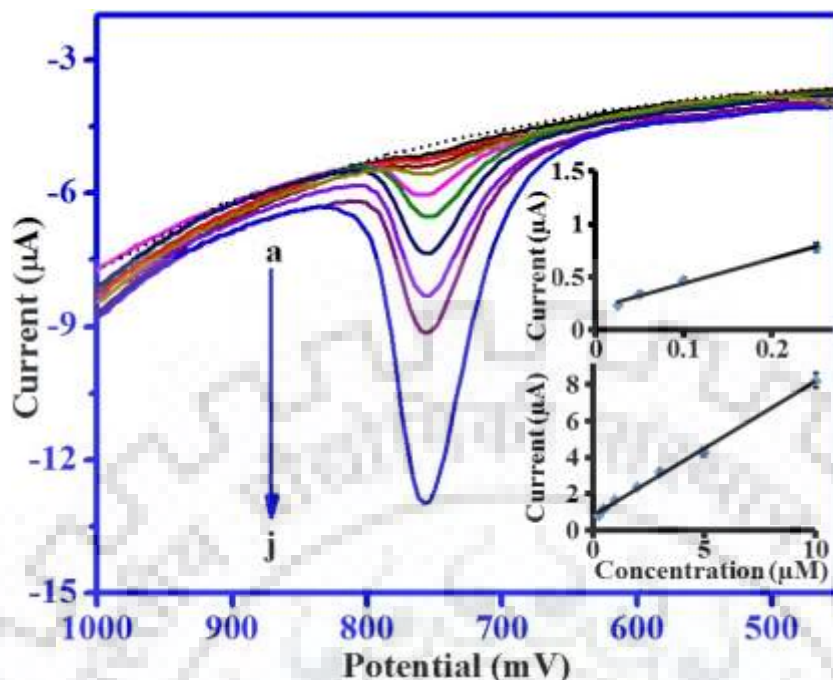
Fig. 5.8: Square wave voltammograms recorded for (a) 0.025 µM, (b) 0.05 µM, (c) 0.1 µM, (d) 0.25 µM, (e) 0.5 µM, (f) 1 µM, (g) 2 µM, (h) 3 µM, (i) 5 µM and (j) 10 µM HCTZ concentrations using MIP/Fe$_3$O$_4$/EPPG. The dotted line represents the background current. Inset are the calibration plots in the concentration range of 0.025–0.25 and 0.25–10.0 µM.

Table 5.1: Statistical parameters obtained for quantitative analysis of HCTZ.

Validation Parameters	Determination of HCTZ		
	Unmodified/EPPG	MIP/Fe$_3$O$_4$/EPPG	
Concentration	2–150 µM	0.025–0.25 µM	0.25–10 µM
Sensitivity (µA/µM)	0.2533	2.3426	0.7411
Correlation coefficient (R^2)	0.996	0.985	0.996
Standard error of slope	0.0065	0.2025	0.0195
Intercept	-0.2295	0.2061	0.7973
Standard error of intercept	0.4043	0.0278	0.0873

The detection limit of the MIP/Fe$_3$O$_4$/EPPG has been calculated by using the formula 3σ/b, where σ is the standard deviation of three repeated blank readings and b is the sensitivity obtained from the calibration plot. The sensitivity was estimated to be 2.3426 µA µM^{-1} and limit of

detection was found to be 0.004 µM. This limit of detection for HCTZ was lowest when compared with the reported in literature in the recent years **(Table 5.2)**.

Table 5.2: A comparison of limit of detection (LOD) obtained for HCTZ using the proposed method with the recently reported using other sensors.

S.No.	Electrode/modified	Linear range (µM)	LOD (µM)	Reference
1.	Ferrocenedicarboxylic Acid/CPE, SWV	0.08–500	0.037	**28**
2.	Benzoylferrocene/CPE	0.03–0.6	0.09	**29**
3.	BDDE, (DPV)	3–74	1.20	**31**
4.	SRE/MWCNTs, DPV	5–70	2.60	**37**
5.	BDDE	1.97–88.1	0.639	**38**
6.	GR-Ferrocene/CPE	0.5–390	0.38	**39**
7.	BDDE	0.51–18.7	0.376	**40**
8.	Fe_3O_4@SiO_2/MWCNT/ionic liquid/CPE	1–600	0.085	**41**
9.	Nickel hydroxide/Ni	13.9–167	7.92	**42**
10.	MIP/Fe_3O_4/EPPG	0.025–0.25 ⎤→ 0.004 0.25–10 ⎦		**Present work**

DPAV: Differential pulse anodic voltammetric, DPV: Differential-pulse voltammetry, BDDE: Boron-doped diamond electrode, SRE/MWCNTs: Multiwall carbon nanotube/silicone rubber

5.3.5 Interference study

The selectivity of the developed MIP/Fe_3O_4/EPPG was evaluated in the presence of interfering substances such as UA, AA, HX, X, telmisartan (TMS) and metoprolol (MTP) with a fixed concentration of HCTZ (1µM). TMS and MTP were selected as HCTZ is also marketed in combination with these drugs, hence, interference of TMS and MTP on oxidation of HCTZ is also examined. The oxidation of TMS did not occur in the working potential range used in the present investigation, hence, no effect of TMS is observed. For other compounds, SW voltammograms of HCTZ at MIP/Fe_3O_4/EPPG were recorded in the presence of different amount of interfering molecules at a fixed concentration of 1µM HCTZ. Practically no effect is found on anodic peak current response of HCTZ in the presence of concentration of UA, AA, X, HX and MTP

respectively (**Fig. 5.9**). Hence, it is concluded that the developed MIP/Fe$_3$O$_4$/EPPG can be effectively used for the selective analysis of HCTZ in the presence of common interfering compounds present in biological systems.
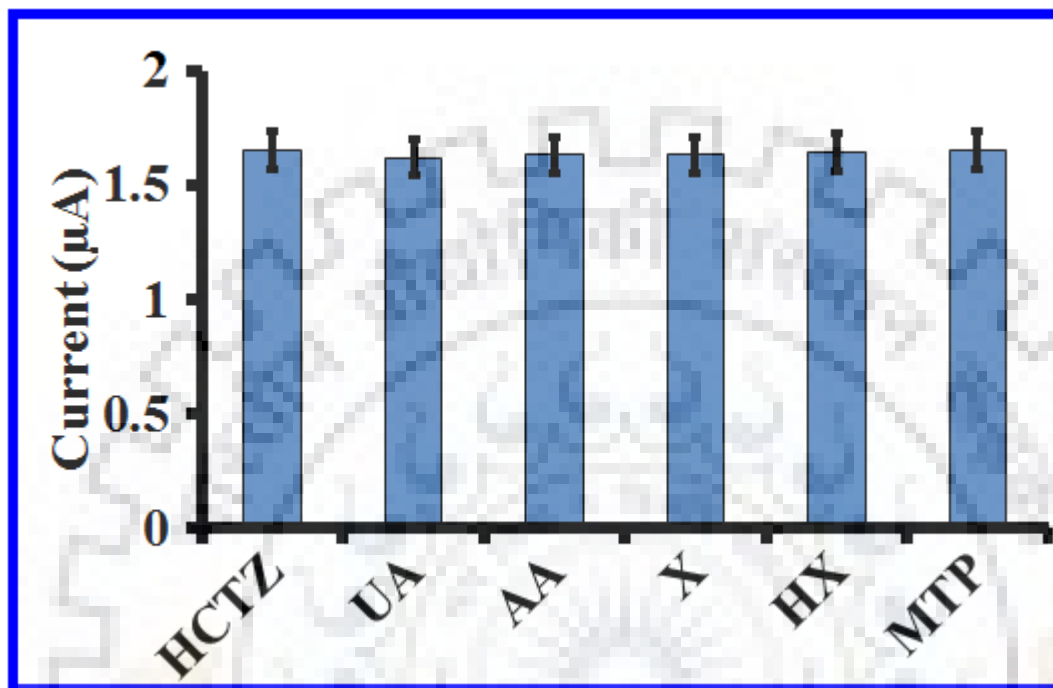
Fig. 5.9: Effect of interferents observed on the peak current of HCTZ for selectivity of imprinted sensor for 1 µM HCTZ. Concentration are 100 µM uric acid; 200 µM ascorbic acid; 100 µM hypoxanthine; 50 µM Xanthine and 100 µM metoprolol.

5.3.6. ANALYTICAL APPLICATION

5.3.6.1 Pharmaceutical Samples

For pharmaceutical analysis, the tablets were crushed and the required amount was dissolved in the double distilled water to prepare 1mM stock solution of HCTZ. To bring the concentration of the solution in the working range, the stock solution was further diluted by using double distilled water and phosphate buffer. SW voltammograms were then recorded at MIP/Fe$_3$O$_4$/EPPG using optimized parameters and identical conditions as were used in above studies. The results obtained are presented in **Table 5.3** and indicated the good similarities between the listed amount and observed amount of HCTZ.

Table 5.3: Determination of HCTZ content in pharmaceutical drug formulations using MIP/Fe$_3$O$_4$/EPPG.

S.No.	Tablet	Stated content (mg)	Observed content (mg)	Error %
1.	Xstan-H	12.5	12.491	0.90
2.	Tazloc-H	12.5	12.487	1.30
3.	Tadil 40-H	12.5	12.493	0.70

5.3.6.2 Recovery study

The analytical utility of the molecular imprinted sensor was determined by carrying out recovery studies. The MIP/Fe$_3$O$_4$/EPPG was used to quantify the HCTZ in the complex matrix, such as human urine samples. For this purpose, the urine samples were diluted 2 fold with pH 7.2 phosphate buffer to minimise the complexity of the samples. Initially the urine samples of the patients undergoing treatment with HCTZ (12–5 g) a day were used. However, no peak for HCTZ was noticed when urine samples collected after 4 h, 8 h and 24 h of oral administration of HCTZ were analyzed. One of the reasons for non-appearance of HCTZ is excretion time, which varies between 6 to 15 h. Hence, it was decided to carry out the recovery studies. The urine samples of healthy persons were spiked with HCTZ in the working range and SW voltammograms were recorded. An excellent agreement was found in the recovery and spiked concentration of HCTZ as shown in **Table 5.4** with low RSD value. The obtained results demonstrated a recovery >99%, indicating thereby the practical utility of the MIP/Fe$_3$O$_4$/EPPG for the quantification of HCTZ in complex matrix.

Table 5.4: Recovery data of HCTZ determination in human urine sample.

S.No.	Spiked amount (µM)	Detected amount (µM)	*Recovery %	Error %
Sample				
1.	0.50	0.501	100.20	0.2
2.	1.0	0.991	99.10	-0.9
3.	2.0	2.010	100.50	0.5
Sample				
1.	0.25	0.251	100.40	-0.4
2.	0.75	0.747	99.60	0.4
3.	3.0	2.991	99.70	0.3

*RSD for the determination was 1.13% for n=3

5.4 Stability and reproducibility of the molecularly imprinted sensor

To examine the stability of the MIP/Fe$_3$O$_4$/EPPG, the oxidation response at a fixed concentration of HCTZ (1 µM) was studied at pH 7.2 by recording the voltammograms over a period of 30 days. The observed results confirmed that MIP/Fe$_3$O$_4$/EPPG exhibited a variation of < ±4.0% during the first 20 days. After 20 days, a current drop up to 6.8% was noticed. Thus, MIP/Fe$_3$O$_4$/EPPG can be safely used for the first 20 days after its fabrication.

In order to evaluate the intraday reproducibility of the MIP/Fe$_3$O$_4$/EPPG, five voltammograms were recorded for HCTZ solution at an interval of 1 h. The R.S.D value for n=5 determinations was found to be ±2.32%. Hence, it is concluded that the MIP/Fe$_3$O$_4$/EPPG has an excellent stability and reproducibility. To monitor the sensor to sensor variation, five different MIP sensors were fabricated by following the same modification protocol. The electrochemical experiment was executed in 1 µM HCTZ solution by using MIP/Fe$_3$O$_4$/EPPG at pH 7.2. A negligible variation was detected in the peak potential and current response of HCTZ. The RSD for peak current was found to be 2.43%. Thus, from the above results it is concluded that the proposed protocol has long term stability and reproducibility.

5.5. Ruggedness studies

To investigate the changes in the interlabortory behavior of the developed MIP/Fe$_3$O$_4$/EPPG, the ruggedness study was performed. To examine the instruments related

deviation in voltammetric response, two voltammetric analyzers viz., Epsilon EC-USB and CV-50 (BAS, West Lafayette, USA) were used. To examine the intermediate precision of the developed MIP/Fe$_3$O$_4$/EPPG, the response was evaluated by two different analysts using different MIP sensors on different days. From the obtained results at different sensors and at different instruments, a variation of ±1.58% in current response of HCTZ was found. The obtained results are listed in **Table 5.5** and suggest that no significant difference is observed between the recovery results. Hence, the proposed MIP/Fe$_3$O$_4$/EPPG presents reliable, robust and rugged approach for analyzing HCTZ in the complex matrix.

Table 5.5: The robustness and ruggedness of the proposed method for the recovery data of HCTZ determination in human urine samples.

Variables	Recovery % ± R.S.D
Robustness at pH=7.2	98.71 ± 1.42
Ruggedness Analyst 1	
Instrument: CV 50W	99.38 ± 1.43
Instrument: Epsilon EC-USB	98.59 ± 1.37
Ruggedness Analyst 2	
Instrument: CV 50W	98.29 ± 1.48
Instrument: Epsilon EC-USB	99.44 ± 1.53

5.6 CONCLUSION

In the present section, a melamine based imprinted sensor was fabricated at the Fe$_3$O$_4$ nanoparticles modified EPPG. The Fe$_3$O$_4$ nanoparticles layer was prepared by using electrochemical method at the EPPG surface. The surface of the MIP/Fe$_3$O$_4$/EPPG was characterized by using Voltammetry, FE-SEM, EDX, EIS and XRD. The electro-catalytic capability of the imprinted sensor has been studied by using the MIP/Fe$_3$O$_4$/EPPG for the quantitative as well as qualitative examination of HCTZ. The calibration curve observed between the peak current and concentration of HCTZ in range of $25 \times 10^{-9} - 10 \times 10^{-6}$ M exhibited a break at 0.25 μM. The MIP/Fe$_3$O$_4$/EPPG exhibited the successful estimation of HCTZ in the presence of interfering substances, such as ascorbic acid, uric acid, xanthine and hypoxanthine. Thus, it is concluded that the MIP/Fe$_3$O$_4$/EPPG can be successfully used for the quantification of HCTZ in

biological fluids and pharmaceutical formulations with excellent selectivity, low detection limit, long-term stability and high reproducibility.

SECTION B: DETERMINATION OF TELMISARTAN BY USING SURFACTANT MODIFIED EDGE PLANE PYROLYTIC GRAPHITE ELECTRODE

Telmisartan ((2-(4-{[4-methyl-6(1-methyl-1H-1,3-benzodiazol-2-yl)-2-propyl-1H1,3-benzodiazol-1-yl]methyl}phenyl) benzoic acid, TMS) is an angiotensin II type I receptor blocker, widely used for the treatment of hypertension and to regulate the blood pressure (BP). Oral administration of TMS dose has been found to reduce the hypertension in several animal models [50-51]. Hypertension increases the undesired symptoms and is associated with many complications like myocardial infarction, coronary heart disease and renal disease [56]. The renin-angiotensin system plays a substantial part in the growth and maintenance of hypertension. TMS selectively inhibits the action of angiotensin type I receptor without affecting the action of other receptors in cardiovascular regulation, which leads to reduced blood pressure, and hence the blood flows smoothly. TMS is a potent, long-term, orally acting non-peptide antagonist, which is utilized for the management of essential hypertension [52-55]. The generally effective dose of TMS is 40-80 mg per day and can be increased to a maximum of 80 mg once a day. TMS is not a pro-drug and suitable for daily dose, which also has a higher half-life (~24 h) [50,52]. The analysis of drugs plays an important role in drug quality control. Thus, the development of simple, selective and reliable method for the analysis of active drug has a valuable impact in the drug manufacture and pharmaceutical analysis. Several methods are available, such as HPLC [57-58], spectrophotometry [59-62], liquid chromatography–tandem mass spectrometry (LC–MS) [63], etc for the analysis of drugs. However, most of these techniques suffer from disadvantages such as expensive, sophisticated processes, time consuming procedure and hectic pre cleaning process using the variety of organic solvents. The electrochemical techniques specially voltammetric approaches are simple, accurate, sensitive, selective and cost effective. Several types of sensors have been made for sensitive, faster and accurate electrochemical investigation of the TMS. Alarfaz [53] and Tasdemir et. al. [64] reported stripping voltammetric approaches for the examination of TMS by using hanging mercury drop electrode. To avoid use of mercury to avoid toxicity, there is still need of a highly sensitive electroanalytical method for the trace analysis of TMS in complex matrix such as human urine. In the present studies an attempt has been made to use a simple protocol to fabricate SDS modified sensor for the analysis of TMS.

It was noticed that TMS strongly adsorb at the surface of pyrolytic graphite. To eliminate adsorption complications, the electrode was dipped in a solution of 10 mM sodium dodecyl sulfate (SDS), an anionic surfactant. It is generally used to overcome adsorption and to improve the

sensor/solution interface in electroanalysis, which increases the rate of electron transfer between the sensor surface and electro-active substances. [65-70].

5.7. EXPERIMENTAL

5.7.1 Materials and instrumentation

TMS, uric acid (UA), ascorbic acid (AA), xanthine (XT), hypoxanthine (HXT) and SDS were obtained from Sigma-Aldrich (USA). Disodium hydrogen phosphate (Na_2HPO_4), sodium dihydrogen phosphate (NaH_2PO_4), sodium hydroxide (NaOH), potassium chloride (KCl) and potassium ferricyanide ($K_3[Fe(CN)_6]$) were purchased from E. Merck (India). The studies were carried out in phosphate buffers (1.0 M) of pH range 2.4–8.0. A pH meter (model pH 700, Eutech) was utilized to assess the pH of the phosphate buffer solutions. To prepare the stock solutions double distilled water was used. The TMS solution (1.0 mM) was prepared by dissolving in 50 µL of 1M NaOH and the solution was made upto the mark using the double distilled water. The electrochemical experiments were performed in single glass cell equipped with three electrode system, a platinum wire an auxiliary electrode, pyrolytic graphite as a working electrode and Ag/AgCl (3M NaCl, Model; BAS MF-2052RB-5B) as a reference electrode. EPPG was obtained as a gift ($15\times3\times3$ mm^3) from Pfizer, USA. The surface of the modified sensor was characterized by using techniques as reported for HCTZ (Section A of this chapter).

5.7.2 Fabrications of sensor and influence of immersion time in SDS

To fabricate the sensor, firstly the EPPG sensor surface was cleaned by rubbing it on an emery paper (P-400) followed by washing with double distilled water. In the preliminary experiments, EPPG was immersed in SDS solutions of different concentrations for constant time. It was noticed that the peak current of TMS increased with increase in the concentration of SDS and became practically constant at higher concentrations (> 8 mM) as shown in **Fig 5.10A**. As critical micelle concentration of SDS is 8 mM in aqueous solution [71], it was concluded that negatively charged surface of micelles played an important role in the electrocatalysis during oxidation of TMS. The peak potential of TMS shifted to less positive values with increase in SDS concentration. This behaviour further indicated the electrocatalytic behaviour of the charged micelles towards oxidation of TMS. Thus, EPPG was immersed in a solution of 10 mM SDS for further studies. After this, the optimization of immersion time in the 10 mM SDS solution was examined. The current response of TMS was recorded using square wave voltammetry (SWV) by

immersing the EPPG between 5–60 s. The peak current response was found to increase till 20 s, after which the current response became constant (**Fig 5.10B**). Hence, an immersion time of 20 s was used in the detailed studies of TMS.
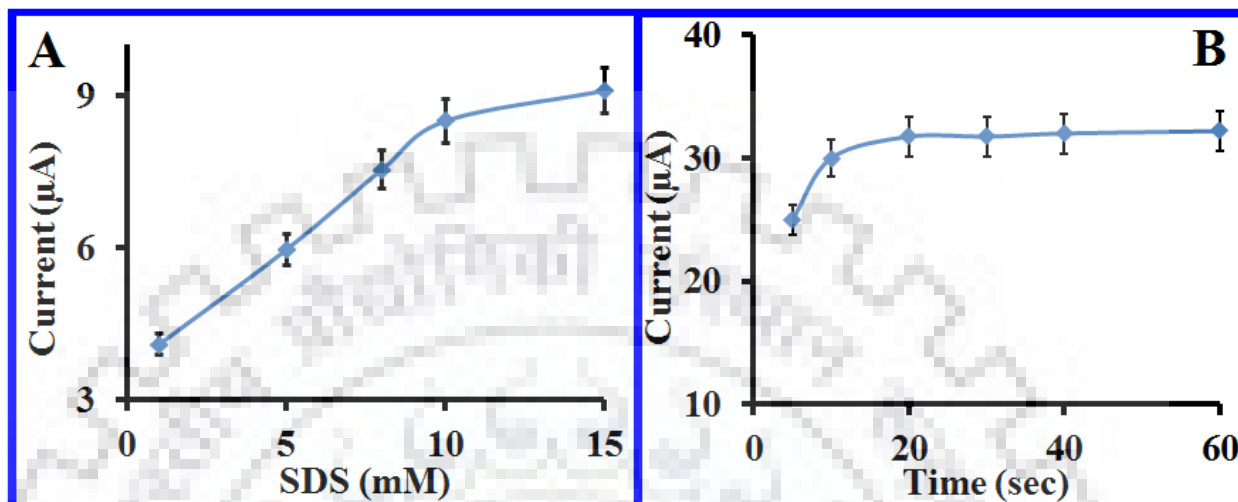

Fig. 5.10: (A) Effect of SDS concentration observed on the peak current of TMS at pH 7.4 Immersion time 20 s and (B) Effect of immersion time on the oxidation peak current response of 100 μM TMS observed using the SDS modified sensor at pH 7.4.

In addition to the use of SDS modified EPPG, the presence of SDS in the solution was also found to affect the peak current of TMS. For this purpose the effect of the concentration of added SDS in the solution was also investigated in the range 20 to 500 μM. A well-defined peak was observed at 100 μM concentration of SDS in the solution and the peak current remained constant at higher concentrations. Hence, 100 μM SDS was also added each time with phosphate buffer in the solution.

5.7.3 Voltammetric procedures

For recording voltammograms the desired concentration of the TMS was added in the cell, which already had 2 mL phosphate buffer. 400 μL of 1 mM SDS solution was then added and double distilled water was used to makes total volume 4 mL. The optimal parameters used for the voltammetric analysis were for experimental parameters for cyclic voltammetry (CV) were initial potential (E_i): 0 mV, switching potential (E): 1500 mV, the final potential (E_f): 0 mV and scan rate 100 mV/s. For square wave voltammetry (SWV) following parameters were optimized; initial potential (E_i): 0 mV, the final potential (E_f): 1500 mV, square wave frequency (f): 15 Hz, square

wave amplitude (E_{sw}): 25 mV, potential step (E): 4 mV. The EPPG surface was renewed each time and immersed in SDS (10 mM) solution for 20 s (optimized) before recording the voltammograms.

5.7.4 Pharmaceutical/ biological samples

To analyse the pharmaceutical formulations three tablets viz; Tazloc-H (USV Ltd, Baddi, Himachal Pradesh), Tadil 40-H (Zee laboratories, Paonta Sahib (HP)), and Xstan-H (Blue Cross PVT Ltd, Mumbai) containing TMS (40 mg) were obtained from the local market of Roorkee, Uttarakhand. The TMS containing tablets were powdered and required amount of the powder was used to prepare the stock solution.

The urine samples of healthy persons and hypertensive patients were collected from the IIT Roorkee hospital after clearance of Human Ethics Committee [Permission No. BIOTECH/IHEC/AP/15/1]. To determine the content of TMS in urine samples after the administration of oral drug, the urine samples of a hypertensive patient (Male, age 67, 75 kg), were collected after 5 h and 24 h of oral administration of TMS tablet (40 mg). To minimize the complexity, the urine samples were diluted three times by using the pH 7.4 phosphate buffer before recording the voltammograms.

The recovery study in urine samples of two volunteers (Male, age 22 and Female, age, 26) were performed. The urine samples were filtered using the Whatman filter paper 42. The phosphate buffer (pH 7.4) was used to dilute the filtrate of urine samples (two times) and the recovery studies were executed by spiking the diluted urine samples after adding known concentration of TMS.

5.8. RESULTS AND DISCUSSION

5.8.1 Characterization of the sensor surface

The morphology of the bare and SDS immersed EPPG surfaces was studied by using the FE-SEM (**Fig. 5.11**). The SEM images clearly indicate the difference in the morphology of the SDS modified surface (**Fig. 5.11 B**) as compared to the bare EPPG (**Fig. 5.11 A**). The surface of bare EPPG was clear, whereas **Fig. 5.11B** represented the deposition of the surfactant in agglomerated form most likely due to the micelles formation as the concentration of SDS was 10 mM (> CMC). This leads to irregular shape and size of the SDS. The irregular aggregation of SDS arises due to various non-covalent interactions leading to different morphologies. The granular and rod like morphologies have also been observed with different concentration of the SDS at the

surface of membrane as well as at glassy carbon electrode [72-74]. **Fig. 5.11 C** displays the EDX data observed at fabricated sensor and exhibits the presence of Na, O, C and S atoms.
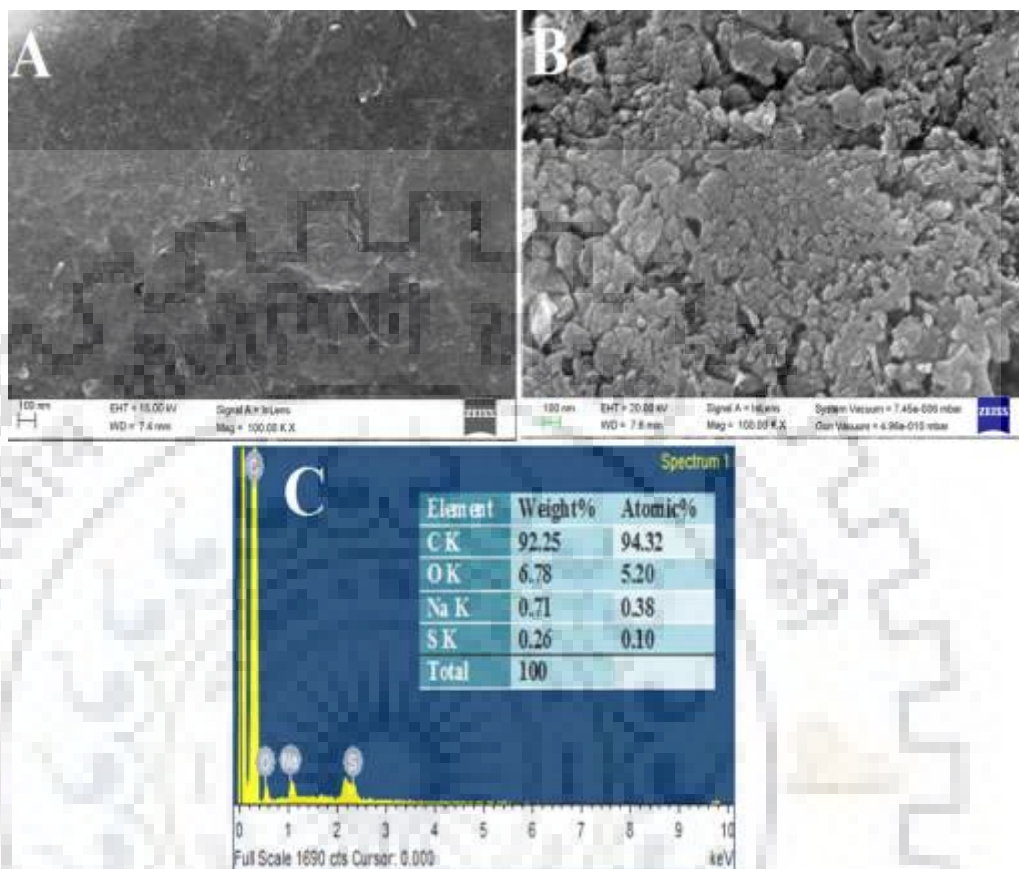

Element	Weight%	Atomic%
C K	92.25	94.32
O K	6.78	5.20
Na K	0.71	0.38
S K	0.26	0.10
Total	100	

Fig. 5.11: FE-SEM images demonstrating surface morphology of (A) bare/EPPG, (B) SDS/EPPG, and (C) EDX data of the SDS modified sensor surface.

The EIS studies have also been performed to evaluate the effect of SDS modified sensor on the electron transport behaviour of TMS. The experiment was performed in the equal proportion of 1 mM KCl and 5 mM $K_3[Fe(CN)_6]$ solution over the 1000 kHz to 0.001 Hz frequency range. Randle's circuit **(inset Fig. 5.12)** has been used to evaluate the data of the SDS immersed EPPG and bare EPPG. The Nyquist plots obtained consist two portions, one is the semi-circular indicating the charge transfer resistance (Rct) and the linear portion represents the mass transfer effects at lower frequency [75-76]. **Fig. 5.12** demonstrates the results observed for impedance studies at SDS modified EPPG and bare EPPG. The R_{CT} values for SDS/EPPG and bare/EPPG were found to 762 Ω **(curve a)**, and 823.1 Ω **(curve b)** respectively. Though, the variation of the Rct for SDS/EPPG in comparison to bare/EPPG was relatively small, still a better peak for TMS

was noticed at the modified electrode (**Fig. 5.12**). Thus, the variation of Rct values before and after modification provides an efficient approach to characterize the conductivity at solution/electrode surface. Thus, it is believed that the SDS reduces the resistance at sensor/solution interface and facilitates the electron transfer process in comparison to bare EPPG. In the presence of the SDS at Pt electrode, the charge transfer resistance has also found to be lower as compared to bare earlier [77]. The presence of SDS surfactant showed the better homogeneity for sample preparation and provided better contact at glassy carbon electrode (GCE) while in case of the carbon paste electrode (CPE) the smooth surface with bundles like structure was obtained [78, 70].
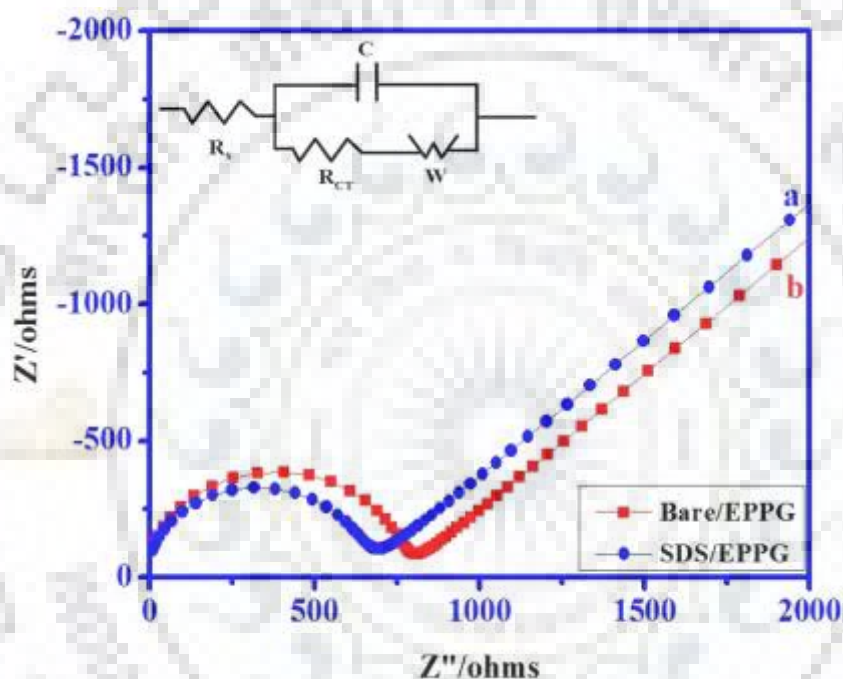
Fig. 5.12: Typical Nyquist plots observed for (a) bare/EPPG and (b) SDS/EPPG in 1:1 mixture of 5 mM $K_3Fe(CN)_6$ and 1 mM KCl solution over the frequency range 1000 kHz to 0.001Hz.

5.8.2 Cyclic Voltammetry

Initial CV studies of the TMS were carried out to examine the nature of electrochemical reactions involved in the oxidation of TMS. Cyclic voltammograms of 100 μM TMS solution were recorded to investigate the effect of SDS at pH 7.4 using the bare/EPPG and SDS/EPPG by scanning the potential from 0 to 1500 mV at a sweep rate of 100 mV/s (**Fig. 5.13**). At the bare EPPG sensor, a small broad peak with very small current was found at 1272 mV corresponding to the anodic oxidation of TMS. At the SDS modified sensor the peak current increased and peak potential shifted to the less positive values (1165 mV). **Fig. 5.13** demonstrates that no oxidation

peak is found in the reverse scan at any of the two sensors, indicating thereby that the oxidation of TMS is irreversible. The increase in the peak current and shift of peak potential of TMS to less positive values clearly indicate the electro-catalytic activity of surfactant (SDS), due to which the oxidation of TMS is facilitated. The similar studies with cationic surfactant, cetyl trimethylammonium bromide and non-ionic surfactant, Tween- 40 did not exhibit any peak in the CV of TMS. Hence, further investigations of TMS were performed by using the SDS/EPPG sensor.
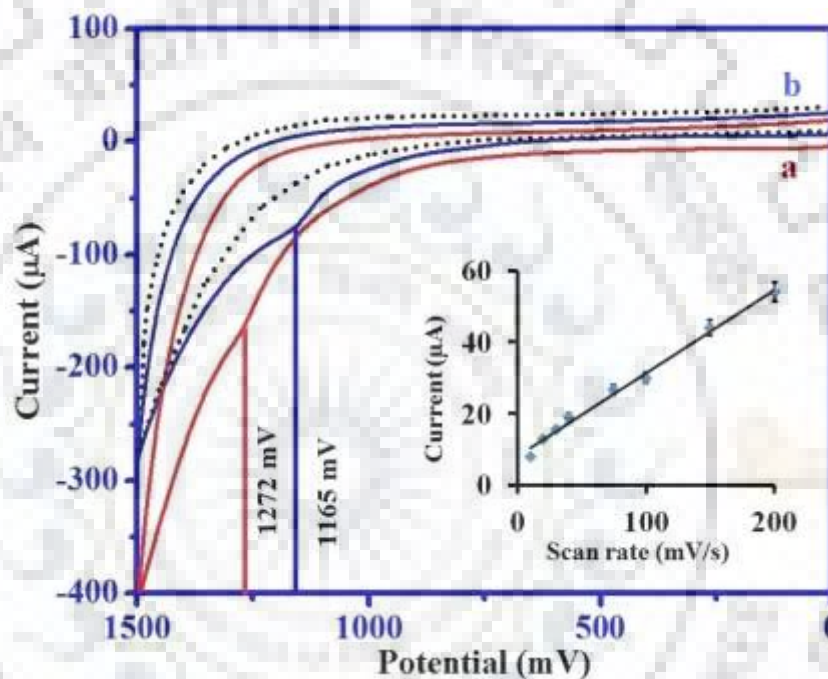
Figure 5.13: A comparison of cyclic voltammograms observed for 75 μM TMS in phosphate buffer of pH 7.4 using 100 μM SDS in the solution at 100 mV/s (a) bare EPPG and (b) SDS/EPPG. dotted line represents the CV of blank solution at modified sensor.

The behaviour of the redox reaction involved in the electro-oxidation of TMS was investigated by using the sweep rate study at SDS/EPPG sensor. In sacn rate study, it was found that with increase in the scan rate (v) in the range 10–200 mV/s, caused an increase in the peak current (i_p) of TMS **(inset Fig. 5.13)**. The plot of i_p versus v was linear and the relation can be described as

$$i_p = 0.2338\ v + 8.0127 \ldots\ldots\ldots\ R^2 = 0.992$$

where, R^2 is the correlation coefficient, v is the scan rate in mV/s, and i_p is the peak current in µA. Further, the linearity of i_p vs. v plot showed that the electro-oxidation of TMS at the surface of SDS/EPPG was adsorption controlled, which is further confirmed by the linear log plot between i_p vs. v. The relation between log i_p vs. log v can be represented by following equation;

$$\textbf{log } \textbf{i}_\textbf{p} = \textbf{0.6174 log } \textbf{\textit{v}} + \textbf{0.2856}……….. \textbf{R}^2 = \textbf{0.993}$$

The slope value (> 0.5) for log plot further indicated that the electron transfer process of TMS proceeded via adsorption controlled path [79]. Thus, it is clear that the SDS modified EPPG and SDS present in the solution are not able to completely remove the adsorption of TMS.

5.8.3 Square Wave Voltammetry

Square wave voltammetry (SWV) is a sensitive technique in comparison to cyclic voltammetry due to the better peak resolution and low background currents. Hence, the detailed electrochemical studies of TMS were performed by using SWV. To investigate the electro-catalytic behavior of the SDS/EPPG, voltammograms were recorded for 75 µM TMS solutions at pH 7.4 with SDS and without SDS in solution. A broad peak with a small peak current was observed at the bare sensor as shown in the **Fig. 5.14 (A)**. The response of the SDS/EPPG sensor was then recorded in both the cases i.e., with SDS and without SDS in solutions as shown in Fig. **5.14 (B)** and **5.14 (C)**. A sharp, well-defined SW voltammetric peak was observed with several fold enhancement in the peak current (i_p) in case of SDS used in solution in comparison to the bare EPPG as represented in **Fig. 5.14 (C)**. Thus, it is concluded that SDS presents in the solution also affects electrocatalysis.
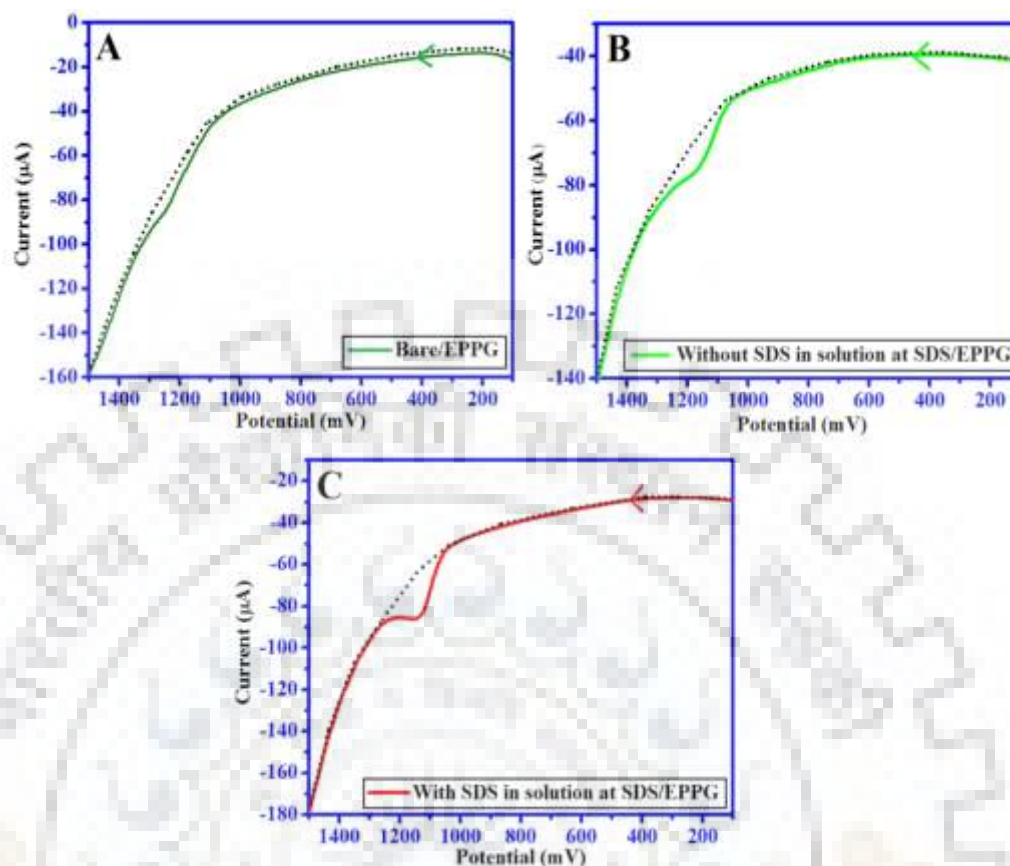
Fig. 5.14: A comparison of SW voltammograms recorded for 75 µM TMS in pH 7.4 phosphate buffer using 100 µM SDS in the solution at (A) bare EPPG, (B) without SDS in solution at SDS/EPPG and (C) with SDS in solution at SDS/EPPG, dotted line represents the SW voltammograms of blank solution.

5.8.3.1 Influence of Frequency

To examine the effect of SW frequency on the anodic peak current response of TMS, frequency study was performed. It has been found that peak current of 75 µM TMS increases with increase in the frequency in the range of 5–50 Hz at SDS/EPPG sensor. The linearity between the frequency (f) and peak current (i_p) at SDS/EPPG sensor indicated adsorption controlled oxidation of TMS. The linear relation of i_p versus f and log i_p versus log f **(Fig 5.15)** can be expressed by the equations;

$$i_p = 0.5685\,f + 6.8507\ldots\ldots\ldots\ldots\ R^2 = 0.993$$

$$\log i_p = 0.6083 \log f + 0.4943\ldots\ldots\ldots\ldots R^2 = 0.998$$

where, f is the square wave frequency in Hz and R^2 is correlation coefficient. As the slope of log plot was > 0.5, it was concluded that the electron transfer process of the electro-oxidation of TMS was adsorption controlled, which supported the results observed using cyclic voltammetry [79].
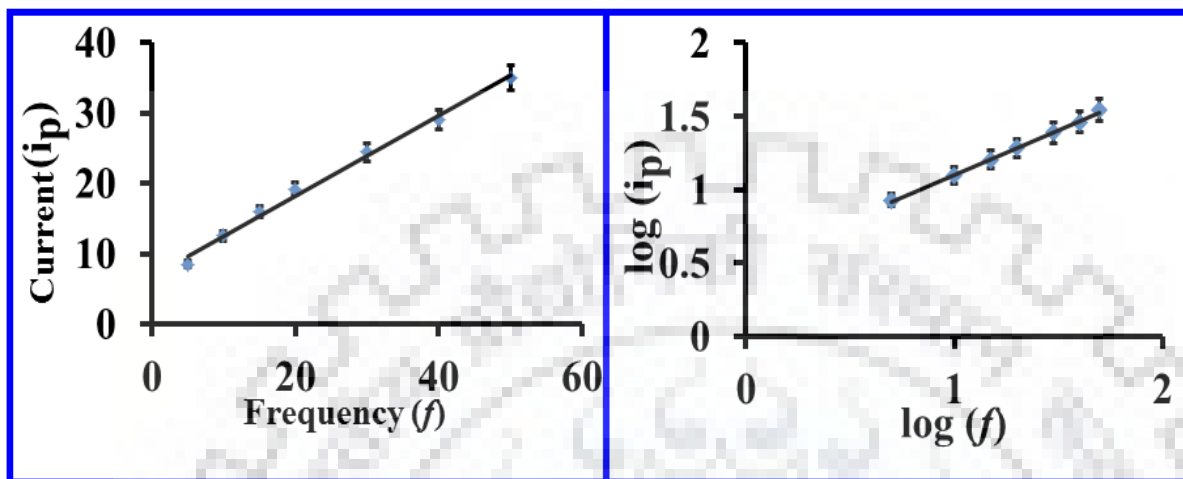
Fig. 5.15: Variation of (A) oxidation peak current (i_p) with the square wave frequency (f), (B) log (i_p) with log (f) for 75 µM TMS using SDS/EPPG sensor.

5.8.3.2 Effect of concentration

The effect of concentration on the peak current of TMS was performed to investigate the feasibility, limit of detection and sensitivity of the developed SDS immersed sensor (SDS/EPPG). The SW voltammograms were recorded at different concentrations of TMS at pH 7.4. The concentration of SDS in the solution was kept constant at 100 µM. An increase in the peak current of TMS was noticed with increase in concentration **(Fig. 5.16)**. A calibration curve was plotted between the peak current (i_p) and concentration of TMS and a linear increase was noticed in the range 5–100 µM as presented in the inset of **Fig. 5.16**. The linear dependence of i_p can be represented by the equation;

$$i_p = 0.2983 \ [C, 5–100] + 2.1733\ldots\ldots\ldots R^2 = 0.995$$
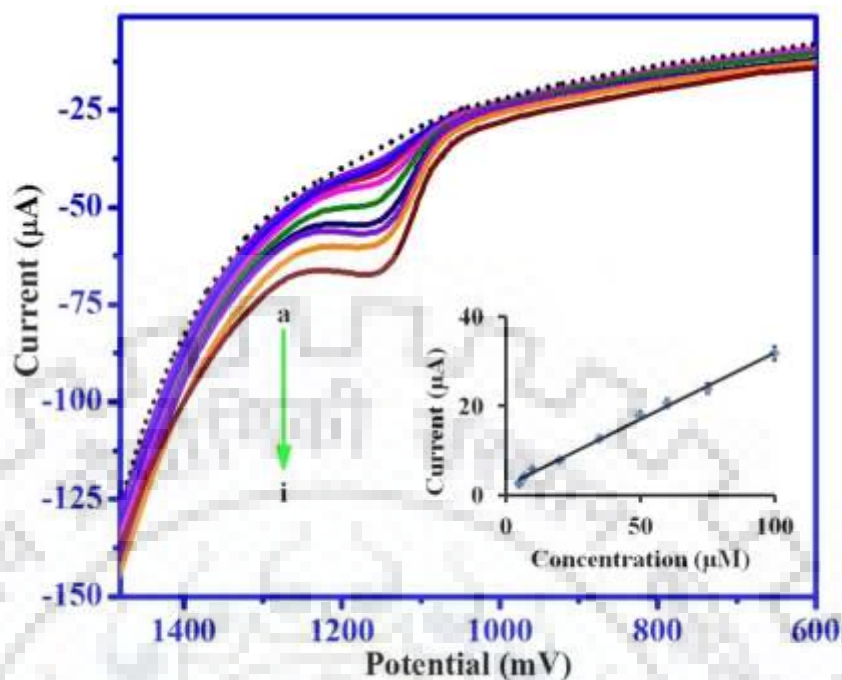
Fig. 5.16: Square wave voltammograms recorded for (a) 5 µM, (b) 7 µM, (c) 10 µM, (d) 20 µM, (e) 35 µM, (f) 50 µM, (g) 60, (h) 75 µM and (i) 100 µM TMS concentrations using SDS/EPPG. The background current is represented by the dotted line. A calibration plot of TMS is presented in the inset.

The limit of detection (LOD) and sensitivity were observed as 82 nM and 0.2983 µA/µM respectively for TMS by using the proposed sensor. The LOD is calculated by applying the 3σ/b, where b is the slope value observed in calibration plot and σ is the standard deviation of the five consecutive blank readings (n=5). A comparison of the L.O.D. of TMS observed at the proposed sensor and reported in recent years by several techniques is summarized in **Table 5.6**.

Table 5.6: A comparison of linear range and Limit of Detection (LOD) observed for TMS at SDS/EPPG with reported methods

S.No.	Technique	LOD (µM)	Concentration range (µM)	Reference
1.	HPLC	2.42	4.85–49.55	57
2.	Spectrophotometric	0.1165	1.94–15.54	59
3.	Spectrophotometric	25.26	77.72–248.7	60
4.	UV Spectroscopy	0.244	1.94–62.18	62
5.	HMDE, SW-AdSV	0.0836	0.1–6	53
6.	HMDE, SWCAdSV	0.00105	0.00169–0.0275	64
7.	SDBS/AB paste electrode	0.75	0.25–20	65
8.	SDS/EPPG, SWV	0.082	5–100	**Present work**

Acetylene black AB; Sodium dodecylbenzene sulfonate SDBS; Square wave cathodic adsorptive stripping voltammetry (SWCAdSV); Hanging mercury drop electrode (HMDE)

It can be clearly seen that a sufficiently low value of L.O.D. is observed using SDS/EPPG. A comparable L.O.D at HMDE was also reported earlier [53,64], however, due to the toxicity of mercury use of HMDE has been restricted/ banned in many countries. The analytical parameters obtained for the proposed method are also compiled in **Table 5.7**.

Table 5.7: Analytical parameters obtained for the quantitative analysis of TMS at SDS/EPPG.

S.No.	Validation Parameters	SDS/EPPG
1.	Concentration range (µM)	5–100
2.	Sensitivity (µA/µM)	0.2983
3.	Correlation coefficient (R^2)	0.9959
4.	Standard error of slope (α, 0.05)	0.0072
5.	Standard error of intercept (α, 0.05)	0.3685
6.	Limit of detection (nM)	82
7.	Limit of quantification (µM)	0.2737

5.8.3.3 Influence of pH

The effect of pH on the electro-oxidation of TMS over the pH range 2.08–8.03 was studied using the SWV. In the entire pH range a well-defined peak was noticed. On observing the oxidation peak of TMS, it was detected that the oxidation potential of TMS shifted as the pH value increased towards the less positive potentials **(Fig. 5.17).** The linear dependence of E_p on pH observed the relation

$$\text{Ep} = \text{-54.21 [pH, 2.08–8.03]} + \text{1530}………… \text{R}^2 = \text{0.951}$$

The dEp/dpH value of 54.21 mV/pH was nearby Nernst's value 59 mV/pH, which shows that number of protons and electrons contributing in the electro-oxidation of TMS are equal at SDS modified EPPG.
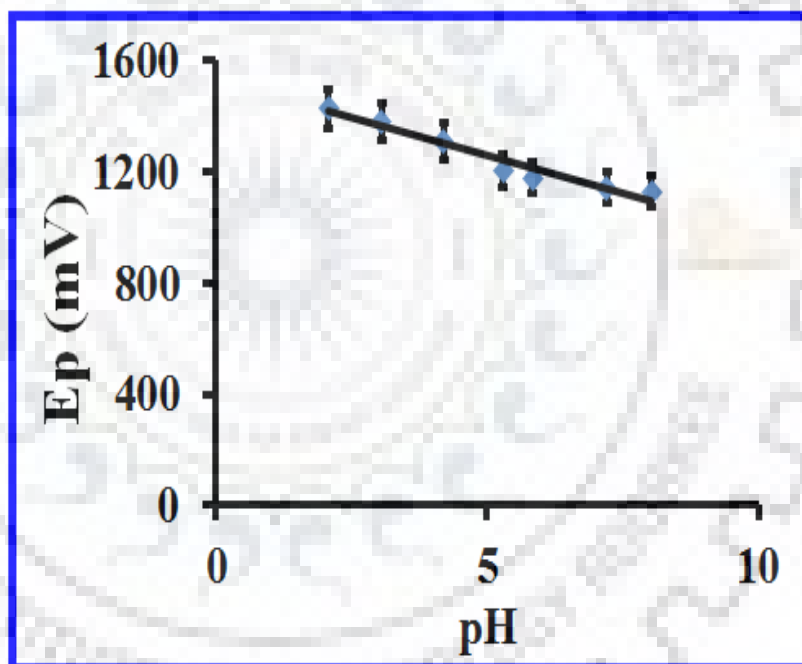
Fig. 5.17: Observed dependence of peak potential of TMS on pH.

To elucidate the number of electrons in the electro-oxidation of TMS, Laviron's equation [48] has been applied:

$$\mathbf{E_P = E^0 + RT/\alpha nF - RT/\alpha nF \ln \nu}$$

where, n is the number of electrons, α is the electron transfer coefficient, F is Faraday constant (96485 C mol^{-1}), T is absolute temperature (298 K) and R is the universal gas constant (8.314 J K^{-1}

mol^{-1}). For this purpose, the cyclic voltammograms of 75 µM TMS were recorded at different scan rates (v) in the range 10 – 150 mV/s. The electro-oxidation potential (E$_p$) increased with increasing the scan rate (v) and the variation can be represented by the relation:

$$\mathbf{E_p = 72.117 \log v + 1023.5\ldots\ldots\ldots R^2 = 0.994}$$

According to the Laviron's equation, the slope value of the plot of E$_p$ vs. log v is equal to 2.303RT/αnF. For a totally irreversible reaction, the value of α (0.5) [49] and electrons are contributing in the oxidation of TMS were observed to be 1.74. The observed value is close to two, so it is concluded that total two electrons are participating in the oxidation of TMS [64]. The most probable oxidation site in TMS is biphenyl carboxylic acid functional moiety. The overall 2e$^-$, 2H$^+$ oxidation of this moiety will give corresponding lactone. Similar oxidation mechanisms for biphenyl carboxylic acid have been reported by electrochemical and chemical reagents [80-81].

TMS
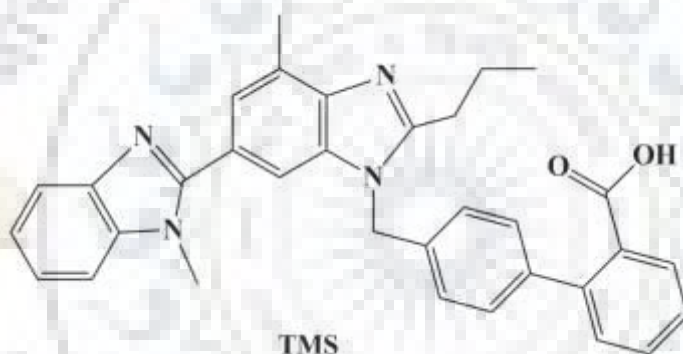
5.8.4 Selectivity of the developed sensor

To look into the effects of the potential interfering molecules, such as UA, XT, AA, which are present in the biological fluids and hydrochlorothiazide (HCTZ), which is given in combination with TMS are evaluated on the peak current and potential of TMS. For this purpose voltammograms were recorded at the fixed concentration of TMS (10 µM), in the presence of 100 fold concentration of the interference substances. The observed experimental results **(Fig. 5.18 A)** indicate that the 100 fold concentration of these interference substances does not affect the peak current of TMS. Hence, the proposed electrochemical method can be used successfully to detect the TMS in the presence of common interfering substance.
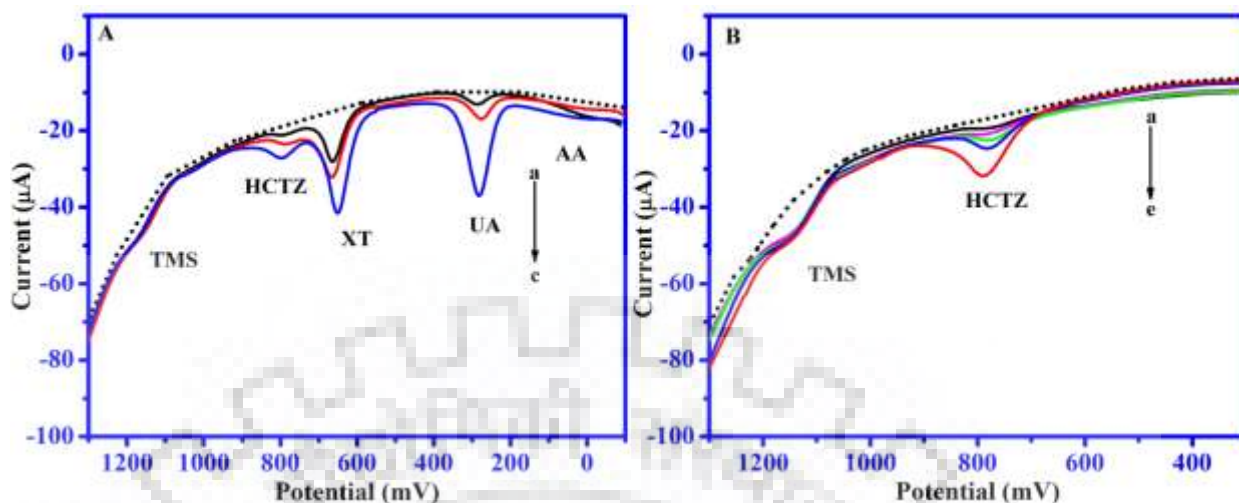
Figure 5.18 (A): Square wave voltammograms recorded in the presence of 10 μM TMS with (a) 50 μM UA + 200 μM XT + 100 μM AA + 100 μM HCTZ, (b) 100 μM UA + 300 μM XT + 200 μM AA + 150 μM HCTZ and (c) 400 μM UA + 400 μM XT + 300 μM AA + 250 μM HCTZ at pH 7.4. Background current is represented by the dotted line. (B): Square wave voltammograms recorded for 20 μM TMS in the presence of (a) 10, (b) 20, (c) 40, (d) 50 and (e) 100 μM HCTZ at pH 7.4.

TMS is also effective when used alone or in combination with other drugs in the treatment of hypertension. A common combination widely used is TMS-HCTZ. Hence, the effect of HCTZ on the oxidation of TMS was also investigated. For this purpose, a fixed concentration of TMS (20 μM) was used with increasing concentrations of HCTZ and voltammograms were recorded. It was observed that HCTZ did not affect the peak current of TMS as shown in the **Fig. 5.18 (B)**. Hence, the observed results indicate the high sensitivity and selectivity of the SDS/EPPG sensor towards TMS.

5.8.5 ANALYTICAL APPLICATION

5.8.5.1 Real sample assay

As TMS binds nearly 99.5% to albumin and alpha-1-acid glycoprotein, it has large half-life (~20–24 h). The inactivation of TMS by liver is less than 3% and ~97% is eliminated in urine in unchanged form [82-83]. Hence, to examine the practical utility of the developed SDS based sensor the determination of TMS in the complex matrix, like urine samples was achieved. For the recovery studies the first urine of the morning of the two healthy volunteers were collected, filtered

and diluted twice by using the phosphate buffer of pH 7.4 in order to minimize the complexity of the samples. The urine samples did not exhibit peak corresponding to TMS, however, peaks of UA, AA were clearly seen at 260 and -100 mV. The recovery studies were carried out by spiking the urine samples with the known concentration of TMS. SW voltammograms were then recorded and a sharp oxidation peak of TMS was observed at 1156 mV with an additional oxidation peak related to the oxidation of uric acid at 260 mV. The concentration of the TMS was determined by using the peak current response. With the help of calibration plot the concentration of TMS is obtained and results are summarized in **Table 5.8**. The observed results indicate a good recovery > 98% for both the urine samples, which demonstrate the excellent applicability of the develop sensor in the complex matrix like human urine.

Table 5.8: Recovery data observed for TMS in healthy human urine samples.

S.No.	Spiked amount (µM)	Detected amount (µM)[*]	Recovery %	Error%
Sample 1				
1	10	9.86	98.60	-1.40
2	20	19.96	99.80	-0.20
3	35	34.85	99.57	-0.43
Sample 2				
1	50	49.62	99.24	-0.76
2	75	74.84	99.78	-0.22
3	100	101.23	101.23	+1.23

*RSD for the determination was 1.68% for n=3

The biological applicability of the developed SDS modified sensor for TMS quantification in urine samples of hypertensive patients has also been evaluated. For this purpose the urine samples of hypertensive patient, who was under the treatment of TMS (40 mg/day) were obtained. The urine samples of hypertensive patient were collected after 6 h and 24 h of oral administration of TMS tablet. The complexity of the collected urine samples was minimized by diluting them three times using a pH 7.4 (phosphate buffer). As the excreted TMS was in small quantity, hence, standard addition method was used. The diluted urine samples were spiked with known concentration of TMS and SW voltammograms were recorded. A peak at 1156 mV

(corresponding to TMS) and a peak at 260 mV (corresponding UA) was clearly seen in the urine samples **(Fig. 5.19)**.
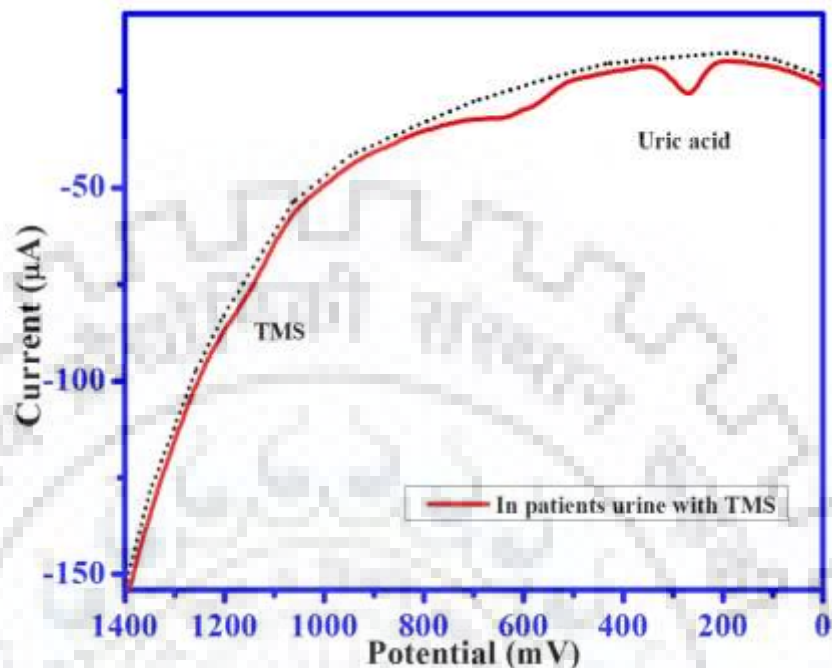
Fig. 5.19: Square wave voltammogram recorded in patient urine sample with spiked TMS.

The concentration of TMS was evaluated by extrapolating the linear curve **(Fig 5.20)**. By considering the dilution factor, the concentration of TMS was detected between 8.0–9.0 µM in all the urine samples. Some typical results of the TMS observed in urine sample after 24 h are shown in **Table 5.9**. The low RSD value ±1.83% (for n=3) in determination demonstrates the good reliability and accuracy of the SDS modified sensor.
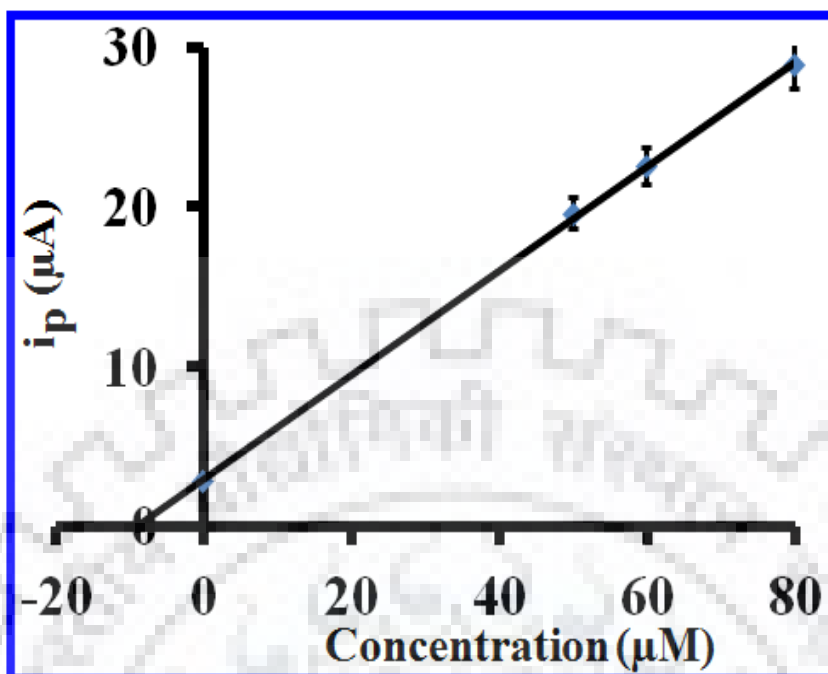
Fig. 5.20: The observed standard addition plot for TMS in the urine sample of a hypertensive patient.

Table 5.9: Observed concentration of TMS in human urine sample of a hypertensive patient after 24 h of oral administration.

S.No.	Spiked (µM)	Observed (µM)	Actual (µM)	*Recovery %	Error%
1.	0	8.82	8.82	--	--
2.	50	58.85	8.85	100.34	+0.34
3.	60	68.91	8.91	101.02	+1.02
4.	80	88.87	8.76	99.31	-0.69

The observed value is the sum of the TMS present in urine + spiked amount

The actual amount is observed – spiked amount

The RSD for determination was ±1.83% (for n=3)

5.8.5.2 Pharmaceutical assay

The amount of TMS present in three tablets marketed by different pharmaceutical companies were also analyzed. The tablets were crushed to powder and the stock solutions (1 mM) were ready by dissolving the required quantity of powder in the double distilled water. Stock solutions were again diluted to carry the concentration in the working range. The SW

voltammograms were then recorded at pH 7.4 at SDS/EPPG. The TMS concentration was calculated using the calibration plot and is presented in **Table 5.10**. The good similarity between the listed amount and observed amount of TMS clearly indicates that SDS/EPPG can be effectively used for the quantitation of TMS.

Table 5.10: Determination of TMS content in pharmaceutical drug formulations using SDS/EPPG sensor.

S.No.	Tablet	Stated content (mg)	Observed content (mg)	Error %
1.	Xstan-H	40	39.86	-0.35
2.	Tazloc-H	40	39.62	-0.95
3.	Tadil 40-H	40	39.54	-1.15

5.9 Stability and reproducibility of sensor

The stability of SDS/EPPG sensor was examined at fixed concentration of TMS (20 µM) under optimized SWV conditions over a period of 30 days. The SW voltammograms were recorded every day, the results demonstrated that current deviated $< \pm 2.89\%$ for first 15 days and after which a deviation in the current up to $\pm 6.32\%$ was noticed. Therefore, the developed SDS/EPPG sensor can be employed safely for 15 days after its fabrication. To examine the intraday reproducibility of the developed sensor, five SW voltammograms were recorded at SDS/EPPG in the blank solution and also for 20 µM TMS at 1 h interval and R.S.D. was determined. By the calculations, the value of R.S.D. was observed to be $\pm 3.72\%$ (n=5), which indicated the excellent reproducibility of the SDS/EPPG sensor. Thus, it was observed that the SDS/EPPG sensor has an outstanding reproducibility. To investigate the sensor to sensor deviation, three EPPG electrodes were modified with SDS by a protocol used earlier. The square wave voltammograms were recorded for a fixed concentration of the TMS (20 µM) by using the each SDS/EPPG sensor and variation in the current response was evaluated. It was found that the current response of the three electrodes was varied by $\pm 2.23\%$. Thus, it is concluded that the proposed protocol shows an excellent sensor to sensor reproducibility.

5.10. Ruggedness studies

To study the interlaboratory behavior of SDS/EPPG sensor, ruggedness study has been performed. To inspect the instruments related variation and analyst to analyst variation in the term of voltammetric response, two voltammetric analyzers viz., Epsilon and CV-50W (Bioanalytical system, WL, USA) were applied. The intermediate precisions of different SDS/EPPG sensors were determined by two analysts on different days. The results observed at different instruments and different sensor exhibited a variation of ±1.58% in the current response of TMS and the obtained results are summarized in **Table 5.11**. Thus, presented SDS/EPPG sensor shows the reliable, robust and rugged approach for the determination of TMS.

Table 5.11: The robustness and ruggedness of the proposed method for the recovery data of TMS determination in human urine samples

Variables	Recovery % ± R.S.D
Robustness at pH=7.2	99.43 ± 1.47
Ruggedness Analyst 1	
Instrument: Epsilon EC-USB	99.27 ± 1.61
Instrument: CV 50W	98.53 ± 1.28
Ruggedness Analyst 2	
Instrument: Epsilon EC-USB	99.32 ± 1.23
Instrument: CV 50W	98.67 ± 1.34

5.11. CONCLUSION

The present section describes, effect of anionic surfactant SDS on the oxidation of TMS; an anti-hypertensive drug. The layer of the SDS was deposited on the surface of EPPG by immersing it in the solution of SDS at a concentration greater than CMC. SDS can easily adsorb at the surface of EPPG via strong hydrophobic interactions and leads to various changes at the electrode/solution interface, due to which electrochemical behaviour of TMS is improved. It is believed that at concentrations greater than CMC, the monomer SDS concentration is very small and most of the SDS species are present in micellar form. The dodecyl sulfate anion then seems to form pseudo complex with cation radical of TMS (which is formed by 1e, $1H^+$ oxidation) due to which oxidation potential shifts to less positive potentials. The binding of cationic free radicals with

negatively charged surface of micelles has been reported for large number of compounds in the literature [84-86]. The loss of second electron and proton then gives corresponding lactone as the final product. The electrochemical response of electroactive compounds has been found to change drastically in the presence of long hydrophobic C-H chain surfactants and hence they are widely used to improve sensitivity and selectivity in determinations [87]. The determination of TMS in the concentration range of 5–100 µM at SDS/EPPG was carried out. The SDS modified surface was characterized by using the FE-SEM, EIS, SWV and CV. The low detection limit at SDS/EPPG sensor was observed. The electron transfer reaction of TMS was facilitated at the SDS/EPPG surface in comparison to bare EPPG. The high reproducibility of the SDS/EPPG sensor makes it a potential candidate for the quantification of TMS in various biological as well as pharmaceutical samples. The proposed method is simple, rapid, sensitive and highly selective.

5.12 REFERENCES

[1] D.T. Lackland, M.A. Weber, "Global burden of cardiovascular disease and stroke: hypertension at the core", Can. J. Cardiology 56931 (2015) 569–571.

[2] N.R. Poulter, D. Prabhakaran, M. Caulfield, "Hypertension", Lancet 386 (2015) 801–812.

[3] S. Laurent, "Antihypertensive drugs", Pharmacol. Res. 124 (2017) 116–125.

[4] K. Haupt, A.V. Linares, M. Bompart, B.T.S. Bui, "Molecularly imprinted polymers", Top Curr. Chem. 325 (2012) 1–28.

[5] W. de J.R. Santos, P.R. Lima, C.R.T. Tarley, N.F. Hoehr, L.T. Kubota, "Synthesis and application of a peroxidase-like molecularly imprinted polymer based on hemin for selective determination of serotonin in blood serum", Anal. Chim. Acta 631 (2009) 170–176.

[6] B. Sellergren, C.J. Allender, "Molecularly imprinted polymers: A bridge to advanced drug delivery", Adv. Drug Deliv. Rev. 57 (2005) 1733–1741.

[7] P. Martin, I.D. Wilson, D.E. Morgan, G.R. Jones, K. Jones, "Evaluation of a molecular-imprinted polymer for use in the solid phase extraction of propranolol from biological fluids", Anal. Commun. 34 (1997) 45–47.

[8] Y.P. Duan, C.M. Dai, Y.L. Zhang, L. Chen, "Selective trace enrichment of acidic pharmaceuticals in real water and sediment samples based on solid-phase extraction using multi-templates molecularly imprinted polymers", Anal. Chim. Acta 758 (2013) 93–100.

[9] F.T.C. Moreira, R.A.F. Dutra, J.P.C. Noronha, M.G.F. Sales, "Myoglobin-biomimetic electroactive materials made by surface molecular imprinting on silica beads and their use as ionophores in polymeric membranes for potentiometric transduction", Biosens. Bioelectron. 26 (2011) 4760–4766.

[10] A. Ribeiro, F. Veiga, D. Santos, J.J.T. Labandeira, A. Concheiro, C.A. Lorenzo, "Bioinspired imprinted PHEMA-hydrogels for ocular delivery of carbonic anhydrase inhibitor drugs", Biomacromolecules 12 (2011) 701–709.

[11] T. Eren, N. Atar, M.L. Yola, H.K. Maleh, "A sensitive molecularly imprinted polymer based quartz crystal microbalance nanosensor for selective determination of lovastatin in red yeast rice", Food Chem. 185 (2015) 430–436.

[12] D.C. Apodaca, R.B. Pernites, R. Ponnapati, F.R.D. Mundo, R.C. Advincula, "Electropolymerized molecularly imprinted polymer film: EIS sensing of bisphenol A", Macromolecules 44 (2011) 6669–6682.

[13] A. McCluskey, C.I. Holdsworth, M.C. Bowyer, "Molecularly imprinted polymers (MIPs): sensing, an explosive new opportunity", Org. Biomol. Chem. 5 (2007) 3233–3244.

[14] B.W. Lu, W.C. Chen, "A disposable glucose biosensor based on drop-coating of screen-printed carbon electrodes with magnetic nanoparticles", J. Magn. Magn. Mater. 304 (2006) e400–e402.

[15] L.M. Rossi, A.D. Quach, Z. Rosenzweig, "Glucose oxidase–magnetite nanoparticle bioconjugate for glucose sensing", Anal. Bioanal. Chem. 380 (2004) 606–613.

[16] S.R. Rudge, T.L. Kurtz, C.R. Vessely, L.G. Catterall, D.L. Williamson, "Preparation, characterization, and performance of magneticiron} carbon composite microparticles for chemotherapy", Biomaterials 21 (2000) 1411–1420.

[17] S.V. Sonti, A. Bose, "Cell separation using protein-A coated magnetic nanoclusters", J. Colloid Interface Sci. 170 (1995) 575–585.

[18] D.H. Chen, M.H. Liao, "Preparation and characterization of YADH-bound magnetic nanoparticles", J. Mol. Catal. B: Enzym. 16 (2002) 283–291.

[19] J. Tucek, K.C. Kemp, K.S. Kim, R. Zboril, "Iron-oxide-supported nanocarbon in lithium-ion batteries, medical, catalytic, and environmental applications", ACS Nano 8(8) (2014) 7571–7612.

[20] A. Kaushik, R. Khan, P.R. Solanki, P. Pandey, J. Alam, S. Ahmad, B.D. Malhotra, "Iron oxide nanoparticles–chitosan composite based glucose biosensor", Biosens. Bioelectron. 24(4) (2008) 676–683.

[21] A.K. Gupta, M. Gupta, "Synthesis and surface engineering of iron oxide nanoparticles for biomedical applications", Biomaterials 26(18) (2005) 3995–4021.

[22] T. Ahuja, I.A. Mir, D. Kumar, Rajesh, "Biomolecular immobilization on conducting polymers for biosensing applications", Biomaterials 28 (2007) 791–805.

[23] M. Gerard, A. Chaubey, B.D. Malhotra, "Application of conducting polymers to biosensors", Biosens. Bioelectron. 17 (2002) 345–359.

[24] B.D. Malhotra, A. Chaubey, S.P. Singh, "Prospects of conducting polymers in biosensors", Anal. Chim. Acta 578 (2006) 59–74.

[25] M. Raj, P. Gupta, R.N. Goyal, "Poly-melamine film modified sensor for the sensitive and selective determination of propranolol, a β-blocker in biological fluids", J. Electrochem. Soc. 163(6) (2016) H388–H394.

[26] S. Baskar, C.W. Liao, J.L. Chang, J.M. Zen , "Electrochemical synthesis of electroactive poly(melamine) with mechanistic explanation and its applicability to functionalize carbon surface to prepare nanotube–nanoparticles hybrid", Electrochim. Acta 88 (2013) 1–5.

[27] F.H. Messerli, H. Makani, A. Benjo, J. Romero, C. Alviar, S. Bangalore, "Antihypertensive efficacy of hydrochlorothiazide as evaluated by ambulatory blood pressure monitoring", J. Am. Coll. Cardiol. 57(5) (2011) 590–600.

[28] H.K. Maleh, A.A. Ensafi, H.R. Ensafi, "Ferrocenedicarboxylic acid modified carbon paste electrode: a sensor for electrocatalytic determination of hydrochlorothiazide", J. Braz. Chem. Soc. 20(5) (2009) 880–887.

[29] H. Beitollahi, F. Ghorbani, "Benzoylferrocene-modified carbon nanotubes paste electrode as a voltammetric sensor for determination of hydrochlorothiazide in pharmaceutical and biological samples", Ionics 19 (2013) 1673–1679.

[30] O.A. Razak, "Electrochemical study of hydrochlorothiazide and its determination in urine and tablets", J. Pharm. Biomed. Anal. 34 (2004) 433–440.

[31] M.C.G. Santos, C.R.T. Tarley, L.H.D. Antonia, E.R. Sartori, "Evaluation of boron-doped diamond electrode for simultaneous voltammetric determination of hydrochlorothiazide and losartan in pharmaceutical formulations", Sens. Actuators B-Chem 188 (2013) 263–270.

[32] M.A. Obando, J.M. Estela, V. Cerda, "Simultaneous determination of hydrochlorothiazide and losartan potassium in tablets by high-performance low-pressure chromatography using a multi-syringe burette coupled to a monolithic column", Anal. Bioanal. Chem. 391(6) (2008) 2349–2356.

[33] A.F.M.E. Walily, S.F. Belal, E.A. Heaba, A.E. Kersh, "Simultaneous determination of enalapril maleate and hydrochlorothiazide by first-derivative ultraviolet spectrophotometry and high-performance liquid chromatography", J. Pharm. Biomed. Anal. 13 (1995) 851–856.

[34] K. Kargosha, A.H.M. Sarrafi, "Spectrophotometric simultaneous determination of triamterene and hydrochlorothiazide in Triamterene-H tablets by multivariate calibration methods", J. Pharm. Biomed. Anal. 26 (2001) 273–279.

[35] N. Erk, "Simultaneous determination of fosinopril and hydrochlorothiazide in pharmaceutical formulations by spectrophotometric methods", J. Pharm. Biomed. Anal. 27 (2002) 901–912.

[36] M.E. MartoAn, O.M. HernaAndez, A.I. JimeAnez, J.J. Arias, F. JimeAnez, "Partial least-squares method in analysis by differential pulse polarography. Simultaneous determination of amiloride and hydrochlorothiazide in pharmaceutical preparations", Anal. Chim. Acta 381 (1999) 247–256.

[37] S.X. dos Santos, E.T.G. Cavalheiro, "Evaluation of the potentialities of a carbon nanotubes/silicone rubber composite electrode in the determination of hydrochlorothiazide", Anal. Lett. 45 (2012) 1454–1466.

[38] A.P.P. Eisele, G.R. Mansano, F.M. de Oliveira, J. Casarin, C.R.T. Tarley, E.R. Sartori, "Simultaneous determination of hydrochlorothiazide and valsartan in combined dosage forms: Electroanalytical performance of cathodically pretreated boron-doped diamond electrode", J. Electroanal. Chem. 732 (2014) 46–52.

[39] M.B. Gholivand, M. Khodadadian, "Simultaneous voltammetric determination of captopril and hydrochlorothiazide on a graphene/ferrocene composite carbon paste electrode", Electroanalysis 25(5) (2013) 1263–1270.

[40] C.A.R.S. Neto, A.P.P. Eisele, V.G. Resta, J. Scremin, E.R. Sartori, "Differential pulse voltammetric method for the individual and simultaneous determination of antihypertensive drug metoprolol and its association with hydrochlorothiazide in pharmaceutical dosage Forms", Sens. Actuators B-chem 230 (2016) 630–638.

[41] H. Beitollahi, F. Ebadinejad, F. Shojaie, M.T. Mahani, "A magnetic core–shell Fe_3O_4@SiO_2/MWCNT nanocomposite modified carbon paste electrode for amplified electrochemical sensing of amlodipine and hydrochlorothiazide", Anal. Methods 8 (2016) 6185–6193.

[42] W.B.S. Machini, D.N.D. Parra, M.F.S. Teixeira, "Electrochemical investigation of the voltammetric determination of hydrochlorothiazide using a nickel hydroxide modified nickel electrode", Mater. Sci. Eng. C 57 (2015) 344–348.

[43] S.J. Makowski, M. Lacher, C. Lermer, W. Schnick, "Supramolecular hydrogen-bonded structures between melamine and N-heterocycles", J. Mol. Struct. 1013 (2012) 19–25.

[44] G.D. Christian, W.C. Purdy, "The residual current in orthophosphate medium", J. Electroanal. Chem. 3(6) (1962) 363–367.

[45] S.Q. Shi, W. Che, K. Liang, C. Xia, D. Zhang, "Phase transitions of carbon-encapsulated iron oxide nanoparticles during the carbonization of cellulose at various pyrolysis temperatures", J. Anal. Appl. Pyrolysis 115 (2015) 1–6.

[46]   F. Yu Cheng, C.H. Su, Y.S. Yang, C.S. Yeh, C.Y. Tsai, C.L. Wu, M.T. Wu, D.B. Shieh, "Characterization of aqueous dispersions of Fe_3O_4 nanoparticles and their biomedical applications", Biomaterials 26 (2005) 729–738.

[47]   R.H. Wopschall, I. Shain, "Effects of adsorption of electroactive species in stationary electrode polarography", Anal. Chem. 39 (1967) 1527–1534.

[48]   E. Laviron, "General expression of the linear potential sweep voltammogram in the case of diffusionless electrochemical systems", J. Electroanal. Chem. 101 (1979) 19–28.

[49]   L. Fotouhi, M. Fatollahzadeh, M.M. Heravi, "Electrochemical behavior and voltammetric determination of sulfaguanidine at a glassy carbon electrode modified with a multi-walled carbon nanotube", Int. J. Electrochem. Sci. 7 (2012) 3919–3928.

[50]   A. Singh, K.K. Jha, A. Mittal, A. Kumar, "A Review on: Telmisartan", J. Sci. & Innov. Res. 2 (2013) 160–175.

[51]   K.J. McClellan, A. Markham, "Telmisartan", Drugs 56 (1998) 1039–1044.

[52]   W. Wienen, M. Entzeroth, J.C.A. van Meel, J. Stangier, U. Busch, T. Ebner, J. Schmid, H. Lehmann, K. Matzek, J.K. Rawson, V. Gladigau, N.H. Hauel, "A Review on telmisartan: A novel, long-acting angiotensin II-receptor antagonist", Cardiovasc. Drug Rev. 18 (2000) 127–154.

[53]   N.A. Alarfaj, "Square-wave adsorptive stripping voltammetric determination of antihypertensive agent telmisartan in tablets and its application to human plasma", J. Anal. Chem. 68 (2013) 335–340.

[54]   A.M. El-Didamony, S.M. Hafeez, A.A. Saad, "Application of bromocresol green and bromothymol blue for the extractive spectrophotometric determination of anti-hypertensive drugs", J. Appl. Pharm. Sci. 5 (2015) 122–129.

[55]   D.P. Navarrete, A.C. Mendoza, E.L. Bojorquez, J.G. Banuelos, V.B. Fraga, M.G. de la Parra, "Bioavailability of two different tablet formulations of telmisartan of two different strengths (40 mg and 80 mg) in healthy male mexican volunteers", J. Bioequiv. Availab. 7 (2015) 164–169.

[56]   X.L. Bao, W.B. Zhu, T.L. Shan, Z. Wu, R.J. Zhang, P.Y. Liao, M.Z. Zheng, H.S. Tang, Y.J. Yan, Z.L. Chen, "Design, synthesis and evaluation of novel angiotensin II receptor 1 antagonists with antihypertensive activities", RSC Adv. 7 (2017) 26401–26410.

[57] S. Jawla, K. Jeyalakshmi, T. Krishnamurthy, Y. Kumar, "Development and validation of simultaneous HPLC method for estimation of telmisartan and ramipril in pharmaceutical formulations", Int. J. PharmTech Res. 2 (2010) 1625–1633.

[58] M. Divya, G. Anusha, Dr. H. Padmalatha, "RP-HPLC method development and validation for simultaneous estimation of telmisartan and ramipril in pharmaceutical dosage forms", Indo Am. J. Pharm. Sci. 3 (2016) 86–91.

[59] D.V. Modi, P.U. Patel, "Development and validation of dual wavelength spectrophotometric method for simultaneous estimation of telmisartan and nifedipine in synthetic mixture", Int. J. Pharm. Pharm. Res. 5 (2016) 48–56.

[60] A.A. Elkheir, H.M. Saleh, M.M. El-henawee, B.E. Ghareeb, "Spectrophotometric determination of terbinafine HCL and telmisartan using potassium permanganate", Int. J. Pharm. Chem. Boil. Sci. 5 (2015) 361–371.

[61] A. Pandey, H. Sawarkar, M. Singh, Dr. P. Kashyap, P. Ghosh, "UV-spectrophotometric method for estimation of telmisartan in bulk and tablet dosage form", Int. J. ChemTech Res. 3 (2011) 657–660.

[62] R.K. Jat, S. Sharma, R.C. Chippa, R. Singh, I. Alam, "Quantitative estimation of telmisartan in bulk drug and tablets by UV-spectroscopy", Int. J. Drug Res. Tech. 2 (2012) 268–272.

[63] V.B. Ravi, J.K. Inamadugu, N.R. Pilli, V. Sreenivasulu, V. Ponneri, "Simultaneous determination of telmisartan and amlodipine in human plasma by LC−MS/MS and its application in a human pharmacokinetic study", J. Pharm. Anal. 2 (2012) 319–326.

[64] I.H. Tasdemir, M.A. Akay, N. Erk, E. Kilic, "Voltammetric behavior of telmisartan and cathodic adsorptive stripping voltammetric method for its assay in pharmaceutical dosage forms and biological fluids", Electroanalysis 22 (2010) 2101–2109.

[65] H. Yi, W. Huang, "Enhancement effect of sodium dodecyl benzene sulfonate (SDBS) and its application into voltammetric determination of telmisartan", Colloids Surf. B 58 (2007) 237–241.

[66] W. Caetano, M. Tabak, "Interaction of chlorpromazine and trifluoperazine with anionic sodium dodecyl sulfate (SDS) micelles: Electronic absorption and fluorescence studies", J. Colloid Interface Sci. 225 (2000) 69–81.

[67]   D. Zheng, J. Ye, W. Zhang, "Some properties of sodium dodecyl sulfate functionalized multiwalled carbon nanotubes electrode and its application on detection of dopamine in the presence of ascorbic acid", Electroanalysis 20 (2008) 1811–1818.

[68]   J. Agrisuelas, M.I.G. Sanchez, E. Valero, "Electrochemical properties of poly(Azure A) films synthesized in sodium dodecyl sulfate solution", J. Electrochem. Soc. 164 (2017) G1–G9.

[69]   M. Kanungo, A. Kumar, A. Q. Contractor, "Studies on electropolymerization of aniline in the presence of sodium dodecyl sulfate and its application in sensing urea", J. Electroanal. Chem. 528 (2002) 46–56.

[70]   O.J. D'Souza, R.J. Mascarenhas, A.K. Satpati, V. Mane, Z. Mekhalif, "Application of a nanosensor based on MWCNT-sodium dodecyl sulphate modified electrode for the analysis of a novel drug, alpha-hydrazinonitroalkene in human blood serum", Electroanalysis 29 (2017) 1–12.

[71]   A. Cifuentes, J.L. Bernal, J.C. Diez-Masa, "Determination of critical micelle concentration values using capillary electrophoresis instrumentation", Anal.Chem. 69 (1997) 4271– 4274.

[72]   Z. Zhao, S. Shi, H. Cao, Y. Li, "Electrochemical impedance spectroscopy and surface properties characterization of anion exchange membrane fouled by sodium dodecyl sulfate", J. Membr. Sci. 530 (2017) 220–231.

[73]   B. Tah, P. Pal, M. Mahato, G. B. Talapatra, "Aggregation behavior of SDS/CTAB catanionic surfactant mixture in aqueous solution and at the air/water interface", J. Phys. Chem. B 115 (2011) 8493–8499.

[74]   J. H. Bang, K. S. Song, M. G. Lee, C. W. Jeon, Y. N. Jang, "Effect of critical micelle concentration of sodium dodecyl sulfate dissolved in calcium and carbonate source solutions on characteristics of calcium carbonate crystals", Mater. Trans. 51(8) (2010) 1486–1489.

[75]   N. Kumar, Rosy, R. N. Goyal, "Palladium nano particles decorated multi-walled carbon nanotubes modified sensor for the determination of 5-hydroxytryptophan in biological fluids", Sens. Actuator B-Chem. 239 (2017) 1060–1068.

[76]   E. Barsoukov, J.R. Macdonald, "Impedance spectroscopy, theory, experiment and applications", 2nd Edition,Wiley Interscience, New Jersey, (2005).

[77]   N.F. Atta, A. Galal, R.A. Ahmed, "Poly(3,4-ethylene-dioxythiophene) electrode for the selective determination of dopamine in presence of sodium dodecyl sulfate", Bioelectrochemistry 80 (2011) 132–141.

[78]   N. Karthikeyan, V.V. Giridhar, D. Vasudevan, "Surfactant effects on methanol oxidation at Pt–Ru/C coated glassy carbon electrode", J. Solid State Electrochem. 14 (2010) 877–881.

[79]   N. Kumar, Rosy, R.N. Goyal, "Nanopalladium grained polymer nanocomposite based sensor for the sensitive determination of Melatonin", Electrochim. Acta 211 (2016) 18–26.

[80]   L. Ebersonl, K. Nyberg, "Studies on electrolytic substitution reactions. I. Anodic acetoxylation", J. Am. Chem. Soc. 88 (1966) 1686–1691.

[81]   G.W. Kenner, M.A. Murray, C.M.B. Tylor, "Oxidative cyclisation of diphenyl-2 carboxylic acid", Tetrahedron 1 (1957) 259–263.

[82]   J. Stangier, C. Su, W. Roth, "Pharmacokinetics of orally and intravenously administered telmisartan in healthy young and elderly volunteers and in hypertensive patients", J. Int. Med. Res. 28 (2000) 149–167.

[83]   P. Gosse, "A review of telmisartan in the treatment of hypertension: blood pressure control in the early morning hours", Vasc. Health Risk Manag. 2 (2006) 195–201.

[84]   J.H. Fendler, E.J. Fendler, "Catlysis in micellar and macromolecular systems", Academic Press, New York, 1997.

[85]   N. Sarmeche, S. Aeiyach, J.J. Aaron, M. Jouini, J.C. Lacroix, P.C. Lacaze, "Improvement of the electrosynthesis and physicochemical properties of poly(3,4-ethylenedioxythiophene) using a sodium dodecyl sulfate micellar aqueous medium", Langmuir 15 (1999) 2566–2574.

[86]   B. Samiey, C. H. Cheng, J. Wu, "Effects of surfactants on the rate of chemical reactions", J. Chem. (2014) doi: 10.1155/2014/908476.

[87]   P. Xie, X. Chen, F. Wang, C. Hu, S. Hu, "Electrochemical behaviors of adrenaline at acetylene black electrode in the presence of sodium dodecyl sulfate", Colloids Surf. B 48 (2006) 17–23.